AD-A168 755 HIGH ANNULAR RESOLUTION STELLAR INTERFEROMETRY(U) 1/3
ROCHESTER UNIV NY INST OF OPTICS J C DAINTY 31 JUL 85
AFOSR-TR-86-0312 AFOSR-81-0003

UNCLASSIFIED F/G 3/1 NL

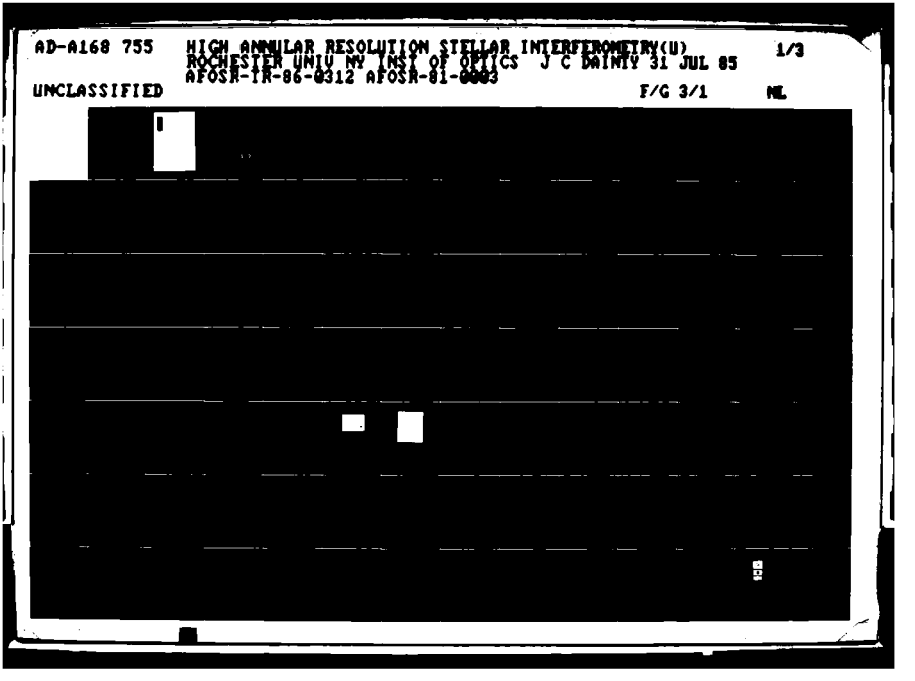

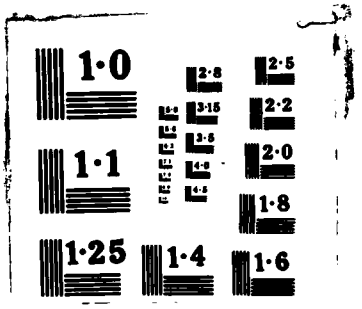
1·0
1·1
1·25
1·4
2·5
2·2
2·0
1·8
1·6

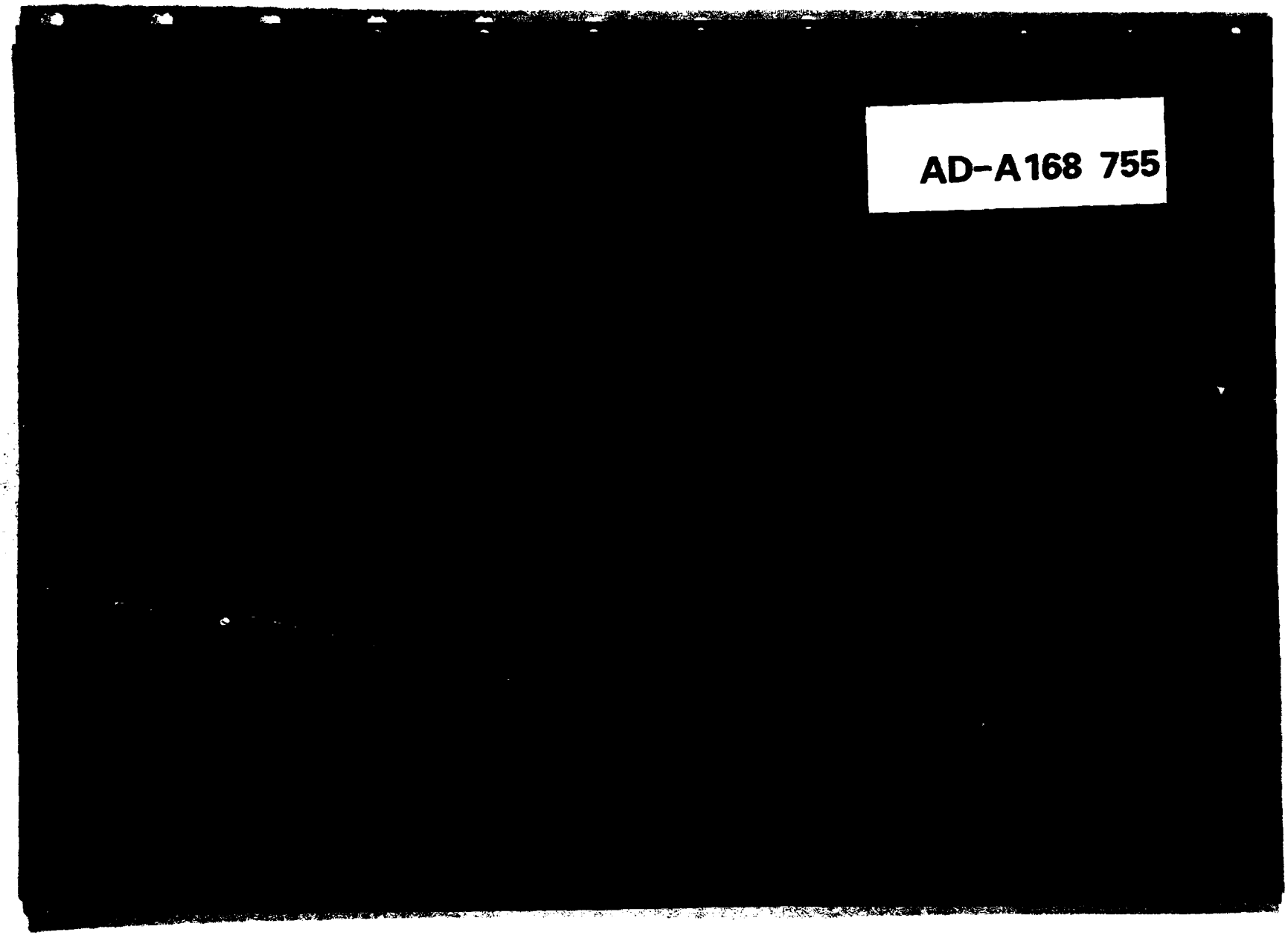

(2)

SECURITY CLASSIFICATION OF THIS PAGE

AD-A168755

REPORT DOCUMENTATION PAGE

1a. REPORT SECURITY CLASSIFICATION: UNCLASSIFIED	1b. RESTRICTIVE MARKINGS
2a. SECURITY CLASSIFICATION AUTHORITY	3. DISTRIBUTION/AVAILABILITY OF REPORT: UNCLASSIFIED/UNLIMITED Approved for public release; distribution unlimited.
2b. DECLASSIFICATION/DOWNGRADING SCHEDULE	
4. PERFORMING ORGANIZATION REPORT NUMBER(S): FINAL REPORT	5. MONITORING ORGANIZATION REPORT NUMBER(S)
6a. NAME OF PERFORMING ORGANIZATION: UNIVERSITY OF ROCHESTER; 6b. OFFICE SYMBOL (If applicable)	7a. NAME OF MONITORING ORGANIZATION
6c. ADDRESS (City, State and ZIP Code): Rochester, NY 14627	7b. ADDRESS (City, State and ZIP Code)
8a. NAME OF FUNDING/SPONSORING ORGANIZATION: AFOSR; 8b. OFFICE SYMBOL (If applicable)	9. PROCUREMENT INSTRUMENT IDENTIFICATION NUMBER: AFOSR-81-0003
8c. ADDRESS (City, State and ZIP Code): Bolling AFB, DC 20332	10. SOURCE OF FUNDING NOS. — PROGRAM ELEMENT NO.: 61102F; PROJECT NO.: 2311; TASK NO.: A1; WORK UNIT NO.
11. TITLE (Include Security Classification): High Angular Resolution Stellar Interferometry	
12. PERSONAL AUTHOR(S): J C DAINTY	
13a. TYPE OF REPORT: FINAL; 13b. TIME COVERED: FROM 12/80 TO 11/84; 14. DATE OF REPORT (Yr., Mo., Day): 31st July 1985; 15. PAGE COUNT	
16. SUPPLEMENTARY NOTATION	
17. COSATI CODES — FIELD / GROUP / SUB. GR.	18. SUBJECT TERMS (Continue on reverse if necessary and identify by block number): Interferometry, Speckle, Astronomy, Phase Problem

19. ABSTRACT (Continue on reverse if necessary and identify by block number)

This report summarises the research carried out under the headings: Atmospheric turbulence, space-time structure of images, speckled speckle, detection of gratings behind diffusers, the phase problem, infra-red speckle interferometry and phase conjugation. Twenty papers resulted from this research program.

20. DISTRIBUTION/AVAILABILITY OF ABSTRACT: UNCLASSIFIED/UNLIMITED ☒ SAME AS RPT. ☐ DTIC USERS ☐	21. ABSTRACT SECURITY CLASSIFICATION: UNCLASSIFIED
22a. NAME OF RESPONSIBLE INDIVIDUAL: Dr H Radoski	22b. TELEPHONE NUMBER (Include Area Code): (202) 767-4906; 22c. OFFICE SYMBOL: NP

DD FORM 1473, 83 APR — EDITION OF 1 JAN 73 IS OBSOLETE.

SECURITY CLASSIFICATION OF THIS PAGE

INTRODUCTION

This report summarises the research carried out during the period 1 December 1980 to 30 November 1984 on Grant AFOSR-81-0003 entitled 'High Angular Resolution Stellar Interferometry'. The AFOSR program manager was H Radoski and the Principal Investigator was J C Dainty. The research was carried out at The Institute of Optics, The University of Rochester, Rochester NY 14627.

CONTENTS

1. SUMMARY OF ACCOMPLISHMENTS

Copies of the 20 papers are provided in the Appendix. In this report we therefore give only a brief outline of the important results that were obtained in each of the topics investigated.

1.1 Atmospheric Turbulence (Refs 3 and 4)

What exposure time Δt should be used in stellar speckle interferometry? The question of the optimum time (for maximum signal-to-noise ratio) when in the photon-limited regime was investigated by O'Donnell and Dainty [J Opt Soc Am, 70, 1354 (1980)], who showed that a good rule of thumb is $\Delta t \simeq 2\tau_c$, where τ_c is the 1/e coherence time of the stellar image. Measurements of the temporal and spatio-temporal correlation were made at Mauna Kea, Hawaii over 10 nights in June/July 1980 [3], showing an average correlation time of 15 ms which implies a speckle exposure time of 30 ms.

Measurements were also made of the wavelength dependence of the variance of stellar scintillation [4] which was shown to follow Tatarski's prediction of $\sigma^2_I/\langle I\rangle^2 \propto \lambda^{-7/6}$.

In unpublished work, J Dugan [Ms Thesis] constructed an anamorphic shearing interferometer for measuring the long-exposure MTF of the atmosphere. This was a prototype instrument which demonstrated the feasibility of constructing a portable interferometer for site testing. Even today, astronomers use the naive 'star trail' method for site testing which is almost totally irrelevant for characterising sites for large optical telescopes.

1.2 Space-Time Structure of Images (Refs 2, 3 and 6)

If one observes the speckle pattern image of an unresolved star, the time evolution would be qualitatively described as a 'boiling' of the image. The spatial structure of a speckle pattern at a given instant of time is quantitatively described by the spatial correlation function $C_1(\Delta\underline{x})$. The temporal structure at a given space-point is described by the temporal correlation $C_2(\Delta t)$. The spatio-temporal structure is described by space-time correlation function $C_3(\Delta\underline{x},\Delta t)$ and we measured this function for stellar speckle images [Dainty et al, J Opt Soc Am, 71, 490-492 (1981) and ref 3].

If the space-time correlation is separable,

$$C_3(\Delta\underline{x},\Delta t) = C_1(\Delta\underline{x})\, C_2(\Delta t),$$

then the spatial structure and time evolution are uncorrelated and under these conditions one would describe the overall time evolution as 'boiling'. We showed experimentally [3] and theoretically [2], that $C_3(\Delta\underline{x},\Delta t)$ is not normally separable in stellar speckle images and therefore there is a coupling between the spatial and temporal structure of the image. This is due physically to the directionality of the turbulence in the telescope pupil due to wind.

It should be possible to make use of the space-time coupling of the image intensity to increase the performance of systems that attempt to image through turbulence. For example, at the moment, speckle interferometry uses data from consecutive frames independently and fails to make use of the fact that photons arriving at the end of one

frame are correlated with those arriving at the start of the following one.

Reference 6 points out the bias obtained on the shape of the normalised spatial correlation function of dynamic speckle under the influence of time integration. The counter-intuitive result is that the speckle size increases slightly with increasing time integration.

1.3 Speckled Speckle (Refs 5 and 14)

'Speckled speckle' arises when a speckle pattern is scattered by a finite rough surface or propagates through a random medium of finite extent. An example is light that has propagated through the atmosphere (i.e. a speckle pattern) and is scattered by an object with a rough surface.

O'Donnell [5] showed that the probability density function of speckled speckle is a K-distribution of order equal to the number of speckles illuminating the second scatterer. In the limiting case of the second scattering area being small compared to the illuminating speckle size, the variance of the intensity equals three times the mean value, whereas for ordinary speckle the variance equals the mean. Newman [14] experimentally confirmed this.

1.4 Detection of Gratings Behind Diffusers (Refs 8 and 10)

This has no direct relevance to stellar imaging but was a spin-off resulting from asking the question: what phase objects can be 'seen' behind strong phase diffusers?

Let the correlation length of the wave that has passed through a phase diffuser be L and the period of a phase grating be b. Then if $L/b \leq .35$, it is impossible to detect the presence of the grating behind the diffuser from simple observation of the intensity in the near- or far-field.

However, the presence (and period) of the grating can be detected by making correlation measurements, either temporal or spatio-temporal depending upon the circumstances. This was first suggested by Baltes et al and experimentally demonstrated in Refs 8 and 10. This has particular application to secure coding of information which can only be detected by special correlation techniques.

1.5 The Phase Problem (Refs 1,7,12,17,19,20 and 21)

1.5.1 Cross-spectrum Method

Given the power spectrum, $\langle F(u)\, F^*(u)\rangle$, and the cross-spectrum, $\langle F(u)\, F^*(u + \Delta)\rangle$ where Δ is a small frequency increment, Knox and Thompson showed that it is possible to recover the object function f(x) uniquely. This is done by finding phase differences in the frequency domain and bootstrapping the phase from the origin outwards. The cross-spectrum method is of course important in astronomy because $\langle F(u)\, F^*(u + \Delta)\rangle$ can be measured using speckle data.

In Ref 1, we showed that it is possible to recover the object function by a zero location technique. The main significance of this result, as Brames discussed in his thesis, is that it proved the uniqueness of the cross-spectrum method. Computationally it would be more straightforward to use the original Knox-Thompson bootstrapping method.

1.5.2 Uniqueness of Modulus-Only Data

(a) Eisenstein's Criterion

In one dimension it is well-known that f(x) cannot be recovered uniquely from $|F(u)|^2$, at least in general. In two dimensions, the number of possible object functions is greatly reduced, and it is frequently stated that f(x,y) is recoverable uniquely from $|F(u,v)|^2$, 'almost always'. Suppose, however, that we wish to guarantee that there is a unique solution. For what class of objects

f(x,y) is uniqueness guaranteed?

The uniqueness of the solution is dependent on the factorisability, or reducability, of the z-transform of the object:

$$F(z_1, z_2) = \sum f_{ij} \, z_1^{\,i} \, z_2^{\,j} \quad ,$$

where z_1 and z_2 are complex spatial frequencies and f_{ij} represents sampled values of the object. If the polynomial $F(z_1, z_2)$ is non-factorisable (or irreducible), then there is a unique solution to the phase problem (i.e. given $|F|^2$, there is a unique f).

Irreducibility of F is guaranteed for certain objects f whose support satisfies Eisenstein's criterion [7,17]. This criterion requires that the object has non-zero points in two particular locations. One of these points is similar to, but not the same as, the reference point in holography. Details are given in Ref 7.

In his thesis and [21], Brames greatly extends the class of irreducible objects. The following is an approximate rule-of-thumb. Enclose the object support by the closest-fitting polygon: if the polygon does not have any two sides parallel, any object with that support has a unique solution to the phase problem.

Testing for Uniqueness

Given either the object or autocorrelation values it is possible to test for factorisability, and hence uniqueness, using a simple algebraic procedure [12]. This procedure uses the following fact: if

the polynomial whose coefficients are reduced modulo p, where p is any prime, is irreducible, then the original polynomial is irreducible. It is much easier to deal with polynomials whose coefficients are reduced modulo p is p is small, e.g. p = 2.

1.5.3 Recovering Solutions from Modulus-Only Data

Extending the above ideas, we see that solving the phase problem is 'simply' a matter of factorising polynomials in two complex variables. For discrete, noiseless data this is a straightforward task [19]. Unfortunately, the technique described in [19] cannot easily be extended to cases of real interest (e.g. noisy data) and the Fienup algorithm is probably still the best technique currently available. Non-linear least squares optimisation only proved useful up to 5 x 5 objects [20].

1.6 Infra-red Speckle Interferometry (Ref 16)

An extensive observational program of infra-red speckle interferometry was carried during the period of this grant in collaboration with Prof J L Pipher (Rochester) and Dr S T Ridgeway (Kitt Peak). The bipolar nebular HD44179, the Red Rectangle, was spatially resolved for the first time [16] and observations on OH26.5, NML Cyg and IRC+10420 are also being prepared for publication.

1.7 Phase Conjugation (Refs 13,15 and 18)

Whilst this subject is not connected with stellar speckle interferometry, it is highly relevant to imaging through turbulent media because of the possibility of the correction for random distortion. Nieto-Vesperinas' work on this relates to Fabry-Perot interferometers with one phase-conjugate mirror [13,15] and to the phase conjugation of evanescent waves [18].

1.8 Bibliography on Stellar Interferometry

During the period of this grant a bibliography on stellar interferometry was maintained and the latest version is attached at the end of the Appendix.

2. LIST OF PUBLICATIONS

1. B J Brames and J C Dainty, 'Method for determining object intensity distributions in stellar speckle interferometry', J Opt Soc Am, 71, 1542-1545 (1981).

2. K A O'Donnell, 'Correlations of time-varying speckle near the focal plane', J Opt Soc Am, 72, 191-197 (1982).

3. K A O'Donnell, B J Brames and J C Dainty, 'Measurements of the spatio-temporal statistics of stellar speckle patterns at Maura Kea, Hawaii', Opt Commun, 41, 79-82 (1982).

4. J C Dainty, B M Levine, B J Brames and K A O'Donnell, 'Measurements of the wavelength dependence and other properties of stellar scintillation at Mauna Kea, Hawaii', Appl Opt, 21, 1196-1200 (1982).

5. K A O'Donnell, 'Speckle statistics of doubly scattered light', J Opt Soc Am, 72, 1459-1463 (1982).

6. T Gonsiorowski and J C Dainty, 'Correlation properties of light produced by quasi-thermal sources', J Opt Soc Am, 73, 234-237 (1983).

7. M A Fiddy, B J Brames and J C Dainty, 'Enforcing irreducibility for phase retrieval in two dimensions', Opt Lett, 8, 96-98 (1983).

8. J C Dainty and D Newman, 'Detection of gratings hidden by diffusers using photon correlation techniques', Opt Lett 8, 608-610 (1983).

9. J C Dainty, 'Stellar speckle interferometry', in Laser Speckle and Related Phenomena, Ed J C Dainty (Springer Verlag 1984) 2nd Edition, 255-320.

10. D Newman and J C Dainty, 'Detection of gratings hidden by diffusers using intensity interferometry', J Opt Soc Am A, 1, 403-411 (1984).

11. T Gonsiorowski, 'Variable threshold discrimination in a photon-limited imaging detector', Appl Opt, 23, 1060-1065 (1984).

12. M Nieto-Vesperinas and J C Dainty, 'Testing for uniqueness of phase recovery in two dimensions', Opt Commun, 52, 94-98 (1984).

13. M Nieto-Vesperinas, 'Regenerative amplifiers with one phase-conjugate mirror', Opt Lett, 9, 555-557 (1984).

14. D Newman, 'K distributions from doubly scattered light', J Opt Soc Am A, 2, 22-26 (1985).

15. M Nieto-Vesperinas, 'Fields generated by a Fabry-Perot interferometer with a phase-conjugate mirror', J Opt Soc Am A, 427-436 (1985).

16. J C Dainty, J L Pipher, M G Lacasse and S T Ridgeway, 'Spatially resolved infrared observations of the Red Rectangle', Astrophys J, 293, 530-536 (1985).

17. M Nieto-Vesperinas and J C Dainty, 'A note on Eisenstein's irreducibility criterion for two dimensions of sampled object', Opt Commun (1985).

18. M Nieto-Vesperinas and E Wolf, 'Phase conjugation and symmetries with wave field in free space containing evanescent components', J Opt Soc Am A, 2 (1985).

19. M Nieto-Vesperinas and J C Dainty, 'Phase recovery for two-dimensional digital objects in polynomial factorisation', submitted to J Opt Soc Am.

20. M Nieto-Vesperinas, 'A study on the performance of non-linear least square optimisation methods in the problem of phase-retrieval', submitted to Optica Acta.

21. B J Brames, in preparation for Optics Letters.

3. CONFERENCE PRESENTATIONS

1. OSA Annual Conference 1981, Orlando, FL: papers FJ1 ThN7 and ThH2.

2. OSA Annual Conference 1982, Tucson, AZ: papers TuR2, WG1 (Invited) and ThM8.

3. Topical Meeting on Signal Recovery, Lake Tahoe, NV: paper ThA11.

4. OSA Annual Conference 1983, New Orleans, LA: paper WV3.

5. Workshop on Image Reconstruction, Oracle, AZ: miscellaneous informal contributions.

6. ECOOSA '84, Amsterdam, Netherlands:

7. OSA Annual Conference 1984, San Diego, CA: papers FL3 and FL5

4. THESES

1. K A O'Donnell, 'Time-Varying Speckle Phenomena in Astronomical Imaging and in Laser Scattering', PhD Thesis, University of Rochester, 1983.

2. B J Brames, 'Uniqueness and Other Aspects of the Optical Phase Problem', PhD Thesis, University of Rochester, 1985.

3. J Dugan, 'Shearing Interferometer for the Measurement of the Atmospheric MTF', MS Thesis, Rochester 1982.

5. PERSONNEL SUPPORTED

J C Dainty (Principal Investigator) 1981-1984

M Nieto-Vesperinas (Post-Doc) 1983-1984

B J Brames (PhD student) 1981-1984

D Newman (PhD student) 1983-1984

K A O'Donnell (PhD student) 1981-1984

J Dugan (MS student) 1982

M Daum (UG assistant) 1981

6. APPENDIX

This appendix contains copies of the 20 publications produced under this research contract. They are numbered as in the List of Publications and presented in chronological order.

1542 J. Opt. Soc. Am./Vol. 71, No. 12/December 1981 JOSA Letters

Method for determining object intensity distributions in stellar speckle interferometry

B. J. Brames and J. C. Dainty

The Institute of Optics, The University of Rochester, Rochester, New York 14627

Received July 2, 1981

We describe a method for finding the intensity distribution of an object from a measurement, or measurements, of its cross-power spectrum. This technique, like the Knox–Thompson algorithm, makes use of the phase information contained in the cross spectrum; it is based on a systematic procedure for locating the complex zeros representing the spectrum of an object.

1. INTRODUCTION

Techniques such as Michelson, intensity, and speckle interferometry usually yield the power spectrum[1] of an object, that is, the modulus of the Fourier transform of some intensity distribution. It is well known[2] that if the phase of the Fourier transform is missing, then there is, in general, no unique solution for the object intensity. Constraints such as object positivity typically do not remove the inherent ambiguity,[3] although it appears that in two spatial dimensions the degree of ambiguity is less than in one.[4–6] (The analysis presented in this Letter will be restricted to the one-dimensional case.)

Additional information about the object is usually available in high-resolution stellar interferometry. In this Letter we use the further information provided by the cross-power spectrum.[7] In 1974 Knox and Thompson[7,8] pointed out that, in speckle interferometry, essentially independent estimates of the object power spectrum $|\mathcal{O}(u)|^2 = \mathcal{O}(u)\mathcal{O}^*(u)$ and its cross-power spectrum $|\mathcal{O}(u)\mathcal{O}^*(u+\Delta)|$ could be obtained for a single small value of $\Delta \leq r_0/\lambda f$, where r_0 is Fried's correlation parameter for atmospheric turbulence,[9] λ is the wavelength, f is the focal length of the telescope, and $\mathcal{O}(u)$ is the Fourier transform of the object intensity $o(x)$. They used this additional information in a boot-strapping algorithm to compute an estimate of the phase of the Fourier transform; the mean square error of this estimate increases linearly with spatial frequency. This procedure has also been successfully implemented by Nisenson *et al.*,[10] whereas other algorithms that combine the information contained in the power spectrum with one or more estimates of the cross-power spectrum have been investigated by Sherman,[11] Frost *et al.*,[12] and Aitken and DeSaulniers.[13] We consider yet another way of using the information in the cross-power spectrum, based on the properties of its complex zeros.

The importance of the zeros of entire functions in interferometry has been discussed by Bates[14] and was recently emphasized by Ross *et al.*[15–17] In Section 2 we summarize some elementary properties of complex polynomials that represent the Fourier transform and power spectrum of an object. In this section we assume that the object can be adequately represented by a set of delta functions, which may be restrictive but is certainly intuitively reasonable.

The proposed method for solving the phase problem (i.e., identifying the correct complex zeros) is described in Section 3, and a computational example is given. As in any technique of phase retrieval, noise plays a crucial role, as is illustrated.

2. ZEROS OF THE OBJECT TRANSFORM AND POWER SPECTRUM

We shall restrict our discussion to objects whose intensity distribution $o(x)$ is a function of only one variable, thus including separable two-dimensional distributions of the form $o(x_1, x_2) = f(x_1)g(x_2)$. Any such distribution that one encounters is square integrable and exists only within a finite region. As a consequence, its Fourier transform $\mathcal{O}(u)$ can be extended into the complex plane as an entire function of $z = u + iv$. It is well known that $\mathcal{O}(z)$ can be uniquely represented by its complex zeros $z_1, \ldots$, in the form of a Hadamard product[18]

$$\mathcal{O}(z) = Ae^{Bz} \prod_{n=1}^{\infty} \left(1 - \frac{z}{z_n}\right) \exp\left(\frac{z}{z_n}\right), \tag{1}$$

where A and B are constants. However, if a discrete transform is taken of the object, only a finite number of zeros, determined by the sampling interval δ, represents object information. It is somewhat more convenient to examine these zeros in the complex w plane, defined by[5]

$$w = re^{i\theta} = \exp(-2\pi i z\delta). \tag{2}$$

We shall define the support of $o(x)$ to be $2a$ and sample at $N+1$ points such that $\delta = 2a/N$. Then, when Eq. (2) is applied, the Fourier integral, Eq. (1), becomes, [illegible] from a factor of $w^{-aN/\delta}$ a polynomial of [illegible] degree N:

$$\mathcal{O}(z) = \int_{-a}^{a} o(x)\exp(-2\pi i z x)\,dx, \tag{3}$$

$$\mathcal{O}(w) = w^{-aN/\delta} \sum_{n=0}^{N} o(n\delta)w^{n} = w^{-aN/\delta} \prod_{n=1}^{N} (w - w_n), \tag{4}$$

$$= w^{-aN/\delta} \sum_{n=0}^{N} a_n w^n = w^{-aN/\delta} \prod_{n=1}^{N} (w - w_n). \tag{5}$$

The w_n [illegible] apart from

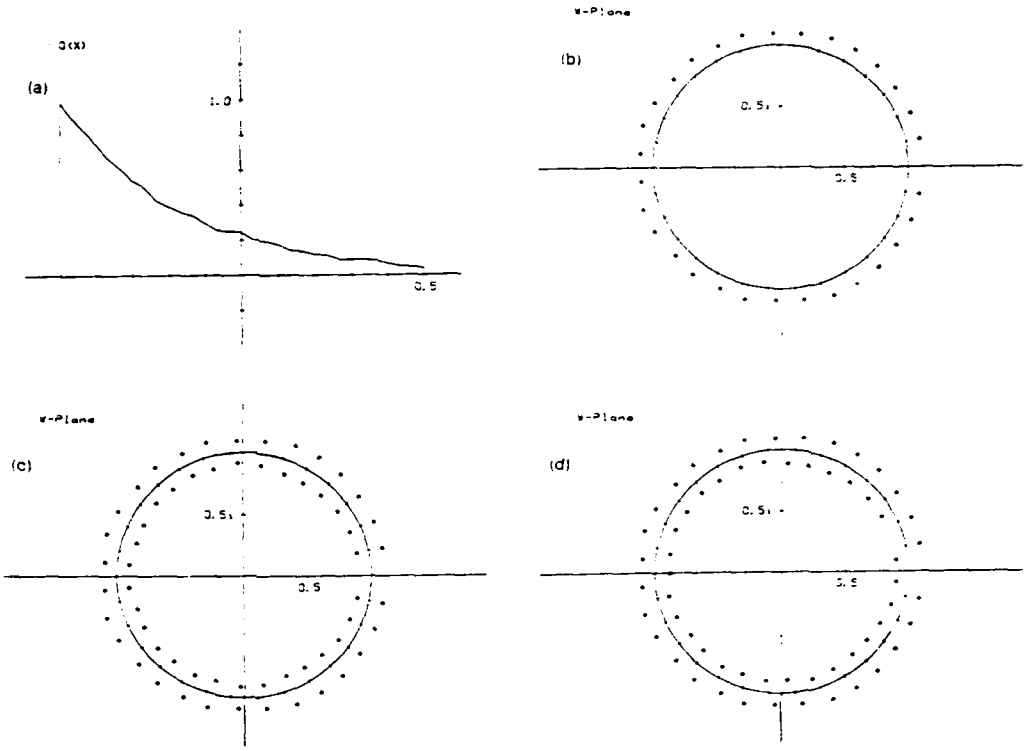

Fig. 1. (a) A simple exponential object with 1% random noise added. (b) Thirty zeros of $O(w)O^*(w^*)$ in the complex w plane that represent the object in (a). (c) The zeros of the power spectrum of (a). Because of the loss of phase information we cannot choose between $|w_i|$ and $|1/w_i|$ for each zero pair. (d) The zeros of the cross spectrum of (a) with $\Delta = 1.5$. The divisions on the unit circle are in increments of Δ. The correct zeros remain unchanged from those in (b), whereas those inside the unit circle are rotated counterclockwise by $\Delta = 1.5$.

a constant factor C, the zeros of the polynomial completely specify $O(w)$ and hence $o(x)$.

If $o(x)$ takes on the particularly simple form of a constant within the interval $2a$, the zeros of $O(w)$ will all lie on the unit circle $|w| = 1$ at base angles $\theta_n = 2\pi n/N$ ($n = \pm 1, \pm 2, \ldots, \pm N/2$). More-complex objects are represented by displacing zeros from these base positions, each w_n affecting a higher spatial frequency as $|n|$ increases.[6] There are only $N/2$ degrees of freedom, however, since the real and positive constraints on $o(x)$, respectively, force the zeros to occur in complex conjugate pairs in the range $0 < |\theta| \leq \pi$. Figure 1(b) shows the zeros associated with a negative exponential object, to which 1% Gaussian random noise was added [see Fig. 1(a)]. This particular object was chosen because all 30 of the zeros are outside the unit circle, near their base angles. This makes the figures that follow somewhat clearer but is not typical of zero distributions, which generally also have zeros within the unit circle.

In a similar manner, we can represent the power spectrum $\Phi(u)$ as an analytic function $\Phi(w) = O(w)O^*(w^*)$. On applying Eqs. (2) and (3) to Eq. (4), we see that the conjugate function $\Phi^*(u) = \Phi(u^*)$ of $\Phi(u)$ becomes

$$\Phi(w) = O(w)O(1/w)$$
$$= C^2\left[\prod_{n=1}^{N}\frac{(-w_n)}{w}\right]\prod_{n=1}^{N}(w - w_n)(w - 1/w_n). \quad (5)$$

The angular distribution of the zeros of $\Phi(w)$ *is identical with* that of $O(w)$ [Fig. 1(c)]. However, without some basis for choosing between $|w_i|$ and $|1/w_i|$ we could construct $2^{N/2}$ equally plausible sets of N zeros, each of which represents a real, possibly positive object.

3. RECOVERING THE PHASE INFORMATION

Let us examine the way the phase information present in the cross-power spectrum $\Phi(u, \Delta) = O(u)O^*(u + \Delta)$ is encoded by its zeros. Extending $\Phi(u, \Delta)$ into the complex w plane by using Eqs. (2) and (3) yields

$$\Phi(w, \Delta) = O(w)O\left(\frac{\exp 2\pi i\Delta}{w}\right)$$
$$= K\prod_{n=1}^{N}(w - w_n)\left(w - \frac{\exp 2\pi i\Delta}{w_n}\right). \quad (6)$$

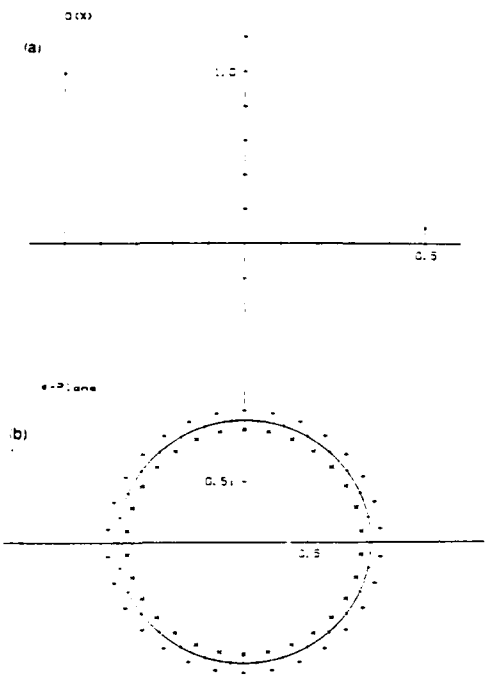

Fig. 2. (a) A simple object $o(x) = \delta(x - 0.5) + 0.5\delta(x - 0.5)$. (b) The zeros of the cross spectrum of (a) for $\Delta = 1$. The inner zeros have been rotated clockwise by one period so that they appear identical with those of the object's power spectrum. Requiring that each zero have a rotated inverse permits only two real solutions for $o(x)$, either those inside (×) the unit circle or those outside (+).

where K is a complex constant.

One complete set of zeros $\{\alpha_n\}$ remains unchanged; however, the other set $\{1/\alpha_n\}$ has been rotated through a known angle of

$$\theta = -2\pi\delta\Delta. \tag{7}$$

In most cases, knowledge of Δ is sufficient to identify the two sets $\{\alpha_n\}$ and $\{1/\alpha_n\}$; thus, in principle, the phase of $O(\omega)$ can be recovered from a single calculation of $\Phi(\omega, \Delta)$ for $0 < \Delta < 1.2\delta$. However, if a subset of the zeros $\{\alpha_n\}$ is invariant under a rotation θ, then there will be more than one possible choice of $\{\alpha_n\}$ and $\{e^{i\theta}\alpha_n\}$ consistent with $\Phi(\omega, \Delta)$ for $\Delta = -\theta/2\pi\delta$. Whereas the number of possible solutions is strongly constrained by Δ and hence is not so formidable an obstacle as with the power spectrum, the problem can be resolved in any case by a different choice of Δ.

In Fig. 2 we have an object that has all its associated zeros outside the unit circle at $\alpha_n = 1.05 \exp(i\pi 2n - 1)/N$, and one cannot obtain a unique phase solution from the cross spectrum for integer values of Δ. Although the positions of the zeros $\{\alpha_n, 1/\alpha_n\}$ are identical with those of the power spectrum, there are only two possible solutions, either those inside the unit [illegible]

In practice it is often the case that the power spectrum can be measured more accurately than the cross spectrum. By using a procedure similar to that suggested by Bates and Napier,[9] it is possible to make use of the more accurate data. We first determine an approximately correct set of zeros $\{\alpha_n\}_\Delta$ from the cross spectrum and then associate them with the more accurate (but ambiguous) zeros of the power spectrum to obtain the new set. The extent to which this will prove successful depends heavily on the noise characteristics of the two measurements, as we can see in Figs. 3–5. Figure 3(a) shows the zeros of a noisy cross spectrum ($\Delta = -1.5$), from which we can find the correct zeros and reconstruct the negative exponential object with $\simeq 2.5\%$ noise. Figure 4 compares the same zeros (×) with those of the less noisy power spectrum (+) in Fig. 1(c). In this case we see that all the correct zeros of the power spectrum can be identified, but using an even noisier set of zeros in Fig. 5 gives ambiguous, and even incorrect, results in several cases.

4. DISCUSSION

In stellar speckle interferometry, estimates of both the power spectrum and cross-power spectrum of the object are available. We have shown that, if the noise is low enough, a single estimate of the cross-power spectrum could be used to find

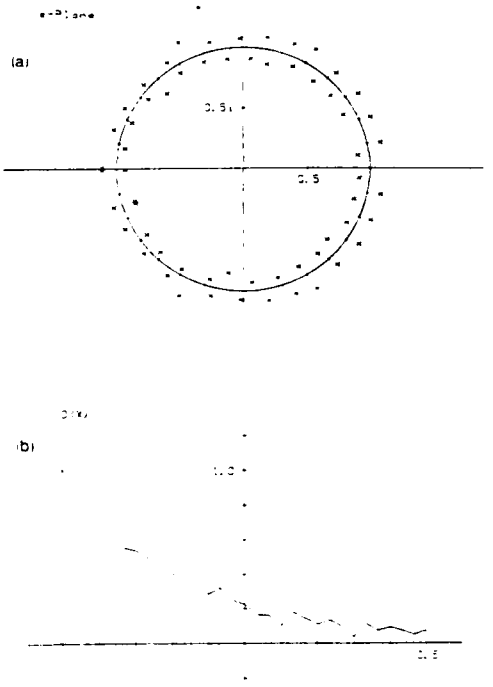

Fig. 3. (a) The zeros of a noisy cross spectrum. As in Fig. 2(b), the inner zeros have been rotated counterclockwise 1.5 units from the [illegible] (b) [illegible] noise restricted to the unrotated

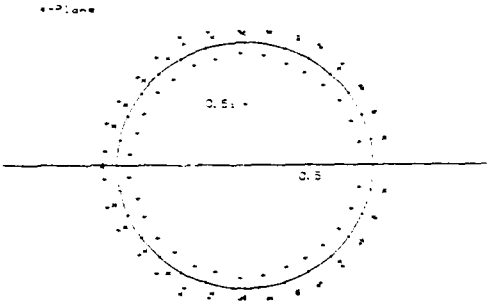

Fig. 4. An improved estimate of the object can be made by comparing the unrotated zeros of Fig. 3(a) (x) with the ambiguous ones of the more accurate power spectrum in Fig. 1(c) (+). In this case, all the correct zeros in the power spectrum can be identified.

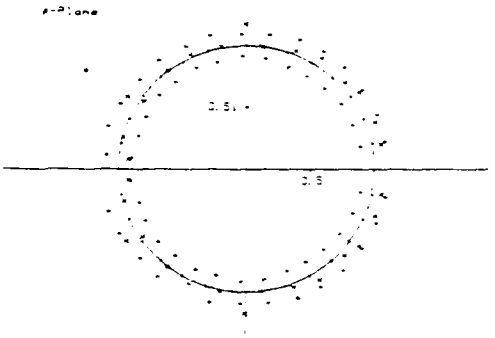

Fig. 5. Comparing the zeros obtained from a much noisier cross spectrum (x) with those of the power spectrum in Fig. 1(c) (+). We find three of the cross spectral zeros to near the unit circle that they are interlacing, whereas two others identify incorrect zeros within the unit circle.

the object spectrum and hence the object. In the presence of more noise, a comparison of the zeros of the power spectrum with those of the cross-power spectrum can allow a more reliable estimate of the object to be made. We do not know whether this technique will produce better reconstructions than the algorithms of Knox and Thompson[7,8] or Sherman.[11] Zero-finding algorithms tend to be laborious, and whereas the method can be extended to the two-dimensional case, the curves (rather than points) of the zeros complicate the situation enormously. Nevertheless, as in the work of Bates[14] and Ross *et al.*,[15–17] the zero-based representation provides insight into the phase problem. Noise perturbs zero locations, and when the noise becomes sufficiently large that we cannot reliably find the zeros corresponding to the object from those of the power spectrum and cross-power spectrum, then a real loss of phase information has taken place. Under these conditions the results of any method of phase reconstruction using the power and cross spectrum must be treated cautiously.

Noise plays such an important role in the phase problem that it would seem useful to study the complex zeros of stochastic processes. The statistics of real-zero crossings have been studied extensively, but, to our knowledge, those of the complex zeros have not.

ACKNOWLEDGMENTS

This research was supported by the U.S. Air Force Office of Scientific Research under grant no. AFOSR 81-0003.

REFERENCES

1. The terms power spectrum and cross-power spectrum are used here to denote the quantities $|O(u)|^2$ and $O(u_2)O^*(u_2)$, where $O(u)$ is the Fourier transform of the object intensity; this terminology is usually reserved for statistical averages in the theory of random processes, but no such averages occur in the present discussion.
2. H. A. Ferwerda, *Inverse Source Problems in Optics*, Vol. 9, H. P. Baltes, ed. (Springer-Verlag, Berlin, 1978), pp. 13–38.
3. J. C. Dainty, M. A. Fiddy, and A. H. Greenaway, "On the danger of applying statistical reconstruction methods in the case of missing phase information," in *Image Formation from Coherence Functions in Astronomy*, C. van Schooneveld, ed. (Reidel, Amsterdam, Holland, 1979), pp. 95–101.
4. J. R. Fienup, "Reconstruction of an object from the modulus of its Fourier transform," Opt. Lett. 3, 27–29 (1978).
5. Yu. M. Bruck and L. G. Sodin, "On the ambiguity of the image reconstruction problem," Opt. Commun. 30, 304–308 (1979).
6. A. M. J. Huiser and P. van Toorn, "Ambiguity of the phase reconstruction problem," Opt. Lett. 5, 499–501 (1980).
7. K. T. Knox and B. J. Thompson, "Recovery of images from atmospherically degraded short-exposure photographs," Astrophys. J. Lett. 193, L45–L48 (1974).
8. K. T. Knox, "Image retrieval from astronomical speckle patterns," J. Opt. Soc. Am. 66, 1236–1239 (1974).
9. D. L. Fried, "Optical resolution through a randomly inhomogeneous medium for very long and very short exposures," J. Opt. Soc. Am. 56, 1372–1350 (1966).
10. P. Nisenson, R. V. Stachnik, C. Papaliolios, and P. Horowitz, "Data recording and processing for speckle image reconstruction," Proc. Soc. Photo-Opt. Instrum. Eng. 243, 88–94 (1980).
11. J. W. Sherman, "Speckle imaging using the principal value decomposition method," Proc. Soc. Photo-Opt. Instrum. Eng. 149, 92–99 (1978).
12. R. L. Frost, C. K. Rushforth, and B. S. Baxter, "Fast FFT-based algorithm for phase estimation in speckle imaging," Appl. Opt. 18, 2056–2061 (1979).
13. G. J. M. Aitken and D. L. DeSaulniers, "Restoration of atmospherically degraded images using complex spectral ratios," Opt. Commun. 28, 26–29 (1979).
14. R. H. T. Bates, "Contributions to the theory of intensity interferometry," Mon. Not. R. Astron. Soc. 142, 413–425 (1969).
15. R. E. Burge, M. A. Fiddy, A. H. Greenaway, and G. Ross, "The phase problem," Proc. R. Soc. London Ser. A 350, 191–212 (1976).
16. G. Ross, M. A. Fiddy, M. Nieto-Vesperinas, and M. W. L. Wheeler, "The phase problem in scattering phenomena: the zeros of entire functions and their significance," Proc. R. Soc. London Ser. A 360, 25–45 (1978).
17. M. A. Fiddy and G. Ross, "Analytic fourier optics: the encoding of information by complex zeros," Opt. Acta 26, 1129–1146 (1979).
18. R. P. Boas, *Entire Functions* (Academic, New York, 1954).
19. R. H. T. Bates and P. J. Napier, "Identification and removal of phase errors in interferometry," Mon. Not. R. Astron. Soc. 158, 405–424 (1972).

Correlations of time-varying speckle near the focal plane

K. A. O'Donnell

The Institute of Optics, University of Rochester, Rochester, New York 14627

Received July 7, 1981

The properties of speckle produced near the focal plane of a lens with a linearly translating diffuser in the pupil are investigated. Expressions for the space–time amplitude and intensity correlations are derived in the Gaussian-field limit. The intensity correlations obtained are not cross-spectrally pure but rather imply some degree of speckle translation in directions both parallel and antiparallel to the diffuser velocity. Lens aberrations are found to have a significant effect on the intensity correlations, and theoretical results are presented for defocus and some of the primary aberrations. Experimental measurements with a two-detector instrument and photon-correlation equipment are found to be in good agreement with the theory.

INTRODUCTION

Laser scattering from moving diffusers has been a subject of considerable interest in recent years. It is well known that when a converging spherical wave is scattered from a linearly translating diffuser, there are two effects that are observed in the diffraction field. First, in diffraction planes that are distant from the focal plane of the wave, the effect more noticeable to the eye is a general linear translation of the speckles before each speckle loses its identity. As the observing plane approaches the focus, the linear speckle motion becomes less apparent, as each speckle decorrelates after traversing a shorter distance. In the focal plane, the speckle field changes its form continuously without an apparent direction of motion. This second effect is commonly called boiling speckle.

The properties of the time-varying speckle field have led to a number of suggestions for measuring the velocity of the diffuser to a high degree of accuracy.[1–5] It has been less widely appreciated that the speckles in the boiling region possess more subtle properties that permit other information about the scattering system to be obtained.

The present paper investigates the properties of the speckle field near the focal plane. It is found that the space–time intensity correlation near the focus is strongly dependent on the shape of the wave front incident upon the diffuser and that it may be useful in measuring aberrations to a high precision. Even in the focal plane, the intensity correlations are shown to imply simultaneous translation of speckles in opposing directions. The results of experiments that support the theory are presented.

THEORY

We consider the experiment shown in Fig. 1. Monochromatic plane waves from a laser are incident upon a lens with a translating diffuser effectively in the pupil plane. In this situation, speckle boiling is observed in the focal plane of the lens, whereas varying degrees of translation are observed elsewhere. If the lens were perfect, one would expect that the contribution of a scattering center of the diffuser to the amplitude in the focus of the lens would be constant, without any dephasing as the diffuser translates across the diameter of the pupil. However, in the focus of an aberrated lens, the amplitude from a scattering center would appear to change phase during its transit across the pupil. This phase variation is due entirely to the deterministic aberration of the lens. Thus it is apparent that the behavior of the focal-plane speckle may provide some insight into the phase properties of the lens pupil.

If the diffuser motion is nearly transverse to the optical axis, Doppler effects will be negligible; this permits the use of complex amplitude in the analysis rather than the analytic signal representation of the optical field. Consider the case when the complex amplitude in the focal plane $A(x, y, t)$ is due to a large number of independent scattering centers of the diffuser. When the random complex amplitude immediately after transmission through the diffuser $a(\xi, \eta)$ has a uniformly probable phase on the interval $(-\pi, \pi)$, and a few other nonrestrictive conditions are satisfied, it has been shown that $A(x, y, t)$ degenerates to a complex circular Gaussian process as a consequence of the central-limit theorem.[6] The statistics of such a process are uniquely defined by the space–time amplitude correlation

$$\langle A^*(x, y, t)\, A(x - \Delta x, y - \Delta y, t + \tau)\rangle, \tag{1}$$

where $\langle\ \rangle$ denotes the ensemble average. We then seek to express this correlation in terms of the parameters of the scattering system.

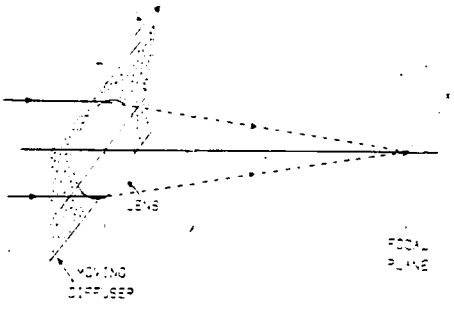

Fig. 1. Experiment under consideration.

The analysis will be restricted to linear diffuser motion, with the velocity vector along the $-\xi$ axis for convenience. Hence if $a(\xi, \eta)$ denotes the amplitude immediately after the diffuser at time $t = 0$, then at time t the amplitude will be denoted by $a(\xi - vt, \eta)$ where v is the diffuser speed. The focal-plane amplitude may now be found from the usual diffraction integral for propagating $a(\xi - vt, \eta)$ from pupil space to the focal plane[7]; that is,

$$A(x, y, t) = \frac{\exp(ikf)}{i\lambda f} \exp\left[\frac{ik}{2f}(x^2 + y^2)\right] \times \iint_{-\infty}^{\infty} a(\xi' - vt, \eta') P(\xi', \eta') \exp\left[\frac{-ik}{f}(x\xi' + y\eta')\right] d\xi' d\eta'. \quad (2)$$

where λ is the wavelength and k is the wave number of the light, $P(\xi', \eta')$ is the complex pupil function of the lens, and f is the focal length of the lens. Forming the product $A^*(x, y, t)\, A(x + \Delta x, y + \Delta y, t + \tau)$ and averaging over the ensemble results in

$$\langle A^*(x, y, t) A(x + \Delta x, y + \Delta y, t + \tau)\rangle = \frac{\exp(i\kappa)}{\lambda^2 f^2} \iiiint_{-\infty}^{\infty} \langle a^*(\xi' - vt, \eta') a[\xi'' - v(t + \tau), \eta'']\rangle P^*(\xi', \eta') P(\xi'', \eta'') \times \exp\left\{\frac{-ik}{f}[x(\xi'' - \xi') + y(\eta'' - \eta') + \Delta x\xi'' + \Delta y\eta']\right\} \times d\xi' d\eta' d\xi'' d\eta''. \quad (3)$$

where

$$\kappa = \frac{k}{2f}(\Delta x^2 + \Delta y^2 + 2x\Delta x + 2y\Delta y). \quad (4)$$

If the diffuser is uniform it is reasonable to assume that $a(\xi, \eta)$ is a statistically stationary process. Its correlation function then depends only on coordinate differences, so that

$$\langle a^*(\xi' - vt, \eta') a(\xi'' - v(t + \tau), \eta'')\rangle \equiv C_a(\xi'' - \xi' + v\tau, \eta'' - \eta'). \quad (5)$$

If Eq. (5) is inserted into Eq. (3), and the sum and difference coordinates

$$\xi_0 = \xi'' - \xi', \quad \eta_0 = \eta'' - \eta', \quad \xi = (\xi' + \xi'')/2, \quad \eta = (\eta' + \eta'')/2 \quad (6)$$

are introduced into the resulting integral, a small amount of algebra then yields

$$\langle A^*(x, y, t) A(x + \Delta x, y + \Delta y, t + \tau)\rangle = \frac{\exp(i\kappa)}{\lambda^2 f^2} \iint_{-\infty}^{\infty} C_a(\xi_0 - v\tau, \eta_0) \Psi(\xi_0, \eta_0)\, d\xi_0 d\eta_0 \quad (7)$$

where

$$\Psi(\xi_0, \eta_0) = \exp\left\{\frac{-ik}{f}[(x - \Delta x/2)\xi_0 + (y - \Delta y/2)\eta_0]\right\} \times \iint_{-\infty}^{\infty} P^*(\xi - \xi_0/2, \eta - \eta_0/2) P(\xi + \xi_0/2, \eta + \eta_0/2) \times \exp\left\{\frac{-ik}{f}(\Delta x\xi + \Delta y\eta)\right\} d\xi d\eta. \quad (8)$$

Thus $\Psi(\xi_0, \eta_0)$ depends only on the properties of the lens, whereas Eq. (7) takes account of the diffuser properties through an autocorrelation type of integral.

To proceed further, it is necessary to make an assumption about the form of the correlation function of $a(\xi, \eta)$. A careful analysis would take into account the interaction of the incident wave with the diffuser structure to determine $C_a(\xi_0, \eta_0)$, but this is a formidable problem. However, a considerable simplification may be obtained in the limit of fine diffuser structure. This limit may be formally taken by replacing the correlation $C_a(\xi_0 - v\tau, \eta_0)$ by the Dirac delta function $\delta(\xi_0 - v\tau, \eta_0)$, with the result that

$$\langle A^*(x, y, t) A(x + \Delta x, y + \Delta y, t + \tau)\rangle = \frac{\exp(i\kappa)}{\lambda^2 f^2} \Psi(v\tau, 0) = \frac{\exp(i\kappa)}{\lambda^2 f^2} \exp\left\{\frac{-ik}{f}(x - \Delta x/2)v\tau\right\} \times \iint_{-\infty}^{\infty} P^*(\xi - v\tau/2, \eta) P(\xi + v\tau/2, \eta) \times \exp\left\{\frac{-ik}{f}(\Delta x\xi + \Delta y\eta)\right\} d\xi d\eta. \quad (9)$$

In this limit the amplitude correlation is thus proportional to the Fourier transform of a pair of displaced pupil functions. It should also be noted that if $C_a(\xi_0, \eta_0)$ were to have a finite width, the correlation of $A(x, y, t)$ would be a smoothed version of Eq. (9), as prescribed by the autocorrelation integral of Eq. (7).

Of more practical interest is the intensity correlation function since, unlike the amplitude correlation, the intensity correlation is directly measurable. The calculation of the correlation of the focal-plane intensity $I(x, y, t)$ is straightforward, since for a complex Gaussian process

$$\langle \Delta I(x, y, t) \Delta I(x + \Delta x, y + \Delta y, t + \tau)\rangle = |\langle A^*(x, y, t) A(x + \Delta x, y + \Delta y, t + \tau)\rangle|^2, \quad (10)$$

where ΔI denotes $I - \bar{I}$. It is also convenient to define the intensity correlation in the normalized form

$$\gamma(\Delta x, \Delta y, \tau) = \frac{\langle \Delta I(x, y, t) \Delta I(x + \Delta x, y + \Delta y, t + \tau)\rangle}{\bar{I}^2}. \quad (11)$$

The quantity $\bar{I}$ may be found from Eq. (9) with $\Delta x = \Delta y = \tau = 0$. The normalized intensity correlation is then found to be

$$\gamma(\Delta x, \Delta y, \tau) = \frac{1}{A^2}\left|\iint_{-\infty}^{\infty} P^*(\xi - v\tau/2, \eta) P(\xi + v\tau/2, \eta) \times \exp\left\{\frac{-ik}{f}(\Delta x\xi + \Delta y\eta)\right\} d\xi d\eta\right|^2, \quad (12)$$

where

$$A = \iint_{-\infty}^{\infty} |P(\xi, \eta)|^2 d\xi d\eta. \quad (13)$$

The result is stationary in both space and time variables; the spatial stationarity is a direct consequence of assuming $a(\xi, \eta)$ to be delta-function correlated. Equation (12) has been obtained elsewhere in different forms.[8,9] It can also be seen that the temporal correlation with $\Delta x = \Delta y = 0$ is the square of the modulation-transfer function of the lens; this has been noted by Yamaguchi *et al.*[10]

In order to include aberrations explicitly, the substitution

$$P(\xi, \eta) = P(\xi, \eta) \exp[ikW(\xi, \eta)] \quad (14)$$

may be made, where $P(\xi, \eta)$ is a purely real pupil function and $W(\xi, \eta)$ describes the aberrations of the pupil. This results in

$$\Lambda(\Delta x, \Delta y, \tau) = \frac{1}{A^2} \left| \iint_{-\infty}^{\infty} P(\xi - v\tau/2, \eta)\, P(\xi + v\tau/2, \eta) \times \exp\{ik[W(\xi - v\tau/2, \eta) - W(\xi + v\tau/2, \eta)]\} \times \exp\left[\frac{-ik}{f}(\Delta x \xi + \Delta y \eta)\right] d\xi d\eta \right|^2. \quad (15)$$

Expanding both aberration functions in the exponential into a Taylor series yields

$$\Lambda(\Delta x, \Delta y, \tau) = \frac{1}{A^2} \left| \iint_{-\infty}^{\infty} P(\xi - v\tau/2, \eta)\, P(\xi + v\tau/2, \eta) \times \exp[ikT(\xi, \eta)] \times \exp\left[\frac{-ik}{f}(\Delta x \xi + \Delta y \eta)\right] d\xi d\eta \right|^2, \quad (16)$$

where

$$T(\xi, \eta) = 2 \sum_{r=0}^{\infty} (v\tau/2)^{2r+1} \left(\frac{\partial}{\partial \xi}\right)^{2r+1} W(\xi, \eta). \quad (17)$$

This is a useful representation, since for defocus and most of the primary aberrations, only the term proportional to $\partial W/\partial \xi$ survives in the series of $T(\xi, \eta)$. It is also interesting to note that $\partial W/\partial \xi$ is proportional to the transverse-ray aberration of geometrical optics, although for other aberrations the higher-order terms become significant.

DISCUSSION

Much of the time-varying speckle work that has been done has pertained to the scattering of Gaussian laser beams from diffusers. In this case the pupil function is Gaussian, and, assuming that it is also purely real,

$$P(\xi, \eta) = \exp[-(\xi^2 + \eta^2)/2\sigma^2], \quad (18)$$

where σ^2 is the variance of the Gaussian beam. Direct substitution shows that

$$P^*(\xi - v\tau/2, \eta)\, P(\xi + v\tau/2, \eta) = \exp(-\xi^2/\sigma^2) \exp(-\eta^2/\sigma^2) \exp[-(v\tau)^2/4\sigma^2]. \quad (19)$$

Since this product of pupil functions factorizes, it immediately follows from Eq. (12) that the space-time intensity correlation factorizes in the sense that

$$\Lambda(\Delta x, \Delta y, \tau) = f_1(\Delta x) f_2(\Delta y) f_3(\tau), \quad (20)$$

where the f_i are functions. This factorization occurs only in the focal plane and does not occur elsewhere.[9]

The factorized correlation of Eq. (20) describes complete speckle boiling with no speckle translation. (Some degree of speckle translation, in the Δx direction, for example, would require a correlation that is a mixed function of Δx and τ.) A correlation that factorizes is commonly referred to as cross-spectrally pure, since an analogous property of correlations in coherence theory is known as the cross-spectral-purity condition.[11,12]

For hard pupils, there is no full factorization in the focal plane as there is for the Gaussian pupil. A particularly simple example is the square pupil described by

$$P(\xi, \eta) = \mathrm{rect}(\xi/a)\,\mathrm{rect}(\eta/a), \quad (21)$$

where $\mathrm{rect}(x)$ is the rectangle function of width 1. One may show from geometry that

$$P(\xi - v\tau/2, \eta) P(\xi + v\tau/2, \eta) = \mathrm{rect}\left(\frac{\xi}{a - |v\tau|}\right) \mathrm{rect}(\eta/a) \text{ for } |v\tau| < a = 0 \text{ for } |v\tau| \geq a. \quad (22)$$

It is also possible to include defocus in the calculation with the aberration function

$$W(\xi, \eta) = \frac{4m\lambda}{a^2}(\xi^2 + \eta^2); \quad (23)$$

where m is the number of wavelengths of defocus at the margin of the pupil. When this is substituted in the series in Eq. (17), only the lowest-order term survives. At this point, straightforward integration of Eq. (16) results in

$$\Lambda(\Delta x, \Delta y, \tau) = \frac{\sin^2\left[\pi\left(1 - \frac{|v\tau|}{a}\right)\left(\frac{8mv\tau}{a} - \frac{a\Delta x}{\lambda f}\right)\right]}{\left[\pi\left(\frac{8mv\tau}{a} - \frac{a\Delta x}{\lambda f}\right)\right]^2} \times \frac{\sin^2\left(\pi \frac{a\Delta y}{\lambda f}\right)}{\left(\pi \frac{a\Delta y}{\lambda f}\right)^2} \quad \text{for } |v\tau| < a,$$

$$\Lambda(\Delta x, \Delta y, \tau) = 0 \quad \text{for } |v\tau| \geq a. \quad (24)$$

Thus even in the focal plane ($m = 0$), there is no factorization of the τ and Δx dependence of $\Lambda(\Delta x, \Delta y, \tau)$. Figure 2 shows a plot of Λ versus τ for $\Delta y = 0$ and several values of Δx. It can be seen that when $\Delta x = (\lambda f/a)$ (the first zero of the spatial intensity correlation), there are correlation peaks placed symmetrically on both sides of the τ axis. A possible interpretation of this is that the speckle translates to some degree in directions both parallel and antiparallel to the direction of diffuser motion. This interpretation of the shifted peaks should be taken somewhat lightly, as for $\Delta x > (\lambda f/a)$ three or more peaks exist in the τ correlation, although these effects become rather weak.

No shifted peaks exist in the temporal correlation for arbitrary Δy when $\Delta x = 0$. This is because the Δy dependence factorizes in Eq. (24); as a result the value of Δy affects only

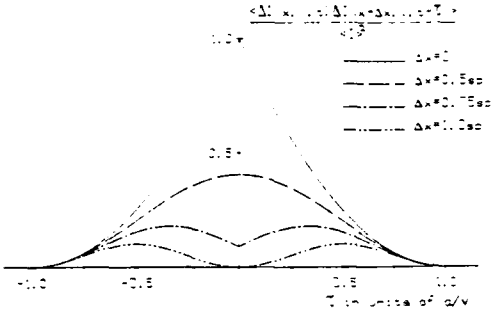

Fig. 2. Space–time intensity correlations in the focal plane of a lens with a square pupil. The curves shown are for $\Delta x = 0, 0.5, 0.75, 1.0$ speckle radii. A speckle radius (ρ) is defined as the position of the first zero of the spatial intensity correlation, which in this case is $\lambda f/a$, where f is the focal length and a is the width of the lens.

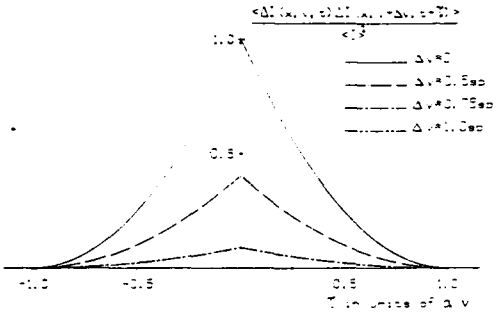

Fig. 3. Space–time intensity correlations in the focal plane of a lens with a square pupil. The curves are for $\Delta x = 0, 0.5, 0.75, 1.0$ speckle radii ($\lambda f/a$).

the strength of the temporal correlation and does not change its form, as is illustrated in Fig. 3. As an aside, it should be noted that the τ derivative of $\Lambda(\Delta x, \Delta y, \tau)$ is often discontinuous at $\tau = 0$. This is unphysical and is purely an artifact of taking the fine diffuser limit in passing from Eq. (9) to Eq. (11).

The space–time correlations are also strongly dependent on the defocus parameter m. The temporal correlations for several values of Δx are shown in Figs. 4 and 5 for $m = 0.025$ waves and $m = 0.09$ waves of defocus, respectively. In these figures the correlation for $\Delta x = 0$ changes only slightly, whereas the other curves become somewhat skewed. This implies that the speckle is beginning to have a preferred direction of translation, which is to be expected away from the focus. It is remarkable, however, that a defocus of $\lambda/40$ causes a noticeable skewness in the correlations.

For defocus greater than about $\lambda/3$, the temporal correlation with $\Delta x = \Delta y = 0$ becomes rather narrow since it is related to the modulation transfer function. The other temporal correlations with $\Delta x \neq 0$ also become narrow with only a single significant displaced peak. This corresponds to speckle translation at a single velocity.

EXPERIMENTS

A series of experiments was carried out in an attempt to measure the intensity correlations of a square pupil. The apparatus used is shown in Fig. 6. A translating ground glass was placed in the pupil of a well-corrected doublet of 365-mm focal length. The lens was mounted on a translator to provide a fine-focus adjustment. In order to obtain a large depth of focus, a 1.30-mm × 1.30-mm aperture stopped down the lens. This allowed the lens defocus to be controlled precisely, since a lens translation that was large enough to be measured accurately produced the small amounts of wave-front defocus that were desired.

A beam splitter after the lens allowed two photomultipliers to be placed in the observation plane. One detector was mounted on a precision translator, and a viewing telescope was used in the initial alignment of the detector apertures. The detector pinhole diameter was 25 μm, which was considerably smaller than the speckle radius ($\lambda f/a$) of 178 μm.

The photomultipliers were operated in the photon-counting mode, and the cross correlation of photon counts was measured with a 128-channel Langley–Ford photon correlator. It may be shown that the normalized cross correlation of photon counts is equivalent to that of the classical intensity.[10] The

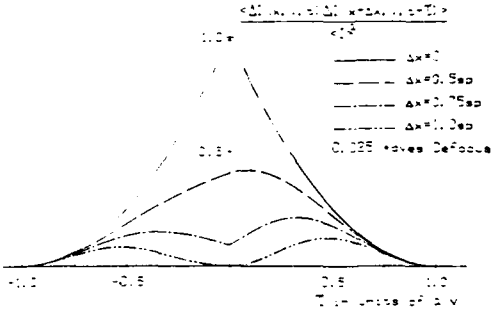

Fig. 4. Space–time intensity correlations of a lens with a square pupil and 0.025λ of defocus. The curves are for $\Delta x = 0, 0.5, 0.75, 1.0$ speckle radii ($\lambda f/a$).

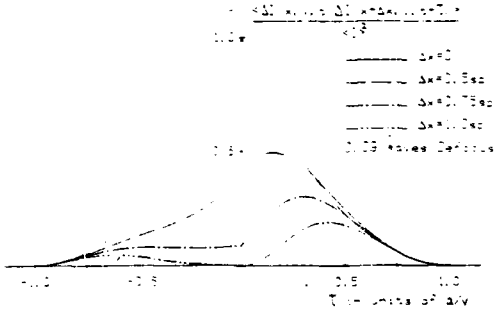

Fig. 5. Space–time intensity correlations of a lens with a square pupil [illegible]. The curves are for $\Delta x = 0, 0.5, 0.75, 1.0$ speckle radii.

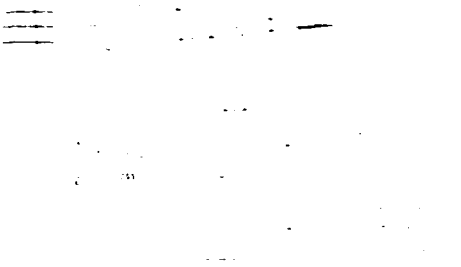

Fig. 6. Experimental apparatus used to measure the space-time correlations. Photomultiplier B was mounted on a translation stage that introduced a known Δx or Δy between the two detectors, and the temporal correlation of the two detector signals was then measured with the correlator.

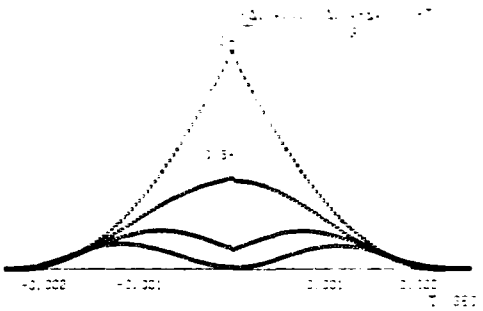

Fig. 7. Measured space–time intensity correlations in the focal plane of a lens with a square pupil. The data runs shown are for Δx = 0, 0.5, 0.75, 1.0 speckle radii (compare with Fig. 2).

photon correlator was interfaced with an HP-85 computer, which processed the data and corrected them for dark current, although this correction was small. Typical signal levels were 4×10^4 photons/sec (0.5 photon per sample time on the average), whereas the dark count rates were typically 10 and 150 photons/sec in the two detectors. Photon rates were sufficiently low so that dead-time effects were small and could be ignored.

Many experimental runs were made, and typical experimental data for the theoretical temporal correlations of Figs. 2–5 are shown in Figs. 7–10. The measurements are based on roughly 2000 statistically independent realizations of the speckle field; the resulting statistical error is 2–3%. Only odd-numbered channels of the correlator output are shown in the figures; otherwise the data points are drawn too closely to be resolved easily.

Some of the data have an apparent discontinuity at $\tau = 0$. This was because the photon correlator measured correlations only for positive τ. The negative-τ part of the correlation was obtained by merely reversing the [illegible] signals in a subsequent measurement. Sometimes the data did not [illegible]

[illegible] the origin because of [illegible] effects; this is most noticeable in Fig. [illegible].

The measured correlations agree well with the theory. Although the statistical error was small, the measurements were limited by deterministic errors in the measurement of Δx and Δy, which were known to within ± [illegible] μm because of

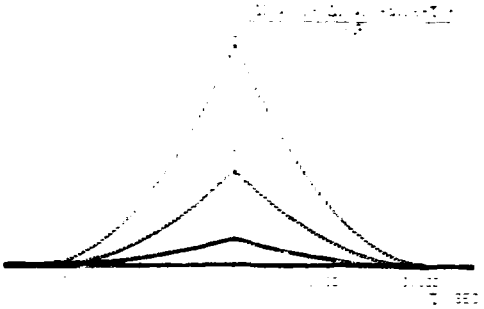

Fig. 8. Measured space–time intensity correlations in the focal plane of a lens with a square pupil. The data runs shown are for Δx = 0, 0.5, 0.75, 1.0 speckle radii (compare with Fig. 3).

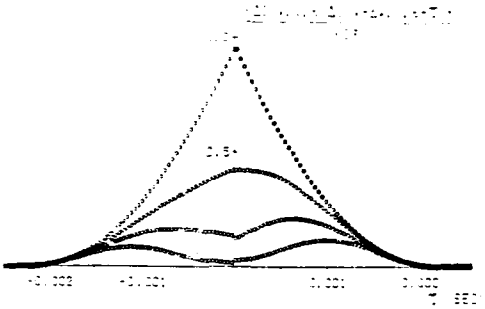

Fig. 9. Measured space–time intensity correlations of a lens with a square pupil and 0.025λ of defocus. The data runs shown are for Δx = 0, 0.5, 0.75, 1.0 speckle radii (compare with Fig. 4).

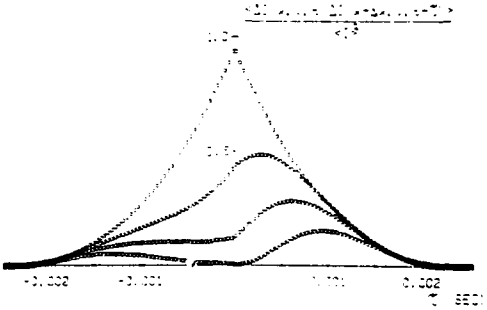

Fig. 10. Measured space–time intensity [illegible] a lens with a square pupil and [illegible] for Δx = [illegible] speckle radii (compare with [illegible]).

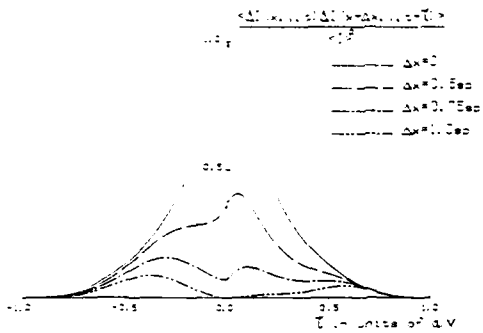

Fig. 11. Theoretical space–time intensity correlations of a lens with a circular pupil and 0.6λ of primary spherical aberrations balanced with −0.6λ of defocus. Shown are curves for $\Delta x = 0, 0.5, 0.75, 1.0$ speckle radii. A speckle radius is defined as $1.22\lambda/a$, the position of the first zero of the spatial intensity correlation.

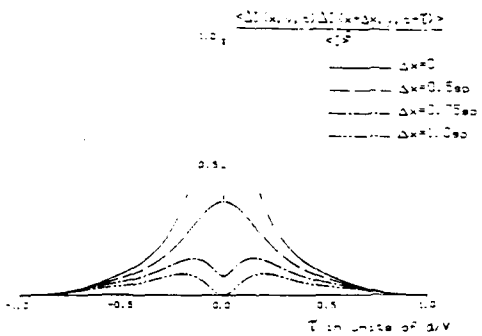

Fig. 12. Theoretical space–time intensity correlations of a lens with a circular pupil and 0.6λ of coma ($W \propto \xi(\xi^2+\eta^2)$, η proportional to $\xi(\xi^2+\eta^2)$). The curves shown are for $\Delta x = 0, 0.5, 0.75, 1.0$ speckle radii $1.22\lambda/a$.

translator and alignment errors. The correlations are, in general, within 0.1 of the theoretical values, with many measurements agreeing considerably better than this.

CIRCULAR PUPILS AND ABERRATIONS

The space–time intensity correlations of circular pupils and pupils with higher-order aberrations are difficult to evaluate. These cases are clearly of interest if the correlations are to be used to assess the state of correction of a lens. It is then necessary to resort to numerical techniques to evaluate $A(\Delta x, \Delta y, \tau)$ in these circumstances.

This integration has been carried out with computer-generated Gauss–Legendre quadrature. It has been found that the correlations for a circular aperture in the diffraction-limited or defocused cases are similar to results that have already been presented for the square aperture, so they will not be shown here. Pure spherical aberration causes the temporal correlations with $\Delta x = 0$ to become skewed, in a manner similar to those with defocus. Figure 11 shows 0.6λ of primary spherical aberration balanced with −0.6λ of defocus. The resulting wave front has a maximum deformation of −0.15λ. This corresponds to the 0.707-aperture zonal-ray focus, which is often considered to be the best focal plane.

Primary astigmatism in the pupil leads to effects identical with those with defocus if the diffuser motion is parallel to the tangential or sagittal planes. This is because $A(\Delta x, \Delta y, \tau)$ depends on $\partial W/\partial\xi$, which is itself independent of η in this case; the correlation is then affected only by the quadratic wave-front curvature in the ξ direction. Other orientations of the diffuser velocity, however, lead to other results. Finally, third-order coma in the pupil does not cause any skewness but rather attenuates the tails of the temporal correlations. This is illustrated in Fig. 12.

SUMMARY

We have seen that the space–time intensity correlations of speckle in the focal plane do not obey the cross-spectral purity condition in the cases of square and round pupils. True speckle boiling is not then observed, and instead there is speckle translation in directions parallel and antiparallel to the direction of diffuser motion. The space–time correlations are strongly dependent on aberrations and may provide a simple method of modulation-transfer-function measurement. The present work may possibly be generalized to include nonlinear diffuser motion and diffusers with a deterministic shape; these considerations would have applications to remote sensing.

It may also be worth noting that the experimental and theoretical results presented here have ties to atmospherically induced speckle patterns in astronomical imaging. The measured correlations of stellar speckle images exhibit displaced time correlation peaks similar to those of Fig. 2.[14] The observed stellar effects are presumably due to the linear translation of the inhomogeneous atmosphere (i.e., a diffuser) across the telescope pupil at the wind speed.

ACKNOWLEDGMENTS

The author gratefully acknowledges many helpful discussions with J. C. Dainty and the aid of B. J. Brames in connection with the numerical integration. This research was supported by U.S. Air Force Office of Scientific Research under grant no. AFOSR81-0093.

REFERENCES

1. G. Stavis, "Optical diffraction velocimeter," Instrum. Control Syst. 39, 99–102 (1966).
2. P. N. Pusey, "Photon correlation study of laser speckle produced by a moving rough surface," J. Phys. D 9, 1399–1409 (1976).
3. J. Ohtsubo and T. Asakura, "Velocity measurement of a diffuse object by using time-varying speckles," Opt. Quantum Electron. 8, 523–529 (1976).
4. A. F. Fercher, "Velocity measurement by first order statistics of time-differentiated laser speckle," Opt. Commun. 33, 129–135 (1980).
5. N. Takai, T. Iwai, and T. Asakura, "Real-time velocity measurement for a diffuse object using zero-crossings of laser speckle," J. Opt. Soc. Am. 70, 450–455 (1980).
6. J. W. Goodman, in *Laser Speckle and Related Phenomena*, J. C. Dainty, ed., Springer-Verlag, Berlin, 1975, p. 35.

7. See, for example, J. W. Goodman, *Introduction to Fourier Optics* (McGraw-Hill, New York, 1968), p. 55.
8. V. V. Anismov, S. M. Kozel, and G. R. Loshkin, "Space–time statistical properties of coherent radiation scattered by a moving diffuse reflector," Opt. Spectrosc. 27, 258–262 (1969).
9. E. Jakeman, "The effect of wavefront curvature on the coherence properties of laser light scattered by target centers in uniform motion," J. Phys. A 8, L23–L28 (1975).
10. I. Yamaguchi, S. Komatsu, and H. Saito, "Dynamics of speckles produced by a moving object and its applications," Jpn. J. Appl. Phys. 14, 301–306 (1975).
11. L. Mandel, "Concept of cross-spectral purity in coherence theory," J. Opt. Soc. Am. 51, 1342–1350 (1961).
12. The reader should not be confused that in coherence theory cross-spectral purity pertains to the factorization of amplitude correlations whereas the present work discusses the factorization of intensity correlations.
13. H. Z. Cummins and E. R. Pike, eds., *Photon Correlation and Light Beating Spectroscopy* (Plenum, London, 1974), p. 75.
14. J. C. Dainty, D. R. Hennings, and K. A. O'Donnell, "Space–time correlations of stellar speckle patterns," J. Opt. Soc. Am. 71, 490–492.

REF. 3

Volume 41, number 2 OPTICS COMMUNICATIONS 15 March 1982

MEASUREMENTS OF THE SPATIAL-TEMPORAL STATISTICS OF STELLAR SPECKLE PATTERNS AT MAUNA KEA, HAWAII

K.A. O'DONNELL, B.J. BRAMES and J.C. DAINTY
The Institute of Optics, The University of Rochester, Rochester, NY 14627, USA

Received 28 October 1981

The spatial-temporal intensity correlations of stellar speckle patterns have been measured over 10 nights (June 24–July 4, 1981) at Mauna Kea, Hawaii. The measurements indicate that the intensity correlation was cross-spectrally pure on most nights of observation. The correlation time of the image was typically 15 ms, while the intensity variance was within the range of 0.4–1.1.

1. Introduction

Because of the fluctuating atmosphere, the stellar image formed by a large earthbound telescope is a time-varying speckle pattern. While the size of the envelope of the stellar speckle image is much larger than the diffraction limit of the telescope, the speckles present within the envelope are comparable to the size of the Airy disc. This high frequency structure is the basis of the important technique of stellar speckle interferometry [1–3], a method of diffraction limited imaging.

In this paper we describe measurements of the temporal and spatial-temporal correlation properties of stellar speckle images over ten nights at Mauna Kea, Hawaii. These measurements are important in choosing the optimum exposure time of speckle interferometry [4–6], and are relevant to other techniques of diffraction limited imaging [6,7]. We define the normalized space-time intensity correlation of the speckle image as

$$C(\boldsymbol{x}_1, \boldsymbol{x}_2, \tau) = \frac{\langle \Delta I(\boldsymbol{x}_1, t)\, \Delta I(\boldsymbol{x}_2, t+\tau)\rangle}{\langle I(\boldsymbol{x}_1, t)\rangle \langle I(\boldsymbol{x}_2, t)\rangle}, \tag{1}$$

where $\boldsymbol{x}_1$ and $\boldsymbol{x}_2$ denote spatial points in the image, and

$$\Delta I(\boldsymbol{x}_1, t) = I(\boldsymbol{x}_1, t) - \langle I(\boldsymbol{x}_1, t)\rangle. \tag{2}$$

Eq. (1) implies stationarity in time but not in space, since the speckle image is not strictly spatially stationary. In our measurements $\boldsymbol{x}_2 - \boldsymbol{x}_1 \equiv \Delta\boldsymbol{x}$ is small compared to the image envelope. The intensity correlation is nearly stationary for such $\Delta\boldsymbol{x}$, so practically we may write the correlation as

$$C(\Delta\boldsymbol{x}, \tau) = \frac{\langle \Delta I(\boldsymbol{x}, t)\, \Delta I(\boldsymbol{x}+\Delta\boldsymbol{x}, t+\tau)\rangle}{\langle I(\boldsymbol{x}, t)\rangle^2}. \tag{3}$$

Measurements of the temporal intensity correlation ($\Delta\boldsymbol{x} = 0$) have been made by Scaddan and Walker [8] and by Parry et al. [9] at Herstmonceux, England; the time scale of the speckle "boiling" was found to be 2–7 ms. The space-time correlations have been measured by Dainty et al. [10] at Bristol Springs, New York. These and subsequent unpublished space–time measurements at the same site imply that the speckles tend to flow in two directions simultaneously; these directions are parallel and antiparallel to the direction of phase translation (wind) in the pupil. Studies of correlations of neighboring frames of motion picture film of the speckle image have been reported by Lohman and Weigelt [11].

The measurements of refs. [8–10] have been made at observing sites where atmospheric seeing is usually poor. To our knowledge the temporal and spatial–temporal intensity correlations have never been measured at a good site. An understanding of image properties at these locations is important, particularly since speckle interferometry is usually implemented at good sites [4]; prior to the present work [12] [illegible]

2. Experiment

The instrument used has been discussed in more detail elsewhere [10] and is shown in fig. 1. The equipment was mounted at the Cassegrain focus of the 61 cm telescope at Mauna Kea. Two photon-counting photomultipliers (an EMI 9862B and a Hammamatsu R928) were positioned to a known Δx within a magnified stellar image. A 128 channel Langley–Ford photon correlator measured the temporal cross correlation of photon counts from the two detectors. It may be shown that the normalized cross correlation of photon counts is equivalent to that of the classical intensity [12]. The space–time correlations were generated by repeating measurements sequentially for a series of values of Δx.

We observed the brightest unresolvable objects near zenith that were available (α-Bootis and α-Lyrae). The speckle images were more compact and had a longer time scale at Mauna Kea than at poor sites: this provided a larger number of detected photons per speckle in a correlation time of the image. As a result, measurements were made with less spatial, temporal, and optical bandwidth integration than previous work. Detector apertures of 70 μm were used, while the Airy disc diameter was 440 μm in the magnified image plane. Chromatic blurring was minimized by interference filters of mean wavelength 550 nm and bandwidth 8 n The integration time was 0.5 ms or 1 ms, depending the image time scale. The correlator was able to obt a low noise correlation (≲ 3% noise) with less than detected photon per sample time on average during 100 s experiment. Atmospheric seeing ranged from 6 arc s during the 10 nights of observation.

An HP-85 computer processed the data and store it on tape. The correlations were corrected for the d current of the detectors (less than 20 counts s^{-1} ty cally). Signal levels were sufficiently low (500–300 photons s^{-1}) so that deadtime effects were small ar could be ignored.

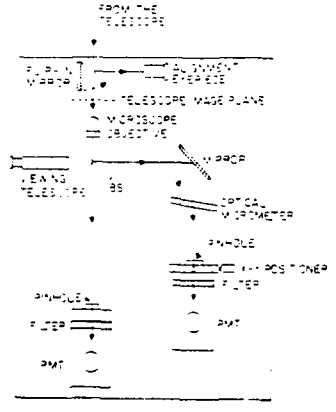

Fig. 1. Diagram of the two-channel instrument. The instrument was mounted at the Cassegrain focus.

3. Results

The measured correlations possess a short time sc component (10–70 ms) due to the speckle boiling a a much longer, nearly linear, component (~1 s) asso ciated with random motion of the speckle image env lope. Since the image motion correlation was rather variable from experiment to experiment, we have divided it out to obtain the correlation due to speckle boiling only. This procedure assumes that speckle boi ing and image motion are statistically independent, a is discussed in refs. [8] and [9].

A selected data series is shown in fig. 2. Each serie included separate measurements of the positive and negative τ part of the correlations for colinear displa

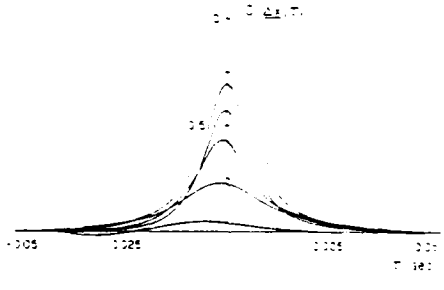

Fig. 2. Cross-spectrally pure image intensity correlations fro night 10 (July 3). The curves are, in order of decreasing intercept, for colinear displacements of $\Delta x = 0$, 0.25, 0.5, 0.75, and 1.0 speckle radii

ments of $\Delta x = 0, 0.25, 0.5, 0.75$ and 1.0 speckle radii [*], with such a measurement requiring roughly 20 min. It can be seen that the correlations weaken without changing their form as Δx increases. This was found to be true regardless of the direction of Δx. Fig. 2 is typical of what was found on 7 of the 10 nights of observation.

These results indicate that the space–time intensity correlation is cross-spectrally pure; that is, the correlation may be written as the product of a space-only part and a time-only part. It has been shown that this is valid if the telescope pupil contains a phase process that evolves or boils without any general linear translation of phase structure [13]. Indeed, visualization of the phase in the pupil by knife-edge testing the telescope mirror revealed that boiling of phase structure occurred predominantly. This is in contrast to previous measurements at Bristol Springs, where phase translation occurred consistently in the pupil and image correlations were decidedly cross-spectrally impure. On only one night (night 6) were cross-spectrally impure correlations observed consistently at Mauna Kea (fig. 3), though the observed effects were rather weak, with small displaced correlation peaks on the $\Delta x = 1.0$ speckle curve.

During nights 2 and 9 (and possibly on night 8),

[*] A speckle radius ("sp") is defined as the location of the first zero of the spatial correlation of intensity. In this case it is equal to $1.22 \lambda f/D$, where f is the focal length and D is the diameter of the telescope.

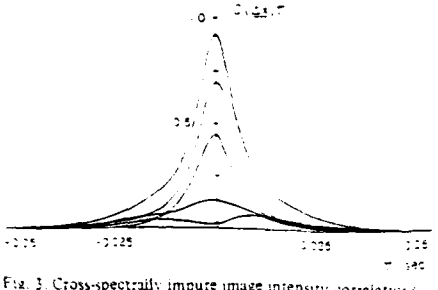

Fig. 3. Cross-spectrally impure image intensity correlations from night 6 (June 29). In order of decreasing y-intercept, the curves are for collinear displacements of $\Delta x = 0, 0.25, 0.75$, and 1.0 speckle radii.

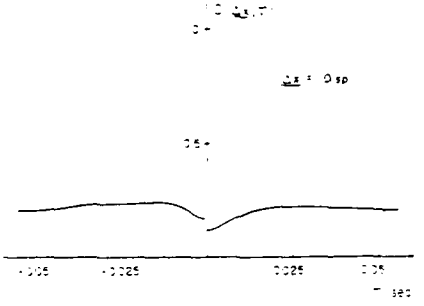

Fig. 4. Image intensity correlations with $\Delta x = 1.0$ speckle radii measured on night 9. The curves have not been corrected for image motion, and hence do not line up at the origin.

we observed an unusual effect. While the measured autocorrelations were not unusual, the correlation with $\Delta x = 1$ speckle had the unexpected shape shown in fig. 4. These correlations have not been corrected for image motion, and so possess the long linear tail. However, the boiling part of the correlation goes *below* the linear part of the correlation. When corrected for image motion as described, this leads to a negative intensity correlation, which cannot occur for a gaussian amplitude process. It is possible that the image was not behaving in a stationary manner during these nights. Also the assumption that image motion and speckle boiling are independent may not have been valid here.

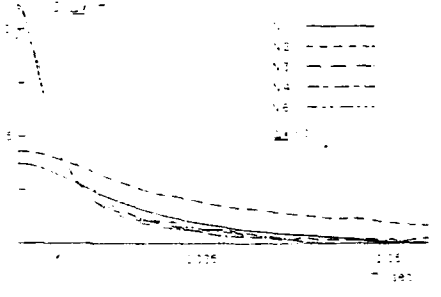

Fig. 2. Temporal image intensity autocorrelations taken during the first five nights of observations (N1–N5). No observations were made on night 5 due to 45 mph winds and freezing mist.

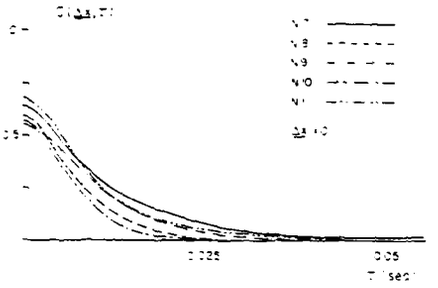

Fig. 6. Temporal image intensity autocorrelations measured on nights 7–11.

Figs. 5 and 6 show intensity autocorrelations ($\Delta x = 0$) for all nights when measurements were made. The average correlation time of the image was 15 ms, though during the second night it increased over two hours from 12 ms to 60 ms. The intensity variance $C(0, 0)$, however, varied considerably between 0.4 and 1.1, though values were reasonably consistent on any one night. If the speckle amplitude were gaussian, the intensity variance should be unity, though inclusion of spatial integration (the most significant effect) would reduce this to approximately 0.92. Gaussian image statistics occur when there are a large number of correlation cells of complex amplitude within the pupil and the wavefront phase has a variance much greater than 1. This may not have been valid for our relatively small telescope during good seeing conditions. We are certain, however, that the low variances were not due to our equipment, which had been checked out carefully on gaussian speckle in the laboratory.

4. Conclusions

In photon-limited speckle interferometry, the optimum exposure time is approximately equal to twice the correlation time of the image [4,6]. Our measurements over 10 nights at Mauna Kea, Hawaii show an average correlation time of 15 ms, implying an exposure time of 30 ms. The intensity variance, however, varied from 0.4 to 1.1. In contrast to measurements at a poor observing site (Bristol Springs, NY), the space–time intensity correlation was cross-spectrally pure on most nights of observation. It showed an anomalous effect which we are unable to explain on two of the nights.

Acknowledgements

We are grateful to the Director of Mauna Kea Observatory, Hawaii for providing observing time on the 61 cm telescope. This research was supported by the Air Force Office of Scientific Research under grant AFOSR 81-0003 and also in part by the Rome Air Development Center Post-Doc Program.

References

[1] A. Labeyrie, Astron. Astrophys. 6 (1970) 85.
[2] J.C. Dainty, in: Laser speckle and related phenomena, Topics in applied physics, Vol. 9 ed. J.C. Dainty (Springer-Verlag, New York, 1975) Chap. 7.
[3] A. Labeyrie, in: Progress in optics, Vol. 14, ed. E. Wolf (North-Holland, Amsterdam, 1976).
[4] J.G. Walker, Optimum exposure time and filter bandwidth in speckle interferometry, IAU Colloquium No. 50, High Angular Resolution Stellar Interferometry, Maryland, Aug.-Sept. 1978 (University of Sydney).
[5] J. Baier, J. Ebersberger, A. Lohman and G. Weigelt, Proc. SPIE, Vol. 264 (1980) 58.
[6] K.A. O'Donnell and J.C. Dainty, J. Opt. Soc. Am. 70 (1980) 1354.
[7] L. Mertz, Appl. Optics 18 (1979) 611.
[8] R.J. Scaddan and J.G. Walker, Appl. Optics 17 (1978) 3779.
[9] G. Parry, J.G. Walker and R.J. Scaddan, Optica Acta 26 (1979) 563.
[10] J.C. Dainty, D.R. Hennings and K.A. O'Donnell, J. Opt. Soc. Am. 71 (1981) 490.
[11] A.W. Lohman and G.P. Weigelt, Optik 53 (1979) 167.
[12] H.Z. Cummins and E.R. Pike, eds., Photon correlation and light beating spectroscopy (Plenum, London, 1974).
[13] E. Jakeman and P.N. Pusey, J. Phys. A8 (1975) 369.

Measurements of the wavelength dependence and other properties of stellar scintillation at Mauna Kea, Hawaii

J. C. Dainty, B. M. Levine, B. J. Brames, and K. A. O'Donnell

The variance of intensity of stellar scintillation has been measured as a function of wavelength using photon counting and on-line digital analysis techniques. The experimental data are consistent with that predicted by the theory of Tatarski. Measurements of the temporal correlation function of intensity and the higher moments of the probability density function of scintillation are also described. Time scales in the 1.7–10-msec range were observed, and the observed higher moments were consistently poorer than those predicted by a log normal distribution. All the measurements were made at Mauna Kea Observatory, Hawaii.

I. Introduction

A large number of measurements of the statistical properties of stellar scintillation have been reported in the literature (see Refs. 1 and 2). To our knowledge, however, no extensive measurements have been made at very high quality astronomical observing sites, and this motivated the experiments described in this paper which were made at Mauna Kea Observatory, Hawaii (altitude 4.2 km) during an eleven night period in June and July, 1981. The main experiment was the measurement of the wavelength variation of the relative variance σ_I^2/I^2; secondary experiments to measure the spatial and temporal properties and the higher moments of stellar scintillation are also described.

II. Equipment and Data Analysis

Observations were made using a 61-cm Boller and Chivens telescope equipped with the dual-channel photometer system shown in Fig. 1. The field lens, which lies in the normal telescope image plane, images the primary mirror onto the detector planes at a magnification of 0.027. The measurement apertures can be selected individually in each channel and adjusted to be superimposed or displaced from each other by a known amount. A typical aperture diameter is 0.73 mm at the detector plane, equivalent to 27 mm in the pupil plane. Interference filters can also be placed in each channel. The photomultipliers (EMI 9862B in channel *A*, Hammamatsu R928P in channel *B*) both have *S*-20 photocathodes and are operated in the photon counting mode.

The statistical properties of the photon counts are measured on-line using a Langley-Ford DC128 digital correlator which is interfaced to a Hewlett-Packard 85 desktop computer. In the experiments described below the correlator was used in either the autocorrelation mode or a dual histogram mode.

The autocorrelation mode yields a 128-channel estimate of the autocorrelation function $C_n(j\Delta t)$ of the photon counts n obtained in successive time intervals spaced Δt apart:

$$C_n(j\Delta t) = \frac{1}{N}\sum_{i=1}^{N} n_i n_{i+j}, \qquad j = 1, 2, \ldots, 128, \tag{1}$$

where N is the total number of samples (typically 10^5–10^6). It is well-known that the normalized correlation function of photon counts simply equals that of the classical measured intensity I (integrated by the measurement procedure) except at the origin:

$$\frac{C_n(j\Delta t)}{C_n(0)} = \frac{C_I(j\Delta t)}{C_I(0)}, \qquad j \neq 0. \tag{2}$$

Thus, in the autocorrelation mode this instrument gives an unbiased estimate of the autocorrelation function of intensity, even though average photon rates typically lie in the 0.5–10 range detected photons per sampling time Δt, depending on the variance of the intensity.

In the dual histogram mode, two 64-channel histograms of the photon counts n_i are measured simultaneously, enabling meaningful comparison experiments

The authors are with University of Rochester, Institute of Optics, Rochester, New York 14627.

Received 22 September 1981.
0003-6935/82/071106-05$01.00/0

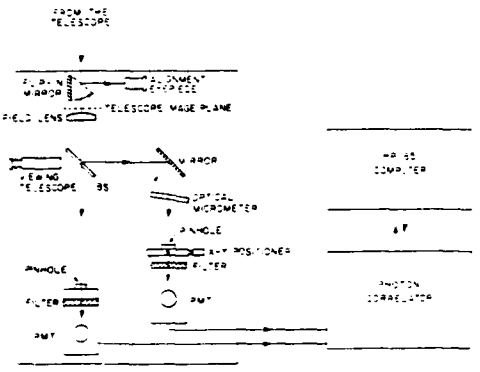

Fig. 1. Dual photometer system for measuring the statistical properties of stellar scintillation.

to be carried out on quasi-stationary processes such as stellar scintillation; this mode was used for the measurement of the wavelength dependence of the variance of scintillation. The probability density function of the measured classical intensity $p(I)$ is related to that of the photon counts $p(n)$ by an inverse Poisson transform.[17] The normalized factorial moments μ_k of the photon counts are simply equal to the normalized moments μ_k of the classical intensity:

$$\mu_k = \langle n(n-1)\cdots(n-k+1)\rangle / \langle n\rangle^k = \langle I^k\rangle / \langle I\rangle^k,$$

$$\mu_k = \mu_k \qquad (3)$$

Thus, the normalized factorial moments of the photon counts which can be calculated from the measured histogram $p(n)$ provide an unbiased estimate of the normalized moments of the intensity. The factorial moments have to be corrected for dark current and the dead time of the photon counting electronics, but for this correction was very small. Typical dark counts were 0.5 and 5 sec^{-1} in channels A and B, respectively, and the photon rates rarely exceeded 2×10^5 sec^{-1}, with a counter dead time of 50 nsec. The use of photon counting methods in the measurement of stellar scintillation is, of course, not new.[4,5,10]

The stars α-Lyrae (Vega) and α-Aquilae (Altair) were used for the observations. The flux from α-Lyrae incident on the earth's atmosphere is $\sim 8.5 \times 10^3$ photons cm^{-2} nm^{-1} sec^{-1} at 550 nm.[11] On the average we detected $\sim 1 \times 10^4$ photons sec^{-1} in channel A using a 5.72-cm^2 aperture area and a green filter [$\lambda = 555$, $\Delta\lambda$(FWHH) = 8 nm], yielding a collection efficiency of 2.5% in channel A and 2% in channel B (i.e., 4.5% overall collection efficiency). This figure includes losses due to atmospheric absorption, telescope optics, and the optical system of the dual photometer as well as the photocathode quantum efficiency, and it would be difficult to substantially increase it. It was not possible to reduce the amount of spatial and temporal integration without increasing the statistical error; for the weak scintillation observed, a photon flux of 5–10 per sample time was required to yield an error of 1–2%.

III. Wavelength Dependence of the Variance

Tatarski's theory[12] of wave propagation in a turbulent medium predicts that, in the absence of aperture averaging, the relative variance of the intensity of scintillation $\sigma_I^2 = \langle I^2\rangle/\langle I\rangle^2 = \mu_2 - 1$ is proportional to $\lambda^{-7/6}$, where λ is the wavelength. Early measurements by Mikeseil *et al.*,[13] Nettelblad,[14] and Protheroe[15] indicated that the relative variance was independent of wavelength, although these measurements involved a significant amount of aperture averaging. A study by Burke[16] using an analog detection scheme and 38-mm diam apertures showed a dependence on wavelength but not as strong as the $\lambda^{-7/6}$ dependence. On the other hand, experiments involving the propagation of laser beams over horizontal paths[17,18] with effectively no aperture averaging are in agreement with Tatarski's theory for unsaturated turbulence. We would not expect the case of vertical propagation to differ appreciably from Tatarski's theory, particularly in view of the fact that the predicted wavelength dependence of astronomical seeing has been confirmed over vertical paths.[19]

A. Theory

The general expression for the relative variance is,[20] ignoring any time integration,

$$\sigma_I^2 = \langle I^2\rangle/\langle I\rangle^2 - 1 = 2\pi \times 0.033\lambda^{-2}\int_0^\infty dh C_n^2(h) \times \int_0^\infty df f^{-8/3}\sin^2(\pi\lambda f^2 z)|T(f)|^2, \qquad (4)$$

where λ is the wavelength,
z is the altitude,
$C_n^2(h)$ is the structure constant of refractive-index fluctuations at altitude h,
f is the spatial frequency, and
$T(f)$ is the transfer function of the measured aperture.

It is clear from Eq. (4) that the relationship between the relative variance and wavelength is not straightforward, and depends in particular on the measurement aperture:[21,22] for a very small aperture [$T(f) = 1$], Eq. (4) reduces to

$$\sigma_I^2 \propto \lambda^{-7/6}, \qquad (5)$$

whereas for a very large aperture of diameter D,

$$\sigma_I^2 \propto \lambda^{-7/6} D^{-4/3}. \qquad (6)$$

The wavelength dependence of the variance for a measurement aperture that is neither very small nor very large depends in general on the variation of the structure constant C_n^2 with altitude h. We shall assume that a single thin layer at altitude h_1 contributes to most of the scintillation. In that case, Eq. (4) can be written for a circular measurement aperture of diameter D as

$$\sigma^2 \propto \lambda^{-7/6} \int_0^\infty x^{-8/3} \sin^2 x \left[\frac{2J_1(cx\sqrt{\lambda})}{cx\sqrt{\lambda}}\right]^2 dx, \quad (7)$$

where $c = D/\sqrt{\pi h_1}$, and $J_1(\cdot)$ is the first-order Bessel function of the first kind. [Unimportant constants of proportionality have been omitted from Eq. (7), and h_1 should be regarded as a constant.]

The right-hand side of Eq. (7) has been evaluated numerically; the results of this calculation are given in Fig. 2 which shows the dependence of the relative variance on wavelength for different diameters of the measurement aperture (expressed by the ratio $D/\sqrt{h_1}$).

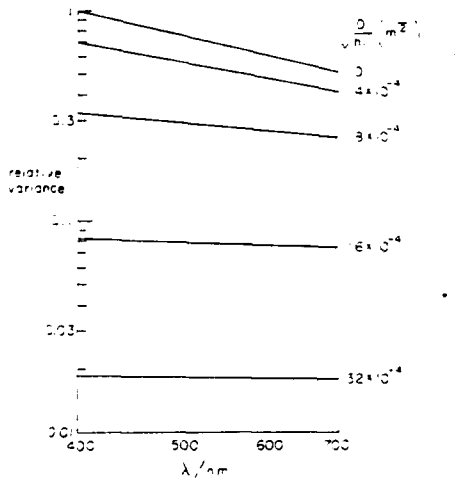

Fig. 2. Variation of the relative variance with wavelength for different diameters of measuring aperture as specified by the ratio $D/\sqrt{h_1}$, where h_1 is the height of the single layer. The variance has been arbitrarily normalized to unity at 550-nm wavelength and $D/\sqrt{h_1} = 0$. The $-7/6$ power law is obeyed for $D/\sqrt{h_1} = 0$, and there is no dependence on wavelength for $D/\sqrt{h_1} \to \infty$.

Thus, if the value of $D/\sqrt{h_1}$ is known or can be estimated from a secondary experiment, the predicted variation of relative variation with wavelength can be found from Fig. 2. Note that for no aperture integration (i.e., $D/\sqrt{h_1} = 0$) the $-7/6$ power law is obeyed; it can also be seen from Fig. 2 that for $0 < D/\sqrt{h_1} < \infty$, there is still an effective power law dependence over the visible spectrum $\sigma^2 \propto \lambda^{-p}$, with $7/6 > p > 0$.

B. Experimental Results

Simultaneous measurements of the probability distribution $p(n)$ of photon counts were made for pairs of wavelengths selected by using the following filters:

red (R) — $\bar{\lambda}$ = 639 nm, $\Delta\lambda$ (FWHH) = 21 nm.

green (G) — $\bar{\lambda}$ = 553 nm, $\Delta\lambda$ = 8 nm.

blue (B) — $\bar{\lambda}$ = 404 nm, $\Delta\lambda$ = 9 nm.

Since the photomultiplier in channel B had a tendency to record a slightly higher variance than the one in channel A (presumably because of nonuniform sensitivity of the photocathode), measurements were always repeated with the filters interchanged between channels A and B. A typical experimental sequence involved taking three pairs of simultaneous histograms for the following filters in channels A and B, respectively: $G/G, G/R, G/B, R/B, R/G, G/G, B/G, B/R$. (This sequencing requires only one filter change between each set of data.)

The sampling interval Δt was varied from night to night depending on the measured correlation time (see Sec. IV); typically, a value of 0.5 or 1 msec was used. A total measurement time of 50 or 100 sec was used, providing $\sim 2 \times 10^4$ statistically independent samples for each pair of histograms. It took about an hour to record and analyze all twenty-four pairs of histograms in a complete filter series. The second factorial moment was computed from each histogram, and hence the ratio of variances was found; the statistical error of the variance due to the finite number of samples and photon

Table I. Relative Variance of Intensity of Stellar Scintillation, Experiment and Theory

	EXPERIMENTAL DATA				APERTURE INTEGRATION			THEORY		
(1) Night	(2) $\frac{\sigma_A^2}{\sigma_B^2}$	(3) $\frac{\sigma_A^2}{\sigma_B^2}$	(4) $\frac{\sigma_A^2}{\sigma_B^2}$	(5) $\frac{\sigma_{AA}^2}{\sigma_B^2}$	(6) $\frac{\sigma_{AA}^2}{\sigma_B^2}$	(7) $\frac{D}{\sqrt{h_1}} \times 10^{-2}$ $\left(\frac{m^2}{m}\right)^{1/2}$	(8) $\frac{\sigma_A^2}{\sigma_B^2}$	(9) $\frac{\sigma_A^2}{\sigma_B^2}$	(10) $\frac{\sigma_A^2}{\sigma_B^2}$
1	1.16±.03	1.33±.02	1.47±.03	.37	.24	5.5	1.12	1.25	1.40
4	1.24±.02	1.35±.02	1.34±.03	.46	.32	5.2	1.11	1.22	1.35
7	1.26±.01	1.24±.04	1.43±.06	.99	.4	4.3	1.14	1.20	1.48
9	1.14±.03	1.27±.04	1.32±.06	.76	.56	3.6	1.15	1.34	1.34
10	1.22±.01	1.22±.03	1.39±.02	.75	.48	4.1	1.14	1.32	1.51

noise was ~1–2%. The absolute values of the normalized variance were 0.02–0.16, and the observations were made at zenith angles <40°.

The results for the most consistent five nights of observations are summarized in columns (2)–(4) of Table I. The values of the ratios of the variances predicted by the $-7/6$ power law are shown in brackets at the top of each column, and it is immediately clear that the measured ratios $\sigma^2_{i_1}/\sigma^2_{i_2}(\lambda_1 < \lambda_2)$ are significantly smaller than those predicted by this power law. In this sense, the results are consistent with those reported by others.[10–16] However, aperture integration also leads to smaller ratios; it should be stressed that spatial and temporal integration was unavoidable in this experiment.

The amount of aperture integration was estimated by measuring, in broadband light of mean effective wavelength 485 nm from a star near the zenith, the ratio of variances for apertures of diameter 27 and 5 mm and 44 and 5 mm, respectively. These ratios are tabulated in columns (5) and (6). We assume that the 5-mm aperture produces a negligible amount of aperture integration. The data in column (5), which employed the 27-mm aperture used in the two wavelength measurements, clearly show that a significant amount of aperture integration must have occurred, particularly on night 4. Using these values and Fig. 2 we can estimate the value of the aperture integration parameter $D/\sqrt{h}$ for the 27-mm aperture that appears in Eq. (7) and hence find the predicted ratios of variances for the different pairs of wavelengths. The values of the integration parameters are shown in column (7), and the predicted ratios are given in columns (8)–(10). (As an aside, it should be observed that the effective single layer heights h_1 calculated from the estimated $D/\sqrt{h_1}$ lie in the 2–5-km range and the effective values of p in the power law are 0.6–0.9.)

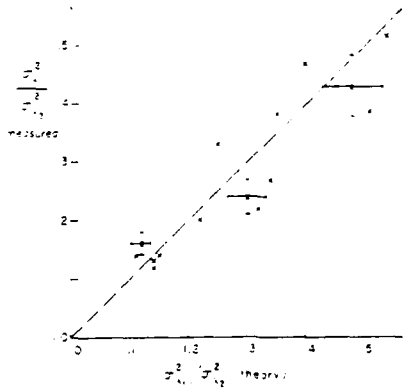

Fig. 3. Measured ratios of variances are plotted against those predicted by theory taking into account the observed aperture integration. The vertical error bars are the standard errors associated with 4–5 independent measurements of the ratios. Horizontal error bars arise from the error in the estimation of the aperture integration parameter. The broken line has slope unity and represents agreement between theory and experiment.

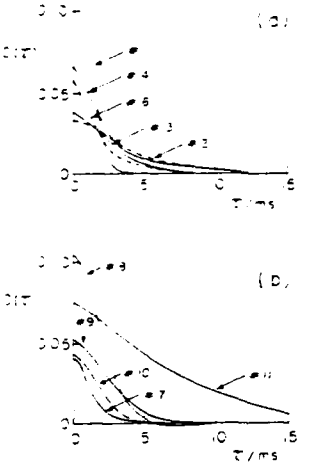

Fig. 4. Temporal correlation functions of stellar scintillation measured over ten nights at Mauna Kea Observatory (observations could not be made on night five). Some curves are shown as broken lines for clarity. Time scales measured at the 1/e point range from 1.7 to 10 msec.

Figure 3 shows a plot of the measured ratios of variances [columns (2)–(4) of Table I] against the predicted ratios [columns (8)–(10)]. The broken line has a slope of unity and represents agreement between theory and experiment: the least squares straight line passing through the data points has a slope of 0.85 ± 0.10.

The data analysis described above ignored the effect of temporal integration. The temporal correlation function consists of two main contributions, a boiling component which is probably wavelength independent and a rigid translation component (the so-called Taylor hypothesis) which is wavelength dependent, since the spatial correlation function is wavelength dependent. Thus, in general, we would expect both temporal and spatial integration to produce measured ratios of variances that are less than those predicted on the basis of spatial integration alone; this trend is observed in Fig. 3. All factors considered, we conclude that the observed behavior with wavelength is consistent with Tatarski's theory.

IV. Temporal Correlation Functions

The temporal correlation function of scintillation was measured on every night of observation using the 27-mm diam aperture, green filter (λ = 553 nm, $\Delta\lambda$ = 8 nm) and sample times ranging from 0.1 to 0.5 msec depending on the correlation time scale. Representative correlation functions of the intensity fluctuation for each night are shown in Figs. 4(a) and (b). The 1/e

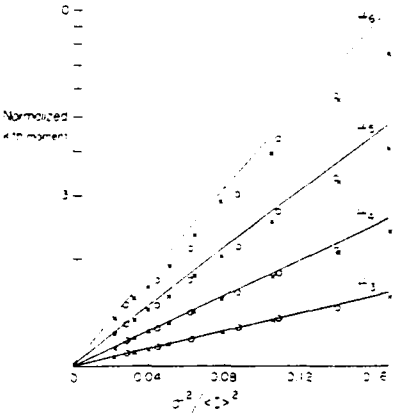

Fig. 5. Measurements of the third, fourth, fifth, and sixth moments plotted as a function of the measured normalized variance. Solid lines are the predictions based on a log normal distribution for stellar scintillation: set 1, (●); set 2, (○); see text.

correlation times vary between 1.7 and 10 msec, with an average value of ~3.5 msec. While these values are similar to the observations of others,[23] they are shorter than correlation times recorded at another excellent observing site (San Pedro Martir Observatory, Baja Calif., Mexico) where values consistently around 10 msec were observed.

V. Normalized Moments of Scintillation

The theory of Tatarski predicts that the probability density function of intensity of stellar scintillation is log normal (assuming that saturation has not been reached). The normalized moments of this distribution are given by[24]

$$\mu_n = \mu_2^{n(n-1)/2} \qquad (5)$$

Some recent experimental results by Parry and Walker[10] show that the measured moments of stellar scintillation agree fairly well with those of the log normal distribution for $\sigma_I^2 \leq 0.65$, although the measured values tend to be lower.

A detailed examination of our data obtained during this observing session (and at Mees Observatory, N.Y. and San Pedro Martir Observatory) shows that the measured moments are always slightly smaller than those predicted by the log normal distribution. A sample of these results is shown in Fig. 5 in which the values of the third, fourth, fifth and sixth normalized moments ($\mu_3 - \mu_6$) are plotted against the measured normalized variance (i.e., $\mu_2 - 1$). The data used to construct Fig. 5 comprised:

Set 1, (●): eighty-nine observations using a 27-mm diam aperture, 0.5–1-msec integration, green filter ($\bar{\lambda}$ = 553 nm, $\Delta\lambda$ = 8 nm), and zenith angle <40°.

Set 2, (○): thirty-seven observations using a 5-mm or smaller diam aperture, 0.5–1-msec integration, broadband light ($\bar{\lambda}$ = 485 nm, $\Delta\lambda \simeq$ 200 nm), and zenith angle <20°.

It is clear from Fig. 5 that the observed higher moments are consistently lower than those associated with the log normal distribution. However, both sets of measurements involved some degree of integration over space, time, or wavelength, and therefore it is possible that the true probability density function of scintillation could be log normal. Finally, it should be noted that the log normal distribution is not uniquely specified by its moments,[24] so that even if our measured moments had been in agreement with those of the log normal distribution this would not have proved that the scintillation was definitely log normal.

We are grateful to the Director of Mauna Kea Observatory, Hawaii, for providing observing time on the 61-cm telescope. This research was supported by the Air Force Office of Scientific Research under grant AFOSR 81 0003 and also in part by the Rome Air Development Center Postdoctoral Program.

References

1. E. Jakeman, G. Parry, E. R. Pike, and P. N. Pusey, Contemp. Phys. **19**, 127 (1978).
2. F. Roddier, Prog. Opt. **19**, 281 (1980).
3. J. C. Dainty, D. R. Hennings, and K. A. O'Donnell, J. Opt. Soc. Am. **71**, 490 (1981).
4. E. Jakeman and P. N. Pusey, "Photon-Counting Statistics of Optical Scintillation," in *Inverse Scattering Problems in Optics*, H. P. Baltes, Ed. (Springer, Heidelberg, 1980), pp. 72–116.
5. L. Mandel, Proc. Phys. Soc. London **72**, 1037 (1958).
6. B. E. A. Saleh, *Photoelectron Statistics* (Springer, Heidelberg, 1978), p. 77.
7. R. F. Chang, V. Korenman, C. O. Alley, and R. W. Detenbeck, Phys. Rev. **178**, 612 (1969).
8. E. Jakeman, E. R. Pike, and P. N. Pusey, Nature **263**, 215 (1976).
9. R. S. Iyer and J. L. Bufton, Opt. Commun. **22**, 377 (1977).
10. G. Parry and J. G. Walker, J. Opt. Soc. Am. **70**, 1157 (1980).
11. C. W. Allen, *Astrophysical Quantities* (Athlone, London, 1973), p. 197.
12. V. I. Tatarski, *Wave Propagation in a Turbulent Medium* (Dover, New York, 1967), p. 53, Eq. 7.44. This result actually pertains to the variance of the log amplitude, which is equal to one-quarter that of the intensity for log normal statistics.
13. A. H. Mikesell, A. A. Hoag, and J. S. Hall, J. Opt. Soc. Am. **41**, 963 (1951).
14. F. Netterblad, *Studies of Astronomical Scintillation, Ser. II*, No. 30 Meddelande Fran Lunds Astronomiska Observatorium, Lund Observatory, Sweden (1953).
15. W. M. Protheroe, Contrib. Perkins Obs. Ser. 2 **4** (1955).
16. J. J. Burse, J. Opt. Soc. Am. **60**, 1262 (1970).
17. M. W. Fitzmaurice, J. L. Bufton, and P. O. Minott, J. Opt. Soc. Am. **59**, 7 (1969).
18. J. R. Kerr, J. Opt. Soc. Am. **62**, 1040 (1972).
19. R. W. Boyd, J. Opt. Soc. Am. **68**, 877 (1978).
20. See Ref. 2, Eq. 5.3, the transfer function of the measurement aperture has been included in Eq. (4).
21. A. T. Young, J. Opt. Soc. Am. **60**, 248 (1970).
22. D. L. Fried, "Theoretical Analysis of Aperture Averaging," Optical Sciences Consultants Technical Report DR-015 (1970).
23. G. Parry, J. G. Walker, and R. J. Scaddan, Opt. Acta **26**, 563 (1979).
24. J. W. Stronbehn, Ting-i Wang, and J. P. Speck, Radio Sci. **10**, 59 (1975).

Speckle statistics of doubly scattered light

K. A. O'Donnell

The Institute of Optics, University of Rochester, Rochester, New York 14627

Received June 19, 1982

The statistical properties of light that has been scattered twice are studied in theory. If each scattering by itself gives rise to Gaussian speckle, it is found that the probability densities of the doubly scattered light amplitude and intensity are approximately K distributions, which imply stronger fluctuations than Gaussian light. The spatial-correlation properties of the doubly scattered light are also examined. The intensity correlations contain non-Gaussian terms, and, although the correlations are spatially stationary, they indicate that the doubly scattered light is not an ergodic process.

1. INTRODUCTION

Although classical speckle theory has become well developed in recent years,[1,2] little attention has been given to the effect of multiple scattering of coherent light. In the context of speckle theory, the only relevant work has been that of Fried,[3] though the correlation structure of doubly scattered light from Brownian particle suspensions has been reported in theory[4,5] and experiment.[5] In the following we examine the effect of scattering a Gaussian speckle pattern from an optically rough surface. It is shown that the probability density of scattered amplitude in the far field is not generally Gaussian in this case; rather, stronger amplitude and intensity fluctuations exist than in the Gaussian case. Finally, the correlation properties of doubly scattered light are discussed in Section 3.

We shall consider the scattering situation shown in Fig. 1. A random complex-amplitude process $a(\xi, \eta)$ is incident upon the hard aperture of a scattering system. The light is then scattered by a diffuser and produces a random complex-amplitude process $A(x, y)$ in the far field of the aperture. Throughout the analysis, two important assumptions will be made. Our first assumption (1) is that the random amplitude $a(\xi, \eta)$ is a spatially stationary circular Gaussian amplitude process. Hence $a(\xi, \eta)$ may be generated by Gaussian scattering from a diffuser, although the details of this initial scattering experiment need not concern us here; rather $a(\xi, \eta)$ will be assumed to be Gaussian *a priori*. The other assumption (2) is that, by itself, the secondary scattering experiment of Fig. 1 gives rise to Gaussian speckle. That is, if $a(\xi, \eta)$ is viewed as a deterministic quantity, $A(x, y)$ will be complex circular Gaussian. The necessary conditions for the second assumption to be valid are well known in speckle theory.[1,2] Most important to the present analysis are the restrictions that the diffuser must introduce optical-path fluctuations greater than the wavelength of light and that a large number of independent scatterers contribute to the amplitude at any given point in the far field. A theory analogous to that presented below may be developed if either $a(\xi, \eta)$ or the secondary scattering experiment (or both) is non-Gaussian. The Gaussian–Gaussian case is presented here because Gaussian speckle is well understood and is easily generated in the laboratory.

2. FIRST-ORDER STATISTICS OF THE DOUBLY SCATTERED LIGHT

Our efforts will presently be directed toward determining the probability densities of the scattered amplitude and intensity in the far field. Within an unessential factor, the scattered amplitude in the far field is given by[6]

$$A(x, y) = \iint_D a(\xi, \eta) t(\xi, \eta) \exp\left[-\frac{ik}{z}(x\xi + y\eta)\right] d\xi d\eta, \tag{1}$$

where D is the domain determined by the shape of the scattering aperture, $t(\xi, \eta)$ is a random function that describes transmission through the diffuser, z is the distance to the far field, and k is the wave number of the incident light. First, consider the case when the correlation scale or speckle size of $a(\xi, \eta)$ is much larger than the aperture. The amplitude $a(\xi, \eta)$ is then approximately constant over the domain of integration so that

$$A(x, y) \cong a_0 \iint_D t(\xi, \eta) \exp\left[-\frac{ik}{z}(x\xi + y\eta)\right] d\xi d\eta, \tag{2}$$

where a_0 is $a(\xi, \eta)$ evaluated at the center of the aperture. The integral remaining is simply the scattered amplitude that is due to a uniformly illuminated aperture. Because of assumption (2), the scattered amplitude is given by the product

$$A(x, y) = a_0 A_0(x, y), \tag{3}$$

where a_0 and A_0 are both complex circular Gaussian variables.

Since a_0 and A_0 are independent and circular, A is circular, although we will now show that it is not Gaussian. The moduli of a_0 and A_0 are Rayleigh distributed according to

$$p(a_0) = \frac{2a_0}{\langle a_0^2 \rangle} \exp\left(-\frac{a_0^2}{\langle a_0^2 \rangle}\right), \tag{4}$$

Reprinted from Journal of the Optical Society of America, Vol. 72, page 1459, November 1982

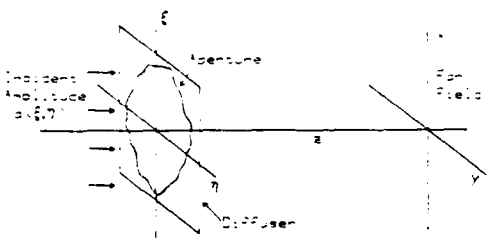

Fig. 1. The scattering geometry under consideration. A Gaussian speckle amplitude process $a(\xi, \eta)$ is scattered by a diffuser into the far field.

and

$$p(|A_{0i}|) = \frac{2|A_{0i}|}{\sigma_2^2} \exp(-|A_{0i}|^2/\sigma_2^2), \tag{5}$$

where

$$\sigma_1^2 = \langle |a_{0i}|^2 \rangle$$

and

$$\sigma_2^2 = \langle |A_{0i}|^2 \rangle. \tag{6}$$

The probability density of $|A| = |a_{0i}| |A_{0i}|$ is then given by

$$p(|A|) = \iint_0^\infty p(|a_{0i}|) p(|A_{0i}|) \delta(|A| - |a_{0i}||A_{0i}|) \, d|a_{0i}| \, d|A_{0i}|, \tag{7}$$

where $\delta(\cdot)$ is the Dirac delta function. After one of the integrals is carried out, this becomes

$$p(|A|) = \frac{4|A|}{\sigma_1^2 \sigma_2^2} \int_0^\infty \frac{1}{x} \exp\left[-\left(\frac{x^2}{\sigma_1^2} + \frac{|A|^2}{x^2 \sigma_2^2} \right) \right] dx, \tag{8}$$

which, with the substitution

$$e^t = x^2 \frac{\sigma_2}{|A| \sigma_1}, \tag{9}$$

may be written in the form

$$p(|A|) = \frac{4|A|}{\sigma_1^2 \sigma_2^2} \int_0^\infty \exp\left[-\frac{2|A|}{\sigma_1 \sigma_2} \cosh(t) \right] dt. \tag{10}$$

This integral is a representation of the zeroth-order modified Bessel function of the second kind[7] so that

$$p(|A|) = \frac{4|A|}{\beta} K_0\left(\frac{2|A|}{\sqrt{\beta}} \right). \tag{11}$$

where we have defined $\beta = \langle |A|^2 \rangle = \sigma_1^2 \sigma_2^2$. Thus $|A|$ is not Rayleigh distributed in the limit of large correlation scale of $a(\xi, \eta)$, so the scattered light is not Gaussian in this case.

We now consider the density function of $A(x, y)$ when the speckle size of $a(\xi, \eta)$ is comparable with or smaller than the scattering aperture. In general this is a difficult problem, although it will be made tractable by using an intuitive approximation. Specifically, the complex amplitude $a(\xi, \eta)$ will be assumed to be spatially constant over any one of a set of equal-sized domains in the scattering aperture, each domain being of the order of a speckle size. Moreover, the amplitude of each domain will be assumed to be a circular Gaussian random variable statistically independent of the other domains, as individual speckles of a Gaussian amplitude process are practically uncorrelated and hence independent in this case. A similar discrete model of a Gaussian speckle pattern has been used to derive the approximate gamma variate form of the integrated speckle intensity.[8]

In this case, the integral of Eq. (1) becomes

$$A(x, y) \simeq \sum_{j=1}^{N} \left\{ a_j \iint_{D_j} t(\xi, \eta) \exp\left[-\frac{ik}{z}(x\xi + y\eta) \right] d\xi d\eta \right\}. \tag{12}$$

where a_j is the spatially constant complex amplitude of $a(\xi, \eta)$ of the jth domain D_j and N is the number of domains present within the scattering aperture. The integral in each term is the random amplitude in the far field that is due to uniform illumination on only a single domain D_j of the diffuser. As long as the domains are considerably larger than the diffuser microstructure, the central-limit theorem may be applied as in Gaussian speckle theory, so that each integral in the sum represents a complex circular Gaussian amplitude. We will also assume that integrals over different domains are statistically independent, which is reasonable for diffusers of much finer scale than D_j.

With these assumptions, expression (12) describes a circular random walk of N independent steps that are, statistically speaking, identical. Since the analysis has been restricted to a hard or unshaded aperture, the N steps of expression (12), which originate from different domains of the aperture, all have an identical mean length. Each step is the product of two circular Gaussian random variables, so the probability density of individual step lengths obeys Eq. (11). Thus we have the purely mathematical problem of determining the density function of a net amplitude A composed of N such steps.

While problems of this sort are often difficult to handle analytically, Eq. (11) belongs to a family of functions known as K distributions that possess a remarkable property. Jakeman and Pusey have demonstrated that, when the step-length distribution is one of the K distributions, the result of a circular random walk leads to a K distribution of higher order for the modulus of the resultant vector.[9] Specifically, the theorem of Jakeman and Pusey may be used to show that, if the step length is distributed according to Eq. (11), the random walk of N steps of expression (12) is distributed as

$$p(|A|) = \frac{4}{\Gamma(N)} \frac{1}{\sqrt{\beta}} \left(\frac{|A|}{\sqrt{\beta}} \right)^N K_{N-1}\left(\frac{2|A|}{\sqrt{\beta}} \right), \tag{13}$$

where

$$\langle |A|^2 \rangle = N\beta.$$

This result will not be proven here; the reader may consult Ref. 9 for details. Equation (13) is approximate for $N > 1$ only because of the somewhat naive model of the scattering process used, although it is exact for $N = 1$, as it reduces to Eq. (11).

Equation (13) has also been found to describe the statistics of singly scattered non-Gaussian light. These K distributions arise in theory when special models of individual scatterers are used[9] or when scatterer number fluctuations are considered[10]; these effects are neglected in the Gaussian scattering experiments discussed here. Rather, the K distributions arise in the present context because of the multiplicative effects of double scattering.

Since A is circular, the probability distribution of amplitude in the complex plane may be written as

$$p(A_r, A_i) = \frac{1}{2\pi A}\, p(A)$$

$$= \frac{2}{\pi\Gamma(N)}\,\frac{1}{\beta}\left[\frac{A_r^2 + A_i^2}{\beta}\right]^{\frac{N-1}{2}} K_{N-1}\left[\frac{2(A_r^2 + A_i^2)^{1/2}}{\sqrt{\beta}}\right], \quad (15)$$

where A_r and A_i denote the real and imaginary parts of A. The cross section of this distribution is shown in Fig. 2 for various values of N in comparison with a circular Gaussian distribution. For $N = 1$ it is singular at the origin, whereas for $N > 15$ it is scarcely different from a circular Gaussian. This is of course because any circular random walk becomes Gaussian for deterministic N as $N \to \infty$, regardless of the properties of the individual steps. In physical terms, if a large number of speckles are present on the scattering aperture, the scattered amplitude statistics are nearly circular Gaussian.

It is also worth noting that the assumption that each integral of the sum of expression (12) is Gaussian will break down as the speckle size becomes comparable with the lateral size of the surface microstructure. However, the scattered amplitude A will still become Gaussian if only because of the central-limit theorem. Hence the approach to Gaussian statistics as N becomes large may be different from that predicted by Eq. (15), but this clearly depends on the value of N necessary to lead to non-Gaussian factors in the terms of inequality (12).

The probability density of intensity I may be found easily by transforming Eq. (13) with $I = A^2$, with the result that

$$p(I) = \frac{2}{\Gamma(N)}\,\frac{1}{\beta}\left(\frac{I}{\beta}\right)^{\frac{N-1}{2}} K_{N-1}\left(2\sqrt{\frac{I}{\beta}}\right), \quad (16)$$

where $\langle I \rangle = N\beta$. This distribution has the normalized moments

$$\frac{\langle I^m \rangle}{\langle I \rangle^m} = m!\,\frac{\Gamma(m+N)}{N^m\Gamma(N)} \quad (17)$$

and normalized variance

$$\frac{\langle I^2 \rangle}{\langle I \rangle^2} - 1 = 1 + 2/N. \quad (18)$$

The distributions of Eq. (16) are shown in Fig. 3 for several values of N. In the case $N = 1$, the normalized moments go as $m!$, which imply strong intensity fluctuations. For large values of N, the K distributions approach a negative exponential distribution. This is illustrated in Fig. 3 and may also be seen from the normalized moments of Eq. (17), which approach the negative exponential moments of $m!$ for large N.

The K distribution of intensity with $N = 1$ has arisen in related problems in the literature. Fried[7] has found that this distribution applies to the statistics of intensity when the eye or a similar imaging system observes a Gaussian speckle pattern reflected from a rough screen. Although it is perhaps not widely appreciated, it has also been shown that, when spatially coherent, quasi-monochromatic thermal light is singly scattered in a Gaussian manner, the intensity statistics obey a K distribution with $N = 1$, as long as the resolution time is much less than the reciprocal of the optical bandwidth.[8] The photon-counting distribution corresponding to this K distribution has also been derived in this context.[9,10] In those references, as in our analysis, the K distribution arises because the intensity is the squared modulus of two independent circular Gaussian factors.

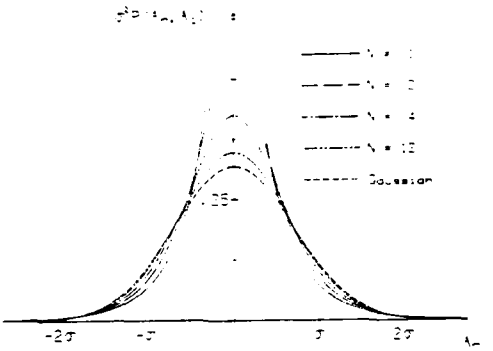

Fig. 2. Cross sections of the K distributions of doubly scattered complex amplitude from Eq. (13). Curves are shown for various values of the N parameter in comparison with a circular Gaussian distribution, which is the limit of the K distributions as $N \to \infty$. All curves are rotationally symmetric in the complex plane.

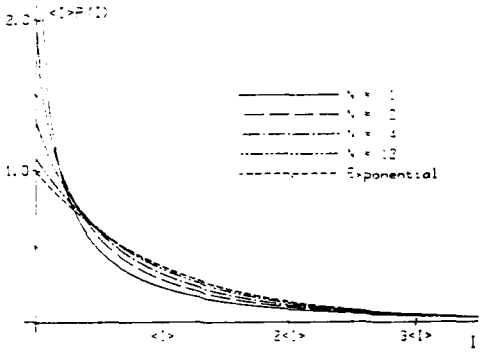

Fig. 3. Probability densities of the doubly scattered intensity from Eq. (16) for various values of the N parameter. A negative-exponential distribution is shown for comparison.

Although the N parameter has been regarded as the number of correlation cells of area $\pi\xi_c\eta_c$ present within the scattering aperture, the precise manner in which N may be calculated for given scattering parameters has been intentionally neglected thus far. Particularly since the probability distributions have been approximate for $N > 1$, one is left with somewhat of an arbitrary decision in the choice of N. We postulate here that N may be chosen most sensibly by matching the variance of the K distribution of Eq. (16) to the exact intensity variance. This is similar to the method of choosing the variance parameter of the gamma variate approximation of spatially integrated speckle intensity.[8] An exact expression for the intensity variance may be deduced from the results of Section 3 as a special case of the exact intensity correlation function. This will not generally lead to integer N, so that our intuitive random-walk model does not strictly hold.

3. CORRELATION STRUCTURE OF THE DOUBLY SCATTERED LIGHT

We now turn our attention to the spatial-correlation properties of the doubly scattered amplitude and intensity in the far field. The approach taken will be first to consider $a(\xi, \eta)$ as a deterministic quantity, in which case from assumption (2) the correlation results are those of conventional Gaussian speckle theory. Then $a(\xi, \eta)$ will be allowed to become random, and the true ensemble average will be obtained by averaging over the Gaussian statistics of $a(\xi, \eta)$. In addition, the hard scattering aperture, which was necessary for identical mean step lengths of the random walk of Section 2, will now be replaced by a more general pupil function $P(\xi, \eta)$, which may include amplitude modulation.

For a given realization of $a(\xi, \eta)$, the results of conventional speckle theory have shown that the correlation function of far-field amplitude $A(x, y)$ is given by[12]

$$\langle A^*(x, y)A(x + \Delta x, y + \Delta y)\rangle_a = e^{i\kappa} \iint_{-\infty}^{\infty} |P(\xi, \eta)|^2 |a(\xi, \eta)|^2 \times \exp\left[-\frac{ik}{z}(\Delta x\xi + \Delta y\eta)\right] d\xi d\eta, \quad (19)$$

where

$$\kappa = \frac{k}{2z}(\Delta x^2 + \Delta y^2 - 2x\Delta x + 2y\Delta y). \quad (20)$$

$\langle Q(a(\xi, \eta))\rangle_a$ denotes the ensemble average of Q for a given realization of $a(\xi, \eta)$, and an unessential scaling factor has been ignored. Also, with $a(\xi, \eta)$ fixed, the Gaussian factorization theorem holds, so that the correlation of far-field intensity is given by[12]

$$\langle I(x, y)I(x - \Delta x, y + \Delta y)\rangle_a = \left|\iint_{-\infty}^{\infty} |P(\xi, \eta)|^2 a(\xi, \eta)|^2 d\xi d\eta\right|^2 - \left|\iint_{-\infty}^{\infty} |P(\xi, \eta)|^2 a(\xi, \eta)|^2 \times \exp\left[-\frac{ik}{z}(\Delta x\xi + \Delta y\eta)\right] d\xi d\eta\right|^2. \quad (21)$$

These results are valid in the paraxial region where the envelope of the speckle pattern is nearly constant. Another important assumption in deriving Eqs. (19) and (21) is that the diffuser surface has much finer structure than $a(\xi, \eta)$ or $P(\xi, \eta)$. This in effect sets a lower limit on the speckle size of $a(\xi, \eta)$ for which the theory to be presented is valid.

These results may now be averaged over the random function $a(\xi, \eta)$. From Eq. (19) we obtain

$$\langle A^*(x, y)A(x + \Delta x, y + \Delta y)\rangle = e^{i\kappa}\langle\cdots\rangle \iint_{-\infty}^{\infty} |P(\xi, \eta)|^2 \times \exp\left[-\frac{ik}{z}(\Delta x\xi + \Delta y\eta)\right] d\xi d\eta, \quad (22)$$

where $\langle\cdots\rangle$ denotes $\langle|a(\xi, \eta)|^2\rangle_a$. $\langle Q\rangle$ denotes the average of Q over the entire ensemble, and we have used the fact that $a(\xi, \eta)$ is spatially stationary. This result is independent of x and y and is rather similar to the Gaussian speckle result. However, in averaging Eq. (21) over the statistics of $a(\xi, \eta)$, fourth-order amplitude moments of $a(\xi, \eta)$ are encountered, which may be simplified with the Gaussian factorization theorem as

$$\langle a(\xi, \eta)|^2 a(\xi', \eta')|^2\rangle_a = \langle\cdots\rangle^2 + C_a(\xi - \xi', \eta - \eta')|^2, \quad (23)$$

where

$$C_a(\xi - \xi', \eta - \eta') \equiv \langle a^*(\xi', \eta')a(\xi, \eta)\rangle_a. \quad (24)$$

A small amount of algebra then yields the spatial intensity correlation as

$$\langle I(x, y)I(x + \Delta x, y + \Delta y)\rangle = \langle I\rangle^2 \iint_{-\infty}^{\infty} |P(\xi, \eta)|^2 d\xi d\eta|^2 + \left|\langle\cdots\rangle \iint_{-\infty}^{\infty} |P(\xi, \eta)|^2 \exp\left[-\frac{ik}{z}(\Delta x\xi + \Delta y\eta)\right] d\xi d\eta\right|^2 + \iiint\iint_{-\infty}^{\infty} |P(\xi, \eta)|^2 |P(\xi', \eta')|^2 C_a(\xi - \xi', \eta - \eta')|^2 \times \left\{1 + \exp\left[-\frac{ik}{z}[\Delta x(\xi - \xi') + \Delta y(\eta - \eta')]\right]\right\} \times d\xi d\xi' d\eta d\eta'. \quad (25)$$

Again the result is independent of the x and y variables, although it is apparent that Eqs. (25) and (22) are not related by the Gaussian-moment theorem. We define the normalized intensity correlation as

$$\Lambda(\Delta x, \Delta y) = \frac{\langle I(x, y)I(x + \Delta x, y + \Delta y)\rangle - \langle I\rangle^2}{\langle I\rangle^2}. \quad (26)$$

The quantity $\langle I\rangle$ may be found from Eq. (22) with $\Delta x = \Delta y = 0$. After introducing sum and difference coordinates in the last integral of Eq. (25), there results

$$\Lambda(\Delta x, \Delta y) = \frac{1}{S^2}\left|\iint_{-\infty}^{\infty} |P(\xi, \eta)|^2 \times \exp\left[-\frac{ik}{z}(\Delta x\xi + \Delta y\eta)\right] d\xi d\eta\right|^2 - \frac{1}{S^2}\iint_{-\infty}^{\infty} T(\xi, \eta)C_a(\xi, \eta)|^2 \times \left\{1 + \exp\left[-\frac{ik}{z}(\Delta x\xi + \Delta y\eta)\right]\right\} d\xi d\eta, \quad (27)$$

where

$$T(\xi, \eta) = \iint_{-\infty}^{\infty} |P(\xi' - \xi/2, \eta - \eta/2)|^2 |P(\xi' + \xi/2, \eta + \eta/2)|^2 d\xi' d\eta', \quad (28)$$

$$S = \iint_{-\infty}^{\infty} |P(\xi, \eta)|^2 d\xi d\eta, \quad (29)$$

and

$$C_a(\xi, \eta) = \langle\cdots\rangle. \quad (30)$$

The first term of Eq. (27) is the Gaussian contribution to the intensity correlation, whereas the other term represents non-Gaussian effects.

It is instructive to consider the intensity correlation in two limiting cases. First, when the speckle size of $a(\xi, \eta)$ is much greater than the scattering aperture size, $T(\xi, \eta) \cong 1$ within the domain of integration. Inserting this in Eq. (27) and

making use of the autocorrelation theorem, we obtain

$$\Gamma(\Delta x, \Delta y) \propto \frac{2}{S^2}\left|\iint_{-\infty}^{\infty} P(\xi,\eta)^2 \times \exp\left[-\frac{ik}{z}(\Delta x\xi + \Delta y\eta)\right] d\xi d\eta\right|^2 - 1. \quad (31)$$

This normalized correlation starts at the value 3 when $\Delta x = \Delta y = 0$ (which is the same as the normalized variance of the K distribution when $N = 1$) and then decays to unity for large Δx or Δy. Correlations never die out; hence $I(x, y)$ is spatially stationary although spatially nonergodic. Physically, when the speckle size is much greater than the scattering aperture size, the intensity in the aperture is spatially constant, although this constant varies over the ensemble with a negative-exponential probability distribution. Moreover, the mean intensity in the far field is proportional to the intensity present in the scattering aperture. Equation (31) is therefore the intensity correlation of a Gaussian speckle pattern whose mean intensity varies as a negative-exponential variable over the ensemble. Thus it is not surprising that a correlation exists between widely separated points.

When $\gamma_a(\xi, \eta)$ is considerably narrower than the scattering pupil, from Eq. (27) we have

$$\Gamma(\Delta x, \Delta y) \propto \frac{1}{S^2}\left|\iint_{-\infty}^{\infty} P(\xi,\eta)^2 \times \exp\left[-\frac{ik}{z}(\Delta x\xi + \Delta y\eta)\right] d\xi d\eta\right|^2 + \frac{T(0,0)}{S^2}\iint_{-\infty}^{\infty} \gamma_a(\xi,\eta)^2 \exp\left[-\frac{ik}{z}(\Delta x\xi + \Delta y\eta)\right] d\xi d\eta + \frac{T(0,0)}{S^2}\iint_{-\infty}^{\infty} \gamma_a(\xi,\eta)^2 d\xi d\eta. \quad (32)$$

In addition to the Gaussian term, the *second term represents* the contribution of the fine structure in $a(\xi, \eta)$ to the intensity structure in the far field. The last term of expression (32) is an energy-conservation term that represents power fluctuations in the scattered light as a whole. This arises for similar reasons as the constant term arose in expression (21), although the nonergodic effects are now considerably weaker.

Finally, it is possible to find a general expression for the N parameter of the K distribution in the manner discussed in Section 2. Comparing Eq. (27) with $\Delta x = \Delta y = 0$ to the expression for the normalized variance of Eq. (13), it is straightforward to show that

$$1/N = \frac{1}{S^2}\iint_{-\infty}^{\infty} T(\xi,\eta)\gamma_a(\xi,\eta)^2 d\xi d\eta. \quad (33)$$

The expression for N^{-1} may indeed be shown to be equal to the normalized variance of Gaussian speckle intensity that has been integrated over the scattering aperture.[14] The normalized variance of Eq. (18) may then be thought of as having two contributions: the Gaussian speckle contribution of unity in addition to a term that represents fluctuations in the net power of the scattered light.

4. SUMMARY

The statistical properties of coherent light that has been scattered twice have been investigated in theory. It has been shown that, if each individual scattering gives rise to Gaussian speckle by itself, the probability densities that describe the doubly scattered light are approximately K distributions. In general, the K distributions predict larger amplitude and intensity fluctuations than arise in Gaussian speckle. The spatial intensity correlation of the doubly scattered light consists of a Gaussian term in addition to terms that represent non-Gaussian effects. Although the intensity correlations are statistically stationary, they do not die out for large spatial separations; hence the doubly scattered light is not spatially ergodic.

The derivation of the K distribution of doubly scattered light amplitude has not been rigorous, as it has made use of a rather idealized model of a Gaussian speckle pattern. However, we believe that a better theory would be considerably more difficult than the intuitive theory presented here. It is expected that the K distribution approximates the exact *probability distribution of doubly scattered* light in the same sense that the gamma variate approximates integrated Gaussian speckle intensity, since similar idealizations are made in both cases. Nevertheless, the ultimate test of validity of the theory presented, as always, would be through comparison with experiment.

ACKNOWLEDGMENTS

The author wishes to thank J. C. Dainty for helpful criticism of an early draft of this manuscript. This work was sponsored by the U.S. Air Force Office of Scientific Research under grant AFOSR81-0003 and by the U.S. Army Research Office under grant DAAG-80-K-0048.

REFERENCES

1. J. W. Goodman, in *Laser Speckle and Related Phenomena*, J. C. Dainty, ed. (Springer-Verlag, Berlin, 1975).
2. J. C. Dainty, in *Progress in Optics*, Vol. XIV, E. Wolf, ed. (North-Holland, Amsterdam, 1976).
3. D. L. Fried, "Laser eye safety: the implications of ordinary speckle statistics and of speckled-speckle statistics," J. Opt. Soc. Am. 71, 914–916 (1981).
4. A. P. Ivanov, A. Ya. Khairullina, and A. P. Chaikovskii, "Angular correlation function of doubly scattered radiation," Opt. Spectrosc. 35, 69–71 (1973).
5. F. C. Van Rijswijk and C. L. Smith, "Fluctuations in doubly scattered laser light," Physica 88A, 121–142 (1976).
6. M. Born and E. Wolf, *Principles of Optics*, 5th ed. Pergamon, Oxford, 1975), Sec. 8.5.
7. G. N. Watson, *A Treatise on the Theory of Bessel Functions*, 2nd ed. (Cambridge U. Press, Cambridge, 1966), p. 172.
8. J. W. Goodman, "Some effects of target-induced scintillation on optical radar performance," Proc. IEEE 53, 1688–1700 (1965).
9. E. Jakeman and P. N. Pusey, "A model for non-Rayleigh sea echo," IEEE Trans. Antennas Propag. AP-24, 806–814 (1976).
10. E. Jakeman and P. N. Pusey, "Significance of K-distributions in scattering experiments," Phys. Rev. Lett. 40, 546–550 (1978).
11. E. Jakeman, "On the statistics of K-distributed noise," J. Phys. A 13, 31–47 (1980).
12. P. N. Pusey, in *Photon Correlation Spectroscopy and Velocimetry*, H. Z. Cummins and E. R. Pike, eds. (Plenum, New York, 1977), Sec. 2.1 and App. 1.
13. M. Bertolotti, B. Crosignani, and P. DiPorto, "On the statistics of Gaussian light scattered by a Gaussian medium," J. Phys. A 3, L37–L40 (1970).
14. B. Saleh, *Photoelectron Statistics* (Springer-Verlag, Berlin, 1978), p. 204.
15. Ref. 1, p. 46.

Correlation properties of light produced by quasi-thermal sources

T. Gonsiorowski and J. C. Dainty*

The Institute of Optics, The University of Rochester, Rochester, New York 14627

Received August 24, 1982

It is well known that narrow-band thermal light can be simulated by moving a ground-glass plate in front of a laser beam (a so-called quasi-thermal source). In this Letter, we show that, when time integration of intensity occurs, the spatial correlation of integrated intensity from a quasi-thermal source does not, in general, behave as it would for a real thermal source. In particular, time integration can increase the spatial coherence area.

1. INTRODUCTION

Shortly after the invention of the laser, Martienssen and Spiller[1] described a quasi-thermal source with an adjustable coherence time between 10^{-5} and 1 sec. This source consists of a rotating diffusing disk, such as a ground-glass plate, illuminated by coherent light, e.g., a laser beam. The field produced by this source has circular complex Gaussian statistics,[2-4] provided that certain restrictions are met. The spatial coherence properties of the scattered field are governed by the Van Cittert–Zernike theorem,[3-5] and the temporal properties are governed by the transit time of the diffuser through the laser beam and by a Doppler-shift term for nonnormal angles of observation.[7]

Recently, rotating diffusers of a more controlled nature[7-9] have been used in experiments designed to illustrate the concept of quasi-homogeneous sources[8,9] and also in studies of the coherence of radiation scattered by gratings covered by a diffuser.[11,12] There is a close correspondence between speckle and coherence theory,[5,13,14] and the theory of time-varying speckle[15-17] is particularly relevant to a study of this relationship.

In this Letter we show that certain spatiotemporal statistics of the light produced by quasi-thermal sources are quite different from those of real thermal sources, such as a primary incoherent source or spectrally filtered blackbody radiation. This difference results from the deterministic motion of the diffuser, which generally produces an amplitude space–time cross-correlation function that is *not* reducible to a product of temporal and spatial correlations. We illustrate this difference by showing that the normalized spatial correlation function of time-integrated intensity increases in width as the integration time increases. If the intensity distribution across the quasi-thermal source is Gaussian (e.g., direct laser illumination), then the space–time cross correlation is reducible; in this case, the quasi-thermal source and a true thermal source *to have the same space–time behavior* but for quite different reasons.

2. GENERAL THEORY

A quasi-thermal source is produced by illuminating a rigidly translating ground-glass plate with a monochromatic plane wave (see Fig. 1). The area illuminated is controlled by an aperture $A(\xi, \eta)$ such that this area is much larger than the correlation area of the diffuser surface but still sufficiently small to fulfill the Fraunhofer condition at the observation plane, a distance z from the source.

If the diffuser is constrained to move transversely to the optical axis, then for small field angles Doppler effects can be ignored, and since the time variations introduced by the diffuser are much slower than the natural fluctuations of the light, the complex amplitude alone provides an adequate description of the optical field. Assuming that the diffuser is rough compared with the illumination wavelength, then the phase of the scattered wave will be uniformly distributed between $-\pi$ and π, and, since the aperture was chosen to encompass many correlation areas, a large number of scattering centers will contribute to the field at each observation point. Under these conditions, the complex amplitude in the far field will obey circular complex Gaussian statistics,[2-4] which may be fully described by the space–time amplitude correlation

$$\langle A^*(x, y, t) A(x + \Delta x, y + \Delta y, t + \Delta t)\rangle,$$

where ⟨ ⟩ denotes an ensemble average. It is assumed here that the optical field is wide-sense stationary in time and quasi-stationary in space, that is, over a certain range of observation points (x, y), governed by the correlation properties of the diffuser, the space–time amplitude correlation is independent of x and y. We will also be interested in the space–time intensity cross correlation

$$\langle \Delta I(x, y, t) \Delta I(x + \Delta x, y + \Delta y, t + \Delta t)\rangle = |\langle A^*(x, y, t) A(x + \Delta x, y + \Delta y, t + \Delta t)\rangle|^2, \quad (1)$$

where $\Delta I = I - \langle I \rangle$ and

$$\langle I \rangle = \langle A^*(x, y, t) A(x, y, t)\rangle. \quad (2)$$

Now let us relate these correlations to the statistics of the diffuser. We assume that the coordinate system is chosen so that the diffuser motion is purely along the ξ axis, with velocity v. If the scattered amplitude immediately after the diffuser at time $t = 0$ is $a(\xi, \eta)$, then at time t it will be $a(\xi - vt, \eta)$. Since the observation plane is in the Fraunhofer regime, the complex amplitude is given by[4]

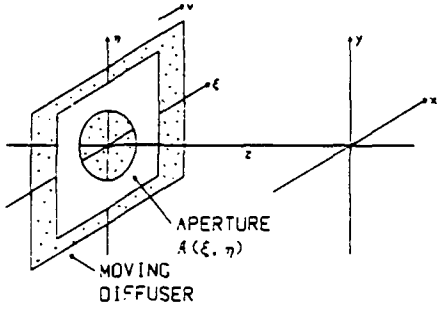

Fig. 1. A quasi-thermal source is produced by illuminating a diffuser moving behind an aperture.

$$A(x, y, t) = \frac{-i}{\lambda z}\exp[ik[z^2 + (x^2 + y^2)/2]/z]\iint_{-\infty}^{\infty} a(\xi' - vt, \eta') \times \mathcal{A}(\xi', \eta')\exp[-ik(x\xi' + y\eta')/z]\,d\xi'\,d\eta', \quad (3)$$

where λ is the wavelength and k is the wave number of the light; the amplitude cross correlation follows directly. Assuming that the diffuser is finely and uniformly ground, we may expect $a(\xi, \eta)$ to be a statistically stationary delta-correlated process; that is, it has a correlation function that depends only on coordinate differences and that can be modeled by a Dirac delta function. This assumption can be shown[17] to result in a normalized space–time intensity correlation of the form

$$\lambda(\Delta x, \Delta y, \Delta t) = \frac{\langle \Delta I(x, y, t)\Delta I(x + \Delta x, y + \Delta y, t + \Delta t)\rangle}{\langle I\rangle^2} = \frac{1}{S^2}\left|\iint_{-\infty}^{\infty} \mathcal{A}\left(\xi - \frac{v\Delta t}{2}, \eta\right)\mathcal{A}\left(\xi + \frac{v\Delta t}{2}, \eta\right) \times \exp[-ik(\Delta x\xi - \Delta y\eta)/z]\,d\xi\,d\eta\right|^2, \quad (4)$$

where

$$S = \iint_{-\infty}^{\infty} |\mathcal{A}(\xi, \eta)|^2 d\xi\,d\eta. \quad (5)$$

To include the effect of time integration, consider the time-averaged intensity

$$\bar{I}(x, y, t) = \frac{1}{T}\int_{t-T/2}^{t+T/2} I(x, y, t')\,dt', \quad (6)$$

where T is the integration time and the bar denotes a time-averaged quantity. Since λ is independent of time, applying [illegible] to Eq. (4) results in

$$\bar{\lambda}(\Delta x, \Delta y, \tau) = \frac{1}{T^2}\int_{t-T/2}^{t+T/2}\int_{t-T/2}^{t+T/2} \lambda(\Delta x, \Delta y, t'' - t')\,dt'\,dt'' \quad (7)$$

This can be simplified to a single integral[20]

$$\bar{\lambda}(\Delta x, \Delta y, \tau) = \frac{1}{T}\int_{-T}^{+T}\left(1 - \frac{|\Delta t - \tau|}{T}\right)\lambda(\Delta x, \Delta y, \Delta t)\,d\Delta t. \quad (8)$$

Together Eqs. (4) and (8) express the time-averaged intensity correlation for spatial separations Δx and Δy at a lag time τ from an aperture $\mathcal{A}(\xi, \eta)$ normally illuminated by a monochromatic plane wave of wave number k and filled by a fine diffuser that is rigidly translating with velocity v in the $+\xi$ direction. Equation (8) shows that time integration effectively convolves the instantaneous correlation with a blurring function that increases the temporal width. Further, if the instantaneous intensity correlation is not reducible (i.e., does not factor into the product of space and time functions), then time integration can also affect the spatial extent of the correlation.

3. APPLICATION TO A RECTANGULAR APERTURE

To demonstrate this phenomenon, consider a rectangular aperture

$$\mathcal{A}(\xi, \eta) = \mathrm{rect}(\xi/a)\,\mathrm{rect}(\eta/b), \quad (9)$$

where $\mathrm{rect}(x)$ is the standard rectangle function of width 1. From a simple geometrical analysis one may show that

$$\mathcal{A}\left(\xi - \frac{v\Delta t}{2}, \eta\right)\mathcal{A}\left(\xi + \frac{v\Delta t}{2}, \eta\right) = \mathrm{rect}\left(\frac{\xi}{a - |v\Delta t|}\right)\mathrm{rect}(\eta/b) \quad \text{for } |v\Delta t| < a; \quad = 0 \quad \text{otherwise.} \quad (10)$$

Hence the instantaneous intensity cross correlation is

$$\lambda(\Delta x, \Delta y, \Delta t) = \frac{1}{S^2}\left|\frac{\sin[\pi(1 - |v\Delta t|/a)a\pi\Delta x/\lambda z]}{\pi\Delta x/\lambda z}\frac{\sin(\pi b\Delta y/\lambda z)}{\pi\Delta y/\lambda z}\right|^2 \quad \text{for } |v\Delta t| < a; \quad = 0 \quad \text{otherwise.} \quad (11)$$

Evaluating S from Eq. (5),

$$S = \iint_{-\infty}^{\infty} |\mathrm{rect}(\xi/a)|^2|\mathrm{rect}(\eta/b)|^2 d\xi\,d\eta = ab, \quad (12)$$

and defining the dimensionless coordinates

$$x_s = \frac{a\Delta x}{\lambda z}, \quad y_s = \frac{b\Delta y}{\lambda z}, \quad (13)$$

where x_s and y_s express the separations in terms of the speckle

size, leads to the relation

$$\Lambda(x_s, y_s, \tau) = \left[\frac{\sin \pi(1 - |v\Delta\tau|, a)x_s}{\pi x_s} \frac{\sin \pi y_s}{\pi y_s}\right]^2 \quad \text{for } |v\Delta\tau| a < 1$$
$$= 0 \quad \text{otherwise.} \tag{14}$$

Note the space–time coupling that prevents factoring $\Lambda(x_s, y_s, \tau)$ into separate space and time functions. Applying Eq. (8) yields

$$\bar{\Lambda}(x_s, y_s, \tau) = \frac{1}{T}\left[\frac{\sin \pi y_s}{\pi y_s}\right]^2 \int_{\Delta\tau_1}^{\Delta\tau_2} \left(1 - \frac{|\Delta\tau - \tau|}{T}\right) \times \left[\frac{\sin(1 - |v\Delta\tau|, a)\pi x_s}{\pi x_s}\right]^2 d\Delta\tau, \tag{15}$$

where

$$\Delta\tau_1 = \max(\tau - T, -a^{-1}), \qquad \Delta\tau_2 = \min(\tau + T, a^{-1}).$$

To simplify this expression, let us introduce a parameter β that measures the relative amount of time integration:

$$\beta = v/Ta. \tag{16}$$

Also, since the space–time coupling affects only the x_s component of the correlation, let us consider only separations along this direction (i.e., set $y_s = 0$). Finally, by choosing a new variable of integration $\tau' = \Delta\tau/T$, we obtain

$$\bar{\Lambda}(x_s, 0, \tau) = \int_{\tau_1}^{\tau_2} \left(1 - \left|\tau' - \frac{\tau}{T}\right|\right) \left[\frac{\sin(1 - \beta|\tau'|)\pi x_s}{\pi x_s}\right]^2 d\tau', \tag{17}$$

where

$$\tau_1 = \max(\tau/T - 1, -\beta^{-1}), \qquad \tau_2 = \min(\tau/T + 1, \beta^{-1}).$$

Equation (17) can be solved analytically or numerically to yield the time-averaged intensity correlation for different values of β. The time integration has two significant effects: the reduction of the variance and the spatial broadening of the correlation.

The variance or zero-point value of the correlation is given by

$$\bar{\sigma}^2 = \bar{\Lambda}(x_s = 0, \tau = 0) = \int_{\tau_1}^{\tau_2} (1 - |\tau'|)(1 - \beta|\tau'|)\, d\tau', \tag{18}$$

where τ_1 and τ_2 are given in Eq. (17). As is shown in Fig. 2, increasing β reduces the variance. This reduction of the variance implies that the far field becomes more incoherent with increased time averaging. This effect is well known and in fact is used to reduce speckle in coherent imaging systems.[3,4]

The second effect is the spreading of the spatial correlation. To show this most clearly, let us renormalize the time-averaged intensity correlation to eliminate the changing variance and select the pure spatial correlation obtained by setting $\tau = 0$. In Fig. 3, the renormalized correlation $\bar{\Lambda}(x_s, 0, 0)/\bar{\sigma}^2$ is plotted for three values of β. The case $\beta = 0$ corresponds to a stationary diffuser with no amount of time averaging or, more importantly, the instantaneous intensity correlation of [illegible]. The curves $\beta = 1$ and $\beta = 100$ show that [illegible]

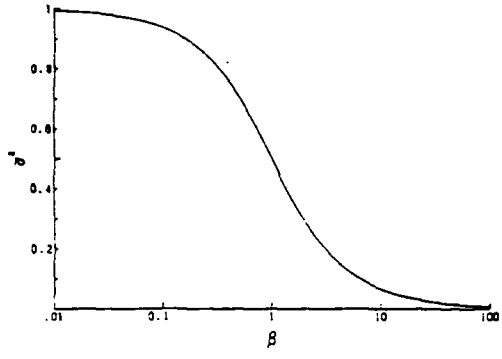

Fig. 2. Variance of the time-averaged intensity cross correlation from a quasi-thermal source. $\beta = v/Ta$ measures the amount of time integration.

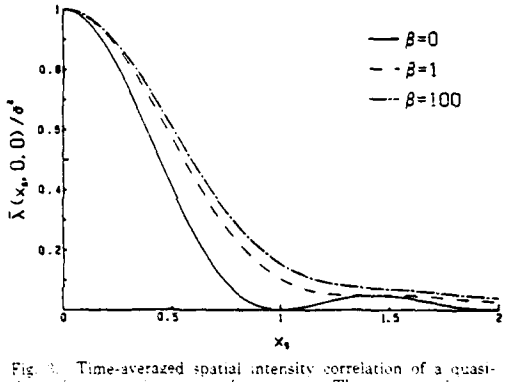

Fig. 3. Time-averaged spatial intensity correlation of a quasi-thermal source with a rectangular aperture. The curves are for various amounts of time integration, β = 0, 1, 100.

relation beyond the instantaneous form. One also sees that the case $\beta = 1$ already represents a significant amount of time integration.

4. APPLICATION TO A GAUSSIAN APERTURE

Quite often the diffuser is directly illuminated with a laser beam; in this case, the appropriate aperture function is

$$A(\xi, \eta) = \frac{1}{2\pi\sigma^2} \exp[(\xi^2 + \eta^2)/2\sigma^2], \tag{19}$$

where σ represents the waist size of the beam. Following an analysis similar to that of Section 3, one obtains the instantaneous intensity cross correlation

$$\Lambda(x_s, y_s, \Delta\tau = 0) = \exp(-2\pi^2 x_s^2 + y_s^2)\exp(-v^2\Delta\tau^2/2\sigma^2), \tag{20}$$

where, in this case,

$$x_s = \frac{\lambda \bar{r}\tau\Delta x}{\Delta\xi}, \qquad y_s = \frac{\lambda \bar{r}\tau\Delta_y}{\Delta\xi}. \tag{21}$$

Here we see that the intensity correlation [illegible]

time-averaged correlation. However, this results from the special properties of the exponential function and does not reflect the general nature of quasi-thermal sources.

5. DISCUSSION

The behavior of the spatial correlation function of time-integrated intensity from a quasi-thermal source, described in Section 3, is quite different from that of a true thermal source. Light propagated from a thermal source, such as a spectrally filtered blackbody with the same intensity at all points on the source, always retains the reducibility property (i.e., it remains cross-spectrally pure), provided that a certain path restriction is obeyed.[21] Thus the shape of the spatial intensity correlation is unaffected by time averaging.

The effect of time integration on the spatial correlation was studied because of its relevance to the original experiments of Hanbury Brown and Twiss[22,23] on intensity interferometry. In those experiments, the time averaging was unavoidable, and it was assumed that the space–time coherence function was reducible; in effect, it was assumed that the spectral intensity across the stellar source was constant. Under this condition of reducibility, the shape of the spatial correlation function was unaffected by time integration, and the usual Van Cittert–Zernike relationship could be used to estimate the angular diameter of the source. As we showed in Section 3 and in Fig. 3, similar experiments using a quasi-thermal source would lead to erroneous estimates of the diameter.

The analysis of Section 3 also illustrates the difference between finite averages over time and over an ensemble. For example, were the diffuser to move in stepwise fashion during the time integration, and if each step presented a completely new section of the diffuser to the illumination region, then the spatial correlation of integrated intensity would retain a constant shape; that is, a finite ensemble average does not yield the same result as a finite time average with uniform diffuser motion.[24] Of course, in the general case, we should assign a velocity function $v(\xi)$ to describe the motion of the diffuser and use the full analytic signal representation for the light.

Although we have reported in this Letter only on the change in shape of the spatial correlation function of time-integrated intensity from a quasi-thermal source, it is obvious that there is a similar effect on the temporal correlation function when spatial integration occurs.

ACKNOWLEDGMENTS

This work was supported by the U.S. Army Research Office under grant DAAG-29-80-K-0045 and by the U.S. Air Force Office of Scientific Research under grant AFOSR-81-0003.

* Also with the Department of Physics and Astronomy, University of Rochester, Rochester, New York 14627.

REFERENCES

1. A. Martienssen and E. Spiller, "Coherence and Fluctuations in Light Beams," Am. J. Phys. 32, 919–926 (1964).
2. M. Roosseau, "Statistical properties of beams of optical fields scattered by random media. Application to the rotating ground glass," J. Opt. Soc. Am. 61, 1707–1713 (1971).
3. J. W. Goodman, in *Laser Speckle and Related Phenomena*, J. C. Dainty, ed., Springer-Verlag, Berlin, 1975, pp. 9–75.
4. M. Born and E. Wolf, *Principles of Optics*, 6th ed., Pergamon, Oxford, 1980, pp. 508–512.
5. J. W. Goodman, "The role of coherence concepts in the study of speckle," Proc. Soc. Photo-Opt. Instrum. Eng. 194, 86–94 (1979).
6. B. Crosignani, B. Daino, and P. DiPorto, "Light scattering by a rotating disk," J. Appl. Phys. 42, 4699–4703 (1971).
7. P. De Santis, F. Gori, G. Guattari, and C. Palma, "An example of a Collett–Wolf source," Opt. Commun. 29, 256–260 (1979).
8. J. D. Farina, L. M. Narducci, and E. Collett, "Generation of highly directional beams from a globally incoherent source," Opt. Commun. 32, 203–208 (1980).
9. W. H. Carter and E. Wolf, "Coherence and radiometry with quasihomogeneous planar sources," J. Opt. Soc. Am. 67, 785–796 (1977).
10. E. Wolf, "Coherence and radiometry," J. Opt. Soc. Am. 68, 6–17 (1978).
11. A. S. Glass and H. P. Baltes, "The significance of far-zone coherence for sources or scatterers with hidden periodicity," Opt. Acta 29, 169–185 (1982).
12. K. M. Baird and H. P. Baltes, "Coherence of radiation scattered by gratings covered by a diffuser," Opt. Acta 28, 1013–1015 (1981).
13. J. C. Leader, "Similarities and distinctions between coherence theory relations and laser scattering phenomena," Opt. Eng. 19, 593–601 (1980).
14. H. M. Pedersen, "Intensity correlation metrology: a comparitive study," Opt. Acta 29, 105–115 (1982).
15. V. V. Anisimov, S. M. Kozel, and G. R. Lokshin, "Space-time statistical properties of coherent radiation scattered by a moving diffuse reflector," Opt. Spectrosc. 27, 258–262 (1969).
16. T. S. McKechnie, "Reduction of speckle in an image by a moving aperture—second order statistics," Opt. Commun. 13, 29–34 (1975).
17. K. A. O'Donnell, "Correlations of time-varying speckle near the focal plane," J. Opt. Soc. Am. 72, 191–197 (1982).
18. For a review of time-varying speckle, see T. Asakura and N. Takai, "Dynamic laser speckles and their application to velocity measurements of the diffuse object," Appl. Phys. 25, 179–194 (1981).
19. J. W. Goodman, *Introduction to Fourier Optics*, McGraw-Hill, New York, 1968, p. 62.
20. A. Papoulis, *Probability, Random Variables, and Stochastic Processes*, McGraw-Hill, New York, 1965, pp. 324–325.
21. L. Mandel, "Concept of cross-spectral purity in coherence theory," J. Opt. Soc. Am. 51, 1342–1350 (1961).
22. R. Hanbury Brown and R. Q. Twiss, "Interferometry of the intensity fluctuations of light. I. Basic theory: the correlation between photons in coherent beams of radiation," Proc. R. Soc. London 242, 300–324 (1957).
23. For a general discussion of intensity correlation interferometry, see L. Mandel, in *Progress in Optics II*, E. Wolf, ed., North-Holland, Amsterdam, 1963, pp. 181–248.
24. J. C. Dainty and W. T. Welford, "Reduction of speckle in image plane hologram reconstructions by moving pupils," Opt. Commun. 3, 289–294 (1971). The rationale of this paper made the erroneous assumption that finite time and finite ensemble averages produced the same spatial correlation function; see Ref. 16.

96 OPTICS LETTERS Vol. 8, No. 2 February 1983

Enforcing irreducibility for phase retrieval in two dimensions

M. A. Fiddy

Department of Physics, Queen Elizabeth College, Campden Hill Road, London W8 7AH, England

B. J. Brames and J. C. Dainty

The Institute of Optics, The University of Rochester, Rochester, New York 14627

Received October 13, 1982

Unique phase recovery from a single two-dimensional intensity data set depends on the complex function's being represented by a globally irreducible entire function. Functions of two complex variables, in general, are likely to be irreducible, but no conditions have been stated to ensure this except for objects consisting of specific arrays of points. A condition based on Eisenstein's criterion for irreducibility is given here that requires two reference points in the object plane.

In one dimension, it is well known that the extent of the ambiguity of phase functions that can be associated with an observed modulus distribution (scattering data, image data, or a coherence function) is expressed by the distribution of complex zeros of the associated analytic function. Unique phase recovery is ensured through zero location, for example, by using a second intensity or prior knowledge about the object, or by the guarantee of a zero-free half-plane, for example, through the addition of a reference wave.[1]

In two dimensions, the field before detection is again analytic, and the phase ambiguity can be expressed by the number of non-self-conjugate irreducible factors in the Osgood product,[2]

$$F(z) = \prod_{m=1}^{N} [F_m(z)e^{\gamma_m}]^{l_m}, \quad N \leq \infty, \quad z = (z_1, z_2),$$

where $F_m(z)$ are globally irreducible factors, e^{γ_m} are convergence factors, γ_m are polynomials, and l_m are integers. It has been shown that the set of polynomial functions of two variables and given degree is a set of measure zero[3]; thus one is tempted to assume that in general $F(z)$ will be irreducible, i.e., that $N = 1$. If this is the case, then a phase unique to within trivial factors can be associated with the observable $|F(x_1, x_2)|^2$.

However, one cannot assume that $F(z)$ is always irreducible, or that reducible $F(z)$ are unimportant,[4] as has been demonstrated.[5,6]

It should be noted that the zeros of $F(z)$ are lines in (z_1, z_2) space and thus extend throughout that space. The use of the Hilbert transform to attempt to construct $\gamma(z)$ from $\log|F(z)|$ will result in a function that, in general, is not even analytic, in distinction from the one-dimensional case.[7] Real and conjugate symmetric factors can occur that do not contribute to the phase ambiguity, and for simply shaped apertures and supports one might expect the asymptotic zeros to reflect these shapes in a reducible function.

Phase-Retrieval Methods in Two Dimensions

In practice, we have data not on continuous variables but only a finite number of discrete samples. Only with an infinite number of samples can a unique representation of $F(z)$ be found; with a finite number of data points an infinite ambiguity is possible unless some estimate for $F(z)$ is selected on the basis of prior knowledge or a chosen model.[8]

Phase-recovery algorithms considered to date include the two-defocus method and those of Gerchberg and Saxton and Fienup. The uniqueness of the first two methods, which require two sets of modulus data, has been discussed.[9] In practice, with sampled data, convergence to the unique solution, if the methods converge at all, is not guaranteed. Fienup's method requires only one modulus data set and, ideally, knowledge of the object support.[10] Only for a nonredundant point-array object can one easily deduce the object support from the autocorrelation support, and in this special case one can also directly determine the point amplitudes[11]; examples of nonredundant arrays have been given by Golay.[12]

We consider here the case for which only one modulus data set is available. The iterative techniques listed above, and hybrid versions of them, have been compared in detail,[13] but for their convergence rather than for possible uniqueness. However, uniqueness of phase is *guaranteed* if we adopt a model for the object based on the Fourier transform's being an irreducible polynomial of degree determined by the number of data points.

Irreducible Polynomials

A polynomial of total degree N in two variables will require $(N + 1)(N + 2)/2$ coefficients and thus this number of data points to represent it uniquely. If we

have N^2 data points, then we may assume that the maximum degree in each variable is $N-1$; thus the N^2 coefficients that are associated with this polynomial. We wish to ensure irreducibility of this polynomial. The example given by Bruck and Sodin[4] in which a reference point is placed to one side of a one-dimensional object array of points ensures irreducibility but is of limited interest.

If the object support is not known, then the simplest step is to assume a constraint for irreducibility outside a simply shaped region within which the object is known to be confined. If the object support is known, a more appropriate and specific constraint can be introduced, and, in addition, it may be possible to model the object by a polynomial of higher degree and thus achieve higher resolution. The following is a sufficient condition for irreducibility of $F(z_1, z_2)$, z complex.

Eisenstein's Criterion.[15] Consider $F(z_1, z_2)$ as a polynomial in z_1, i.e.,

$$F(z_1, z_2) = a_0(z_2) + a_1(z_2)z_1 \ldots a_{N-1}(z_2)z_1^{N-1}.$$

Thus the coefficients are polynomials in z_2. If there exists a prime (irreducible) factor $p(z_2)$, which divides $a_0, a_1 \ldots a_{N-2}$ but not a_{N-1}, and if $p^2(z_2)$ does not divide a_0, then $F(z_1, z_2)$ is irreducible. In C the only prime is of the form $z_2 + b$, where b is complex.

Consider the general form of a polynomial in two variables having maximum powers J and K in z_1 and z_2:

$$F(z_1, z_2) = \sum_0^J \sum_0^K f(j, k) z_1^j z_2^k.$$

The coefficients of the polynomial are samples of the object.[14] We can construct an irreducible polynomial in, for example, the following way. Assume that the region containing the object support is a rectangle defined by $0 \leq j \leq J-1$ and $1 \leq k \leq K$. A single reference point at $(J, 0)$ ensures irreducibility, provided that the point at $(0, 1)$ is nonzero. The simplest prime, z_2, divides all coefficients except that of the z_1^J term, and z_2^2 does not divide the z_1^0 coefficient.

Figure 1 shows the location of the reference points A and B at $(J, 0)$ and $(0, 1)$, respectively. Points A and B should be nonzero. Clearly, if the object support is known, it may be possible in special cases to choose a point on its perimeter as B and then select an optimum location for A chosen by rotating the support and redefining the axes; irreducibility is maintained under any linear transformation.

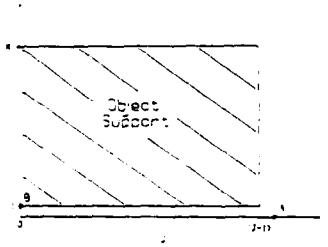

Fig. 1. Sufficient conditions for a two-dimensional array to be irreducible are satisfied when the object is contained within the shaded support and points A and B are nonzero.

Fig. 2. The test object (a) is a 64 × 64 element array with the magnitude of the brightest point normalized to one and point B of Fig. 1 arbitrarily set to one. The result, after 250 iterations, of applying the Fienup algorithm directly to the Fourier modulus and support of (a) is shown in (b). Although certain general features are recognizable, the image has a noisy appearance, which is only slightly reduced by continued iteration. Including point A of Fig. 1 ensures a unique solution, and the Fienup algorithm converges rapidly. Pictures (c) and (d) show the results after 20 iterations for $A = 100$ and $A = 10$, respectively.

The reference function introduced can be arbitrarily close to the object support, provided that the Eisenstein criterion is satisfied. The method has similarities to off-axis holography, a holographic reconstruction failing because of the overlap of the autocorrelation and cross-correlation terms. The object support may be such that this is naturally satisfied.

Implementation of Phase-Retrieval Methods on Irreducible Polynomials

Having shown that our object model generates an irreducible polynomial of degree compatible with the number of data points available, we still have to find a way of recovering the unique phase from the modulus data. It has yet to be proved that, when only one pos-

sible phase function exists, the Fienup algorithm, if it converges, does converge to the correct phase. Nevertheless, we have compared object reconstructions by using this algorithm with and without the reference points of A and B. These are illustrated in Fig. 2. The results are encouraging, showing a rapid convergence with the reference points when there is no sign of convergence to the correct solution without them. The computer simulations indicate that, when a unique phase exists, there is no advantage in imposing the positivity constraint (when relevant) other than to speed up the rate of convergence.

Conclusions

It has been argued that, despite the likelihood of irreducibility for functions of more than one variable, the lack of consistent success of phase-retrieval algorithms suggests that irreducibility should be guaranteed beforehand. In addition, because of the inevitable limitation of discrete data, a model is adopted of a finite-degree irreducible polynomial consistent with the available data. The Eisenstein criterion provides one particular sufficient condition for irreducibility; necessary conditions do not appear to exist, but other sufficient conditions may exist.

Having imposed the irreducibility criterion by adding nonzero reference points to the object, we found that the Fienup algorithm quickly converged to the correct missing phase. This therefore offers a possible means for analyzing the Fienup method to determine necessary conditions for its unique convergence. An analysis in terms of alternating orthogonal projections onto the boundaries of convex sets[16] suggests that, without additional constraints, Feinup's algorithm could reach all solutions that are band limited and have a given modulus; thus, if the number of solutions is guaranteed to be one, the method will work.

This work was supported by the U.S. Air Force Office of Scientific Research under grant AFOSR 81 0003.

References

1. R. E. Burge *et al.* Proc. R. Soc. London Ser. A 350, 191–212 (1976).
2. I. Manoliksakis, J. Math. Phys. (to be published).
3. M. H. Hayes and J. H. McClellan, Proc. IEEE 70, 197–198 (1982).
4. R. H. T. Bates, J. Opt. Soc. Am. (to be published).
5. B. L. McGlamery, RADC Tech. Rep. TR-81-237 (Rome Air Development Center, Griffis AFB, N.Y., 1981).
6. P. van Toorn, A. H. Greenaway, and A. M. J. Huiser (to be published).
7. M. Nieto-Vesperinas, Optik 56, 376–384 (1980).
8. M. A. Fiddy and T. J. Hall, J. Opt. Soc. Am. 71, 1406–1407 (1981).
9. H. A. Ferwerda, AIP Conf. Proc. 65, 402–411 (1980).
10. J. R. Fienup, Opt. Lett. 3, 27–29 (1978).
11. J. R. Fienup, T. R. Crimmins, and W. Holstynski, J. Opt. Soc. Am. 72, 610–624 (1982).
12. M. J. E. Golay, J. Opt. Soc. Am. 61, 272–273 (1971).
13. J. R. Fienup, Appl. Opt. 21, 2758–2769 (1982).
14. Yu. M. Bruck and L. G. Sodin, Opt. Commun. 30, 304–308 (1979).
15. B. L. van der Waerden, *Algebra* (Ungar, New York, 1970), Vol. 1, p. 94.
16. D. C. Youla, Rep. POLY-MRI-1420-81 (Polytechnic Institute of New York, New York, 1981).

Reprinted from Optics Letters, Vol. 8, page 608, December, 1983

Detection of gratings hidden by diffusers using photon-correlation techniques

J. C. Dainty and D. Newman

Department of Physics and Astronomy, University of Rochester, Rochester, New York 14627

Received August 16, 1983

Photon-correlation experiments have verified the theoretical prediction of Baltes *et al.* that a phase grating hidden by a diffuser can be detected by correlation measurements. We have additionally demonstrated that a simpler method of detecting the presence of the grating, valid for arbitrarily fine diffusers, is to measure the temporal autocorrelation of the intensity of the scattered field at a single point.

In a series of recent theoretical papers,[1-10] Baltes and co-workers have shown that the presence of a phase grating placed behind a diffuser can be detected by correlation (coherence) measurements of the scattered radiation, even when a simple intensity measurement does not reveal the grating.

In this Letter, we present measurements of the strengths of the correlation peaks as a function of the diffuser and grating parameters obtained using photon-correlation techniques; our results confirm Baltes's theory.[1-6] We also report measurements of temporal-correlation functions in which the presence of the grating manifests itself as a cosinusoidal modulation.

Measurements are made in the far field of the grating–diffuser plane (see Fig. 1). In the absence of the grating, the diffuser alone would give a broad diffraction cloud of width *inversely proportional* to the correlation length L; the sinusoidal phase grating in the absence of the diffuser would give a series of diffraction orders with an angular separation inversely proportional to the grating period b. With both grating and diffuser present, the diffraction pattern consists of a series of coherently superposed diffraction clouds centered at each diffraction order of the grating, as shown in Figs. 1 and 2. If the ratio L/b is small enough ($L/b < 0.33$), then the average intensity distribution does not reveal the presence of the grating, as shown in Fig. 2(c).

Using one-dimensional notation, we model the complex amplitude in the scattering plane as the product

$$U(\xi) = P(\xi)e^{i\phi(\xi)}T(\xi), \tag{1}$$

where $P(\xi)$ is a real pupil function, $\phi(\xi)$ is the random phase that is due to the diffuser, and $T(\xi)$ is the transmission function of the phase grating. In our case,

$$P(\xi) = I_0^{1/2}\exp(-\xi^2/4a^2), \tag{2}$$

where a is the beam width, and

$$T(\xi) = \exp[i\,\alpha\sin(2\pi\xi/b)], \tag{3}$$

where α is the optical depth and b is the period of the grating. In our experiments, $a = 0.33$ mm, $\alpha \approx 0.85$, and $b = 5.1$ and 9.2 μm.

The diffusers were made in photoresist by multiple exposure to Gaussian speckle patterns[11,12]; this produces a surface height with a Gaussian probability distribution of standard deviation σ_h and a Gaussian correlation function of parameter equal to l_h. If $\sigma_h \gtrsim \lambda$, it can be shown that the correlation function of the complex amplitude transmittance of the diffuser is also approximately Gaussian, with width equal to L (Ref. 13):

$$\langle\exp i[\phi(\xi_1) - \phi(\xi_2)]\rangle \approx \exp(-|\xi_1 - \xi_2|^2/2L^2), \tag{4}$$

where

$$L = l_h\left[\frac{2\pi(n-1)\sigma_h}{\lambda}\right]. \tag{5}$$

λ is the wavelength (633 nm), and n is the refractive index of the photoresist (≈ 1.67). In our experiments, $L = 1.3, 2.5, 3.3, 6.4, 7.1$, and 10.3 μm.

For computational simplicity we expand the grating transmission $T(\xi)$ in a discrete Fourier series:

$$T(\xi) = \exp[i\,\alpha\sin(2\pi\xi/b)] = \sum_{n=-\infty}^{\infty} g_n\exp(i2\pi n\xi/b), \tag{6}$$

where $g_n = J_n(\alpha)$, the Bessel function of the first kind of order n and argument α.

The correlation $\Gamma(x_1, x_2)$ of the complex amplitude in the far field is given by, ignoring the unimportant phase-factor and scaling constants,

$$\Gamma(x_1, x_2) = \int\int_{-\infty}^{\infty} \langle U(\xi_1)U^*(\xi_2)\rangle \times \exp\left[-i\,\frac{2\pi}{\lambda R}(x_1\xi_1 - x_2\xi_2)\right] d\xi_1 d\xi_2. \tag{7}$$

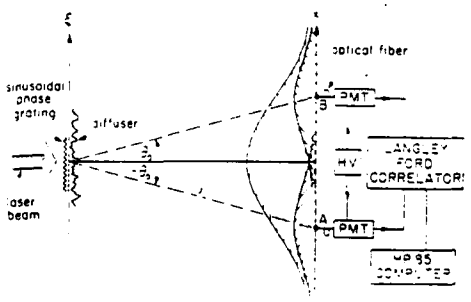

Fig. 1. Experimental arrangement.

0146-9592/83/120608-03$1.00/0

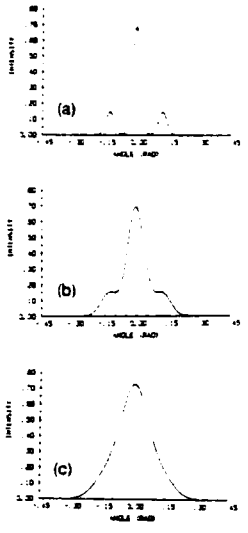

Fig. 2. Theoretical average intensity in the far field of phase grating–diffuser combinations: (a) $L/b = 1.0$, (b) $L/b = 0.50$, and (c) $L/b = 0.33$. (L is the $1/e$ correlation length of the complex amplitude transmittance of the diffuser and b is the period of the sinusoidal phase grating).

and the normalized correlation is defined by

$$\gamma(x_1, x_2) = \frac{\Gamma(x_1, x_2)}{[\Gamma(x_1, x_1)\Gamma(x_2, x_2)]^{1/2}}. \tag{8}$$

Defining the sum and difference coordinates in the far field, $x = (x_1 + x_2)/2$ and $\Delta x = (x_1 - x_2)$, and the angular sum and difference coordinates, $s = x/R = (\sin\theta_1 + \sin\theta_2)/2$ and $\sigma = \Delta x/R = \sin\theta_1 - \sin\theta_2$, we find that a straightforward calculation yields

$$\gamma(s, \sigma) = \frac{\sum_{n,m=-\infty}^{\infty} g_m g_n \exp\left\{-\tfrac{1}{2}k^2a^2\left[\sigma - \frac{(m-n)\lambda}{b}\right]^2\right\} \exp\left\{-\tfrac{1}{2}k^2L^2\left[s - \frac{\frac{1}{2}(m+n)\lambda}{b}\right]^2\right\}}{\left\{\sum_n |g_n|^2 \exp\left[\frac{2\pi^2L^2}{b^2}\left(s + \frac{\sigma}{2} - \frac{n\lambda}{b}\right)^2\right]\right\}^{1/2}\left\{\sum_n |g_n|^2 \exp\left[-\frac{2\pi^2L^2}{b^2}\left(s - \frac{\sigma}{2} - \frac{n\lambda}{b}\right)^2\right]\right\}^{1/2}}, \tag{9}$$

where $k = 2\pi/\lambda$, $s + \sigma/2 = \sin\theta_1$, $s - \sigma/2 = \sin\theta_2$, and we have made use of the fact that $a \gg b$ in evaluating the denominator.

Photon-correlation measurements[14] estimate the normalized correlation, defined by

$$C_I(x_1, x_2) = \frac{\langle I(x_1)I(x_2)\rangle}{\langle I(x_1)\rangle\langle I(x_2)\rangle} - 1. \tag{10}$$

Since $a \gg L$, the far-field speckle has Gaussian statistics, so the intensity and amplitude correlations are simply related[15]:

$$C_I(x_1, x_2) = |\gamma(x_1, x_2)|^2. \tag{11}$$

Although the sums in Eq. (9) appear quite formidable, it turns out that, for $g_n = J_n(\alpha)$, $\alpha \approx 0.35$, only the terms 0, ±1, and ±2 are significant. The average intensity $\Gamma(x_1, x_1) \equiv \Gamma(s = \sin\theta_1, \sigma = 0)$ shows broad peaks centered on the grating diffraction orders; the angular width of these peaks is equal to $(kL)^{-1}$ (see Fig. 2). The amplitude cross-correlation in the so-called "antisymmetric" scan,[3] $\Gamma(x_1, -x_1) \equiv \Gamma(s = 0, \sigma = 2\sin\theta_1)$, shows sharp correlation peaks whenever $\sin\theta_1 = \pm(n\lambda/b)$, i.e., whenever one correlates pairs of diffraction orders. The angular width of the correlation peaks is equal to $(ka)^{-1}$, or a speckle diameter; note that these peaks are usually very narrow compared with the intensity peaks, $(ka)^{-1} \ll (kL)^{-1}$.

Measurements of the peaks of the normalized intensity cross-correlation were made for the antisymmetric scan ($\theta_0 = \lambda/b$), using standard photon-correlation equipment described elsewhere.[16] The diffuser was rigidly translated across the illuminated region, and the spatial correlation at the two angles was estimated from measurements of the temporal cross-correlation at zero time lag. The angular width of the correlation peaks does equal $(ka)^{-1}$, as found (approximately) by Jauch and Baltes[3]; these results are not repeated here. The experimental values of the peak of the normalized intensity cross-correlation are plotted in Fig. 3 for eight different values of the ratio L/b, where L is the correlation length of the complex amplitude transmission of the diffuser and b is the grating period; the theoretical curve [Eqs. (9)–(11)] is also plotted in Fig. 3.

The agreement between theory and experiment in Fig. 3 is excellent. It should be noted that, for values of $L/b \lesssim 0.33$, the average intensity distribution as shown in Fig. 2 does not reveal the presence of the grating; however, the intensity correlation still has a measurable value for $L/b \gtrsim 0.15$, so there is a small but important range of values $0.15 \lesssim L/b \lesssim 0.33$ where the grating is revealed by correlation measurements but not by average intensity measurements.

As our experimental apparatus measures temporal cross-correlations of dynamic speckle intensities, we shall expand the previous ($v = 0$) theory[1–6] and allow the diffuser to have a linear velocity $\mathbf{v} = v_\xi\hat{\xi} + v_\eta\hat{\eta}$, where $\hat{\xi}$ and $\hat{\eta}$ are unit vectors,

$$\phi[\xi(t), \eta(t)] = \phi(\xi - v_\xi\tau, \eta - v_\eta\tau).$$

The only difference here is that the spatiotemporal correlation of the complex amplitude transmission of the diffuser is given by

$$\langle \exp\{i[\phi(\xi_1(t), \eta_1(t)] - \phi[\xi_2(t+\tau), \eta_2(t+\tau)]\}\rangle \approx \exp[-(|\xi_1 - \xi_2 - v_\xi\tau|^2 + |\eta_1 - \eta_2 - v_\eta\tau|^2)/2L^2], \tag{12}$$

where $\sigma_h \gtrsim \lambda$, L is defined by Eq. (5), and time stationarity is assumed. The expression for the amplitude cross-correlation evaluated at coordinates $(s_x, 0, \sigma_x, 0, \tau)$ becomes

$$\mathrm{Re}[\gamma(s_x, 0, \sigma_x, 0, \tau)] \approx \exp(-|v|^2\tau^2/2a^2) \times \sum_{n,m}\left(\cos\left[\frac{2\pi v_\xi\tau}{b}\left(\frac{s_x}{\sin\theta_0} - \frac{n+m}{2}\right)\right] g_n g_m \times \exp\left\{-\tfrac{1}{2}k^2a^2\left[\sigma_x - \frac{(n-m)\lambda}{b}\right]^2\right\} \times \exp\left\{-\tfrac{1}{2}k^2L^2\left[s_x - \frac{\frac{1}{2}(n+m)\lambda}{b}\right]^2\right\}\right). \tag{13}$$

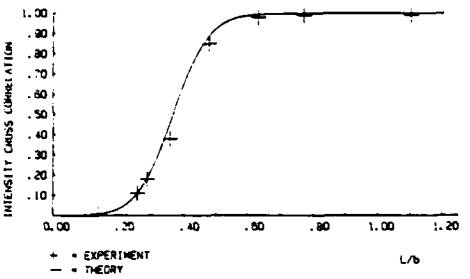

Fig. 3. Peak values of the intensity cross-correlation measured at angles $(-\theta_0, \theta_0)$ as a function of L/b.

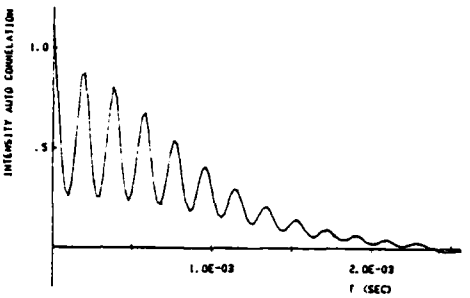

Fig. 4. The temporal-intensity autocorrelation function measured at the center of the far field with parameters $L \approx 1\ \mu m$, $b = 9.2\ \mu m$, $a = 0.33$ mm, $v_\xi \approx 50$ mm sec^{-1}, and $v_\eta \approx 560$ mm sec^{-1}. Note that the period of the modulation is b/v_ξ.

where $\sin\theta_0 = \lambda/b$. The imaginary part of γ has an identical form to expression (13) except that the cosine is replaced by a sine.

A more complete analysis of the spatiotemporal correlation [expression (13)] will be given in a forthcoming paper. Here we evaluate and present a measurement of the intensity autocorrelation at the center of the diffraction field:

$$C_I(0,0,0,0,\tau) \approx \frac{\exp(-\tfrac{1}{4}|\mathbf{v}|^2\tau^2/4a^2)\left[|g_0|^2 + 4|g_1|^2\exp\left(\frac{-2\pi^2L^2}{b^2}\right)\cos\left(\frac{2\pi v_\xi \tau}{b}\right)\right]}{|g_0|^2 + 4|g_1|^2\exp\left(\frac{-2\pi^2L^2}{b^2}\right)}. \quad (14)$$

Thus the intensity temporal autocorrelation has the usual Gaussian envelope[17] $\exp(-\tfrac{1}{4}|\mathbf{v}|^2\tau^2/4a^2)$ of width $\approx 2a/|\mathbf{v}|$, within which there is a cosinusoidal modulation. The period of this modulation is simply b/v_ξ; that is, the period equals the time taken for any point on the diffuser to move across a single spatial period of the grating. The strength of the modulation depends on the Fourier efficients g_0 and g_1 of the series expansion of the grating profile and on the ratio L/b; the modulation is strongest for small values of L/b.

The above analysis shows that detection of the presence of the phase grating and measurement of its period b may easily be achieved by a simple measurement of the intensity temporal-correlation function. Figure 4 shows an example of such a measurement, which is in excellent agreement with theory.

The physical origin of the modulation can be understood by considering a diffuser correlation cell, of linear dimension L, moving across the phase grating of period b. For $L \ll b$, each diffuser element has added to it a periodic phase component, which gives rise in the far field to a strong cosinusoidal modulation of period b/v_ξ. As L increases, the diffuser element still has a periodic component added to it, but the strength of the component is now smaller since it is the value of the phase of the grating averaged over a distance L; thus the modulation disappears as $L/b \to \infty$.

This research was supported by grants from the U.S. Army Research Office (DAAG-29-80-K-0048) and the U.S. Air Force Office of Scientific Research (AFOSR-81-0003).

J. C. Dainty is also with The Institute of Optics, University of Rochester. The address of both authors beginning January 1, 1984, will be Blackett Laboratory, Imperial College, London SW7 2BZ, England.

References

1. H. P. Baltes, H. A. Ferwerda, A. S. Glass, and B. Steinle, Opt. Acta **28**, 11–28 (1981).
2. H. P. Baltes and H. A. Ferwerda, IEEE Trans. Antennas Propag. **AP-29**, 405–406 (1981).
3. H. P. Baltes, A. S. Glass, and K. M. Jauch, Opt. Acta **28**, 873–876 (1981).
4. H. P. Baltes and K. M. Jauch, J. Opt. Soc. Am. **71**, 1434–1439 (1981).
5. A. S. Glass and H. P. Baltes, Opt. Acta **29**, 169–185 (1982).
6. A. S. Glass, H. P. Baltes, and K. M. Jauch, Proc. Soc. Photo-Opt. Instrum. Eng. **369**, 681–686 (1982).
7. K. M. Jauch and H. P. Baltes, Opt. Acta **28**, 1013–1015 (1981).
8. A. S. Glass, Opt. Acta **29**, 575–583 (1982).
9. K. M. Jauch and H. P. Baltes, Opt. Lett. **7**, 127–129 (1982).
10. K. M. Jauch, H. P. Baltes, and A. S. Glass, Proc. Soc. Photo-Opt. Instrum. Eng. **369**, 687–690 (1982).
11. P. F. Gray, Opt. Acta **25**, 765–775 (1978).
12. B. M. Levine and J. C. Dainty, Opt. Commun. **45**, 252–257 (1983).
13. J. W. Goodman, in *Laser Speckle and Related Phenomena*, J. C. Dainty, ed. (Springer-Verlag, Heidelberg, 1975), p. 63.
14. H. Z. Cummins and E. R. Pike, eds., *Photon Correlation and Light Beating Spectroscopy* (Plenum, London, 1974), p. 75.
15. J. C. Dainty, in *Progress in Optics XIV*, E. Wolf, ed. (North-Holland, Amsterdam, 1976), p. 1.
16. K. A. O'Donnell, J. Opt. Soc. Am. **72**, 191–197 (1982).
17. T. Asakura and N. Takai, Appl. Phys. **25**, 179–194 (1981).

7. Stellar Speckle Interferometry

J. C. DAINTY

With 19 Figures

The use of optical interferometry to determine the spatial structure of astronomical objects was first suggested by FIZEAU in 1868 [7.1]. Stellar interferometers measure, in modern terminology, the spatial coherence of light incident upon the Earth, and the object intensity (or some parameter such as its diameter) is calculated using the van Cittert–Zernike theorem [7.2]. FIZEAU's suggestion led to the development of specialized long baseline interferometers; MICHELSON's stellar interferometer [7.3, 4] directly applied Fizeau's method (amplitude interferometry), whilst the intensity interferometer of HANBURY BROWN and TWISS [7.5] enabled the squared modulus of the spatial coherence function to be measured for thermal sources.

Until recently, single optical telescopes were used in a conventional (non-interferometric) way, their spatial resolution being limited to approximately 1".0* due to the presence of atmospheric turbulence or "seeing". In 1970, LABEYRIE invented the technique of stellar speckle interferometry [7.6], in which diffraction-limited resolution is obtained from a large single telescope despite the seeing. The diffraction-limited angular resolution $\Delta\alpha$ of a telescope of diameter D operating at wavelength λ is conveniently expressed by the Rayleigh criterion,

$$\Delta\alpha = 1.22\frac{\lambda}{D}, \tag{7.1}$$

yielding approximately 0".025 at $\lambda = 400$ nm for a 4 m telescope. The first results by LABEYRIE and collaborators were published in 1972 [7.7] and since then approximately 250 papers on speckle interferometry have been published [7.8].

Labeyrie's important contribution was to recognize that the speckles formed at the focus of a large telescope have an angular size determined by diffraction, i.e. their smallest dimension is given by (7.1). Diffraction-limited information about an astronomical object can therefore be extracted from short-exposure, narrow-band images by an appropriate method of data reduction.

* One arc second.

This chapter is divided into six sections. The basic principles are outlined in non-mathematical terms in Sect. 7.1, and this is followed by a detailed mathematical discussion of the technique in Sect. 7.2. In astronomy, the objects under observation are often faint and only a limited observing time is available, so that the question of signal-to-noise ratio is very important; this is evaluated in Sect. 7.3. In Sect. 7.4 we discuss the problem of finding images (or maps) of astronomical objects using speckle data. This is an area of considerable activity at the moment both by theoreticians and observers. The equipment required to implement speckle interferometry is described in Sect. 7.5; this section includes a discussion of the technique of one-dimensional infra-red speckle interferometry which has proved so fruitful in recent years. Finally, we conclude with a brief summary of the astronomical results produced by speckle interferometry—these range from measurements of asteroids to quasars.

Certain topics have been deliberately omitted or are considered only very briefly. Other methods of interferometry, such as rotation-shearing interferometry [7.9] and long baseline interferometry [7.10, 15], are not considered. The discussion in Sect. 7.4 of the phase problem is incomplete due partly to the uncertainty in the field at the moment; a more complete exposition of this subject may be found in the review paper by BATES [7.11] which is complementary in content to this chapter. Earlier reviews of stellar interferometry may be found in [7.12–15]; some useful references are also contained in two conference proceedings [7.16, 17].

7.1 Basic Principles

Figure 7.1 shows highly magnified images of an unresolvable ("point") and a resolved star taken using a large telescope with an exposure time of approximately 10^{-2} s through a filter of bandwidth 10 nm. In the case of the point source (upper row), the image has a speckle-like structure and it is found that, as with conventional laser speckle patterns, the minimum speckle "size" is of the same order of magnitude as the Airy disc of the telescope. A long-exposure image is simply the sum of many short-exposure ones, each with a speckle structure that is different in detail, and is therefore a smooth intensity distribution whose diameter is typically 1″.0 in good seeing. Long-exposure images of the point source and resolved star of Fig. 7.1 would show little, if any, difference. The minimum speckle size, on the other hand, is approximately 0″.025 for a 4 m telescope at a mean wavelength of 400 nm; by extracting correctly the information in short-exposure images, it is possible to observe detail as

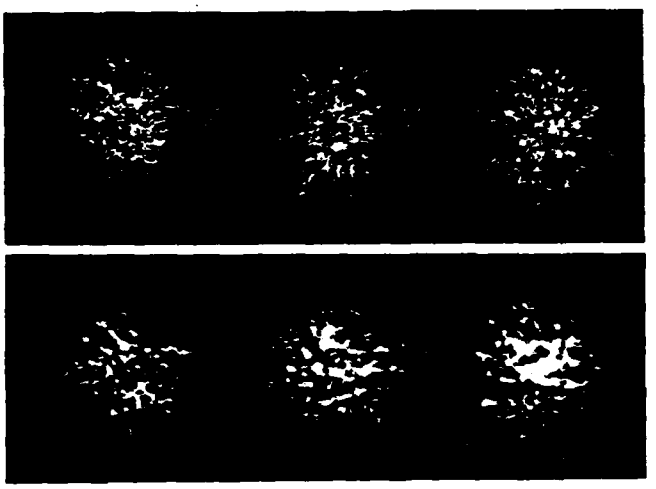

Fig. 7.1. Short exposure photographs of an unresolved point source (*upper row*) and a resolved star, α-Orionis, (*lower row*) taken on a 4 m-class telescope. The exposure time and filter bandwidth are 10^{-2} s and 10 nm, respectively (courtesy of B. L. Morgan and R. J. Scaddan, *Imperial College, London*)

small as the limit imposed by diffraction and not be limited to the 1".0 resolution of conventional images.

A laboratory simulation illustrating the basic method is shown in Fig. 7.2 for an unresolved star, binary stars of two separations, and a resolved star (shown as a uniformly illuminated disc). A large number of short-exposure records are taken, each through a different realization of the atmosphere, typical examples being shown in row B. For a binary star, each component produces an *identical* speckle pattern (assuming isoplanatism and neglecting photon noise) and a "double-speckle" effect may be visible in each short-exposure image in favourable circumstances. The optical diffraction pattern, or squared modulus of the Fourier transform, of a typical short-exposure record is shown in row C for each object. The signal-to-noise ratio is low for a single record and may be improved by adding many such diffraction patterns (row D). The unresolved object has a diffraction halo of relatively large spatial extent, the binaries give fringes of a period inversely proportional to their separation, and the resolved object gives a diffraction halo whose diameter is inversely proportional to the diameter of the object. By taking a further

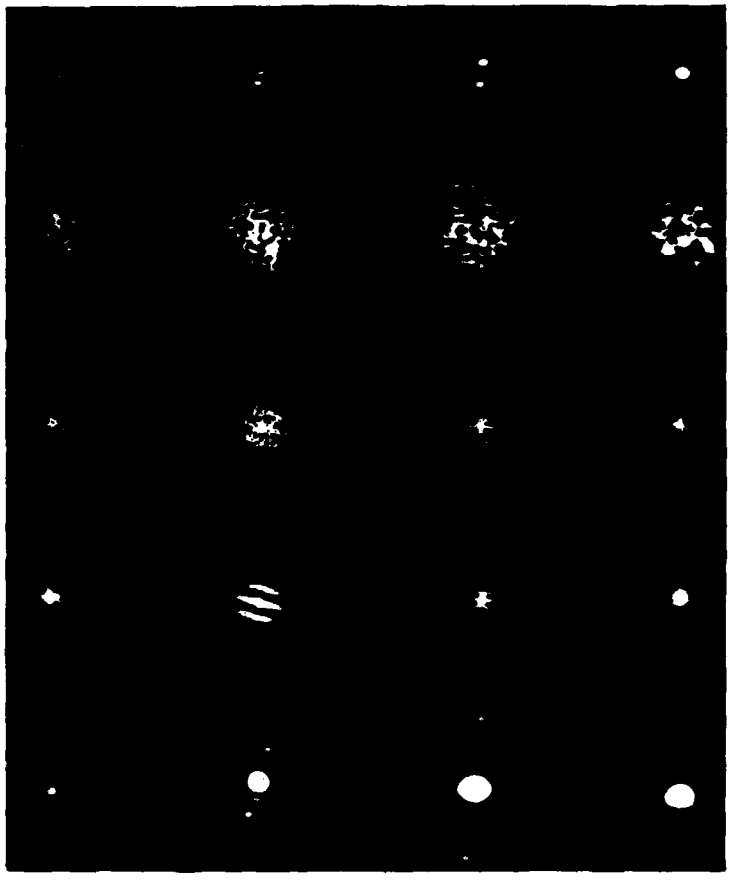

Fig. 7.2A–E. Laboratory simulation showing the principles of stellar speckle interferometry. (A: objects, B: typical short exposure pinnograms; C: diffraction patterns of row B; D: sum of 20 diffraction patterns; E: diffraction pattern of row D) (courtesy of A. Labeyrie, CERGA)

Fourier transform of each ensemble-average diffraction pattern we obtain the average spatial (or angular) autocorrelation of the diffraction-limited images of each object (row E).

The term "speckle interferometry" was adopted by GEZARI et al. [7.7]. The interferometer is, in fact, the telescope—light from all parts of the pupil propagates to the image plane where it interferes to become a speckle pattern. In other forms of stellar interferometry, the light in the pupil is combined in a different way, for example, using a rotation-shearing interferometer. The beauty of the speckle technique is that the interferometer (i.e., the telescope) is already constructed to the required tolerances.

7.2 The Theory of Speckle Interferometry

7.2.1 Outline of Theory

For each short-exposure record, the usual quasi-monochromatic, isoplanatic imaging equation applies, provided that the angular extent of the object is not too large[1]:

$$I(\alpha,\beta)=\int_{-\infty}^{\infty}\int O(\alpha',\beta')P(\alpha-\alpha',\beta-\beta')d\alpha'd\beta'$$

or, in notation,

$$I(\alpha,\beta)=O(\alpha,\beta)\circledast P(\alpha,\beta)\,, \tag{7.2}$$

where $I(\alpha,\beta)$ is the instantaneous image intensity as a function of angle (α,β), $O(\alpha,\beta)$ is the object intensity, $P(\alpha,\beta)$ is the instantaneous point spread function of the atmosphere/telescope system normalized to unit volume, and $\circledast$ denotes the convolution integral.

As we demonstrated in Sect. 7.1, the analysis of this data may be carried out in two equivalent ways. In the angular, or spatial, domain, the ensemble averaged angular autocorrelation function of the image is found; this is defined as

$$C_I(\alpha,\beta)\equiv\left\langle\int_{-\infty}^{\infty}\int I(\alpha',\beta')I(\alpha'+\alpha,\beta'+\beta)d\alpha'd\beta'\right\rangle.$$

or, in notation,

$$C_I(\alpha,\beta)\equiv\langle I(\alpha,\beta)\star I(\alpha,\beta)\rangle\,, \tag{7.3}$$

[1] Throughout this review, the object and image plane coordinates are taken to be angles (α,β), the coordinates in the Fourier transform plane being angular frequencies (arcsec^{-1}).

where $\asymp$ denotes angular autocorrelation. Combining (7.2 and 3) yields the following relationship between object and image autocorrelation functions,

$$C_I(\alpha,\beta) = C_O(\alpha,\beta) \circledast \langle P(\alpha,\beta) \asymp P(\alpha,\beta) \rangle , \tag{7.4}$$

where $C_O(\alpha,\beta)$ is the angular autocorrelation function of the object intensity. Note that (7.4) for the object and image autocorrelation functions is similar in form to (7.2) for object and image intensities, but with an impulse response equal to $\langle P(\alpha,\beta) \asymp P(\alpha,\beta) \rangle$.

In the angular (or spatial) frequency domain, the average squared modulus of the Fourier transform of the image intensity is found: this is correctly referred to as the average energy spectrum,[2]

$$\Phi_I(u,v) \equiv \langle |i(u,v)|^2 \rangle , \tag{7.5}$$

where

$$i(u,v) \equiv \int_{-\infty}^{\infty}\int I(\alpha,\beta) \exp[-2\pi i(u\alpha + v\beta)] d\alpha\, d\beta . \tag{7.6}$$

Combining (7.2, 5 and 6) yields the following simple relationship between the energy spectrum of the image $\Phi_I(u,v)$ and that of the object $\Phi_O(u,v)$:

$$\Phi_I(u,v) = \Phi_O(u,v) \cdot \mathcal{T}(u,v), \tag{7.7}$$

where

$$\mathcal{T}(u,v) \equiv \langle |T(u,v)|^2 \rangle ,$$

and $T(u,v)$, the instantaneous transfer function, is equal to the Fourier transform of the point spread function,

$$T(u,v) = \int_{-\infty}^{\infty}\int P(\alpha,\beta) \exp[-2\pi i(u\alpha + v\beta)] d\alpha\, d\beta . \tag{7.8}$$

Because of the similarity between (7.7) and the Fourier-space isoplanatic imaging equation (in which image frequency components are equal to object frequency components multiplied by an optical transfer function [7.19]), the quantity $\mathcal{T}(u,v)$ is referred to as the transfer function for speckle interferometry or *speckle transfer function*. Equations (7.4 and 7) in the real (angular) and Fourier (angular frequency) domains re-

[2] The *energy spectrum* of a function equals the squared modulus of its Fourier transform. If the function is a realization of a square-integrable non-stationary random process, an *ensemble-averaged energy spectrum* can be defined as in (7.5). A realization of a stationary random process does not possess a Fourier transform, but a *power spectrum* can be defined in terms of a generalized Fourier transform [7.18].

spectively are completely equivalent; (7.7) is simply obtained by taking the Fourier transform of both sides of (7.4).

The conventional ("long-exposure") image intensity is found from (7.2) by ensemble averaging:

$$\langle I(\alpha,\beta)\rangle = O(\alpha,\beta) \circledast \langle P(\alpha,\beta)\rangle , \tag{7.9}$$

where $\langle P(\alpha,\beta)\rangle$ is the average point spread function of the atmosphere/telescope system. In Fourier space, (7.9) becomes

$$\langle i(u,v)\rangle = o(u,v)\langle T(u,v)\rangle , \tag{7.10}$$

where $o(u,v)$ is the Fourier transform of the object intensity, and $\langle T(u,v)\rangle$ is the average, or long-exposure, transfer function.

Comparing conventional long-exposure imaging, (7.10), to speckle interferometry, (7.7), it is clear that the resolution of conventional imaging is governed by the form of the average transfer function $\langle T(u,v)\rangle$, whereas in speckle interferometry the relevant transfer function is $\mathcal{T}(u,v) \equiv \langle |T(u,v)|^2 \rangle$. In the following sections we shall show that the latter function retains high angular-frequency information that is lost in conventional imaging. However, it must be remembered that $\mathcal{T}(u,v)$ is a transfer function for energy spectra, whereas $\langle T(u,v)\rangle$ is a transfer function for Fourier components; the loss of Fourier phase information in speckle interferometry is a severe limitation to its usefulness and possible methods of retrieving the Fourier phase will be discussed in Sect. 7.4.

7.2.2 The Long-Exposure Transfer Function

To find the optical transfer function of a system, we must consider the imaging of a quasi-monochromatic point source as in Fig. 7.3. For an isoplanatic, incoherent imaging system, the optical transfer function $T(u,v)$ is equal to the normalized spatial autocorrelation of the pupil function $H(\xi,\eta)$,

$$T(u,v) = \frac{\int_{-\infty}^{\infty} H(\xi,\eta)H^*(\xi+\lambda u,\eta+\lambda v)d\xi\,d\eta}{\int_{-\infty}^{\infty} |H(\xi,\eta)|^2 d\xi\,d\eta} , \tag{7.11}$$

where (u,v) are angular frequency coordinates, (ξ,η) are distance coordinates in the pupil and λ is the mean wavelength [7.20]. The pupil function $H(\xi,\eta)$ is the complex amplitude in the exit pupil, relative to a reference sphere centered on the Gaussian focus, due to a point source

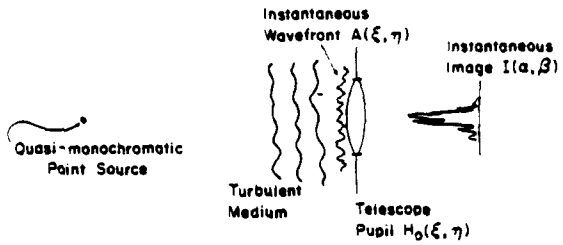

Fig. 7.3. The formation of an instantaneous image of a point source through the atmosphere

and in the case of propagation through the turbulent atmosphere may be written as

$$H(\xi,\eta) = A(\xi,\eta)H_0(\xi,\eta), \tag{7.12}$$

where $A(\xi,\eta)$ is the complex amplitude of light from a point source that has propagated through the atmosphere and $H_0(\xi,\eta)$ is the pupil function of the optical system alone.

Substitution of (7.12) into (7.11) gives

$$T(u,v) = \frac{\int_{-\infty}^{\infty}\int A(\xi,\eta)A^*(\xi+\lambda u,\eta+\lambda v)H_0(\xi,\eta)H_0^*(\xi+\lambda u,\eta+\lambda v)d\xi\,d\eta}{\int_{-\infty}^{\infty}\int |A(\xi,\eta)|^2\,|H_0(\xi,\eta)|^2 d\xi\,d\eta}. \tag{7.13}$$

The long-exposure or average transfer function is found by averaging (7.13). The lower line is simply the intensity of light integrated over the telescope pupil and is effectively constant for a large telescope and/or weak scintillation. We also assume that $A(\xi,\eta)$ is a (wide-sense) stationary process [i.e., its mean and autocorrelation function in (7.13) are independent of the ξ,η coordinates], so that the expression for the long-exposure transfer function becomes [7.21]

$$\langle T(u,v)\rangle = T_s(u,v)T_0(u,v), \tag{7.14}$$

where $T_s(u,v)$ is the atmospheric or "seeing" transfer function,

$$T_s(u,v) = \frac{\langle A(\xi,\eta)A^*(\xi+\lambda u,\eta+\lambda v)\rangle}{\langle |A(\xi,\eta)|^2\rangle}. \tag{7.15}$$

and $T_0(u, v)$ is the optical transfer function of the telescope alone,

$$T_0(u, v) = \frac{\int\int_{-\infty}^{\infty} H_0(\xi, \eta) H_0^*(\xi + \lambda u, \eta + \lambda v) d\xi\, d\eta}{\left\langle \int\int_{-\infty}^{\infty} |H_0(\xi, \eta)|^2 d\xi\, d\eta \right\rangle}. \tag{7.16}$$

Thus the long-exposure transfer function is equal to the product of the transfer functions of the atmosphere and telescope.

A detailed discussion of the atmospheric transfer function and other relevant properties of turbulence may be found in [7.22–25], particularly in the comprehensive review by RODDIER [7.24]. For a Kolmogorov spectrum of turbulence, the average transfer function is rotationally symmetric and is given by

$$T_s(w) = \exp\left[-3.44\left(\frac{\lambda|w|}{r_0}\right)^{5/3}\right], \tag{7.17}$$

where $w = \sqrt{u^2 + v^2}$ and the parameter r_0, first defined by FRIED [7.22], is equal to the diameter of the diffraction-limited telescope whose Airy disc has the same area as the seeing disc. The parameter r_0 plays an important role in both long-exposure imaging and speckle interferometry; it can be shown that [7.24]

$$r_0 \propto \lambda^{6/5}(\cos\gamma)^{3/5}, \tag{7.18}$$

where γ is the zenith angle. Typical values of r_0 lie in the range 5 to 20 cm at a good observing site in the visible range; since an r_0 value of 10 cm at $\lambda = 500$ nm is equivalent to $r_0 = 3.6$ m at $\lambda = 10\,\mu$m, it follows that a 4 m class telescope is severely seeing-limited in the visible but essentially diffraction-limited at 10 μm.

The angular "diameter" of the seeing disc, or seeing angle ω, is defined by

$$\omega \equiv \frac{\lambda}{r_0}, \tag{7.19}$$

and is therefore proportional to $\lambda^{-1/5}$. At $\lambda = 500$ nm and $r_0 = 10$ cm, the seeing disc has a diameter of approximately 5×10^{-6} rad or 1".0.

Measurements of the long-exposure transfer function and the parameter r_0 have been reported by DAINTY and SCADDAN [7.26], RODDIER [7.27], and BROWN and SCADDAN [7.28] and there is good agreement with (7.17).

7.2.3 The Speckle Transfer Function

The transfer function of speckle interferometry, $\mathcal{T}(u,v) \equiv \langle |T(u,v)|^2 \rangle$, relates the average energy spectrum of the image to that of the object. Using (7.13), we can write $|T(u,v)|^2$ as $|T(u,v)|^2 = \mathcal{A}(u,v)/\mathcal{B}$, where

$$\mathcal{A}(u,v) = \int\int\int\int_{-\infty}^{\infty} A(\xi_1,\eta_1)A^*(\xi_1+\lambda u,\eta_1+\lambda v)A^*(\xi_2,\eta_2) \cdot A(\xi_2+\lambda u,\eta_2+\lambda v)H_0(\xi_1,\eta_1)H_0^*(\xi_1+\lambda u,\eta_1+\lambda v) \cdot H_0^*(\xi_2,\eta_2)H_0(\xi_2+\lambda u,\eta_2+\lambda v)d\xi_1 d\eta_1 d\xi_2 d\eta_2$$

and

$$\mathcal{B} = \left[\int\int_{-\infty}^{\infty} |A(\xi,\eta)|^2 |H_0(\xi,\eta)|^2 d\xi\, d\eta\right]^2. \tag{7.20}$$

As before, $A(\xi,\eta)$ is assumed to be a stationary random process with weak scintillation; for convenience we define $\langle |A|^2 \rangle \equiv 1$ and the pupil area $\mathcal{S}$,

$$\mathcal{S} \equiv \int\int_{-\infty}^{\infty} |H_0(\xi,\eta)|^2 d\xi\, d\eta \tag{7.21}$$

(this is the true pupil area for an unapodized, or clear, pupil).

With the substitution $\xi' = \xi_2 - \xi_1$ and $\eta' = \eta_2 - \eta_1$, (7.20) yields the following expression for the speckle transfer function:

$$\mathcal{T}(u,v) = \mathcal{S}^{-2} \int\int_{-\infty}^{\infty} \mathcal{M}(u,v;\xi',\eta')\mathcal{H}(u,v;\xi',\eta')d\xi' d\eta',$$

where $\mathcal{M}$ is a fourth-order moment,

$$\mathcal{M}(u,v;\xi',\eta') \equiv \langle A(\xi_1,\eta_1)A^*(\xi_1+\lambda u,\eta_1+\lambda v)A^*(\xi_1+\xi',\eta_1+\eta') \cdot A(\xi_1+\xi'+\lambda u,\eta_1+\eta'+\lambda v)\rangle \tag{7.22}$$

and

$$\mathcal{H}(u,v;\xi',\eta') = \int\int_{-\infty}^{\infty} H_0(\xi_1,\eta_1)H_0^*(\xi_1+\lambda u,\eta_1+\lambda v) \cdot H_0^*(\xi_1+\xi',\eta_1+\eta')H_0(\xi_1+\xi'+\lambda u,\eta_1+\eta'+\lambda v)d\xi_1 d\eta_1.$$

Clearly, the quantity $\mathcal{M}$ characterizes the atmospheric contribution and $\mathcal{H}$ the telescope contribution to the speckle transfer function.

Further simplification of (7.22) requires that an assumption about the joint probability distribution of the process $A(\xi,\eta)$ be made. The most

satisfactory distribution is the log normal, in which the log modulus and phase each have a Gaussian probability density. KORFF [7.29] evaluated the speckle transfer function using this model and results will be shown below; however, neither this model or the zero-scintillation versions of it [7.24] have a simple analytical solution and require extensive numerical calculations.

In order to illustrate in a qualitative way the form of the speckle transfer function, we shall assume that $A(\xi,\eta)$ is a complex Gaussian process [7.30]. This is a poor assumption in good seeing, although it improves as the seeing deteriorates; this assumption also violates the weak scintillation requirement for normalization. For a complex Gaussian process, the fourth-order moment of (7.22) reduces to a product of second-order moments

$$\begin{aligned}\mathscr{M}(u,v;\xi',\eta') = &\langle A(\xi_1,\eta_1)A^*(\xi_1+\lambda u,\eta_1+\lambda v)\rangle\\ &\cdot\langle A^*(\xi_1+\xi',\eta_1+\eta')A(\xi_1+\xi'+\lambda u,\eta_1+\eta'+\lambda v)\rangle\\ &+\langle A(\xi_1,\eta_1)A^*(\xi_1+\xi',\eta_1+\eta')\rangle\\ &\cdot\langle A^*(\xi_1+\lambda u,\eta_1+\lambda v)A(\xi_1+\xi'+\lambda u,\eta_1+\eta'+\lambda v)\rangle,\end{aligned}$$

which, when substituted into (7.22) yields

$$\begin{aligned}\mathscr{T}(u,v) = &|T_s(u,v)|^2|T_0(u,v)|^2+\mathscr{S}^{-2}\int_{-\infty}^{\infty}\int|T_s(\xi'/\lambda,\eta'/\lambda)|^2\\ &\cdot\mathscr{H}(u,v;\xi',\eta')d\xi'd\eta'.\end{aligned}\tag{7.23}$$

Now $|T_s(\xi'/\lambda,\eta'/\lambda)|^2$ is of width of order r_0/λ and $\mathscr{H}$ is essentially constant for such values of ξ',η', provided that $\sqrt{u^2+v^2}<(D-r_0)/\lambda$. The second term of (7.23) therefore reduces to

$$\mathscr{S}^{-2}\int_{-\infty}^{\infty}\int|T_s(\xi'/\lambda,\eta'/\lambda)|^2d\xi'd\eta'\times\mathscr{H}(u,v;0,0),\tag{7.24}$$

except for $\sqrt{u^2+v^2}>(D-r_0)/\lambda$.

The first integral in (7.24) can be evaluated using (7.17) to give $0.109\pi r_0^2$; the quantity $\mathscr{H}(u,v;0,0)$ is simply

$$\mathscr{H}(u,v;0,0)=\int_{-\infty}^{\infty}\int|H_0(\xi_1,\eta_1)|^2|H_0(\xi_1+\lambda u,\eta_1+\lambda v)|^2d\xi_1d\eta_1,$$

which, when multiplied by $\mathscr{S}^{-1}$ is the *diffraction-limited* optical transfer function $T_D(u,v)$ for an unapodized, or clear, pupil; and finally, the remaining $\mathscr{S}^{-1}$ equals $4/\pi D^2$.

Thus the expression for the speckle transfer function reduces to

$$\mathcal{T}(u,v)=|\langle T(u,v)\rangle|^2+0.435(r_0/D)^2T_D(u,v), \tag{7.25}$$

or, defining the number of speckles as

$$N_{sp}=2.3\left(\frac{D}{r_0}\right)^2,$$
$$\mathcal{T}(u,v)=|\langle T(u,v)\rangle|^2+\frac{1}{N_{sp}}T_D(u,v). \tag{7.26}$$

In both equations it is assumed that $\sqrt{u^2+v^2}\leqq(D-r_0)/\lambda$.

The essential feature of the speckle transfer function, (7.25 or 26), is that there is a term proportional to the diffraction-limited optical transfer function, that extends almost up to the diffraction-limited cut-off D/λ; expressions (7.25 and 26) indicate that this result is *independent of telescope aberrations* [7.30], although there is, in fact, a weak dependence on aberrations to be discussed in Sect. 7.2.4. With $D\cong 4$ m and $r_0\cong 0.1$ m,

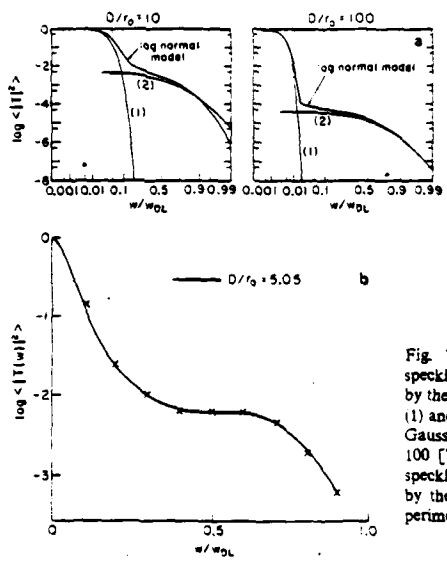

Fig. 7.4. (a) Comparison of the speckle transfer function predicted by the log normal model with terms (1) and (2) of (7.26) for the complex Gaussian model, for $D/r_0\approx 10$ and 100 [7.49]. (b) Comparison of the speckle transfer function predicted by the log normal model with experimental results [7.32]

the number of speckles N_{sp} is approximately 3.7×10^3, indicating that the diffraction-limited information in the image may be carried with a low signal-to-noise ratio. However, the normalization of (7.25, 26) to unity at zero spatial frequency gives a misleading impression of the signal-to-noise ratio which is best evaluated by other methods (Sect. 7.3).

Since (7.25, 26) are based on the assumption that $A(\xi, \eta)$ is a complex Gaussian process, they give only the qualitative behaviour of the transfer function. The speckle transfer function can be calculated using the log normal model and these results are compared to (7.26) in Fig. 7.4a for $D/r_0 = 10$ and 100 [7.49]; the main differences lie in the region between the low- and high-frequency terms. In fact, at low spatial frequencies, the correct asymptotic form of the speckle transfer function is $|\langle T \rangle_{SE}|^2$, where $\langle T \rangle_{SE}$ is the so called "short-exposure" average [7.22, 29] (i.e., the average when each point image is re-centered). Careful measurements by ABME et al. [7.31] and CHELLI et al. [7.32] are in excellent agreement with the log normal model, particularly if the effect of the central obstruction and the (small) effect of defocus are allowed for. Fig. 7.4b shows the result of a measurement in the infra-red.

7.2.4 Effect of Aberrations

Telescope aberrations have two potential effects on the speckle transfer function. If they are very severe, optical-path differences greater than the coherence length of the light may be introduced and this would lead to a strong attenuation of the transfer function. A proper analysis of this effect requires a detailed consideration of temporally partially coherent imaging; this is not carried out here since the effects in normal circumstances are small, as the following analysis shows.

Consider the simplest aberration—*defocus*—of magnitude m waves at the edge of the pupil; the longitudinal and angular transverse ray aberrations Δz and $\Delta\alpha$, respectively, are given by

$$\Delta z = \frac{8m\lambda f^2}{D^2}$$

and (7.27)

$$\Delta\alpha = \frac{8m\lambda}{D}.$$

Under most observing conditions, focus can be established to a tolerance $\Delta\alpha$ of less than 1".0, giving a maximum value of m of approximately 5λ for a 4 m telescope. The coherence length l_c of light of bandwidth $\Delta\lambda$ is given

approximately by

$$l_c \cong \frac{\bar{\lambda}^2}{\Delta\lambda}, \tag{7.28}$$

and with typical bandwidths ($\Delta\lambda = 20$ nm, $\bar{\lambda} = 500$ nm) it is clear that $l_c > m\lambda$. In practice, aberrations only introduce path differences greater than the coherence length if the bandwidth is large or the aberrations are severe.

Aberrations also affect the shape of the speckle transfer function in the quasi-monochromatic case; their effect reduces as the ratio D/r_0 increases and disappear in the limit $D/r_0 \to \infty$. The effect of several aberrations was investigated by DAINTY [7.33] using the complex Gaussian model for the atmospheric turbulence. More precise calculations for defocus and astigmatism were made by RODDIER et al. [7.34] using the log normal model and were compared to the measurements of KARO and SCHNEIDERMAN [7.35]. These results are shown in Fig. 7.5: it should be emphasized that the defocus in this case was made artifically large to illustrate the effect, with $m \cong 6.4\lambda$ corresponding to an angular transverse ray aberration (of extremal rays) of $\Delta\alpha \cong 3''.3$.

For aberrations other than defocus, intuitive reasoning based on the approximations necessary to obtain (7.25, 26) suggests that the effect of aberrations is small if the seeing disc is larger than the point spread function due to telescope aberrations alone. Thus, a telescope of poor optical quality achieves *diffraction-limited* angular resolution if suf-

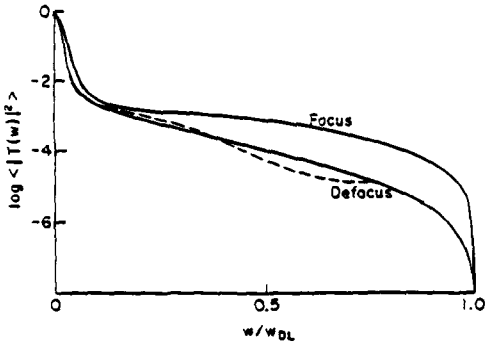

Fig. 7.5. *Solid lines*—theoretical speckle transfer functions for $D/r_0 = 19.2$ in focus and defocused by 6.4λ. *Broken line*—curve observed by Karo and Schneiderman under defocused conditions [7.34]

ficiently severe atmospheric turbulence (real or artificially induced) is present [7.30]. Unfortunately, poor seeing (small r_0) also results in a low signal-to-noise ratio (Sect. 7.3).

7.2.5 Effect of Exposure Time

In practice, each image is the result of a finite exposure time Δt, which always has the effect of attenuating the speckle transfer function. Let the instantaneous point spread function at time t be denoted $P(\alpha, \beta, t)$ and the instantaneous transfer function be $T(u, v, t)$. The speckle transfer function for instantaneous exposures ($\Delta t \to 0$) is defined by

$$\mathscr{T}(u, v) \equiv \langle |T(u, v, t)|^2 \rangle , \tag{7.29}$$

whereas for an exposure time Δt it is equal to

$$\mathscr{T}_{\Delta t}(u, v) = \frac{1}{\Delta t^2} \int_0^{\Delta t} \int \langle T^*(u, v, t) T(u, v, t') \rangle dt\, dt' . \tag{7.30}$$

The term $\langle \cdot \rangle$ in (7.30) is called the temporal cross-energy spectrum and plays an important role in time-integration effects. Assuming temporal stationarity of the process $T(u, v, t)$, (7.30) may also be written

$$\mathscr{T}_{\Delta t}(u, v) = \frac{1}{\Delta t} \int_{-\Delta t}^{+\Delta t} \left(1 - \frac{|\tau|}{\Delta t}\right) \langle T^*(u, v, t) T(u, v, t + \tau) \rangle d\tau . \tag{7.31}$$

The finite exposure time speckle transfer function, $\mathscr{T}_{\Delta t}(u, v)$, is always less than (or equal to) the instantaneous transfer function $\mathscr{T}(u, v)$, as the following analysis shows [7.36]. The Schwartz inequality implies that

$$|\langle T^*(u, v, t) T(u, v, t + \tau) \rangle| \leqq \langle |T(u, v, t)|^2 \rangle$$

so that, using (7.31),

$$\begin{aligned} \mathscr{T}_{\Delta t}(u, v) &\leqq \frac{1}{\Delta t} \int_{-\Delta t}^{+\Delta t} \left(1 - \frac{|\tau|}{\Delta t}\right) |\langle T^*(u, v, t) T(u, v, t + \tau) \rangle| d\tau \\ &\leqq \frac{1}{\Delta t} \int_{-\Delta t}^{+\Delta t} \left(1 - \frac{|\tau|}{\Delta t}\right) \langle |T(u, v, t)|^2 \rangle d\tau \\ &= \langle |T(u, v, t)|^2 \rangle \equiv \mathscr{T}(u, v) , \end{aligned}$$

i.e.,

$$\mathscr{T}_{\Delta t}(u, v) \leqq \mathscr{T}(u, v) . \tag{7.32}$$

This is a general result which is independent of the detailed nature of the turbulence. The magnitude of the attenuation of $\mathcal{T}(u, v)$ due to an exposure time Δt depends, from an experimental point of view, on the form of the temporal cross-energy spectrum $\langle T^*(u, v, t)T(u, v, t+\tau)\rangle$; only qualitative estimates of this function have been reported [7.37].

The temporal cross-energy spectrum is equal to the Fourier transform of the spatially averaged space-time[3] intensity correlation function.

$$\langle T^*(u, v, t)T(u, v, t+\tau)\rangle = \int_{-\infty}^{\infty}\int\left[\int_{-\infty}^{\infty}\int\langle P(\alpha, \beta, t)P(\alpha+\Delta\alpha, \beta+\Delta\beta, t+\tau)\rangle d\alpha d\beta\right] \cdot \exp[-2\pi i(u\Delta\alpha + v\Delta\beta)]d\Delta\alpha d\Delta\beta, \tag{7.33}$$

where $\langle P(\alpha, \beta, t)P(\alpha+\Delta\alpha, \beta+\Delta\beta, t+\tau)\rangle$ is the space-time cross-correlation function of the instantaneous point spread function. A few measurements of the spatially integrated space-time cross-correlation function have been made [7.38, 39]. They show that, in general, this function is not cross-spectrally pure, so that it cannot be written as the product of two separable functions of (u, v) and t,

$$\langle T^*(u, v, t)T(u, v, t+\tau)\rangle \neq \mathcal{T}(u, v)C(\tau). \tag{7.34}$$

(This result is referred to in Sect. 7.3.3 on the optimum exposure time.)

When $\Delta\alpha = \Delta\beta = 0$, the space-time cross-correlation is simply equal to the temporal autocorrelation of the point spread function $\langle P(\alpha, \beta, t)P(\alpha, \beta, t+\tau)\rangle$. Several measurements of this function have been reported [7.38–41] and a sample of results taken at Mauna Kea, Hawaii, are shown in Fig. 7.6; the average correlation time of the image intensity was 15 ms (61 cm telescope). In site testing for new locations for stellar interferometry, it is important to measure both the spatial and temporal properties of seeing.

Although it is the cross-energy spectrum that most directly influences the effect of a finite exposure time Δt, from a more fundamental point of view the important quantity is the fourth order correlation function of the complex amplitude in the pupil:

$$\langle A(\xi, \eta, t)A^*(\xi+\xi_1, \eta+\eta_1, t) \cdot A^*(\xi+\xi_2, \eta+\eta_2, t+\tau)A(\xi+\xi_3, \eta+\eta_3, t+\tau)\rangle \tag{7.35}$$

[3] As given in (7.33), this is an angle-time correlation function; the name space-time is more widely used, distances (x, y) in the image plane being related to angles (α, β) by $x = \alpha f$, $y = \beta f$, where f is the focal length.

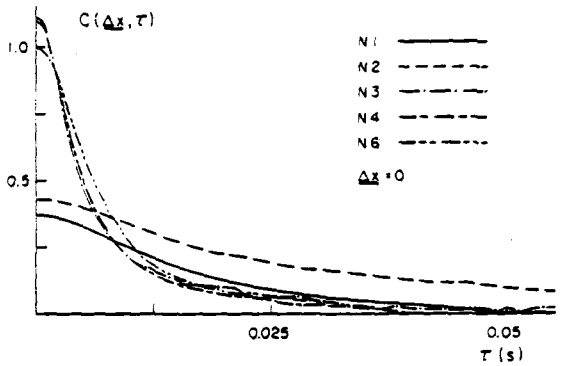

Fig. 7.6. Temporal image intensity autocorrelations over 5 nights at Mauna Kea, Hawaii, measured using a 61 cm telescope [7.39]

[compare with the expression for $\mathcal{M}$ in (7.22)]. For both complex Gaussian and log normal complex amplitude, this fourth order moment is determined by the behaviour of the second order moment. RODDIER and coworkers [7.42, 43] have calculated the effect of a finite exposure time on the speckle transfer function using the log-normal model and the assumption that the complex amplitude $A(\xi, \eta, t)$ moves rigidly across the telescope pupil (the Taylor approximation). For a velocity v along the ξ axis,

$$\langle A(\xi, \eta, t) A^*(\xi + \Delta\xi, \eta + \Delta\eta, t + \tau) \rangle = f(\Delta\xi - v\tau, \Delta\eta), \tag{7.36}$$

For a telescope of diameter D, a velocity v of the turbulence implies a characteristic image time scale of D/v; the results in [7.42] show that the attenuation of the transfer function is not too severe provided that $\Delta t < D/v$.

Spatio-temporal measurements (of $|A|^2$) imply that, in addition to the rigid translation described by (7.36), there is also a strong decorrelation due to "boiling" of $A(\xi, \eta, t)$. This can be explained by a multilayer model for the turbulence [7.24] with a velocity distribution Δv of the atmospheric layers; this leads to a characteristic time scale of $r_0/\Delta v$ and a uniform attenuation of the high-frequency part of the speckle transfer function.

KARO and SCHNEIDERMAN [7.44] have measured the effect of a finite exposure time on the speckle transfer function; their results obtained on

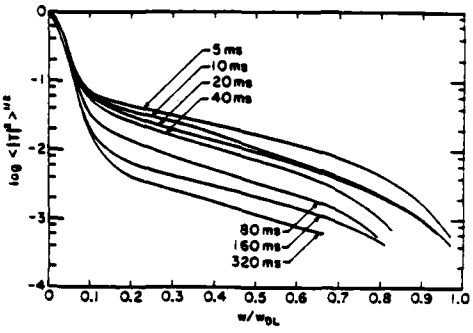

Fig. 7.7 The effect of finite exposure time on the speckle transfer function [7.44]

the 1.6 m telescope at Maui, Hawaii, are shown in Fig. 7.7. Unfortunately, the spatio-temporal atmospheric data required to compare these measurements with theory were not available. However, the uniform attenuation suggests that the wavefront "boiling" dominated over simple rigid translation and implies a time-scale consistent with $r_0/\Delta v \cong 20$ ms.

7.2.6 Effect of Finite Bandwidth

A finite bandwidth $\Delta\lambda$, centered at $\bar{\lambda}$, has two effects both of which attenuate the speckle transfer function. These effects are identical to those observed in polychromatic laboratory-generated Fraunhofer plane speckle patterns discussed in Chap. 3. The two effects are (i) a radial dispersion effect similar to that produced by a grating and (ii) a loss of speckle contrast caused by atmospheric (or, possibly, telescope induced) optical path differences being comparable to the coherence length $l_c \equiv \bar{\lambda}^2/\Delta\lambda$ of the radiation.

In accordance with simple first order grating theory, a spread of wavelengths $\Delta\lambda/\bar{\lambda}$ causes a spread in diffraction angles $\Delta\omega/\bar{\omega}$,

$$\frac{\Delta\omega}{\bar{\omega}} = \frac{\Delta\lambda}{\bar{\lambda}}.$$

Taking $\bar{\omega}$ to be the seeing angle λ/r_0 (7.19), and defining ω_0 to be the angular diameter of a speckle ($\equiv \lambda/D$), we find that the fractional radial

elongation of speckles, $\Delta\omega/\omega_0$ at the seeing angle to be given by

$$\frac{\Delta\omega}{\omega_0} = \frac{\Delta\lambda}{\bar{\lambda}} \frac{D}{r_0}.$$

To determine a criterion for the maximum permissable value of $\Delta\lambda/\bar{\lambda}$, we require that $\Delta\omega/\omega_0 < 1$, yielding

$$\left[\frac{\Delta\lambda}{\bar{\lambda}}\right]_1 < \frac{r_0}{D}. \tag{7.37}$$

In order to calculate a criterion for coherence length effects to be negligible, we require a formula for the root-mean-square optical path fluctuation $\sigma_s(\xi)$ between two points spaced ξ apart in the telescope pupil; the Kolmogorov theory [7.24] predicts that

$$\sigma_s(\xi) \cong 0.42\bar{\lambda}\left(\frac{\xi}{r_0}\right)^{5/6}, \tag{7.38}$$

in which $\sigma_s(\xi)$ is in fact independent of wavelength since $r_0 \propto \lambda^{6/5}$. Thus over a telescope aperture of diameter D we may estimate σ_s by substituting $\xi = D$ in (7.38); requiring that the coherence length $l_c > \sigma_s$, we obtain

$$\left[\frac{\Delta\lambda}{\bar{\lambda}}\right]_2 < 2.4\left(\frac{r_0}{D}\right)^{5/6}. \tag{7.39}$$

Other, more stringent, criteria have been suggested [7.23]. For a typical $r_0 = 0.1$ m and $D = 4$ m, criteria (7.37, 39) yield

$$\left[\frac{\Delta\lambda}{\bar{\lambda}}\right]_1 < 0.025, \quad \left[\frac{\Delta\lambda}{\bar{\lambda}}\right]_2 < 0.111,$$

implying that the chromatic dispersion effect is dominant and that, for $\bar{\lambda} = 500$ nm, the bandwidth $\Delta\lambda$ should be less than 12.5 nm.

Measurements by KARO and SCHNEIDEMAN [7.44] with $D/r_0 \cong 14$ show no discernable effect on the speckle transfer function for $\Delta\lambda/\bar{\lambda} < 0.06$; this is consistent with $[\Delta\lambda/\bar{\lambda}]_1 < 0.07$ given by criterion (7.37). Even for $\Delta\lambda/\bar{\lambda} \cong 0.14$, the mid-frequencies of $\mathcal{T}(u, v)$ were attenuated by only a factor of two.

Since the chromatic dispersion effect is important, it may be worthwhile to design a relay optical system that removes the dispersion [7.45].

Various optical systems have been suggested for this [7.46], but they suffer by having a very small effective field angle and no design has yet been successfully incorporated into a speckle camera system.

7.2.7 Isoplanicity

If a linear system is non-isoplanatic (i.e., if its point spread function depends on both object and image coordinates), then the elementary convolution relationship of (7.2) is replaced by

$$I(\alpha,\beta)=\int_{-\infty}^{\infty}\int O(\alpha',\beta')P(\alpha-\alpha',\beta-\beta';\alpha',\beta')d\alpha'\,d\beta', \tag{7.40}$$

where $P(\Delta\alpha,\Delta\beta;\alpha',\beta')$ is the instantaneous point spread function for an object point at (α',β'). There is now no meaningful concept of an instantaneous transfer function or a speckle transfer function. However, defining $T(u,v;\alpha',\beta')$ to be the Fourier transform of $P(\alpha-\alpha',\beta-\beta';\alpha',\beta')$ with respect to the variables (α,β), the average image energy spectrum $\Phi_i(u,v)$ reduces to

$$\Phi_i(u,v)\equiv\langle|i(u,v)|^2\rangle=\int_{-\infty}^{\infty}\int C_O(\alpha_1,\beta_1)\langle T(u,v;\alpha',\beta')\cdot T^*(u,v;\alpha'-\alpha_1,\beta'-\beta_1)\rangle\exp[-2\pi i(u\alpha_1+v\beta_1)]d\alpha_1 d\beta_1, \tag{7.41}$$

where $\alpha_1=\alpha-\alpha'$ and $\beta_1=\beta-\beta'$.

If the function $T(u,v;\alpha',\beta')$ is independent of the object point (α',β'), i.e. the imaging is isoplanatic, then (7.41) simplifies to the usual result.

$$\Phi_i(u,v)=\Phi_O(u,v)\langle|T(u,v)|^2\rangle. \tag{7.7}$$

However, according to (7.41), there is no longer a simple relationship between object and image properties, and the form of the cross-spectrum,

$$\langle T(u,v;\alpha',\beta')T^*(u,v;\alpha'-\alpha_1,\beta'-\beta_1)\rangle$$

between speckle patterns produced by two point sources separated by angle (α_1,β_1) plays an important role.

KORFF et al. [7.47], SHAPIRO [7.48], and FRIED [7.49] have investigated this problem using the log-normal model for atmospheric turbulence. However, a more complete analysis can be carried out if the complex Gaussian model of the wavefront $A(\xi,\eta)$ is used, as shown by RODDIER et al. [7.50]. Using a multiple-layer model for the turbulence,

they estimate the "atmospheric isoplanatic angle" $\delta\omega$ to be given by

$$\delta\omega \cong 0.36 \frac{r_0}{\Delta h}, \tag{7.42}$$

where Δh is a measure of the altitude dispersion of the turbulent layers [7.50]. This simple relationship does not reveal the fact that high angular frequencies decorrelate more rapidly than lower ones as the angle of separation (α_1, β_1) increases, but gives a good estimate of the extent of the isoplanatic region. Based on measured profiles of the variation of turbulence with altitude (see Vernin in [7.42]), predicted isoplanatic angles were in the range 1".9 to 5".4 over six nights at Haute Provence Observatory, with an average of 3".1 [7.50].

Several measurements of the isoplanatic angle or related quantities have been reported [7.37, 51–53]. The values vary widely, the most reliable quantitative estimates being in the range 1".5–5".0 [7.51, 52], i.e. the same order of magnitude as the theoretical predictions. Qualitative estimates, based on the successful implementation of speckle holography [7.37, 53], indicate some correlation of image intensity for stars as far apart as 22".0.

7.2.8 Self-Calibration of Speckle Interferometry

In order to recover the energy spectrum of the object $\Phi_O(u, v)$, the average energy spectrum of the image $\Phi_I(u, v)$ is divided by the speckle transfer function

$$\Phi_O(u, v) = \Phi_I(u, v) / \mathcal{T}(u, v). \tag{7.43}$$

In practice, *the speckle transfer function is estimated by finding the* average energy spectrum for a point source (or reference star). Unfortunately, as we have seen in previous sections, the speckle transfer function depends on a number of atmospheric parameters (such as r_0 and time scale) and these parameters themselves vary considerably over both short (~seconds) and long (~hours) periods of time. Under stable atmospheric conditions, application of (7.43) is straightforward, but under (more typical) unstable conditions, the use of (7.43) can lead to considerable errors in the estimation of the object's spectrum. This is less critical for measurements of simple structural features of an object (e.g., the vector separation of a binary star) but crucial for photometric features (e.g., magnitude difference of a binary star).

Two approaches to this problem have been suggested. The first is to make simultaneous measurements of r_0 and use the established theory to

predict the form of the speckle transfer function [7.24]. The measurements of AIME et al. [7.31] and CHELLI et al. [7.32] suggest that the instantaneous ($\Delta t \to 0$), narrowband ($\Delta\lambda \to 0$) speckle transfer function can be predicted for an aberration-free telescope, but in practice focussing errors, aberrations, the finite exposure time and other effects may influence it. Nevertheless, this appears to be a promising technique, particularly in the infra-red where the second approach is less reliable.

The second approach, originally suggested by WORDEN and coworkers [7.54, 55], involves subtracting the cross-correlation of uncorrelated images from the autocorrelation of individual frames. Let $I(\alpha, \beta)$ be an instantaneous short-exposure image and $I'(\alpha, \beta)$ be another instantaneous short-exposure image taken some time after the first one so as to be uncorrelated with it; then, denoting the result by $C_1'(\alpha, \beta)$,

$$C_1'(\alpha, \beta) = \langle I(\alpha, \beta) \star I(\alpha, \beta) \rangle - \langle I(\alpha, \beta) \star I'(\alpha, \beta) \rangle . \tag{7.44}$$

In fact, no second image is required, since (7.44) is exactly the same as [7.56]

$$C_1'(\alpha, \beta) = \langle I(\alpha, \beta) \star I(\alpha, \beta) \rangle - \langle I(\alpha, \beta) \rangle \star \langle I(\alpha, \beta) \rangle , \tag{7.45}$$

i.e. the average of the angular autocorrelation minus the autocorrelation of the average image.

These equations may equally well be written in the angular frequency domain, giving a resultant image energy spectrum $\Phi_1'(u, v)$,

$$\Phi_1'(u, v) = \Phi_0(u, v)\mathcal{T}'(u, v) , \tag{7.46}$$

where the transfer function for this technique is given by

$$\mathcal{T}'(u, v) = \langle |T(u, v)|^2 \rangle - |\langle T(u, v) \rangle|^2 . \tag{7.47}$$

The original hypothesis [7.45] was that the shape of $\mathcal{T}'(u, v)$ is independent of atmospheric seeing, and this is correct for the complex gaussian model of the pupil amplitude $A(\xi, \eta)$, as can be seen by substituting (7.26) into (7.47):

$$\mathcal{T}'(u, v) = \frac{1}{N_{sp}} T_D(u, v) , \tag{7.48}$$

where N_{sp} is the number of speckles ($\equiv 2.3(D/r_0)^2$), and $T_D(u, v)$ is the diffraction-limited transfer function.

Two factors combine to invalidate this result for the lower angular frequencies. First, as remarked upon earlier, the asymptotic form of the low frequency dependence of the speckle transfer function is $|\langle T(u,v)\rangle_{SE}|^2$, where $\langle T\rangle_{SE}$ is the average transfer function of centroided (tilt-removed) images; this could be taken into account, in principle, by centroiding each image [7.56] or by other methods [7.57].

Second, the additive form (7.26) of the speckle transfer function is not predicted by the more accurate log-normal model, and the end result is to invalidate this method for frequencies (u, v) less than approximately the seeing limit, i.e. $(u,v) \lesssim r_0/\lambda$ [7.55, 58]. When D/r_0 is large, say >10, the seeing-limited frequencies constitute only a small fraction of the available frequency plane and this method may be the most satisfactory way of self-calibration. But in the infra-red, where $D/r_0 < 10$, it is not appropriate.

7.3 Signal-to-Noise Ratio

In the visible region of the spectrum, the signal-to-noise ratio of a measurement and the limiting magnitude of speckle interferometry are ultimately determined by the fluctuations imposed by the atmospheric turbulence and the quantum nature of radiation. Although early film-based speckle cameras were limited by other types of noise, the improvement in detector technology over the past decade has made available detectors that are photon-noise limited [7.59]. Thus in this section we shall discuss only the fundamental noise sources relevant to visible light speckle interferometry (the infra-red case is discussed in Sect. 7.5.2).

Let Q be some quantity that is to be estimated by speckle interferometry; Q may be (a) a point in the energy spectrum $\Phi_0(u,v)$ of the object, (b) a point in the autocorrelation function $C_0(\alpha,\beta)$ of the object, or (c) a parameter derived from the autocorrelation function or energy spectrum, such as the diameter of a star, binary separation or magnitude difference.

We define the signal-to-noise ratio, SNR, of this measurement as

$$\text{SNR} \equiv \frac{\text{expected value of quantity}}{\text{standard deviation of estimate}},$$

or

$$\text{SNR} \equiv \frac{\langle Q\rangle}{[\text{var}(Q)]^{1/2}}, \tag{7.49}$$

where $\mathrm{var}(Q) \equiv \langle Q^2 \rangle - \langle Q \rangle^2$ is the variance of Q. In the analysis that follows, the SNRs relate to an estimate of Q based on a single frame of data. Normally, one would take M frames of data and, provided these are statistically independent, the overall SNR for the M frames $(\mathrm{SNR})_M$, is simply given by

$$(\mathrm{SNR})_M = \mathrm{SNR} \cdot M^{1/2} . \tag{7.50}$$

The signal-to-noise ratio is the inverse of the relative error of measurement and in a given astronomical application we would normally be interested in the relative error on some parameter (such as diameter), as in (c). However, each problem has its own specific parameters of interest and to keep our results as general as possible we shall consider the SNR of the energy spectrum or autocorrelation function.

Several investigations of the SNR of a measurement of the autocorrelation function have been made [7.33, 57, 60–63] and the review in the first edition of this volume [7.12] outlines this approach. However, it has been shown [7.64] that the autocorrelation and energy spectrum approaches give exactly equivalent signal-to-noise ratios, although the detailed expressions show little apparent similarity. The decision whether to use the autocorrelation method or the energy spectrum method of data reduction should be based on operational considerations and not on SNR considerations. Thus in the following subsection we evaluate only the SNR of the energy spectrum of the object.

7.3.1 Signal-to-Noise Ratio (SNR) at a Point in the Energy Spectrum

The SNR at a point in the energy spectrum was first evaluated by RODDIER [7.65] and subsequently in more detail by several authors [7.66–69] and reviewed in detail in [7.70]. In this analysis we shall use one-dimensional notation for simplicity, and it is convenient to deal with energy spectra of the image and object that are normalized to unity at zero angular frequency, denoted by $\hat{\Phi}_I(u)$ and $\hat{\Phi}_O(u)$, respectively. These are related in the usual way,

$$\hat{\Phi}_I(u) = \hat{\Phi}_O(u) \mathcal{T}(u), \tag{7.51}$$

where the speckle transfer function $\mathcal{T}(u)$ in the frequency range of interest is given by (7.26):

$$\mathcal{T}(u) = \frac{1}{N_{sp}} T_D(u), \quad \frac{r_0}{\lambda} < u < \frac{(D - r_0)}{\lambda}. \tag{7.26}$$

We model the jth image, $D_j(\alpha)$, as an inhomogeneous or compound Poisson process which has a rate proportional to the classical image intensity $I_j(\alpha)$, i.e.,

$$D_j(\alpha) = \sum_{k=1}^{N_j} \delta(\alpha - \alpha_{jk}),$$

where each delta function represents a detected photon event, α_{jk} is the location of the kth event in the jth frame and N_j is the number of detected photons in the jth frame. In an observation, the squared modulus of the Fourier transform $|d_j(u)|^2$ is computed for each frame. It is straightforward to show that the average of this is given by [7.66]

$$\langle |d_j(u)|^2 \rangle = \bar{N}^2 \hat{\Phi}_i(u) + \bar{N}, \tag{7.52}$$

where $\bar{N}$ is the average number of detected photons per frame. It follows that the energy spectrum of the photon data, $\langle |d_j(u)|^2 \rangle$, is a biased estimate of $\hat{\Phi}_i(u)$ to the presence of the $\bar{N}$ term; in the realistic case in which the photon events are not delta functions but have a unit volume spread function $S(\alpha)$, the second term would be $\bar{N}|s(u)|^2$.

There are two estimators Q whose average yield an unbiased estimate of the image energy spectrum. One possibility is to subtract the average number $\bar{N}$ from each $|d_j(u)|^2$,

$$Q_1 = |d_j(u)|^2 - \bar{N}, \tag{7.53}$$

and the second possibility is to subtract the actual number N_j,

$$Q_2 = |d_j(u)|^2 - N_j. \tag{7.54}$$

In either case, the average values of Q are unbiased estimators,

$$\langle Q_1 \rangle = \langle Q_2 \rangle = \bar{N}^2 \hat{\Phi}_i(u). \tag{7.55}$$

For the first estimator, the variance is equal to [7.67]

$$\text{var}(Q_1) = \bar{N} + \bar{N}^2 + 2(2+N)N^3 \hat{\Phi}_i(u) + \bar{N}^2 \hat{\Phi}_i(2u) + \bar{N}^4 \hat{\Phi}_i^2(u). \tag{7.56}$$

As in all problems of this type, the fluctuation at frequency u is influenced by the value of the energy spectrum at frequency $2u$. At exceedingly low light levels $\bar{N} \ll 1$ (probably of no practical interest!), the SNR per frame for estimate Q_1 is, using (7.49, 55 and 56),

$$\text{SNR} = \bar{N}^{3/2} \hat{\Phi}_i(u), \quad \bar{N} \ll 1. \tag{7.57}$$

The use of definition (7.53) for the estimate Q_1 has the disadvantage that the noise associated with Q_1 contains a contribution arising from N_j, the actual number of photons per frame. These fluctuations are related to the brightness of the object and not to its structure. If one is interested in the morphology of the object, Q_2 is a better estimate; its variance is given by [7.69]

$$\text{var}(Q_2) = \bar{N}^2 + \bar{N}^2\hat{\Phi}_i(2u) + 2\bar{N}^3\hat{\Phi}_i(u) + \bar{N}^4\hat{\Phi}_i^2(u). \tag{7.58}$$

If we consider only frequencies $u > \frac{1}{2}D/\lambda$, the second term in (7.58) can be ignored, yielding a SNR per frame of

$$\text{SNR} = \frac{\bar{N}\hat{\Phi}_i(u)}{1 + \bar{N}\hat{\Phi}_i(u)}. \tag{7.59}$$

Equation (7.59) is the general expression for the signal-to-noise ratio at any point ($u > \frac{1}{2}D/\lambda$) in the energy spectrum of the image. If the speckle transfer function is known exactly (this is never true in practice), then (7.59) is also the SNR at a point in the energy spectrum of the object. Substituting (7.26, 51) into (7.59), and defining the average number of detected photons per speckle $\bar{n}$ as

$$\bar{n} \equiv \frac{\bar{N}}{N_{sp}} = \frac{\bar{N}}{2.3}\left(\frac{r_0}{D}\right)^2, \tag{7.60}$$

we find that the SNR per frame becomes

$$\text{SNR} = \frac{\bar{n}T_D(u)\hat{\Phi}_O(u)}{1 + \bar{n}T_D(u)\hat{\Phi}_O(u)}. \tag{7.61}$$

Two limiting cases are of interest: very bright objects and very faint ones.

(i) For very bright objects, such that

$$\bar{n}T_D(u)\hat{\Phi}_O(u) \gg 1,$$

then,

$$\text{SNR} \cong 1. \tag{7.62}$$

Note that the SNR per frame cannot exceed unity in speckle interferometry and this is one of the disadvantages of the speckle technique, compared to pupil plane interferometry, for bright objects.

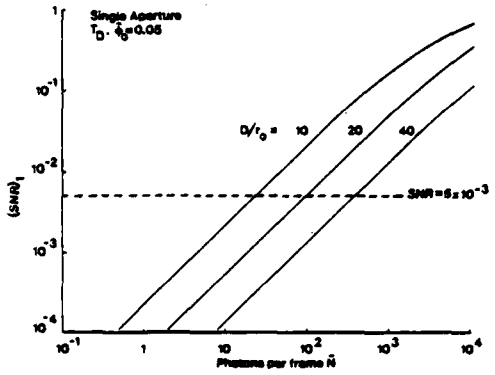

Fig. 7.8. The variation of SNR per frame with the average number of detected photons per frame $\bar{N}$ for $D/r_0 = 10$, 20, and 40, for $T_D\hat{\phi}_0 = 0.05$ [7.70]

(ii) For very faint objects, such that

$$\bar{n}T_D(u)\hat{\Phi}_O(u) \ll 1$$

then

$$\begin{aligned} \mathrm{SNR} &\cong \bar{N}\hat{\Phi}_I(u) \\ &\cong \bar{n}T_D(u)\hat{\Phi}_O(u), \end{aligned} \tag{7.63}$$

where, as before, $\bar{N}$ is the average number of detected photons per frame and $\bar{n}$ is the average number per speckle. This particularly simple formula for the SNR per frame at a point ($u > \frac{1}{2}D/\lambda$) in the energy spectrum of the object is in practice valid for all fainter objects.

An example of the variation of SNR per frame as a function of $\bar{N}$ is shown in Fig. 7.8 for $D/r_0 = 10$, 20, and 40. For faint objects, the SNR is proportional to r_0^2, so that there is a strong dependence of SNR on the seeing. On the other hand, since the average number of photons per speckle (7.60) is independent of telescope diameter, the SNR at a point in the energy spectrum is also independent of telescope diameter, for faint objects. Of course, a larger telescope yields more independent points in the energy spectrum.

7.3.2 Optimum Exposure Time

In the low-light-level case, the SNR at a point in the energy spectrum for M statistically independent frames is, from (7.50, 63),

$$(\mathrm{SNR})_M \cong \sqrt{M}\,\bar{N}\,\hat{\Phi}_1(u). \tag{7.64}$$

It appears at first sight that a larger exposure time (i.e., increasing $\bar{N}$) leads to a higher SNR; however, this is true only up to an optimum exposure time, after which the decrease in M and $\hat{\Phi}_1(u)$ dominates. The optimum exposure time has been evaluated by WALKER [7.62], and O'DONNELL and DAINTY [7.71].

Let the exposure time be denoted by Δt, the experiment time by T_e and the photon rate by $\mu \equiv \bar{N}/\Delta t$; then, assuming that neighboring exposures are always statistically independent[4] (7.64) can be re-written as

$$(\mathrm{SNR})_M \cong \mu\sqrt{T_e \Delta t}\,\hat{\Phi}_{1,\Delta t}(u), \tag{7.65}$$

where $\hat{\Phi}_{1,\Delta t}(u)$ is the measured image energy spectrum for an exposure time Δt. The temporal behaviour of the image intensity has been discussed in Sect. 7.2.5; there we showed that the measured image energy spectrum may always be written, see (7.31),

$$\hat{\Phi}_{1,\Delta t}(u) = \frac{1}{\Delta t}\int_{-\Delta t}^{\Delta t}\left(1-\frac{|\tau|}{\Delta t}\right)\langle i^*(u,t)i(u,t+\tau)\rangle d\tau. \tag{7.66}$$

Both theory and experiment show that, in general, the cross-spectrum $\langle i^*(u,t)i(u,t+\tau)\rangle$ is *not* separable. On the other hand, measurements [7.39] indicate that the approximation, see (7.34),

$$\langle i^*(u,t)i(u,t+\tau)\rangle \cong \hat{\Phi}_1(u)C(\tau) \tag{7.67}$$

may not be unreasonable under typical observing conditions; in (7.67), $\hat{\Phi}_1(u)$ is the normalized instantaneous energy spectrum and $C(\tau)$ is the normalized temporal autocorrelation function of the stellar image (some measurements are shown in Fig. 7.6). Substituting (7.66, 67) into (7.65) we obtain

$$(\mathrm{SNR})_M \cong \hat{\Phi}_1(u)2\mu\sqrt{\frac{T_e}{\Delta t}}\int_0^{\Delta t}\left(1-\frac{|\tau|}{\Delta t}\right)C(\tau)d\tau. \tag{7.68}$$

[4] Clearly, neighboring exposures cannot be statistically independent unless $\Delta t \gg$ correlation time of the image intensity; when there are only a small number of detected photons per frame, however, there is an approximate statistical independence for neighboring frames.

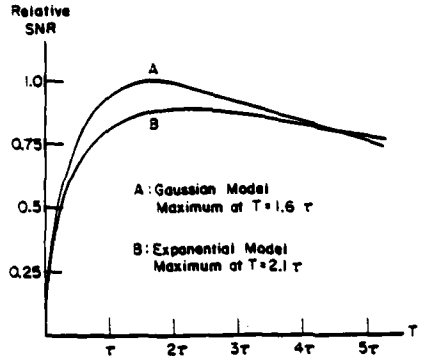

Fig. 7.9. Relative SNR at a point in the power spectrum as a function of the length of the individual short exposures for two models of the time-correlation of the image intensity. The overall time of observation is assumed to be constant and it is also assumed that the average number of detected photons per speckle is very much less than one [7.71]

In Fig. 7.9, the SNR is plotted as a function of exposure time for two models of the temporal correlation function $C(\tau)$, Gaussian and negative exponential, each having a 1/e correlation time of τ_c; the Gaussian model appears to give a better fit to the experimental data of Fig. 7.6. It can be seen that the overall SNR is highest for exposure times Δt equal to $1.6\tau_c$ for the Gaussian model and $2.1\tau_c$ for the exponential one. This is somewhat larger than might be expected and certainly much larger than desirable at high light levels where photon noise is negligible. Since the SNR decreases rather slowly for exposure times longer than $\cong 2\tau_c$, we can also conclude that, if there is some doubt as to the value of τ_c, longer rather than shorter exposures should be used.

7.3.3 Limiting Magnitude

LABEYRIE concluded his original paper on speckle interferometry [7.6] with the comment that "the technique appears to be limited to objects brighter than $m_v = 7$". It was quickly recognized by LABEYRIE and others that, in fact, the faintest objects that can be resolved by this technique are a factor of 10^5 fainter, of apparent visual magnitude $m_v \cong 20$.

Any estimate of the limiting or just-observable magnitude depends on the criterion adopted for "just-observable" as well as on the usual

parameters such as detector quantum efficiency, bandwidth, exposure time and so on. Three examples are given below: an estimate of the complete object energy spectrum, the detection of a binary star, and the measurement of the diameter of a star. In each case we define a factor F to be the product of the exposure time Δt [s], the optical bandwidth $\Delta\lambda$ [nm] and the quantum efficiency q of the detector,

$$F \equiv \Delta t \Delta\lambda q. \tag{7.69}$$

We also use the fact that a source of apparent visual magnitude m_v gives rise to an average number of detected photons per m^2 per frame, $\bar{N}_A$, of [7.72]

$$\bar{N}_A = F\,10^{(8-0.4m_v)}. \tag{7.70}$$

Estimation of the Object Energy Spectrum

At low light levels, combination of (7.50, 63 and 70) gives a SNR of

$$(\mathrm{SNR})_M = M^{1/2}\frac{\pi D^2}{4} F\,10^{(8-0.4m_v)}\left[0.435\left(\frac{r_0}{D}\right)^2\right]\hat{\Phi}_O(u)T_D(u),$$

which can be re-arranged to give [7.70]

$$m_v = 18.8 + 2.5\log F - 2.5\log(\mathrm{SNR})_M + 1.25\log M + 2.5\log[\hat{\Phi}_O(u)T_D(u)] + 5\log r_0. \tag{7.71}$$

For $r_0 = 0.1$ m, $M = 10^5$, $\Delta t = 0.02$ s, $\Delta\lambda = 25$ nm, $q = 0.1$, $\hat{\Phi}_O(u)T_D(u) = 0.2$ and a limiting $(\mathrm{SNR})_M = 5$, (7.71) predicts a limiting apparent visual magnitude of approximately $m_v = 13.3$, corresponding to approximately 300 detected photons per frame in a 4 m telescope. Note that the limiting magnitude defined in this way is independent of telescope diameter and depends quite strongly on the seeing parameter r_0; in fact, the dependence on r_0 is stronger than (7.71) indicates since the bandwidth and exposure time both change with r_0 [7.23] (Sects. 7.2.5, 6). The value $m_v = 13.3$ is a conservative estimate of the limiting magnitude for many purposes, since it is based on the criterion that the SNR have the value 5 at every point in the energy spectrum.

Detection of Binary Stars

Using a formula for the SNR based on the autocorrelation approach [7.61, 70], in which the estimated quantity is the height of the binary star

autocorrelation peak above its local background, we can derive the following limiting magnitude for a binary whose components are equally bright:

$$m_v = 17.3 + 2.5\log F - 2.5\log(\mathrm{SNR})_M + 1.25\log M + 2.5\log D + 2.5\log r_0 . \quad (7.72)$$

Substituting the same parameters as above now leads to a limiting magnitude $m_v = 17.6$, corresponding to approximately 5 detected photons per frame an average. By increasing the number of independent frames to 10^6 and slightly increasing the exposure time and bandwidth, binaries as faint as $m_v = 20$ should be observable.

The limiting magnitude predicted by (7.72) has been effectively achieved by HEGE et al. [7.73] in their measurement of the 16.2 magnitude component of the triple quasar PG 1115+08 using approximately 20,000 independent frames.

Estimation of Object Diameter

WALKER [7.57] has made a comprehensive study of the accuracy with which the diameter of an object can be estimated by speckle interferometry, assuming a known limb darkening profile of the star. His

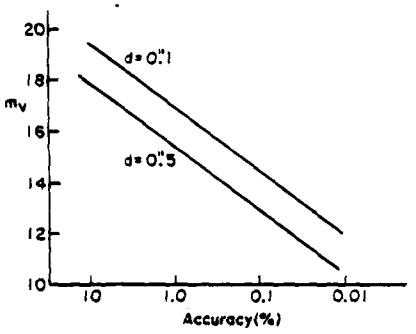

Fig. 7.10. Limiting magnitude m_v as a function of the desired fractional accuracy for a typical set of observing parameters on a 4 m-class telescope (observing period: 2000 s) [7.58]

results are summarized in Fig. 7.10 for a collection of observing parameters that are similar (but not identical) to the previous two cases. For 1% statistical error in a diameter whose value is 0."5, the limiting magnitude is approximately $m_v = 16$. Of course, other deterministic effects such as those due to atmospheric calibration are not included in this or previous cases.

7.3.4 Space-Time Speckle Interferometry

In the analysis of the optimum exposure time in Sect. 7.3.2, we found that exposures as long as twice the temporal correlation time of the image could be optimum from the point of view of signal-to-noise ratio. Such long exposure times result in attenuation of the high angular frequency components in the measured energy spectrum, and those remain uncorrected. Another drawback of the straightforward speckle method is that no use is made of the fact that photons detected at the end of one exposure are associated with essentially the same classical intensity as those detected at the beginning of the next exposure; thus there is a potential loss of information.

"Space-time" speckle interferometry [7.71, 74] is an extension of speckle interferometry that includes correlations in the time domain as well as in the spatial or angular domain. In one such scheme, the temporal cross-energy spectrum $\langle i^*(u,v,t)i(u,v,t+\tau)\rangle$ is estimated and used to find an estimate of $\Phi_i(u,v)$ that is not biased by the effects of a finite exposure time. However, the signal-to-noise ratio of this technique does not appear to be any higher than that associated with the "optimum exposure time" method [7.71]. It does not appear to be worthwhile implementing space-time speckle interferometry unless other benefits can be found (such as obtaining object maps [7.74]).

7.4 Reconstruction of the Object Intensity

The fundamental equation of speckle interferometry relates the average energy spectrum of the image $\Phi_i(u,v)$ to that of the object $\Phi_O(u,v)$,

$$\Phi_i(u,v) = \Phi_O(u,v)\mathcal{T}(u,v), \tag{7.7}$$

where $\mathcal{T}(u,v)$ is the speckle transfer function. Under favorable conditions this equation can be inverted to yield an estimate of the object energy spectrum

$$\Phi_O(u,v) \equiv |o(u,v)|^2 = \left| \int_{-\infty}^{\infty} O(\alpha,\beta)\exp[-2\pi i(\alpha u+\beta v)]\,d\alpha\,d\beta \right|^2, \tag{7.73}$$

where $O(\alpha,\beta)$ is the angular distribution of object intensity and $o(u,v)$ is its Fourier transform. It should be noted that, by the van Cittert-Zernike theorem [7.2], $o(u,v)$ is a spatial coherence function (strictly, the mutual intensity) and $|o(u,v)|$ is often called a visibility function.

It is impossible, *in general*, to calculate a unique object intensity $O(\alpha, \beta)$ from a knowledge of only its energy spectrum $\Phi_O(u, v)$; this simple fact cannot be stressed too strongly. In some special cases, unique reconstruction of $O(\alpha, \beta)$ is possible; in a second set of special cases, unique reconstructions can be formed almost always; and in a third set of special cases, additional information is available that enables a unique solution to be found.

The object energy spectrum $\Phi_O(u, v)$ contains no obvious information about the phase of the Fourier transform of $O(\alpha, \beta)$ and for this reason the problem of reconstructing the object intensity from $\Phi_O(u, v)$ is referred to as the "phase problem". Phase problems arise in many branches of physics—scattering, x-ray diffraction, coherence theory and microscopy—and a detailed review is beyond the scope of this chapter (see [7.75, 76]). Our review will be strictly limited to the phase problem as it occurs in the measurement of angular coherence functions by stellar speckle interferometry; short reviews of this may be found in [7.12–15, 77] and a comprehensive review was given by. BATES [7.11]. It is interesting to note that some of the earliest work on the phase problem by Lord RAYLEIGH [7.78] and, in the modern era, by WOLF [7.79] was also concerned with coherence theory.

The plan of this section is as follows. In Sect. 7.4.1 we discuss the basic reason for the ambiguity of the phase problem. The next two Sects. 7.4.2, 3 deal with attempts at object reconstruction from the energy spectrum only, whilst in Sects. 7.4.4–7 we describe other methods that incorporate information in addition to the energy spectrum. The subject is summarized in Sect. 7.4.8. The review is limited to the speckle method of stellar interferometry; in this regard it should be noted that there is increasing evidence [7.9, 80–82] that other methods of stellar interferometry are probably more appropriate for object reconstruction.

7.4.1 Ambiguity of the Phase Problem

An essentially theoretical restriction in the phase problem, which is always satisfied in practice, is that the object intensity $O(\alpha, \beta)$ has a finite angular extent with support (2a, 2b); thus $o(u, v)$ is the *finite* Fourier transform,

$$o(u, v) = \int_{-a}^{a} \int_{-b}^{b} O(\alpha, \beta) \exp[-2\pi i(u\alpha + v\beta)] \, d\alpha \, d\beta \,. \tag{7.74}$$

It can be shown that the analytic continuation of $o(u, v)$ to the complex plane, $o(z_1, z_2)$ where z_1, z_2 are complex variables, is an entire function of

exponential type. Such functions are completely specified by their (complex) zeros. The zeros provide a unifying concept for the study of all phase retrieval methods; their importance in interferometry was discussed by BATES [7.83] and in a more general context by ROSS and colleagues [7.85–87]. Although the zeros are the unifying concept, they are not necessarily of practical value in computer-based algorithms due to the complexity of determining their locations.

Before discussing the reason for the ambiguity of the phase problem, we should note that certain phase ambiguities do not affect the form of the object intensity and are ignored in the following analysis. Defining the phase of $o(u, v)$ as phase $\{o(u, v)\}$, we are not concerned with the following variants:

$$\text{phase } \{o(u, v)\} + \phi, \text{ where } \phi \text{ is a constant,} \tag{7.75a}$$

$$\text{phase } \{o(u, v)\} + 2\pi(u\alpha_1 + v\beta_1), \text{ where } (\alpha_1, \beta_1) \text{ is a constant vector,} \tag{7.75b}$$

$$-\text{ phase } \{o(u, v)\}. \tag{7.75c}$$

The addition of a constant phase, (7.75a), does not alter the object intensity $O(\alpha, \beta)$; the second variant, (7.75b), leads to a shifted object $O(\alpha + \alpha_1, \beta + \beta_1)$; the third case, (7.75c), gives $O(-\alpha, -\beta)$, which is a 180° rotated version of the object. In the discussion below, these trivial ambiguities are ignored.

Our approach to describing the phase problem is, following BRUCK and SODIN [7.88], to represent the object by a finite number of samples, equally spaced (for simplicity) by Δ on a grid of $(N+1)$ by $(M+1)$ points. Defining new complex variables w_1 and w_2

$$w_1 = \exp(-2\pi i z_1 \Delta), \quad w_2 = \exp(-2\pi i z_2 \Delta), \tag{7.76}$$

the Fourier transform $o(w_1, w_2)$ can be written as a finite polynomial in w_1 and w_2

$$o(w_1, w_2) = w_1^{-a/\Delta} w_2^{-b/\Delta} \sum_{n=0}^{N} \sum_{m=0}^{M} O(n\Delta - a, m\Delta - b) w_1^n w_2^m.$$

The terms $w_1^{-a/\Delta}$ and $w_2^{-b/\Delta}$ merely define the (α, β) origin; ignoring these, and simplifying the notation we write

$$o(w_1, w_2) = \sum_{n=0}^{N} \sum_{m=0}^{M} O_{nm} w_1^n w_2^m. \tag{7.77}$$

The most important feature of (7.77) is that the (discrete) Fourier transform of the object intensity can be written as a finite polynomial in the complex variables w_1 and w_2, the coefficients of the polynomial being the sampled values of the object intensity. In this approach to the phase problem, the mathematics of polynomials is important; note, however, that this approach is less general than required by the original problem, which was for continuous, not discrete, object functions.

Consider now the one dimensional case,

$$o(w_1) = \sum_{n=0}^{N} O_n w_1^n. \tag{7.77a}$$

A one-dimensional polynomial can always be factorized, or reduced, into prime factors,

$$o(w_1) = C \prod_{j=1}^{N} (w_1 - w_{1,j}), \tag{7.78}$$

where C is a constant and $w_{1,j}$ are the roots or zeros. The N zeros and the constant C completely determine the Fourier transform $o(w_1)$ and hence the object O_n. If the object is real, as in the present case, the zeros lie on the unit circle or in complex conjugate pairs around the unit circle and only $N/2$ zero locations are required to specify the object; positivity

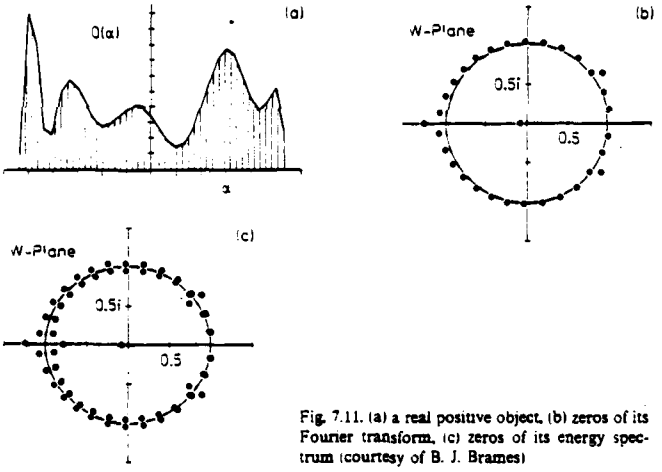

Fig. 7.11. (a) a real positive object, (b) zeros of its Fourier transform, (c) zeros of its energy spectrum (courtesy of B. J. Brames)

requires that no zeros lie on the positive real w_1 axis. Figures 7.11a and b illustrate these results.

In a similar manner, we can represent the energy spectrum $\Phi_O(u)$ as an analytic function $o(z_1)o^*(z_2^*)$; the conjugate function to $o(w_1)$ is just $o(1/w_1)$ so that $\Phi_O(w_1)$ can be written as a polynomial of degree $2N$:

$$\Phi_O(w_1) = C^2 \prod_{j=1}^{N} (w_1 - w_{1,j})(w_1 - 1/w_{1,j}^*). \tag{7.79}$$

That is, the complex zeros of $\Phi_O(w_1)$ consist of the original N zeros of the object transform plus their inverses. This is illustrated in Fig. 7.11c.

Thus, the essence of the phase problem is that, without some basis for choosing between the correct zero and its inverse, we could construct $2^{N/2}$ equally valid sets of N zeros each representing a real, possibly positive, object. In the one-dimensional case, there is no unique solution to the phase problem, in either a theoretical or practical sense; additional information is required to find the object intensity.

Consider now the two-dimensional case, where the Fourier transform of the object intensity can be written as a polynomial in two complex variables,

$$o(w_1, w_2) = \sum_{n=0}^{N} \sum_{m=0}^{M} O_{nm} w_1^n w_2^m. \tag{7.77}$$

NAPIER and BATES [7.89] were the first to find that a unique solution to the phase problem was more likely to occur in this case. In one dimension, ambiguity resulted from the factorizability of the polynomial (7.77a); in two dimensions, as shown by BRUCK and SODIN [7.88], ambiguity may also exist if the two variable polynomial (7.77) is factorizable (or reducible) and the degree of ambiguity is determined by the number of non-self-conjugate irreducible factors. However, there is a very small probability that any two-dimensional polynomial is reducible; in fact, reducible polynomials in two dimensions are a set of measure zero [7.90]. Thus one is tempted to assume that the two-dimensional phase problem has a unique solution "almost always".

The uniqueness of the two-dimensional phase problem is the subject of much current research. The results of applying the algorithms to be described in Sect. 7.4.3 strongly suggest that effectively unique solutions may exist for certain objects, although of course it is always possible to produce counter-examples [7.91, 92]. FIDDY et al. [7.93] and FIENUP [7.94] have used Eisenstein's irreducibility theorem to define one particular class of objects for which a unique solution is guaranteed.

There are three basic approaches to solving the phase problem in stellar speckle interferometry. In the first, it is assumed that something about the object is known. For example, for a symmetric object intensity

$$O(\alpha, \beta) = O(-\alpha, -\beta), \tag{7.80}$$

the Fourier transform $o(u, v)$ is purely real and continuity arguments enable it to be found from $|o(u, v)|$; a rotationally symmetric object is included in this category. Speckle holography, to be discussed in the next subsection, also assumes that the object has a known property. In the second approach, one assumes that the two-dimensional phase problem is almost unique and seeks an algorithm to recover the object intensity from the modulus information alone. In the third approach, additional information is extracted from the speckle images in a number of different ways (Sects. 7.4.4–7).

7.4.2 Speckle Holography

The technique of speckle holography, in its original and most elementary form [7.95, 96], relies on the presence of a reference object, preferably a point source. Let the object field be written as the sum of a point centered at the origin and the object under investigation $O_1(\alpha, \beta)$ centered at (α_1, β_1),

$$O(\alpha, \beta) = \delta(\alpha)\delta(\beta) + O_1(\alpha - \alpha_1, \beta - \beta_1). \tag{7.81}$$

The spatial autocorrelation of (7.81) consists of four terms

$$\begin{aligned} C_O(\alpha, \beta) = & \int_{-\infty}^{\infty}\int \delta(\alpha')\delta(\beta')\delta(\alpha' + \alpha)\delta(\beta' + \beta)d\alpha' d\beta' \\ & + \int_{\infty}^{\infty}\int O_1(\alpha', \beta')O_1(\alpha' + \alpha, \beta' + \beta)d\alpha' d\beta' \\ & + O_1(\alpha - \alpha_1, \beta - \beta_1) + O_1(-\alpha - \alpha_1, -\beta - \beta_1). \end{aligned} \tag{7.82}$$

The first two terms are located in the region of the origin, the third is the object centered at (α_1, β_1) and the fourth term is a 180° rotation of the object centered at $(-\alpha_1, -\beta_1)$. Provided that $\alpha_1 > 3a/2$ and $\beta_1 > 3b/2$, where the object extent is (a, b), the third and fourth terms are separated in angle from the first two and a reconstruction of the object is obtained (with the 180° rotatic ↑ ambiguity). WEIGELT [7.97–99] has demonstrated that this is a useful astronomical technique and Fig. 7.12 shows an

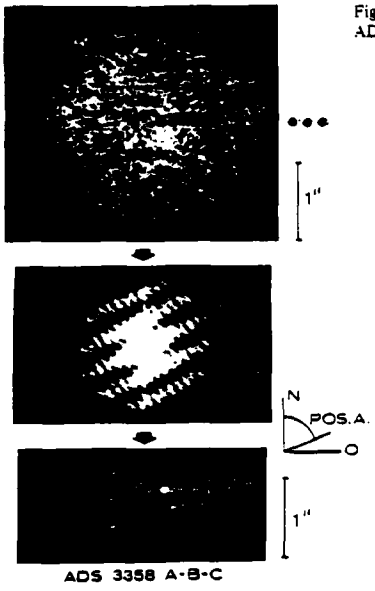

Fig. 7.12. Speckle holography of ADS 3358 [7.98]

example of the reconstruction of a triple star using speckle holography. The extent of the atmospheric isoplanatic angle is clearly important in speckle holography (Sect. 7.2.7).

If the reference point is not separated by the "holographic distance" then, in general, the object intensity cannot be reconstructed unambiguously unless further information is available. For example, LIU and LOHMANN [7.100] suggested using the long-exposure image as a mask, and BALDWIN and WARNER [7.101] used the knowledge that one star is brighter than the others to unravel the object (star clusters) from the autocorrelation function. Indeed, if the object consists of a discrete set of points and no vector separation between points occurs more than once (i.e., non-redundant spacings) then a unique solution to the problem exists [7.102, 103]. In another special case described by BRUCK and SODIN [7.87], a one-dimensional object can be reconstructed uniquely provided that the reference point is not in line with the object in the two-dimensional plane. The irreducibility criterion described by FIDDY et al. [7.93] also involves the use of reference points less than the usual holographic distance.

WEIGELT [7.104, 105] has suggested a technique called "speckle masking" that is related to holography in the sense that the speckle short-exposure images are preprocessed to yield an approximation to the instantaneous point spread function. In a more general sense, the speckle masking method involves the determination of the triple correlation

$$C_I(\alpha,\beta;\alpha_0,\beta_0) \equiv \langle I(\alpha,\beta)\cdot I(\alpha-\alpha_0,\beta-\beta_0) * I(\alpha,\beta)\rangle ,$$

from which the triple correlation of the object,

$$C_O(\alpha,\beta;\alpha_0,\beta_0) \equiv [O(\alpha,\beta)\cdot O(\alpha-\alpha_0,\beta-\beta_0)] * O(\alpha,\beta),$$

can be determined by subtraction of bias terms [7.105]. Depending upon the complexity of the object, it is possible to determine $O(\alpha,\beta)$ from the triple correlation $C_O(\alpha,\beta;\alpha_0,\beta_0)$.

7.4.3 Modulus—Only Algorithms

In this approach to object reconstruction in stellar speckle interferometry, it is implicitly assumed that the two-dimensional problem *does* have a unique solution. Three algorithms that attempt to recover this solution are described below. Any result produced by these algorithms is therefore subject to two uncertainties: a) did a unique solution to the phase problem exist, even in principle? b) if it did exist, did the algorithm converge to this solution? Strictly speaking, uniqueness of the solution to the two-dimensional phase problem is not guaranteed and none of the algorithms described here have been shown to always converge to the unique solution when one is known, a priori, to exist. On the other hand, the overwhelming proportion of experimental evidence suggests that, for simple objects, some of these methods are successful in reconstructing object maps.

Iterative Algorithm

FIENUP has suggested a number of iterative algorithms [7.106–110] for computing the object intensity from a knowledge of only the modulus of its Fourier transform and an estimate of the support of the object. Two possible schemes are shown in Fig. 7.13. The first scheme, called the error reduction method because the mean square error between iterations always decreases [7.110], is a generalized form of the GERCHBERG-SAXTON algorithm [7.111]. Starting with an estimate of the object intensity at the k th iteration $\hat{O}_k(\alpha,\beta)$, the transform $\hat{o}_k(u,v)$ is calculated.

AD-A168 755 HIGH ANNULAR RESOLUTION STELLAR INTERFEROMETRY(U) 2/3
ROCHESTER UNIV NY INST OF OPTICS J C DAINTY 31 JUL 85
AFOSR-TR-86-0312 AFOSR-81-0003

UNCLASSIFIED F/G 3/1 NL

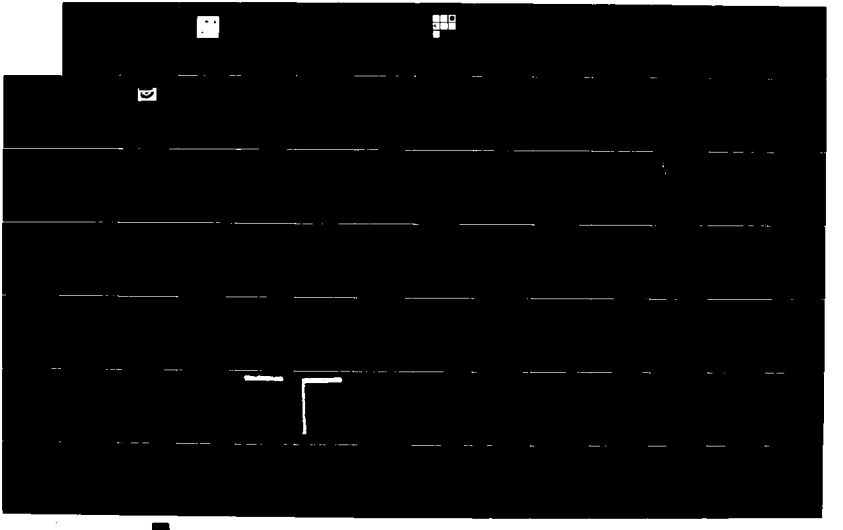

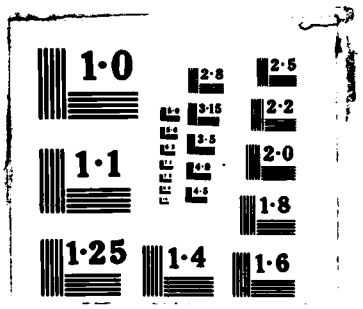
1·0
1·1
1·25
1·4
1·6
1·8
2·0
2·2
2·5
2·8
3·15
3·5

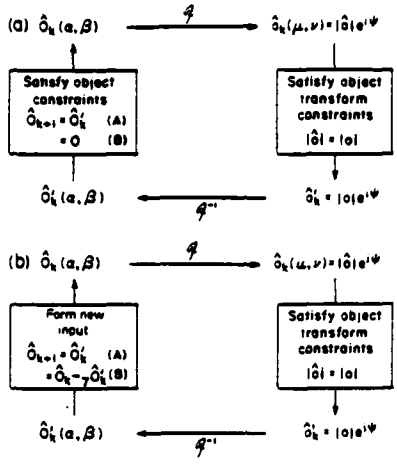

Fig. 7.13a, b. Two iterative algorithms for solving the phase problem. (a) error reduction—in object space, (A) is where object constraints are satisfied, (B) is where they are not satisfied; (b) hybrid input-output [7.110]

The modulus of this transform is replaced by the given modulus, forming a new estimate $\hat{o}'_k(u,v)$ that satisfies the constraints of the problem in the Fourier transform domain. This is inverse-transformed to give a new estimate of the object $\hat{O}'_k(\alpha,\beta)$ which is set to zero in the region where the object is known to be zero and set equal to zero where negative object values exist, thus forming a new estimate $\hat{O}_{k+1}(\alpha,\beta)$ which is the starting point for the next cycle. In practice, the error reduction algorithm converges very slowly and it is generally most useful when applied with one of the "input-output" algorithms.

The second scheme is shown in Fig. 7.13b and is called the "input-output" algorithm. The only difference between this and the error reduction scheme lies in how the next starting input $\hat{O}_{k+1}(\alpha,\beta)$ is derived from the previous output estimate $\hat{O}'_k(\alpha,\beta)$ and input $\hat{O}_k(\alpha,\beta)$. To a first-order approximation, a small change in the input gives a small change in the output proportional to that in the input (plus nonlinear terms); thus, by changing the input it should be possible to drive the output in the desired direction. The most satisfactory version of this scheme, called the hybrid input-output algorithm is

$$\begin{aligned}\hat{O}_{k+1}(\alpha,\beta) &= \hat{O}'_k(\alpha,\beta) \quad \text{when object constraints satisfied}\\ &= \hat{O}_k(\alpha,\beta)-\gamma\hat{O}'_k(\alpha,\beta) \quad \text{when not satisfied,}\end{aligned} \tag{7.83}$$

where γ is a parameter, typically on the order of unity.

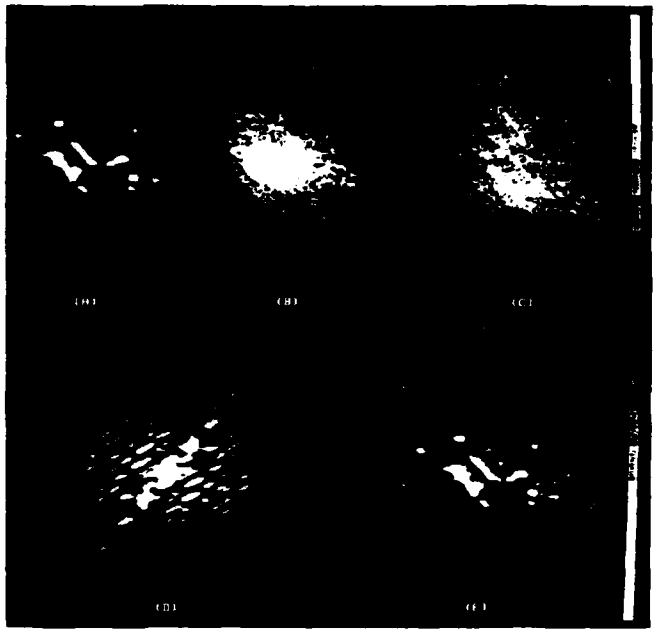

Fig. 7.14. (A) Original object: (B), (C) examples of simulated degraded images: (D) Fourier modulus estimate computed from degraded images: (E) image reconstructed using iterative algorithm [7.110]

A discussion of the relative merits of different iterative algorithms is given in [7.110]; at the present time, these algorithms are still rather ad hoc and their success appears to depend to some extent on the skill of the programmer. Figure 7.14 shows some results obtained by Fienup. These algorithms tends to successfully recover the object intensity for simple, but non-symmetric, objects; the shape of the support of the object also appears to affect the success of the iterative method. It should be stressed that this (and other) algorithms can fail to converge to the correct solution for complicated objects.

Phase-Closure Algorithms

BATES and coworkers [7.112–114] have suggested an algorithm that, in its original form, may be useful as a starting point for the Fienup

algorithm [7.115–117], and in a future improved form may be valuable on its own. Consider an array of N by M values of the Fourier transform of an object (for a real object of size N by N, $M = N/2 + 1$); the aim of this algorithm is to calculate the phases of each point θ_{ij}, allowing any one point (usually the origin) to be set to zero. Bates and coworkers suggested the following two step procedure:

i) Estimate the magnitude of the $(N-1)$ by M phase differences along the u-axis, $|\theta_{i+1,j} - \theta_{i,j}|$ and the N by $(M-1)$ v-phase differences $|\theta_{i,j+1} - \theta_{i,j}|$.

ii) Compute the N by M phases from the magnitudes of these $(2NM - N - M) \cong 2NM$ phase differences.

Let us assume, for the moment, that step (i) is possible and see how phase closure might be used to determine the phases. Consider the rectangle comprising the first four points (0, 0), (1, 0), (1, 1), and (0, 1) and assume that the magnitudes of the four phase differences are known:

$$\begin{aligned} |\theta_{1,0} - \theta_{0,0}| &= \psi_1, \\ |\theta_{1,1} - \theta_{1,0}| &= \psi_2, \\ |\theta_{1,1} - \theta_{0,1}| &= \psi_3, \\ |\theta_{0,1} - \theta_{0,0}| &= \psi_4. \end{aligned} \tag{7.84}$$

Clearly, we can set

$$\theta_{0,0} = 0 \tag{7.85a}$$

and

$$\theta_{1,0} = +\psi_1. \tag{7.85b}$$

(If in fact $\theta_{1,0} = -\psi_1$, the object reconstruction will be rotated by 180°.) Proceeding around the rectangle anti-clockwise,

$$\theta_{1,1} = \psi_1 \pm \psi_2 \tag{7.85c}$$

and this leads to four possible values of $\theta_{0,1}$,

$$\theta_{0,1} = \psi_1 \pm \psi_2 \pm \psi_3. \tag{7.85d}$$

On the other hand, going directly from (0, 0) to (0, 1) yields

$$\theta_{0,1} = \pm\psi_4 \tag{7.85e}$$

BATES [7.112] argued that only one of the four solutions (7.85d) will equal one of the two solutions (7.85e), thus determining the phases at each of

the four points. If this is the case, then this procedure could be repeated for all points in the Fourier plane and the object intensity could be found by inverse Fourier transformation. Since the number of phase difference magnitudes is roughly twice the number of phases, it may be possible to use the methods mentioned in Sect. 7.4.7 for improving the phase estimates.

Even if the above step (ii) works, it is still necessary to find the magnitudes of phase differences, step (i). These can be estimated by oversampling the modulus in a scheme in which the Shannon interpolation formula is replaced by two point interpolation [7.112]; this provides only a crude estimate of the phase differences (for example, a large proportion have to be set equal to 0 or π) and requires improvement for reliable object restoration by itself. Combined with a modified Fienup algorithm that incorporates a preprocessing step to remove the strong central lobe in the Fourier plane, this technique has been shown [7.116, 117] to produce excellent reconstructions of simple objects.

Maximum Entropy Algorithm

In general terms, the maximum entropy method reconstructs the smoothest object intensity distribution consistent with the available data. It was first suggested for use with phaseless data by GULL and DANIELL [7.118]; as with the other algorithms, there is of course no way that the maximum entropy algorithm can resolve any inherent ambiguities [7.119]. If there are ambiguities, this method restores the smoothest object map.

7.4.4 Use of Exponential Filters

The ambiguity of the phase problem arises because the $2N$ zeros of the object energy spectrum consist of the N zeros associated with the Fourier transform of the object, plus their inverses. Given only the $2N$ zeros of the energy spectrum, it is impossible, in general, to select the correct zeros from each zero pair. By making a second measurement of the energy spectrum of a modified object intensity distribution [the original $O(\alpha, \beta)$ multiplied by $\exp(-2\pi\alpha a)$, where a is a constant], it is possible to unambiguously recover the correct N zeros and hence the object intensity itself. This was first suggested by WALKER [7.120] and WOOD et al. [7.121].

The basic principle of the method is shown in Fig. 7.15, where, for illustration, there are only three sets of zeros. The zeros corresponding to the original object are shown as solid circles ● and their inverses as ○; given only the object energy spectrum it is impossible to determine which

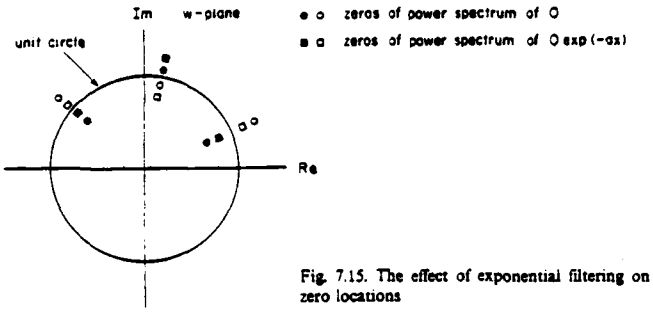

Fig. 7.15. The effect of exponential filtering on zero locations

is the "correct" one. When the object is multiplied by $\exp(-2\pi xa)$, $a>0$, the zeros in terms of the z-variable move from z_j to $z_j - ia$, and in terms of the w-variable, $w=\exp(-2\pi iz\Delta)$, from w_j to $w_j\exp(2\pi a\Delta)$; that is, the correct zeros all move radially outwards by a constant factor, as shown in Fig. 7.15 (●→■). The energy spectrum of the modified object contains both these zeros (■) and their inverses (□); given both pairs of zeros (●, ○, ■ and □) the correct zero (●) can always be located. Although our description has been in terms of one dimension, the uniqueness of the solution also applies to the two-dimensional case.

In astronomy, it is, of course, impossible to place an exponential filter over the object! WALKER [7.122] showed that this is not necessary and that the exponential filter may be placed in the image plane. Denote the instantaneous image intensity by $I(\alpha,\beta)$ and the exponential filter transmittance by $G(\alpha,\beta)$. The energy spectra of the image intensity and the modified image intensity ($I(\alpha,\beta)\cdot G(\alpha,\beta)$) are

$$\Phi_i(u,v)=|o(u,v)|^2\langle|T(u,v)|^2\rangle \tag{7.5}$$

and

$$\begin{aligned}\Phi_i'(u,v)&=\langle|i(u,v)\circledast g(u,v)|^2\rangle\\&=\langle|\{o(u,v)T(u,v)\}\circledast g(u,v)|^2\rangle\,,\end{aligned} \tag{7.86}$$

where $\circledast$ denotes convolution and the other symbols are defined in Sect. 7.2.1.

Provided that

$$G(\alpha_1+\alpha_2,\beta_1+\beta_2)\equiv G(\alpha_1,\beta_1)G(\alpha_2,\beta_2)\,, \tag{7.87}$$

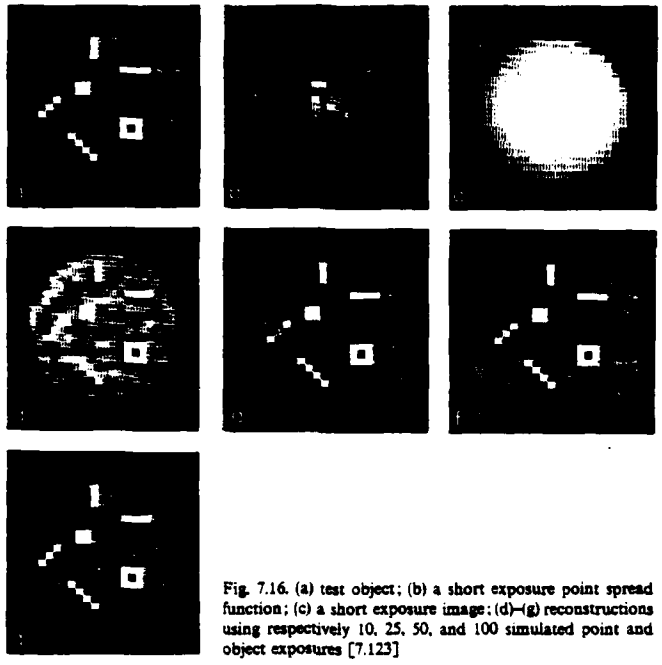

Fig. 7.16. (a) test object; (b) a short exposure point spread function; (c) a short exposure image; (d)–(g) reconstructions using respectively 10, 25, 50, and 100 simulated point and object exposures [7.123]

which is satisfied by the real exponential function, the convolution of (7.86) simplifies to yield

$$\Phi_i'(u,v) = |o'(u,v)|^2 \langle |T'(u,v)|^2 \rangle \tag{7.88}$$

where,

$$o'(u,v) = o(u,v) \circledast g(u,v)$$

and

$$T'(u,v) = T(u,v) \circledast g(u,v).$$

Assuming that the forms of the two transfer functions $\langle |T(u,v)|^2 \rangle$ and $\langle |T'(u,v)|^2 \rangle$ can be found (using a reference star, for example), we can find

the energy spectra of the object and of the modified object which are sufficient data for a unique solution to the phase problem.

Having shown that a unique object reconstruction can be found from $|o(u,v)|^2$ and $|o'(u,v)|^2$, there remains the problem of finding a practical two-dimensional algorithm that converges to this unique solution. WALKER [7.122, 123] has used an extended version of the Fienup algorithm that includes both sets of Fourier constraints. Figure 7.16 shows an example of reconstructions obtained by WALKER in a computer simulation, using this algorithm. It should be noted that this proposed method of object reconstruction uses only a single set of data for the object and for the reference, as the exponential filter can be applied numerically on the raw data.

7.4.5 Shift and Add

The short-exposure speckle images shown in Fig. 7.1 are of an unresolvable star in the upper row and α-Orionis, or Betelgeuse, which is a red giant star in the lower row. In simplistic terms, each "speckle" in both sets of images may be regarded as an "image"; for the upper row, it is an image of a point source and for the lower row it is an image of α-Orionis. Such reasoning led HARVEY and coworkers [7.124, 125] to obtain the first diffraction-limited map of a star other than our own sun.

In the original method, a few bright speckles are selected from each exposure and superimposed with the aid of a digital microdensitometer and computer. Figure 7.17 shows the result of this process for a point object (a) and α-Orionis in the continuum (b) and TiO absorption band (c); clearly the giant star is resolved and the difference |(b–c)| indicates possible temperature variation over the surface of the star. MCDONNELL and BATES [7.126] have applied superresolution techniques to produce an enhanced image of Betelgeuse from this data.

This approach to forming object maps has been extended by BATES and CADY [7.127, 128] in a technique they call "shift and add". Let (α_j, β_j) denote the coordinates of the center of the brightest speckle in the jth image; each image is shifted such that (α_j, β_j) is at the origin and then added to all other similarly shifted images, giving the result

$$R(\alpha,\beta)=\frac{1}{N}\sum_{j=1}^{N} I_j(\alpha-\alpha_j,\beta-\beta_j). \tag{7.89}$$

This process is carried out for both the object under study and a reference star; the image of the object is de-convolved using that of the reference and an algorithm such as "CLEAN" [7.129]. A theoretical study [7.130]

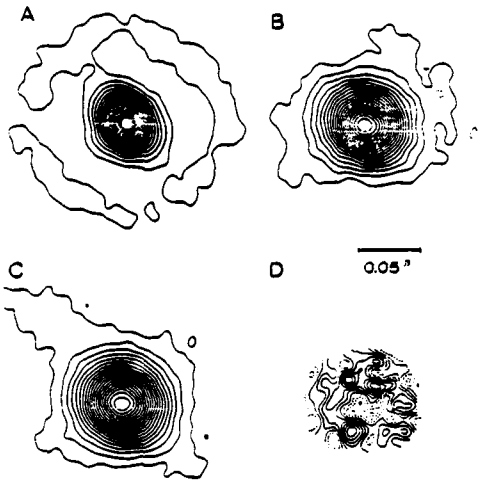

Fig. 7.17A–D. Diffraction-limited images computed from short exposure photographs by LYNDS et al. [7.124]. (A) unresolved star (γ-Ori), (B) α-Ori or Betelgeuse, in the continuum, (C) α-Ori in the TiO band and (D) the difference image (B)–(C). The contour levels are 5% of the peak intensity (A)–(C); in (D) the interval is 2%, with the broken curve indicating that the continuum is brighter

has recently confirmed that diffraction-limited information is preserved in the shift and add method.

7.4.6 Phase Averaging

In the technique of speckle interferometry, the Fourier transforms of the instantaneous image intensity and the object intensity are related by

$$i(u,v) = o(u,v)T(u,v), \tag{7.90}$$

where $T(u,v)$ is the instantaneous transfer function. The quantities $\langle|i(u,v)|^2\rangle$ and $\langle|T(u,v)|^2\rangle$ are measured and an estimate of the object energy spectrum $|o(u,v)|^2$ is obtained. Taking the logarithm of (7.90) we obtain

$$\text{phase}\{i(u,v)\} = \text{phase}\{o(u,v)\} + \text{phase}\{T(u,v)\} \tag{7.91}$$

and, taking the average

$$\langle \text{phase}\{i(u,v)\}\rangle = \text{phase}\{o(u,v)\} + \langle \text{phase}\{T(u,v)\}\rangle , \tag{7.92}$$

where, in all cases, the phase is the value in the interval $-\infty$ to ∞. Thus, provided that $\langle \text{phase}\{T(u,v)\}\rangle$ is known (or zero), the phase of the object transform can be obtained from the average phase of the image transforms; this method was first suggested by MCGLAMERY [7.131].

Using arguments based on the central limit theorem, it is not difficult to show that, for $D \gg r_0$ and angular frequencies

$$r_0/\lambda < (u,v) < (D-r_0)/\lambda ,$$

the quantity $T(u,v)$ is a circular complex Gaussian random process; it follows that

$$\langle \text{phase}\{T(u,v)\}\rangle = 0 ,$$

and that the phase $\{T(u,v)\}$ folded into the primary interval $-\pi$ to π is statistically uniformly distributed.

The crucial step in implementing the phase-averaging method is therefore the determination of the "unwrapped" phase (i.e., that in the interval $-\infty$ to ∞) from the phase in the primary interval $-\pi$ to π. In principle, this may be done by assuming continuity of the phase and following it out from the origin where it can be assumed to be zero. This procedure is subject to error when the modulus $|i(u,v)|$ is small; O'DONNELL [7.36] has shown that the root-mean-square absolute error σ in the unwrapped phase is given approximately by

$$\sigma \simeq \frac{1}{(2\bar{N})^{1/2}|\hat{i}(u,v)|} , \tag{7.93}$$

where $\bar{N}$ is the average number of detected photons per frame and $\hat{i}(u,v)$ is the Fourier transform of the instantaneous image intensity normalized to unity at the origin. Clearly, a small value of $|\hat{i}(u,v)|$ leads to a large error. For example, for a point object $[\hat{\Phi}_O(u,v) = 1]$ at an intermediate frequency $[T_D(u,v) \simeq 0.5]$ and a large telescope $(D/r_0 \simeq 40)$, an *average* value of $|\hat{i}(u,v)|$ is on the order of 10^{-2}, implying $\bar{N} > 8 \times 10^4$ detected photons per frame for a phase error of less than 0.25 rad.

Despite the above analysis, computer simulations of the phase averaging method have shown some promise [7.132, 133], particularly for providing a starting point to the Fienup algorithm. Other algorithms

for phase unwrapping have been suggested by TRIBOLET [7.134] and SWAN [7.135]; in the latter, the average phase is calculated without explicit unwrapping. Finally, MERTZ [7.74] has suggested following the phases of the angular frequency components in time in order to find their average value; the error has not yet been evaluated for this approach.

7.4.7 Knox-Thompson Method

In this method, first suggested by KNOX and THOMPSON [7.136, 137], the cross-energy spectrum of the image intensity is computed; following the notation of Sect. 7.2.1

$$\langle i(u',v')i^*(u'',v'')\rangle = o(u',v')o^*(u'',v'')\langle T(u',v')T^*(u'',v'')\rangle . \tag{7.94}$$

Taking logarithms of each side and equating imaginary parts, we find that,

$$\begin{aligned}&\text{phase}\{\langle i(u,v)i^*(u+\Delta u,v+\Delta v)\rangle\}\\&\quad=\text{phase}\{o(u,v)\}-\text{phase}\{o(u+\Delta u,v+\Delta v)\}\\&\qquad+\text{phase}\{\langle T(u,v)T^*(u+\Delta u,v+\Delta v)\rangle\},\end{aligned} \tag{7.95}$$

where we have made the substitutions

$$\Delta u = u''-u' \quad \text{and} \quad \Delta v = v''-v' \quad \text{in (7.94).}$$

Thus, provided that

i) $\langle T(u,v)T^*(u+\Delta u,v+\Delta v)\rangle \neq 0$ and

ii) phase $\{\langle T(u,v)T^*(u+\Delta u,v+\Delta v)\rangle\}$ is either known or zero, it is possible to find *phase differences* in the object spectrum. This information is then used to find the phase of the object spectrum and hence the object intensity (if the energy spectrum is known). In the following we show that (i) is satisfied when $(u,v)<r_0/\lambda$ and that phase $\{\langle T(u,v)T^*(u+\Delta u,v+\Delta v)\rangle\}$ is approximately zero; we then discuss how the phase difference information can be used to restore the actual phases.

To evaluate the quantity $\langle T(u',v')T^*(u'',v'')\rangle$ we use a similar approach to that given in Sect. 7.2.3 to evaluate the approximate speckle transfer function. In particular, it is assumed that the complex amplitude of the wave in the telescope pupil from a point source is a circular complex Gaussian process. Instead of (7.23) we now have the following

expression for $\langle T(u',v')T^*(u'',v'')\rangle$:

$$\begin{aligned}
&\langle T(u',v')T^*(u'',v'')\rangle \\
&\quad = T_0(u',v')T_0^*(u'',v'')T_s(u',v')T_s^*(u'',v'') \\
&\qquad + \mathscr{S}^{-2}\int\int_{-\infty}^{\infty}\int\int T_s\left(\frac{\Delta\xi}{\lambda},\frac{\Delta\eta}{\lambda}\right)T_s^*\left(\frac{\Delta\xi}{\lambda}+\Delta u,\frac{\Delta\eta}{\lambda}+\Delta v\right) \\
&\qquad \cdot H_0(\xi_1,\eta_1)H_0^*(\xi_1+\lambda u',\eta_1+\lambda v')H_0^*(\xi_2,\eta_2) \\
&\qquad \cdot H_0(\xi_2+\lambda u'',\eta_2+\lambda v'')d\xi_1 d\eta_1 d\xi_2 d\eta_2 ,
\end{aligned} \tag{7.96}$$

where

$$\Delta\xi=\xi_1-\xi_2, \quad \Delta\eta=\eta_1-\eta_2,$$
$$\Delta u=u''-u', \quad \Delta v=v''-v',$$

and the other symbols were defined in Sect. 7.2.3. Assuming that $H_0(\xi,\eta)$ is constant where $T_s(\xi/\lambda,\eta/\lambda)$ is effectively non-zero, the second term reduces to, see (7.24),

$$\begin{aligned}
&\mathscr{S}^{-2}\int\int_{-\infty}^{\infty}T_s\left(\frac{\Delta\xi}{\lambda},\frac{\Delta\eta}{\lambda}\right)T_s^*\left(\frac{\Delta\xi}{\lambda}+\Delta u,\frac{\Delta\eta}{\lambda}+\Delta v\right)d\Delta\xi\, d\Delta\eta \\
&\quad \cdot \int\int_{-\infty}^{\infty}|H_0(\xi,\eta)|^2\left|H_0\left\{\xi+\lambda\left(\frac{u''+u'}{2}\right),\eta+\lambda\left(\frac{v''+v'}{2}\right)\right\}\right|^2 d\xi\, d\eta .
\end{aligned} \tag{7.97}$$

Bearing in mind that the seeing transfer function $T_s(u,v)$ has a width $\simeq r_0/\lambda$, that it is clear from (7.97) that $\langle T(u,v)T^*(u+\Delta u,v+\Delta v)\rangle$ can only be non-zero if $|\Delta u|$ and $|\Delta v|<r_0/\lambda$ [otherwise the first integral in (7.97) is zero].

If we make the further approximation that the seeing transfer function has a Gaussian shape [it is more accurately described by (7.17)], then it is straightforward to show that

$$\begin{aligned}
&\langle T(u,v)T^*(u+\Delta u,v+\Delta v)\rangle \\
&\quad \simeq \langle|T(u,v)|^2\rangle\,|T_s(\Delta u/2,\Delta v/2)|^2 .
\end{aligned} \tag{7.98}$$

That is, the Knox-Thompson transfer function is simply the product of the speckle transfer function at (u,v) and the squared modulus of the seeing transfer function at $(\Delta u/2,\Delta v/2)$. It follows from (7.98) that

$$\text{phase}\,\langle T(u,v)T^*(u+\Delta u,v+\Delta v)\rangle \simeq 0 .$$

Since (7.98) results from an oversimplified atmospheric model, it cannot be relied upon quantitatively, but it does provide the correct qualitative condition on $|\Delta u|$ and $|\Delta v|$. Using the log-normal model, FRIED [7.48] suggests that the optimum value of $|\Delta u|$ and $|\Delta v|$ is approximately $0.2 r_0 / \lambda$.

If we consider the Fourier transform of the object to be sampled on a grid of N by M points there are approximately $2NM$ phase differences for a single choice of $(\Delta u, \Delta v)$; several schemes have been suggested for efficiently computing the required NM phases [7.138–145]. This problem is similar to that of calculating phases from shearing interferograms. It may be helpful to use more than one value of $(\Delta u, \Delta v)$ [7.140].

In a variation of the Knox-Thompson technique, AITKEN and DESAULNIERS [7.146] suggest computing average ratios $\langle i(u, v)/i(u + \Delta u, v + \Delta v)\rangle$, a possible advantage being that a separate reference calibration may not be required. SHERMAN [7.147] has extended the technique to non-isoplanatic imaging. BRAMES and DAINTY [7.148] have given an interpretation of the method in terms of the complex zero picture of Sect. 7.4.1; this picture may be useful for studying the role of noise in the technique. The effects of photon noise on speckle image reconstruction with the Knox-Thompson algorithm have recently been investigated [7.149]. Photon noise introduces a frequency-dependent bias which must be corrected for successful reconstruction. In the photon-limited case (low light levels), NISENSON and PAPALIOLIOS [7.149] gave the lower bound on the number of frames M required for "good" image reconstruction of a point-like object as

$$M \geqq 125 \left(\frac{N_{sp}}{\bar{N}} \right)^2 ,$$

where N_{sp} is the average number of speckles per frame and $\bar{N} (< N_{sp})$ is the average number of detected photons per frame.

7.4.8 Summary

In this section we have reviewed a number of possible techniques for solving the phase problem, that is, reconstructing the object intensity, in stellar speckle interferometry. The methods fall into two categories; those that require only the modulus of the object Fourier transform (covered in Sects. 7.4.2 and 3) and those that utilize other information present in the original speckle exposures (Sects. 7.4.4 to 7). It seems obvious that methods in the latter category are preferable for this particular phase problem, since they make use of additional information present in the available data.

Although substantial progress in this topic has been made in the last few years, the map of Betelgeuse obtained by HARVEY and coworkers in 1975 remains the *only* non-trivial stellar object reconstructed from speckle data. The practical difficulties in implementing the algorithms on real astronomical data are frequently underestimated. Part of this difficulty arises because the implementation of ordinary speckle interferometry also has a number of practical problems that have to be overcome if photometric accuracy is desired; some of these practical problems are discussed in the following section.

7.5 Implementation

7.5.1 Data Collection and Processing

Speckle camera systems have been constructed by a number of groups [7.143, 150–154]. As an example, we shall describe a "first-generation" system used at Kitt Peak National Observatory for many years [7.153], a diagram of which is shown in Fig. 7.18.

Referring to Fig. 7.18, light from the telescope passes through an electromechanical shutter (1) at the front of the speckle camera system and reaches the Cassegrain or Richey-Chretien focus at (2). At the 4 m Mayall telescope, the image scale at this focus is approximately 6.5 arcsec/mm so that a lens (3) is required to magnify the image 10 or 20 times giving final image scales of approximately 0.65 and 0.32 arcsec/mm, respectively. At 500 nm, the diffraction-limited angular frequency of a 4 m telescope is approximately 40 arcsec^{-1}, and the sampling theorem therefore requires image plane sampling at $\Delta\alpha \leqq 0''.012$, or 0.04 mm or less in the 20 × magnified image plane; this value also determines the resolution (or MTF) of the image detection system.

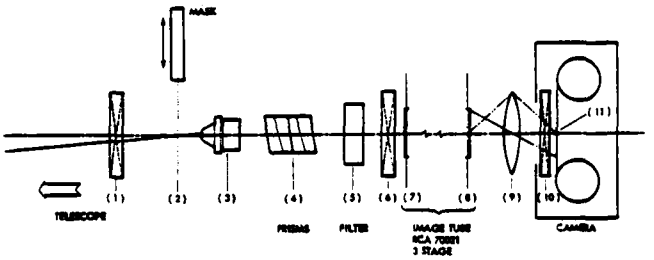

Fig. 7.18. Schematic cross-section view of a speckle camera [7.153]

It is necessary to correct for atmospheric dispersion except when observing close to the zenith. The magnitude of atmospheric dispersion depends upon a number of factors [7.155], but it is approximately given by

$$\Delta z \cong 0.3 \tan z \quad \text{arcsec/100 nm},$$

in the middle of the visible spectrum. Either a grating system [7.150, 152] or a pair of Risley prisms [7.151, 153] can be used to correct this; Fig. 7.18 shows the use of a prism pair. The optimum choice of glasses for the prisms are LaK24 and KF9 [7.156]—these match the dispersion of air over the broadest wavelength range. A narrow-band interference filter (5) selects the mean wavelength and bandpass (see Sect. 7.2.6 for a discussion of the permissable bandpass).

The most critical element in a speckle camera system is the image detector. Figure 7.18 shows an image intensifier/photographic film combination, which has the advantage of simplicity. A variety of image intensifiers may be suitable—magnetically or electrostatically focussed cascade systems, or microchannel plate devices; a variable (high) gain and low background are two practical requirements for the intensifier. Recently constructed speckle cameras and those under construction all use some form of electronic readout; this has the potential advantages of overcoming the noise and nonlinearity of photographic film and of allowing the possibility of real-time analysis of the data.

The type of electronic image detector required depends to a certain extent on the type of astronomical speckle observations that are planned and the intended method of data analysis. Before describing possible detectors it is therefore appropriate to discuss methods of data reduction. In the first-generation speckle cameras, the photographic images were analyzed in a coherent optical processor; this extremely simple analog device gives as output the energy spectrum of the complex amplitude transmittance of the film, the average energy spectrum being found by summation of the energy spectra of M frames ($M < 1000$ in practice). This technique could also be used for other "real-time" photographic-type detectors [7.139], but these analog systems tend to suffer from nonlinearities and noise. Digital processing appears to offer more flexibility and is the only way of implementing some of the object reconstruction algorithms described in Sect. 7.4.

For conventional speckle interferometry, there are two approaches to calculating the object information; one is via the average energy spectrum, as in (7.5), and the other is via the average spatial autocorrelation function as in (7.3). Allowing for moderate oversampling, large telescope speckle data requires a format of at least 256×256 pixels and a

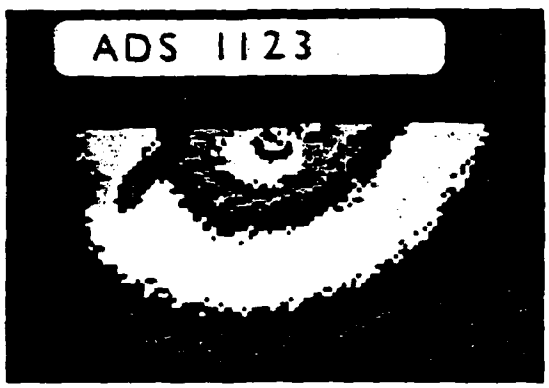

Fig. 7.19. Output of a vector autocorrelator display in real time when observing a binary star (courtesy of B. L. Morgan and H. Vine, Imperial College, London)

desirable frame rate is approximately $50\,s^{-1}$. Devices that compute Fourier transforms of this size at this rate are becoming available, but their cost may not be justified in this application. Consequently, the average energy spectrum method of analysis is currently done after the observations have been made and stored on a suitable medium such as videotape.

On the other hand, the autocorrelation method of analysis lends itself to real-time computation. VOKAC [7.157] has described a prototype on-line digital autocorrelator for 16-level (4 bit) 64×64 pixel images taken at a rate of $2\,s^{-1}$, and predicted that full-scale throughout would be possible with current technology. BLAZIT [7.158] and the London group [7.159] have constructed one-bit vector autocorrelators that process images containing a few photons (< 200) at $25\,s^{-1}$. Vector autocorrelators work on the principle that the autocorrelation function of an image consisting entirely of ones and zeros (presence or absence of a photon) is equal to the histogram of vector differences between all possible pairs of photons. This algorithm can either be hardwired in a special purpose device or programmed into a fast commercial or customized microcomputer. An example of the resolution of a binary star obtained with such a device (in real-time) is shown in Fig. 7.19. Another approach suggested by COLE [7.160] uses optical circuit elements to allow higher photon rates.

Depending upon the type of data analysis to be used, there are several possible electronic detector systems. One of the most straightforward is

to use an intensified television camera or intensifier plus television camera combination. The format of the data allows easy storage on videotape, but digital computer analysis, via a video-digitiser system, may be tedious. Another possibility is to replace the television camera by a charge-coupled device (CCD) [7.161]. The advantage of both of these approaches is that either analog (intensity) or digital (photon counting) data may be processed. For low light levels, photon counting devices in which the position and time of photoelectron events are recorded may be preferable [7.162, 163], particularly since the recorded data is already in a suitable format for vector autocorrelation processing.

It should also be noted that speckle interferometry can also be accomplished using a single or twin photomultipliers [7.164] or with a linear array [7.165], but there seems no advantage apart from cost and only bright objects can be studied. Equipment for laboratory simulation of stellar speckle interferometry has also been described [7.166].

7.5.2 One-Dimensional Infrared Speckle Interferometry

Efficient two-dimensional array detectors in the near infrared (2–5 μm) are not yet widely available and therefore infrared speckle interferometry has to be practised using only a single detector element. This feature, some other special problems that are encountered and its demonstrated astronomical success, make it worthwhile to devote a section of this review to infrared speckle interferometry.

At first glance, infrared speckle interferometry would seem less fruitful then that in the visible range, particularly in view of the restriction to a single detector element. Table 7.1 summarizes the resolution according to the diffraction-limit for a 4 m telescope (column 2) and the seeing limit (column 4) for the wavelengths of 0.5, 2.2(K), 3.45(L), and 4.8(M) μm. From column (2), it can be seen that the diffraction-limited angular resolution (Rayleigh criterion) is approximately 0.″03 at 0.5 μm,

Table 7.1.

(1) Wavelength [μm]	(2) $\Delta\alpha$ (D = 4 m) [arcsec]	(3) r_0 [m]	(4) ω [arcsec]
0.5	0.03	0.1	1.00
2.2 (K)	0.14	0.6	0.74
3.45 (L)	0.22	1.0	0.68
4.8 (M)	0.30	1.5	0.64

but only 0".30 at 4.8 μm, whereas a 1".0 seeing limited image at 0.5 μm is slightly smaller, 0".64, at 4.8 μm. Thus, taking the ratio of columns (2) and (4), we see that there is typically a 33 times increase in angular resolution possible by doing speckle interferometry at 0.5 μm, whereas the improvements at 2.2, 3.45, and 4.8 μm are only 5, 3 and 2, respectively (this does assume "good" seeing). The reason why infrared speckle has been so valuable is that, despite the relatively poorer angular resolution, there are many more potentially resolvable (i.e., large) bright objects in the near infrared than in the visible. Some infrared speckle observations are summarized in Sect. 7.6.5.

The technique of one dimensional infrared speckle interferometry is described in [7.167–171], particularly the comprehensive paper by SIBILLE et al. [7.168]. In the method developed by the French group, the image is scanned over a long, narrow slit and the light collected by a single indium antimonide (InSb) detector cooled to liquid nitrogen or helium temperature. The bandwidth restrictions are much less severe in the infrared than in the visible [see (7.37) and Table 7.1] the maximum $\Delta\lambda/\bar{\lambda}$ being on the order of 0.13 at 2.2 μm and 0.37 at 4.8 μm. The scanning speed of the image across the slit has to be sufficient to "freeze" the speckle, rates of 50–100 arcsec s^{-1} being typical; the effect of scanning rate is described by AIME et al. [7.172].

If the scan is assumed to be along the x-axis (corresponding to the u-axis in the angular frequency plane), the temporal average energy spectrum $\langle|i(f)|^2\rangle$ of the image intensity $I(t) \equiv I(\alpha/\nu)$, where ν is the scan rate, is given by

$$\langle|i(f)|^2\rangle = |o(u,0)|^2\langle|T(u,0)|^2\rangle T_{\text{slit}}^2(u)\,, \tag{7.99}$$

where the temporal frequency f is related to the angular frequency u by $f = u\nu$ and where the slit transfer function for a slit of width x_{slit} is

$$T_{\text{slit}}(u) = \frac{\sin(\pi u x_{\text{slit}})}{\pi u x_{\text{slit}}}\,. \tag{7.100}$$

The one-dimensional temporal energy spectrum can easily be computed on-line using a commercial microcomputer. By observing a reference star, the speckle transfer function can be found, so that a section through the modulus of the object energy spectrum $|o(u,0)|$ can be found. The complete modulus could in principle be found by rotating the scan direction, although because of practical problems connected with atmospheric instability only north-south and east-west scans are usually made.

One of the greatest problems encountered in implementing infrared speckle interferometry is the instability of atmospheric turbulence.

Because the seeing limited angular frequency portion of the speckle transfer function is a significant part of the whole transfer function, it is not possible to use Worden's scheme for self-calibrating the method (Sect. 7.2.8). Accordingly, a typical observing sequence is object→sky→reference→sky→object, taking perhaps 100–1000 scans of each and repeating the sequence until consistent results are obtained. The "sky" measurement is required in the infrared due to emission from both the sky and the telescope, and an estimate of the energy spectrum of the object is obtained from

$$|o(u,0)|^2 \cong \frac{\langle |i_{obj}(f)|^2\rangle - \langle |i_{sky}(f)|^2\rangle}{\langle |i_{ref}(f)|^2\rangle - \langle |i_{sky}(f)|^2\rangle}. \tag{7.101}$$

The signal-to-noise ratio of the slit scan method is derived by SIBILLE et al. [7.168]. In addition to the atmospheric fluctuation and photon noise of the signal that are the only fundamental contributions in the visible, there is now also the photon noise of the "sky" background and noise inherent in the detector, such as Johnson noise. Limiting magnitudes, based on the value of the object intensity that yields an energy spectrum equal to that of the noise sources for a single 100 ms scan, were predicted to be of the order of 5 to 6 for the K, L, and M wavelengths, although practical experience indicates limiting magnitudes of approximately 7 (K) to 2 (M). SELBY et al. [7.167] used a grating rather than a slit, thus measuring only a single-frequency component at a time; they claim fainter limiting magnitudes but these have not yet been achieved.

In a new development of one-dimensional speckle interferometry (visible or infrared) AIME et al. [7.173] suggested the use of a telescope with a one-dimensional aperture (e.g. $10 \times 800\,cm^2$). This gives a contrast gain over a circular aperture and, associated with a spectroscope, allows investigation of the spectral-angular plane with no loss in light.

7.6 Astronomical Results

Observational speckle interferometry is now over a decade old, and approximately 80 papers primarily concerned with astronomical results have been published, some of which are referenced below. Despite the enthusiasm of a few astronomers, it is only realistic to point out that the technique is not widely used or accepted by the astronomical community at large. Some possible reasons for this are: (i) relatively few objects, particularly in the visible, are resolvable by 4 m class telescopes, whose diffraction-limit at 400 nm are 0".02; (ii) calibration problems make it

difficult to obtain photometric energy spectra of sufficient accuracy for the particular astronomical problem; and (iii) only the most expensive equipment yields faint limiting magnitudes and enables the vast amounts of data to be reduced.

The summary of astronomical results given below is divided into four parts; solar system objects, binary stars, single stars and infrared objects. In addition to these, some more unusual objects have also been observed using speckle interferometry. For example, HEGE et al. [7.73] resolved one of the components of the "triple" quasar PG 1115+08 as a binary, one of the faintest objects studied by the speckle method ($m_v \simeq 16.2$). The Seyfert galaxy NGC 1068 has been observed in the visible [7.159] and at 2.2 μm [7.174], both results revealing a nuclear core containing most of the luminosity.

7.6.1 Solar System Objects

The angular diameters of the asteroids Pallas and Vesta were measured by WORDEN et al. [7.54, 175, 176], the results for Pallas indicating some elongation of the object. The diameter of the planetary satellites Rhea and Iapetus [7.176] and Titan [7.177] have also been measured.

Observations of the planet Pluto and its moon Charon are near to the limiting magnitude of speckle interferometry, their magnitudes being approximately 15.3 and 16.9, respectively. ARNOLD et al. [7.178] estimate Pluto's diameter to be 3000 ± 400 to 3600 ± 400 km depending upon whether limb darkening is incorporated in the model. This is slightly smaller than that measured by BONNEAU and FOY [7.179], 4000 ± 400 km with no limb darkening, who also estimate the diameter of Charon to be 2000 ± 200 km and propose a revised orbit for the moon. Both results imply a mean density of Pluto (and Charon) $\simeq 0.5\ \mathrm{g\,cm^{-3}}$.

The Solar granulation has also been measured by speckle interferometry [7.180–182]; the main technical problem here is the absence of any reference source for estimation of the speckle transfer function. Image reconstruction techniques (using the Knox-Thompson algorithm) have been applied to solar features [7.182].

7.6.2 Binary Stars

Speckle interferometry has been most successful when used to determine the angular separation and position angle of binary stars. MCALISTER [7.183–188] has reported over 1000 measurements of resolved binaries, and 500 binary stars unresolved by the speckle method [7.189, 190], as well as a number of detailed studies of individual systems [7.191–198].

Several hundred observations have also been reported by three other groups [7.7, 45, 199–206]. Several reasons have contributed to the success of speckle interferometry in this area; the measurements are amongst the simplest speckle observations to make, can be made rapidly on brighter stars (MCALISTER [7.207] reported 125 to 175 observations per clear night) and yield an accuracy far exceeding visual observations. MCALISTER [7.207] mentioned typical errors of 0.6% on the separation and $\pm 2°$ on the position angle, although other groups gave more conservative error estimates [7.201].

In principle, the fringe visibility can be used to estimate the magnitude difference of the two components of a binary star, but this requires proper calibration of the system using a reference star. MORGAN et al. [7.199] have built doubly-refracting prisms and a polarizer to enable artifical double-stars of known magnitude difference to be recorded for calibration purposes. It is typical of the gap between the theory and practice of speckle interferometry that the measurement of Δm, which is so simple in theory is, in practice, elusive.

The aim of making binary star measurements is usually to estimate the masses of each component. For a double-lined spectroscopic binary (i.e., one for which the radial velocities of both components are known) a minimum of two measurements of the angular separation and position angle yields both the masses of each component and the absolute distance (parallax). One example measured by MCALISTER [7.193] is 12 Persei; the masses are 1.25 ± 0.20 and 1.08 ± 0.17 times the mass of the Sun and parallax is $0''.046 \pm 0''.002$ which combined with the known apparent magnitudes gives absolute visual magnitudes of 3.8 ± 0.1 and 4.1 ± 0.1, respectively.

Binaries that are both double-lined spectroscopic and resolvable by speckle interferometry are rather rare. If the binary is single-lined, then speckle observations cannot unambiguously give the individual masses and distances. However, if masses appropriate to the spectral type are assumed, a distance can be found. MCALISTER [7.192] and MORGAN et al. [7.201] have applied this to binaries in the Hyades cluster, a distance marker in the universe, to confirm that its mass-luminosity relationship is normal and that its distance is approximately 10% greater than the original proper motion studies indicated.

BECKERS [7.208, 209] has suggested a modification of the speckle technique called "differential speckle interferometry" that may enable sub-milliarcsecond separation of binary stars to be measured on a 4 m class telescope in the visible. The technique uses the Doppler shift and observation at two closely spaced wavelengths to modulate the position of speckles in the short-exposure photographs; since the speckle procedure measures shifts to an accuracy of a fraction of the speckle size,

resolution of binaries whose separation is much less than the diffraction-limit may be possible.

7.6.3 Single Resolvable Stars

One of the first stellar discs to be resolved by speckle interferometry was the supergiant α-Orionis (Betelgeuse) [7.7] which has subsequently been observed on several occasions [7.124, 125, 203, 210–212], including the first example of a map of a star apart from our Sun [7.124]. Whilst there is evidence for substantial limb darkening on α-Orionis, the speckle energy spectrum provides rather low quality data for comparison with models. Measurements reported by Goldberg et al. [7.212] at H_α wavelength and the neighboring continuum reveal a mean diameter of 0".060 with an unresolvable bright feature near the SW limb in the continuum and significant H_α emission at large distances (radii exceeding 0".25). The diameter of the giant star α-Bootis has also been estimated [7.213].

Several *Mira variable stars*—*o-Ceti* (Mira), R. Leo and χ Cygni [7.210, 214, 215]—have been observed by speckle interferometry. These results indicate that Mira-type stars probably have smaller diameters than was previously supposed.

Finally we note that the first results of long-baseline two telescope speckle interferometry have resolved the individual components of the binary star Capella, yielding values of 5 ± 1 and $4 \pm 2 \times 10^{-3}$ arcsec [7.216].

7.6.4 Infrared Stars

Although infrared speckle interferometry is at the moment still restricted to a single detector across which the image is scanned, many interesting measurements have been made. This work is likely to expand when array infrared detectors become available.

The diameters of several protostar candidates have been measured, particularly WS–IRS 5, MonR 2–IRS 3, S 140–IRS 1 and the BN object [7.169, 171, 217–219]. MCCARTHY's measurements of the triple nature of MonR 2–IRS 3 [7.219] are a good example of the results possible with careful data analysis. The bright carbon star IRC + 10216 has been observed both the continuum and in the CO lines [7.220, 221]. Several Mira variables [7.171, 220] and the dust shells around Wolf-Rayet stars [7.222] and the supergiant α-Orionis [7.169] have also been observed. The star T-Tauri, after which the class of T-Tauri variable stars is named,

has been shown to be double [7.223]. Finally, object restoration via the Knox-Thompson algorithm and image enhancement techniques have been applied to the extended object η-Carinae [7.224].

Acknowledgements. This review was written whilst the author was on leave from the University of Rochester at the School of Electrical Engineering, The University of Sydney as the recipient of a Norman I. Price Scholarship. It is a pleasure to acknowledge the hospitality of Professor T. W. Cole, Dr. J. Davis, and Dr. W. H. Steel in Sydney and also the financial support of the U.S. Air Force under Grant AFOSR-81-0003. I wish to thank Evelyn Snyder for her expert typing of the manuscript.

References

7.1 Fizeau: Compt. Rend. **66**, 932 (1868)
7.2 M. Born, E. Wolf: *Principles of Optics*, 6th ed. (Pergamon, London 1980) p. 508
7.3 A. A. Michelson: Nature **45**, 160 (1891)
7.4 A. A. Michelson, F. G. Pease: Astrophys. J. **53**, 249 (1921)
7.5 R. Hanbury Brown: *The Intensity Interferometer* (Taylor and Francis, London 1974)
7.6 A. Labeyrie: Astron. Astrophys. **6**, 85 (1970)
7.7 D. Y. Gezari, A. Labeyrie, R. V. Stachnik: Astrophys. J. **173**, L 1 (1972)
7.8 J. C. Dainty: Symposium on Recent Advances in Observational Astronomy, ed. by H. L. Johnson and C. Allen (Ensenada, Mexico 1981) p. 95. A bibliography on stellar interferometry is maintained by the author and is available on request
7.9 C. Roddier, F. Roddier: In *Image Formation from Coherence Functions in Astronomy*, ed. by C. van Schooneveld (Reidel, Dordrecht 1979) p. 175
7.10 J. Davis: NZ J. Science **22**, 451 (1979)
7.11 R. H. T. Bates: Phys. Rep. **90**, 203 (1982)
7.12 J. C. Dainty (ed.): *Laser Speckle and Related Phenomena*, Topics Appl. Phys., Vol. 9 (Springer, Berlin, Heidelberg, New York 1975) Chap. 7
7.13 A. Labeyrie: *Progress in Optics* **14**, 47 (North-Holland, Amsterdam 1976)
7.14 S. P. Worden: Vistas in Astron. **20**, 301 (1977)
7.15 A. Labeyrie: Ann. Rev. Astron. Astrophys. **16**, 77 (1978)
7.16 High Angular Resolution Stellar Interferometry, Proceedings IAU Colloquium No. 50 (University of Sydney 1979)
7.17 Applications of Speckle Phenomena, Proc. SPIE **243** (SPIE, 1980)
7.18 A. Papoulis: *Probability, Random Variables and Stochastic Processes* (McGraw-Hill, New York 1965) p. 338 and 447
7.19 J. W. Goodman: *An Introduction to Fourier Optics* (McGraw-Hill, New York 1968), Chap. 6
7.20 J. W. Goodman: [Ref. 7.19, Eq. (6–26)], note that the form used in (7.11) assumes that $H(\xi, \eta)$ is the pupil function, and not its mirror image
7.21 R. E. Hufnagel, N. R. Stanley: J. Opt. Soc. Am. **54**, 52 (1964)
7.22 D. L. Fried: J. Opt. Soc. Am. **56**, 1372 (1966)
7.23 F. Roddier: Scientific Importance of High Angular Resolution at Infrared and Optical Wavelengths. Proc. ESO Conf. (March 1981) p. 5
7.24 F. Roddier: *Progress in Optics* **19**, 281 (North-Holland, Amsterdam 1980)
7.25 R. L. Fante: Proc. IEEE **63**, 1669 (1975) and **68**, 1424 (1980)
7.26 J. C. Dainty, R. J. Scaddan: Mon. Not. R. Astr. Soc. **170**, 519 (1975)

7.27 C. Roddier: J. Opt. Soc. Am. 66, 478 (1976)
7.28 D. S. Brown, R. J. Scaddan: Observatory 99, 125 (1979)
7.29 D. Korff: J. Opt. Soc. Am. 63, 971 (1973)
7.30 J. C. Dainty: Opt. Commun. 7, 129 (1973)
7.31 C. Aime, S. Kadiri, G. Ricort, C. Roddier, J. Vernin: Opt. Acta 26, 575 (1979)
7.32 A. Chelli, P. Lena, C. Roddier, F. Sibille: Opt. Acta 26, 583 (1979)
7.33 J. C. Dainty: Mon. Not. R. Astr. Soc. 169, 631 (1974)
7.34 F. Roddier, G. Ricort, C. Roddier: Opt. Commun. 24, 281 (1978)
7.35 D. P. Karo, A. M. Schneiderman: J. Opt. Soc. Am. 67, 1277 (1977)
7.36 K. A. O'Donnell: Thesis, University of Rochester (1983)
7.37 A. W. Lohmann, G. P. Weigelt: Optik 53, 167 (1979)
7.38 J. C. Dainty, D. R. Hennings, K.A. O'Donnell: J. Opt. Soc. Am. 71, 490 (1981)
7.39 K. A. O'Donnell, B. J. Brames, J. C. Dainty: Opt. Commun. 41, 79 (1982)
7.40 R. J. Scaddan, J. G. Walker: Appl. Opt. 17, 3779 (1978)
7.41 G. Parry, J. G. Walker, R. J. Scaddan: Opt. Acta 26, 563 (1979)
7.42 C. Roddier, F. Roddier: J. Opt. Soc. Am. 65, 664 (1975)
7.43 F. Roddier, J. M. Gilli, G. Lund: J. Opt. 13, 263 (1982)
7.44 D. P. Karo, A. M. Schneiderman: J. Opt. Soc. Am. 68, 480 (1978)
7.45 B. L. Morgan, D. R. Beddoes, R. J. Scaddan, J. C. Dainty: Mon. Not. R. Astr. Soc. 183, 701 (1978)
7.46 G. M. Morris: Appl. Opt. 20, 2017 (1981)
C. G. Wynne: Opt. Commun. 28, 21 (1979)
7.47 D. Korff, G. Dryden, R. P. Leavitt: J. Opt. Soc. Am. 65, 1321 (1975)
7.48 J. H. Shapiro: J. Opt. Soc. Am. 66, 469 (1976)
J. H. Shapiro: In *Laser Beam Propagation in the Atmosphere*, ed. by J. W. Strohbehn, Topics Appl. Phys., Vol. 25 (Springer, Berlin, Heidelberg, New York 1978) Chap. 3
7.49 D. L. Fried: Op. Acta 26, 597 (1979)
7.50 F. Roddier, J. M. Gilli, J. Vernin: J. Opt. 13, 63 (1982)
7.51 P. Nisenson, R. V. Stachnik: J. Opt. Soc. Am. 68, 169 (1978)
7.52 A. M. Schneiderman, D. P. Karo: J. Opt. Soc. Am. 68, 338 (1978)
7.53 G. P. Weigelt: Opt. Acta 26, 1351 (1979)
7.54 S. P. Worden, M. K. Stein, G. D. Schmidt, J. R. P. Angel: Icarus 32, 450 (1977)
G. L. Welter, S. P. Worden: J. Opt. Soc. Am. 68, 1271 (1978)
7.55 Yu. M. Bruck, L. G. Sodin: Astron. Astrophys. 87, 188 (1980)
7.56 S. P. Worden: SPIE Proc. 243, 66 (1980)
7.57 J. G. Walker: Opt. Acta 28, 885 (1981)
7.58 R. L. Fante: J. Opt. Soc. Am. 69, 1394 (1979)
7.59 R. J. Keyes (ed.): *Optical and Infrared Detectors*, 2nd ed., Topics Appl. Phys., Vol. 19 (Springer, Berlin, Heidelberg, New York 1980)
7.60 M. E. Barnett, G. Parry: Opt. Commun. 21, 60 (1977)
7.61 J. C. Dainty: Mon. Not. R. Astr. Soc. 183, 223 (1978)
7.62 J. G. Walker: High Angular Resolution Stellar Interferometry, Proc. IAU Colloquium No. 50 (Univ. Sydney 1979)
7.63 J. G. Walker: Opt. Commun. 29, 273 (1979)
7.64 A. H. Greenaway, J. C. Dainty: Opt. Commun. 35, 307 (1980)
7.65 F. Roddier: Imaging in Astronomy, AAS/SAO/OSA/SPIE Topical Meeting, Reprints ThC6 (Boston 1975)
7.66 J. W. Goodman, J. F. Belsher: Proc. SPIE 75, 141 (1976)
7.67 J. W. Goodman, J. F. Belsher: RADC-TR-76-50 (March 1976), RADC-TR-76-382 (December 1976), RADC-TR-77-175 (May 1977). All ARPA Order No. 2646 (Rome Air Development Center, Griffin AFB, NY 13441)
7.68 M. G. Miller: J. Opt. Soc. Am. 67, 1176 (1977)

7.69 J. C. Dainty, A. H. Greenaway: J. Opt. Soc. Am. **69**, 786 (1979)
7.70 J. C. Dainty, A. H. Greenaway: High Angular Resolution Stellar Interferometry, Proc. IAU Colloquium No. 50 (Univ. Sydney 1979)
7.71 K. A. O'Donnell, J. C. Dainty: J. Opt. Soc. Am. **70**, 1354 (1980)
7.72 A. D. Code: *Astronomical Techniques* (University of Chicago Press, Chicago, IL 1962) pp. 50–87
7.73 E. K. Hege, E. N. Hubbard, P. A. Strittmatter, S. P. Worden: Astrophys. J. **248**, L 1 (1981)
7.74 L. N. Mertz: Appl. Opt. **18**, 611 (1979)
7.75 H. A. Ferwerda: In *Inverse Source Problems*, ed. by H. P. Baltes, Topics Curr. Phys., Vol. 9 (Springer, Berlin, Heidelberg, New York 1978) Chap. 2
7.76 L. S. Taylor: IEEE Trans AP-**29**, 386 (1981)
7.77 A. H. Greenaway: J. Optics (Paris) **10**, 308 (1979)
7.78 Lord Rayleigh: Phil. Mag. **34**, 407 (1892)
7.79 E. Wolf: Proc. Phys. Soc. **80**, 1269 (1962)
7.80 K. Itoh, Y. Ohtsuka: Appl. Opt. **20**, 4239 (1981)
7.81 A. H. Greenaway: Opt. Commun. **42**, 157 (1982)
7.82 A. M. J. Huiser: Opt. Commun. **42**, 226 (1982)
7.83 R. H. T. Bates: Mon. Not. R. Astr. Soc. **142**, 413 (1969)
7.84 R. H. T. Bates, P. J. Napier: Mon. Not. R. Astr. Soc. **158**, 405 (1972)
7.85 R. E. Burge, M. A. Fiddy, A. H. Greenaway, G. Ross: Proc. R. Soc. Lond. Ser. A **350**, 191 (1976)
7.86 G. Ross, M. A. Fiddy, M. Nieto-Vesperinas, M. Wheeler: Proc. R. Soc. Lond. Ser. A **360**, 25 (1976)
7.87 M. A. Fiddy, G. Ross: Opt. Acta **26**, 1139 (1979)
7.88 Yu. M. Bruck, L. G. Sodin: Opt. Commun. **30**, 304 (1979)
7.89 P. J. Napier, R. H. T. Bates: Astron. Astrophys. Suppl. **15**, 427 (1974)
7.90 M. H. Hayes, J. H. McClellan: Proc. IEEE **70**, 197 (1982)
7.91 A. M. J. Huiser, P. van Toorn: Opt. Lett. **5**, 499 (1980)
7.92 P. van Toorn, A. H. Greenaway, A. M. J. Huiser: Preprint
7.93 M. A. Fiddy, B. J. Brames, J. C. Dainty: Opt. Lett. **8**, 96 (1983).
7.94 J. Fienup: J. Opt. Soc. Am. **73**, 1421 (1983)
7.95 R. H. T. Bates, P. T. Gough, P. J. Napier: Astron. Astrophys. **22**, 319 (1973)
7.96 P. T. Gough, R. H. T. Bates: Opt. Acta **21**, 243 (1974)
7.97 G. P. Weigelt: Optik **43**, 111 (1975)
7.98 G. P. Weigelt: Appl. Opt. **17**, 2660 (1978)
7.99 G. P. Weigelt: Proc. SPIE **243**, 103 (1980)
7.100 C. Y. C. Liu, A. W. Lohmann: Opt. Commun. **8**, 372 (1973)
7.101 J. E. Baldwin, P. J. Warner: Mon. Not. R. Astr. Soc. **182**, 411 (1978)
7.102 J. Christou: Opt. Commun. **37**, 331 (1981)
7.103 J. R. Fienup, T. R. Crimmins, W. Holsztynski: J. Opt. Soc. Am. **72**, 610 (1982)
7.104 G. P. Weigelt: Opt. Commun. **21**, 55 (1977)
7.105 G. Weigelt, B. Wirnitzer: Opt. Lett **8**, 389 (1983)
7.106 J. R. Fienup: Opt. Lett. **3**, 27 (1978)
7.107 J. R. Fienup: Opt. Engrg. **18**, 529 (1979)
7.108 J. R. Fienup: *Transformations in Optical Signal Processing* (SPIE, Bellingham, Washington 1982)
7.109 J. R. Fienup: RADC-TR-81-63 (May 1981) (Rome Air Development Center, Griffiss AFB, NY 13441)
7.110 J. R. Fienup: Appl. Opt. **21**, 2758 (1982)
7.111 R. W. Gerchberg, W. O. Saxton: Optik **35**, 237 (1972)
7.112 R. H. T. Bates: Optik **61**, 247 (1982)

7.113 K. L. Garden, R.H.T. Bates: Optik **62**, 131 (1982)
7.114 W. R. Fright, R. H. T. Bates: Optik **62**, 219 (1982)
7.115 R. H. T. Bates, W. R. Fright: J. Opt. Soc. Am. **73**, 358 (1983)
7.116 R. H. T. Bates: Comp. Graph. & Image Proc. (in press)
7.117 R. H. T. Bates, W. R. Fright: *Advances in Computer Vision and Image Processing*, Vol. 1, ed. by T. S. Huang (JAI Press, 1983) Chap. 5
7.118 S. F. Gull, G. J. Daniell: Nature **272**, 686 (1978)
7.119 J. C. Dainty, M. A. Fiddy, A. H. Greenaway: In *Image-Formation from Coherence Functions in Astronomy*, ed. by C. van Schooneveld (Reidel, Dordrecht 1979) p. 95
7.120 J. G. Walker: Opt. Acta **28**, 735 (1981)
7.121 J. W. Wood et al.: Opt. Lett., **8**, 54 (1981)
7.122 J. G. Walker: Opt. Acta **28**, 1017 (1981)
7.123 J. G. Walker: Appl. Opt. **21**, 3132 (1982)
7.124 C. R. Lynds, S. P. Worden, J. W. Harvey: Astrophys. J. **207**, 174 (1976)
7.125 S. P. Worden, C. R. Lynds, J. W. Harvey: J. Opt. Soc. Am. **66**, 1243 (1976)
7.126 M. J. McDonnell, R. H. T. Bates: Astrophys. J. **208**, 443 (1976)
7.127 R. H. T. Bates, F. M. Cady: Opt. Commun. **32**, 365 (1980)
7.128 F. M. Cady, R. H. T. Bates: Opt. Lett. **5**, 438 (1980)
7.129 J. A. Hogbom: Astron. Astrophys. Suppl. **15**, 417 (1974)
7.130 B. R. Hunt, W. R. Fright, R. H. T. Bates: J. Opt. Soc. Am. **73**, 456 (1983)
7.131 B. L. McGlamery: NASA TR SP-256, 167 (1971)
7.132 W. J. Cocke: Steward Obs. Reprint No. **264** (1980)
7.133 B. T. O'Conner, T. S. Huang: Comp. Graph. Image Proc. **15**, 25 (1981)
7.134 J. M. Tribolet: IEEE Trans. ASSP **25**, 170 (1977)
7.135 H. W. Swan: Ph.D. Thesis, Stanford University (1982)
7.136 K. T. Knox, B. J. Thompson: Astrophys. J. **193**, L45 (1974)
7.137 K. T. Knox: J. Opt. Soc. Am. **66**, 1236 (1976)
7.138 P. Nisenson, D. C. Ehn: Proc. SPIE **75**, 83 (1976)
7.139 M. P. Rimmer: Appl. Opt. **13**, 623 (1974)
7.140 J. W. Sherman: Proc. SPIE **74**, 249 (1976)
7.141 R. L. Frost, C. K. Rushforth, B. S. Baxter: Appl. Opt. **18**, 2056 (1979)
7.142 B. R. Hunt: J. Opt. Soc. Am. **69**, 393 (1969)
7.143 P. Nisenson, R. Stachnik, C. Papaliolios, P. Horowitz: Proc. SPIE **243**, 88 (1980)
7.144 R. Stachnik, P. Niesenson, C. Papaliolios: *Solar Instrumentation – What's Next?* (Sunspot, New Mexico 1980)
7.145 P. Nisenson, R. Stachnik, C. Papaliolios: In *Optical and Infrared Telescopes for the 1990s*, ed. by A. Hewitt (Kitt Peak National Observatory, Tucson, AZ 1980) p. 401
7.146 G. J. M. Aitken, D. L. Desaulniers: Opt. Commun. **28**, 26 (1979)
7.147 J. W. Sherman: Proc. SPIE **243**, 51 (1980)
7.148 B. J. Brames, J. C. Dainty: J. Opt. Soc. Am. **71**, 1542 (1981)
7.149 P. Nisenson, C. Papaliolios: Opt. Commun. **45**, 311 (1983)
7.150 A. Labeyrie: Auxiliary Instrumentation for Large Telescopes (ESO/CERN, 1972) p. 389
7.151 D. R. Beddoes, J. C. Dainty, B. L. Morgan, R. J. Scaddan: J. Opt. Soc. Am. **66**, 1247 (1976)
7.152 A. M. Scheiderman, D. P. Karo: Opt. Engrg. **16**, 72 (1977)
7.153 J. B. Breckinridge, H. A. McAlister, W. G. Robinson: Appl. Opt. **18**, 1034 (1979)
7.154 G. Hubbard, K. Hege, M. A. Read, P. A. Strittmatter, N. J. Woolf, S. P. Worden: Astron. J. **84**, 1437 (1979)
7.155 G. W. Simon: Astron. J. **71**, 190 (1966)
7.156 E. P. Wallner, W. B. Wetherell: J. Opt. Soc. Am. **69**, 1413 (1979) (abstract only)
7.157 P. R. Vokac: Proc. SPIE **119**, 223 (1977)

7.158 A. Blazit: *Image Processing Techniques in Astronomy* (Reidel, Dordrecht 1975)
7.159 J. Meaburn, B. L. Morgan, H. Vine, A. Pedlor, R. Spencer: Nature **296**, 331 (1982)
7.160 T. W. Cole: Proc. ASA **4**, 19 (1980)
7.161 D. F. Barbe (ed.): *Charge-Coupled Devices*, Topics Appl. Phys., Vol. 38 (Springer, Berlin, Heidelberg, New York 1980)
7.162 C. Papaliolios, L. Mertz: Proc. SPIE **331**, 360 (1982)
7.163 L. N. Mertz, T. D. Tarbell, A. Title: Appl. Opt. **21**, 628 (1982)
7.164 A. A. Tokovinin: Sov. Astron. Lett. **4**, 204 (1978)
7.165 G. D. Schmidt, J. R. P. Angel, R. Harms: Publ. Astr. Soc. Pac. **89**, 410 (1977)
7.166 A. M. Schneiderman, P. F. Kellen, M. G. Miller: J. Opt. Soc. Am. **65**, 1287 (1975) D. P. Karo, A. M. Schneiderman: Appl. Opt. **18**, 828 (1979)
7.167 M. J. Selby, R. Wade, C. S. Magro: Mon. Not. R. Astr. Soc. **187**, 553 (1979)
7.168 F. Sibille, A. Chelli, P. Lena: Astron. Astrophys. **79**, 315 (1979)
7.169 R. R. Howell, D. W. McCarthy, F. J. Low: Astrophys. J. **251**, L 21 (1981)
7.170 C. Perrier: ESO Messenger **29**, 26 (1981)
7.171 J. M. Mariotti, A. Chelli, R. Foy, P. Lena, F. Sibille, G. Tchountonov: Astron. Astrophys. **120**, 237 (1983)
7.172 C. Aime, S. Kadiri, G. Ricort: Opt. Commun. **35**, 169 (1980)
7.173 C. Aime, J. Demarcq, F. Martin, G. Ricort: Opt. Engrg. **22**, 224 (1983)
7.174 D. W. McCarthy, F. J. Low, S. G. Kleinmann, F. C. Gillett: Astrophys. J. **257**, L 7 (1982)
7.175 S. P. Worden, M. K. Stein: Astron. J. **84**, 140 (1979)
7.176 S. P. Worden: *Asteroids* (Univ. Arizona Press 1979) p. 119
7.177 P. Nisenson, J. Apt, R. Goody, P. Horowitz: Astron. J. **86**, 1690 (1981)
7.178 S. J. Arnold, A. Boksenburg, W. L. W. Sargent: Astrophys. J. **234**, L 159 (1979)
7.179 D. Bonneau, R. Foy: Astron. Astrophys. **92**, L 1 (1980) (*See also* G. Baier, N. Hetterich, G. Weigelt: ESO Messenger **30**, 23 (1982))
7.180 J. W. Harvey, J. B. Breckinridge: Astrophys. J. **182**, L 137 (1973)
7.181 J. W. Harvey, M. Schwarzschild: Astrophys. J. **196**, 221 (1975)
7.182 R. V. Stachnik, P. Nisenson, D. C. Ehn, R. H. Hudgin, V. E. Shirf: Nature **266**, 149 (1977)
7.183 H. A. McAlister: Astrophys. J. **215**, 159 (1977)
7.184 H. A. McAlister: Astrophys. J. **225**, 932 (1978)
7.185 H. A. McAlister, K. A. DeGioia: Astrophys. J. **228**, 493 (1979)
7.186 H. A. McAlister: Astrophys. J. **230**, 497 (1979)
7.187 H. A. McAlister, F. C. Fekel: Astrophys. J. Suppl. Ser. **43**, 327 (1980)
7.188 H. A. McAlister, E. M. Hendry: Astrophys. J. Suppl. Ser. **48**, 273 (1982)
7.189 H. A. McAlister: Publ. Astron. Soc. Pac. **90**, 288 (1978)
7.190 H. A. McAlister, E. M. Hendry: Publ. Astron. Soc. Pac. **93**, 221 (1981)
7.191 H. A. McAlister: Publ. Astron. Soc. Pac. **88**, 957 (1976)
7.192 H. A. McAlister: Astrophys. J. **212**, 459 (1977)
7.193 H. A. McAlister: Astrophys. J. **223**, 526 (1978)
7.194 H. A. McAlister: Astrophys. J. **236**, 522 (1980)
7.195 H. A. McAlister: Astron. J. **85**, 1265 (1980)
7.196 H. A. McAlister: Astron. J. **86**, 795 (1981)
7.197 H. A. McAlister: Astron. J. **86**, 1397 (1981)
7.198 H. A. McAlister, W. I. Hartkopf: Publ. Astr. Soc. Pac. **94**, 832 (1982)
7.199 B. L. Morgan, D. R. Beddoes, R. J. Scaddan, J. C. Dainty: Mon. Not. R. Astr. Soc. **183**, 701 (1978)
7.200 B. L. Morgan, G. K. Beckmann, R. J. Scaddan: Mon. Not. R. Astr. Soc. **192**, 143 (1980)

7.201 B. L. Morgan, G. K. Beckmann, R. J. Scaddan, H. A. Vine: Mon. Not. R. Astr. Soc. **198**, 817 (1982)
7.202 A. Labeyrie, D. Bonneau, R. V. Stachnik, D. Y. Gezari: Astrophys. J. **194**, L 147 (1974)
7.203 A. Blazit, D. Bonneau, L. Koechlin, A. Labeyrie: Astrophys. J. **214**, L 79 (1977)
7.204 D. Bonneau, A. Blazit, R. Foy, A. Labeyrie: Astron. Astrophys. Suppl. Ser. **42**, 185 (1980)
7.205 D. Bonneau, R. Foy: Astron. Astrophys. **86**, 295 (1980)
7.206 G. Weigelt: Astron. Astrophys. **68**, L 5 (1978)
7.207 H. A. McAlister: Modern Astrometry (IAU Colloquium No. 48, University Observatory Vienna 1978) p. 325
7.208 J. M. Beckers: Current Techniques in Double and Multiple Star Research (IAU Colloquium No. 62, Flagstaff, 1981)
7.209 J. M. Beckers: Opt. Acta **29**, 361 (1982)
7.210 D. Bonneau, A. Labeyrie: Astrophys. J. **181**, L 1 (1973)
7.211 M. S. Wilkerson, S. P. Worden: Astron. J. **82**, 642 (1977)
7.212 L. Goldberg, E. K. Hege, E. N. Hubbard, P. A. Strittmatter, W. J. Cocke: preprint C. Roddier, F. Roddier: Astrophys. J. **270**, L23 (1983)
7.213 S. P. Worden: Publ. Astr. Soc. Pac. **88**, 69 (1976)
7.214 A. Labeyrie, L. Koechlin, D. Bonneau, A. Blazit, R. Foy: Astrophys. J. **218**, L 75 (1977)
7.215 J. Christou, S. P. Worden: Astron. J. **85**, 302 (1980)
7.216 A. Blazit, D. Bonneau, M. Josse, L. Koechlin, A. Labeyrie, J. L. Onéto: Astrophys. J. **217**, L 55 (1977)
7.217 A. Chelli, P. Lena, F. Sibille: Nature **278**, 143 (1979)
7.218 H. M. Dyck, R. R. Howell: Astron. J. **87**, 400 (1982)
7.219 D. W. McCarthy: Astrophys. J. **257**, L 93 (1982)
7.220 R. Foy, A. Chelli, F. Sibille, P. Lena: Astron. Astrophys. **79**, L 5 (1979)
7.221 H. M. Dyck, S. Beckwith, B. Zuckerman: In press
7.222 D. A. Allen, J. R. Barton, P. T. Wallace: Mon. Not. R. Astr. Soc. **196**, 797 (1981)
7.223 H. M. Dyck, T. Simon, B. Zuckerman: Astrophys. J. **255**, L103 (1982)
7.224 A. Chelli, C. Perrier, Y. G. Biraud: Astron. Astrophys. **117**, 199 (1983)

Reprinted from Journal of the Optical Society of America A, Vol. 1, page 403, April, 1984.

Detection of gratings hidden by diffusers using intensity interferometry

D. Newman* and J. C. Dainty*

Department of Physics and Astronomy, The University of Rochester, Rochester, New York 14627

Received October 14, 1983; accepted November 29, 1983

Photon-correlation experiments have verified the theoretical prediction of Baltes *et al.* [Opt. Acta 28, 11–28 (1981)] that a phase grating hidden within a diffuse medium may be detected by correlation measurements. By extension of this theory to the space–time domain we have additionally verified that a simple and more reliable method of detecting the grating, valid for arbitrarily fine diffusers, is possible by temporal autocorrelation measurements of the scattered field at a single point. This method is shown to yield detailed information about the deterministic and stochastic features of the source and the source plane motion.

1. INTRODUCTION

This paper investigates the use of coherence properties in detecting the presence of a phase grating that has been obscured by an optically diffuse medium. A theoretical analysis and complete experimental verification of two detection methods involving photon correlation techniques are presented.

A recent series of theoretical papers[1–6] has shown that the spatial period of the grating may be determined in such circumstances by correlation (coherence) measurements of the scattered radiation even when a simple intensity measurement does not reveal its presence. The grating period is revealed through the existence of sharp correlation peaks that are present whenever one correlates pairs of the grating diffraction orders in the far field.[5] The width of these peaks has been estimated[7–10] by using (amplitude) interferometry. The strength of these peaks as a function of diffuse scattering has also been measured by using photon-correlation techniques.[11]

An extension of Baltes' analysis is made by allowing the diffuser to move with respect to the optical axis and grating. The spatiotemporal correlation function in this case is seen to be a direct generalization of Baltes' ($t = 0$) result. More importantly, the spatiotemporal analysis provides an entirely different and more reliable method of extracting the hidden grating period through a temporal autocorrelation measurement at a single point in the far field. The presence of the grating manifests here as a cosinusoidal modulation whose frequency is linearly proportional to the grating frequency and the diffuser velocity. The strength of the modulation depends on both the amplitude correlation length of the diffuser and the spatial period of the grating. Therefore the characteristic parameters of both deterministic and stochastic features in the compound source are easily identified by temporal autocorrelation measurements of the scattered radiation.

Previous theoretical work was phrased by using the language of coherence theory; however, we use that of speckle theory since the experiment is concerned with a scattering problem, not a source problem. It is well known[12–14] that there is a close analogy between speckle and coherence. In the present case the terminology of either may be used equally well.

2. GENERAL THEORY

Measurements are made in the far field of the grating/diffuser plane (see Fig. 1). Coherent illumination of the compound source produces in the far field an array of diffraction clouds centered on the grating diffraction orders. If the diffuser acts as a deep random phase screen (or scatterer), the angular intensity distribution of each diffraction (speckle) cloud is a Gaussian whose angular width is inversely proportional to the complex amplitude correlation length L characterizing the diffuser. The far-field angular displacement of the respective diffraction clouds is inversely proportional to the spatial period b characterizing the grating. The parameter L/b is then a measure of the degree of intensity overlap between these diffraction clouds. For $L/b \leq 0.33$, the average intensity distribution will not reveal the presence of the grating, as shown in the theoretical curves of Fig. 2.

Theoretical Model

We investigate the two-point correlation function of a time-evolving speckle intensity fluctuation produced in the far-field diffraction plane by laser illumination of a diffuse object moving with velocity $\mathbf{v} = v_\xi\hat{\xi} + v_\eta\hat{\eta}$ with respect to the optical axis and grating. The unit vectors $\hat{\xi}$ and $\hat{\eta}$ define the object plane in this notation. The diffuser is modeled as a deep random phase screen whose surface-height probability distribution is a Gaussian of standard deviation σ_h and has a surface-height correlation length denoted by l_h. The diffuser is assumed to be homogeneous, i.e., spatially stationary in the statistical sense.

Using two-dimensional notation, we express the complex amplitude in the scattering plane as a product

$$U(\xi, \eta, t) = P(\xi, \eta)\exp[i\phi(\xi, \eta, t)]T(\xi, \eta), \qquad (1)$$

where

0740-3232/84/040403-09$02.00

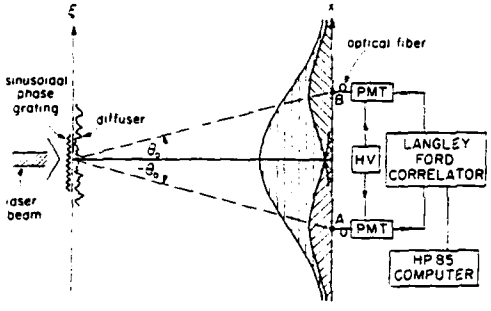

Fig. 1. Experimental arrangement.

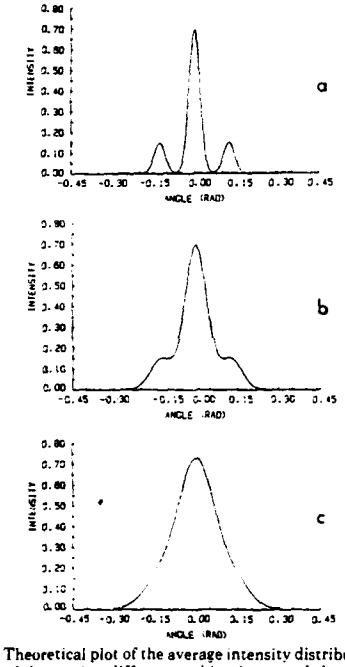

Fig. 2. Theoretical plot of the average intensity distribution in the far field of the grating/diffuser combinations: a. $L/b = 1.0$, b. $L/b = 0.5$, and c. $L/b = 0.33$. L is the 1/e correlation length of the complex amplitude transmittance of the diffuser and b is the spatial period of the sinusoidal phase grating).

$P(\xi, \eta)$ is a real pupil function.

$\varphi(\xi, \eta, t)$ is a time-evolving random phase that is due to the diffuser.

$T(\xi, \eta)$ is the sinusoidal phase grating transmission.

In our case

$$P(\xi, \eta) = I_0 \exp[-(\xi^2 + \eta^2)/4a^2],$$

where a is the laser-beam radius

$$T(\xi, \eta) = \exp[i\alpha(\sin 2\pi\xi/b)],$$

where α is the effective optical depth and b is the spatial period of the grating and

$$\varphi(\xi, \eta, t) = \varphi(\xi - v_\xi t, \eta - v_\eta t)$$

is the explicit time dependence of the random phase.

For computational simplicity we expand the grating transmission term in a discrete Fourier series

$$\exp[i\alpha \sin(2\pi\xi/b)] = \sum_{n=-\infty}^{\infty} g_n \exp(in2\pi\xi/b), \quad (2)$$

where $g_n = J_n(\alpha)$ is the Bessel function of the first kind with argument α (α is real and nonnegative).

The correlation of complex amplitudes is defined as

$$\Gamma(x_1, y_1; x_2, y_2, \tau) = \langle U(x_1, y_1, t) U^*(x_2, y_2, t + \tau) \rangle, \quad (3)$$

where $\langle\rangle$ denotes an ensemble average. As is well known, we may express the far-field complex amplitude $U(x_1, y_1, t)$ in terms of the source plane complex amplitude $U(\xi_1, \eta_1, t)$ by means of the Fresnel–Kirchhoff diffraction formula. Since measurements are made in the far field of the grating/diffuser plane, the simplifying requirements of Fraunhofer zone diffraction are assumed to be satisfied, that is,

$$ka \gg 1, \quad (3a)$$

$$R \gg ka^2, \quad (3b)$$

where $k = 2\pi/\lambda$ is the laser wave number and R is the distance from the detector to the source plane. The far-field correlation of amplitudes may then be expressed as a fourfold Fourier transform:

$$\Gamma(x_1, y_1, x_2, y_2, \tau) = \iint_{-\infty}^{\infty} d\xi_1 d\xi_2 \times \iint_{-\infty}^{\infty} d\eta_1 d\eta_2 \langle U(\xi_1, \eta_1, t) U^*(\xi_2, \eta_2, t + \tau) \rangle \times \exp\left[-\frac{2\pi i}{\lambda R}(x_1\xi_1 - x_2\xi_2 + y_1\eta_1 - y_2\eta_2)\right]. \quad (4)$$

where we have ignored the unimportant phase factors and scaling constants. Evaluation of Eq. (4) requires that we first evaluate the correlation of complex amplitudes that are due to the diffuser, namely,

$$\langle \exp[i[\varphi(\xi_1, \eta_1, t) - \varphi(\xi_2, \eta_2, t + \tau)]] \rangle.$$

If the diffuser satisfies our initial assumptions and is in addition optically rough, $\sigma_h \geq \lambda$, it can be shown[15] that the correlation of complex amplitude transmittance is approximately Gaussian of width equal to L:

$$\langle \exp[i[\varphi(\xi_1, \eta_1, t) - \varphi(\xi_2, \eta_2, t + \tau)]] \rangle \approx \exp\{-[(\xi_1 - \xi_2 - v_\xi\tau)^2 + (\eta_1 - \eta_2 - v_\eta\tau)^2]/2L^2\}, \quad (5)$$

where

$$L = l_{1/e}[2\pi(n - 1)\sigma_h/\lambda]$$

and n is the bulk index of refraction within the diffuse medium. The limit of a delta correlated source ($L \to 0$) often used in the literature yields a correlation of complex amplitudes [Eq. (4)] that does not depend on the deterministic source plane phase; rather it depends only on the source intensity. This approximation is therefore insufficient for our purposes. The source correlation of complex amplitude is now

$$\langle U(\xi_1, \eta_1, t)U^*(\xi_2, \eta_2, t+\tau)\rangle$$
$$= \exp\left\{-\left[\frac{(\xi_1 - \xi_2 - v_\xi\tau)^2 + (\eta_1 - \eta_2 - v_\eta\tau)^2}{2L^2}\right]\right\}$$
$$\times \langle P(\xi_1, \eta_1)T(\xi_1)[P(\xi_2, \eta_2)T(\xi_2)]^*\rangle. \quad (6)$$

A simple change of variables proves quite useful here. By defining the sum and difference coordinates

$$\xi_0 = (\xi_1 + \xi_2)/2, \qquad \eta_0 = (\eta_1 + \eta_2)/2,$$
$$\xi = \xi_1 - \xi_2, \qquad \eta = \eta_1 - \eta_2,$$

we find that

$$\langle P(\xi_1, \eta_1)T(\xi_1)[P(\xi_2, \eta_2)T(\xi_2)]^*\rangle$$
$$= \sum_{n,m=-\infty}^{\infty} g_n g_m^* \exp[-(\xi^2 + \eta^2)/8a^2]\exp[i2\pi(n+m)\xi/b]$$
$$\times \exp[-(\xi_0^2 + \eta_0^2)/2a^2]\exp[i2\pi(n-m)\xi_0/b]. \quad (7)$$

Equation (4) now separates into four closed Fourier integrals, and a straightforward calculation shows that

$$\Gamma(s, \sigma, 0, 0, \tau) = \exp(-|v|^2\tau^2/8a^2)$$
$$\times \sum_{n,m=-\infty}^{\infty} g_n g_m^* \exp\left[\frac{-i2\pi v_\xi \tau}{b}\left(s/\sin\theta_0 - \frac{n+m}{2}\right)\right]$$
$$\times \exp\left\{-\tfrac{1}{2}k^2a^2\left[\sigma - (n-m)\frac{\lambda}{b}\right]^2\right\}$$
$$\times \exp\left\{-\tfrac{1}{2}k^2L^2\left[s - \tfrac{1}{2}(n+m)\frac{\lambda}{b}\right]^2\right\}. \quad (8)$$

where

$$s \equiv \frac{x_1 + x_2}{2R} = \frac{\sin\theta_1 + \sin\theta_2}{2}$$

and

$$\sigma \equiv \frac{x_1 - x_2}{R} = \sin\theta_1 - \sin\theta_2$$

are the angular sum and difference coordinates. $\sin\theta_0 = \lambda/b$ is the first grating diffraction order, and we concern ourselves here only with correlation measurements along the far-field x axis; hence $y_1 = y_2 = 0$.

Photon-correlation experiments do not measure Γ directly; rather they are capable of measuring a related quantity, the correlation of intensity fluctuation, whose normalized form in one-dimensional notation is

$$C_I(x_1, x_2, \tau) = \frac{\langle I(x_1, t)I^*(x_2, t+\tau)\rangle}{|\langle I(x_1, 0)\rangle||\langle I(x_2, 0)\rangle|} - 1, \quad (9)$$

where $I(x_1, t) = U(x_1, t)U^*(x_1, t)$.

If $L/a \ll 1$, the far-field speckle has Gaussian statistics so that the intensity and amplitude correlations are simply related:

$$C_I(x_1, x_2, \tau) = \frac{|\Gamma(x_1, x_2, \tau)|^2}{|\Gamma(x_1, x_1, 0)||\Gamma(x_2, x_2, 0)|} \equiv |\gamma(x_1, x_2, \tau)|^2, \quad (10)$$

where $\gamma(x_1, x_2, \tau)$ is commonly termed the complex degree of coherence and satisfies $0 \le |\gamma| \le 1$ by virtue of the Schwarz inequality.

3. EXPERIMENTAL PROCEDURE

The experimental setup is shown in Fig. 1. Correlation measurements are all made in the far field using standard photon-correlation equipment. The detectors consist of thin optical fibers of 50-μm core diameter coupled to Hamamatsu R928 photomultipliers. The signals are passed through a preamplifier/discriminator and the photon counts analyzed by a Langley Ford correlator that estimates the correlation function with 128-channel resolution, each channel corresponding to a time increment $\Delta\tau$. Typical time increments used in our experiment were $\Delta\tau$ = 50–200 μsec, and photon rates of approximately one photon per $\Delta\tau$ or 5×10^3–2×10^4 sec^{-1}, with a dark count of approximately 100 sec^{-1}. Typical measurement times were 10–20 sec (about 10^5 samples).

Measurements of the spatial cross correlation of intensities in the so-called antisymmetric scan[5] ($\sin\theta_1 = -\sin\theta_2 = \lambda/b$) are estimated from the temporal cross correlation at zero time delay.

A series of diffusers was produced in photo resist. Multiple exposure of these plates to different speckle patterns and subsequent development yields an optically rough surface whose surface-height probability distribution is approximately Gaussian.[16,17] The standard deviation σ_h of this distribution and the surface-height correlation length l_h of each diffuser are measured by using a Dektak profilometer (mechanical stylus device). The resulting value of the complex amplitude correlation length L is then determined for a particular wavelength by Eq. (5) whenever $\sigma_h \ge \lambda$. The refractive index n of photoresist is approximately 1.67 at the He–Ne wavelength λ = 633 nm. The diffusers used here give correlation lengths of L = 0.9, 1.4, 2.3, 2.7, 3.3, 6.4, 7.1, and 10.3 μm.

Two thin sinusoidal phase gratings of spatial periods b = 5.1 and 9.2 μm were produced holographically by using Kodak 131-02 holographic film. The optical depth of the gratings was estimated from standard intensity measurements, and

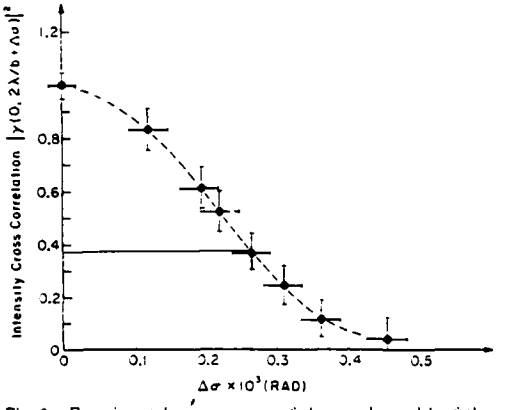

Fig. 3. Experimental measurement of the angular width of the cross-correlation peak in the antisymmetric scan, $\sigma = 2\lambda/b + \Delta\sigma$ versus $\Delta\sigma$. The $1/e$ width of this peak occurs at $\Delta\sigma \approx 1.26 \times 10^{-3}$ rads, which is approximately equal to $1/ka$, where $k \approx 10^{-2}$ mm is the He–Ne wave number and a = 0.33 mm is the laser-beam radius ($L/a \approx 1.2$ for this measurement).

both gratings used in the experiment had an effective optical depth of $\alpha \cong 0.85$. The values of the first four Fourier coefficients are then

$$g_0 \cong 0.826,$$
$$g_1 \cong 0.385,$$
$$g_2 \cong 0.08,$$
$$g_3 \cong 0.012,$$

The experimental error associated with α is less than 5%, whereas the error in measurement of the amplitude correlation length L is in the 5–10% range.

A precise estimate of the spatial cross-correlation peak value in the antisymmetric scan is made difficult because of the sharpness of this peak, as shown experimentally in Fig. 3. Great care was taken in aligning the detectors, and measurements were repeated on several occasions with consistent results. The sharpness of this peak may be appreciated by considering our arrangement. For a laser beam width of $2a \cong 0.66$ mm and wavelength $\lambda \cong 633$ nm, the angular width of this peak has a predicted value[5] of $1/ka \cong 3 \times 10^{-4}$ rad. For $R = 2$ m, a 0.1-mm alignment error yields only 90% of the true correlation peak, and this peak vanishes whenever the net alignment error exceeds a speckle diameter, which in our case is approximately 2 mm.

The diffuser translation was effected by a continuous rotation in the (ξ, η) plane. The diffuser's relative component of velocity parallel to the far-field x axis, v_ξ, is equal to $2\pi\omega_d r_\eta$, where r_η is the vertical displacement of the laser beam with respect to the center of the rotation and ω_d is the angular speed of the diffuser. The relative velocity v_η is then equal to $2\pi\omega_d r_\xi$, where r_ξ is the horizontal displacement. It is understood here that the diffuser plane (ξ, η) is perpendicular to the beam axis at all times.

For measurements involving only one-dimensional translations $|v| = v_\xi$, $(v_\eta = 0)$, a variable-speed linear translator was used that allowed for accurate measurements of v_ξ and hence the modulation period as a function of b/v_ξ.

Experimental values for the modulation strength of the beats in the autocorrelation function were made with a pencil and a ruler after obtaining a hard copy of the correlator output. It would not be difficult to measure these quantities electronically as the correlation function is being processed. This would reduce the total measurement time to a few seconds and therefore might be practical as an information-coding scheme.

4. SPATIAL CORRELATION AT ZERO TIME DELAY

For zero time delay, $\tau = 0$, the complex degree of coherence, or normalized amplitude correlation function, is given from Eq. (3) by

$$\gamma(s, \sigma, 0) = \frac{\sum_{n,m} g_n g_m \exp\left\{-\tfrac{1}{2}k^2a^2\left[\frac{\sigma - (n-m)\lambda}{b}\right]^2\right\} \exp\left\{-\tfrac{1}{2}k^2L^2\left[s - \tfrac{1}{2}\frac{(n+m)\lambda}{2}\right]^2\right\}}{\left(\left\{\sum_n |g_n|^2 \exp\left[\frac{-2\pi^2L^2}{b^2}(s + \sigma/2 - n\lambda/b)^2\right]\right\}\left\{\sum_n |g_n|^2 \exp\left[\frac{-2\pi^2L^2}{b^2}(s - \sigma/2 - n\lambda/b)^2\right]\right\}\right)^{1/2}} \tag{11}$$

where $s + \sigma/2 = \sin\theta_1$, $s - \sigma/2 = \sin\theta_2$, and we have made use of the fact that $a, b \gg 1$ in evaluating the denominator. There is no loss of generality here, as $a/b \gg 1$ for all situations of practical interest. This expression was first derived in Refs. 1–6 and has a number of interesting related properties. The average intensity, defined as $\Gamma(x_1, x_1) \equiv \Gamma(s = \sin\theta_1, \sigma = 0)$, exhibits broad peaks centered on the far-field grating diffraction orders $\sin\theta_1 = n\lambda/b$. The angular width of these peaks is approximately equal to $(kL)^{-1}$. The amplitude cross correlation in the so-called antisymmetric scan,[15] $\Gamma(x_1, -x_1) \equiv \Gamma(s = 0, \sigma = 2\sin\theta_1)$, is sharply peaked whenever $\sin\theta_1 = \pm n\lambda/b$, i.e., whenever one correlates pairs of diffraction orders. The angular width of the correlation peaks is approximately equal to $(ka)^{-1}$ and is narrow compared with $(kL)^{-1}$ in situations of practical interest.

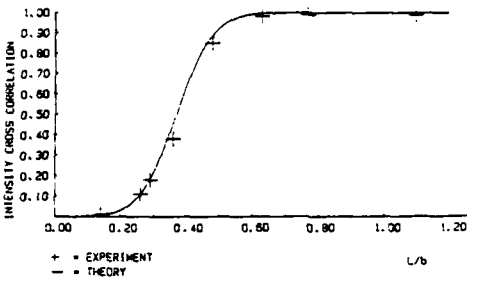

Fig. 4. Peak values of the intensity cross correlation measured at angles $(-\theta_0, \theta_0)$ as a function of L/b $(\sin\theta_0 \equiv \lambda/b)$.

We now examine in detail a correlation of the ±1 diffraction orders, $\sin\theta_1 = -\sin\theta_2 = \lambda/b$ (thus $\sigma = 2\lambda/b$, $s = 0$ in our notation). Direct evaluation of Eq. (11) appears to be a difficult task in this case; however, because of our particular values of the Fourier coefficients g_n and the fact that $a/b \gg 1$, it is shown that $\gamma(0, 2\lambda/b)$ has a simple form.

In particular, note that the term

$$\exp[-\tfrac{1}{2}k^2a^2[\sigma - (n-m)\lambda/b]^2] = \exp\left\{-\frac{2\pi^2a^2}{b^2}[2 - (n-m)]^2\right\} \cong \delta_{2,n-m}$$

for $\sigma = 2\lambda/b$. Thus only the terms $n - m = 2$ contribute to the sum. Further, if the optical depth of the grating satisfies $0 \le \alpha \le 1.5$, it is seen that the Fourier coefficients $g_n = J_n(\alpha)$ are a rapidly decreasing function of n. For our case, $\alpha = 0.85$, only the terms $n = 0, \pm1, \pm2$ contribute significantly. Therefore to a high degree of accuracy we may express the normalized correlation of complex amplitudes as

$$\gamma(0, 2\lambda/b) \cong \frac{2g_0g_2\exp(-2\pi^2L^2/b^2) + |g_1|^2 + 2g_1g_3\exp(-8\pi^2L^2/b^2)}{|g_1|^2 + (|g_0|^2 + |g_1|^2)\exp(-2\pi^2L^2/b^2)} \tag{12}$$

where $2g_0g_2 + 2g_1g_3 = |g_1|^2$ to four significant places. This is due to the general result that

$$0 = \sum_{k=0}^{2n} (-1)^k J_k(z) J_{2n-k}(z) + 2 \sum_{k=1}^{\infty} J_k(z) J_{2n+k}(z) \quad (n \geq 1).$$

The minus on $|g_1|^2$ arises from the fact that $J_{-n}(\alpha) = (-1)^n J_n(\alpha)$ and has the physical interpretation here that the ± 1 diffraction orders are antiphased. We see that $|\gamma(0, 2\lambda/b)| \to 1$ for $L/b \to \infty$, which is the extreme coherent limit.

where γ is the normalized version of Eq. (8) with time delay $\tau > 0$, and $s + \sigma/2 = \sin\theta_1$, $s - \sigma/2 = \sin\theta_2$ as before. We again restrict the far-field analysis to measurements along the x axis ($y_1 = y_2 = 0$); however, one should recall that the diffuser has a linear velocity $\mathbf{v} = v_\xi \hat{\xi} + v_\eta \hat{\eta}$ in the object plane, where $\hat{\xi}$ is parallel to $\hat{x}$ and $\hat{\eta}$ is perpendicular to $\hat{x}$. The spatiotemporal correlation of intensities is

$$|\gamma(s, \sigma, \tau)|^2 = \exp(-|v|^2\tau^2/4a^2) \frac{\left|\sum_{n,m} A_{nm}(s, \sigma) \exp\left\{-\frac{i2\pi v_\xi \tau}{b}\right\} [s/\sin\theta_0 - \tfrac{1}{2}(n+m)]\right|^2}{\left\{\sum_n |g_n|^2 \exp\left[-\frac{2\pi^2 L^2}{b^2}(s + \sigma/2 - n\lambda/b)^2\right]\right\}\left\{\sum_n |g_n|^2 \exp\left[-\frac{2\pi^2 L^2}{b^2}(s - \sigma/2 - n\lambda/b)^2\right]\right\}}. \quad (14)$$

and $|\gamma(0, 2\lambda/b)| \to 0$ for $L/b \to 0$, which is the extreme incoherent limit. A plot of the normalized correlation of intensities in the antisymmetric scan $|\gamma(0, 2\lambda/b)|^2$ against the parameter L/b is shown in Fig. 4. The experimental agreement is seen to be excellent. Note that, for $L/b \leq 0.33$, the far-field intensity distribution is completely diffuse (see Fig. 2), whereas correlation measurements reveal the presence of the grating for all $L/b \geq 0.15$. Hence there is a small but important range of values $0.15 \leq L/b \leq 0.33$ for which correlation measurements detect the presence of the grating even when simple intensity measurements would fail, i.e., when the intensity information is hidden in speckle noise.

It should be stressed here that the curve in Fig. 4 depends critically on the Fourier coefficients g_n of the grating. The range of values of L/b for which the hidden periodicity may be revealed by either correlation measurements or interferometry[3] will then depend on the particular choice of phase grating and must be evaluated from Eq. (11) in each case. An example of this effect using a lamellar phase grating that nullifies the even diffraction orders was worked out theoretically by Baltes[5] and has similar characteristics to our case.

In principle, an amplitude interferometry experiment will yield a larger range of values for which the coherence effect is noticeable because interferometry measures γ directly, whereas photon correlation experiments measure $|\gamma|^2$. No detailed experiment along these lines has yet been reported.

5. SPATIOTEMPORAL CORRELATION FUNCTION

Our experiment is capable of measuring the spatiotemporal correlation function of dynamic speckle intensity fluctuations. We therefore present the time-dependent features of this quantity here. The normalized correlation of intensity fluctuations is defined by

$$\gamma(s, \sigma, \tau)|^2 = \frac{|\Gamma(s, \sigma, \tau)|^2}{|\Gamma(s + \sigma, 0, 0)||\Gamma(s - \sigma, 0, 0)|}. \quad (13)$$

For $\tau > 0$, the normalized correlation of amplitudes $\gamma(s, \sigma, \tau)$ is a complex function; hence in evaluating $|\gamma|^2$ both real and imaginary parts are relevant. The numerator in Eq. (14) is seen to have the form

$$|\gamma(s, \sigma, \tau)|^2 \propto \exp(-|v|^2\tau^2/4a^2)\{|\sum_{n,m} A_{nm}(s, \sigma) \times \cos[\omega_{nm}(s)\tau]|^2 + |\sum_{n,m} A_{nm}(s, \sigma)\sin[\omega_{nm}(s)\tau]|^2\}, \quad (15)$$

where

$$A_{nm}(s, \sigma) = g_n g_m \exp\left\{-\tfrac{1}{2}k^2a^2\left[\sigma - \frac{(n-m)\lambda}{b}\right]^2\right\} \times \exp\left\{-\tfrac{1}{2}k^2L^2\left[s - \tfrac{1}{2}\frac{(n+m)\lambda}{b}\right]^2\right\},$$

where

$$\omega_{nm}(s) = \frac{2\pi v_\xi}{b}\left(s/\sin\theta_0 - \frac{n+m}{2}\right)$$

and $\sin\theta_0 \equiv \lambda/b$ is the first grating diffraction order.

The spatiotemporal correlation function has the usual Gaussian envelope[18] of width $t_0 \equiv 2a/|v|$ within which are a series of harmonic oscillations. For the case of an intensity autocorrelation it is shown that the modulation of this Gaussian envelope is entirely cosinusoidal and is heavily weighted in favor of a fundamental frequency $\omega_0 = 2\pi v_\xi/b$.

An autocorrelation of intensities is defined as $|\gamma(x_1, x_2, \tau)|^2 \equiv |\gamma(s = \sin\theta_1, \sigma = 0, \tau)|^2$. Since $a/b \gg 1$, we find that

$$A_{nm}(s, 0) \cong g_n g_m \exp\left\{-\tfrac{1}{2}k^2L^2\left[s - \tfrac{1}{2}\frac{(n+m)\lambda}{b}\right]^2\right\}\delta_{n,m}, \quad (16)$$

where $s \equiv \sin\theta$ defines the detection location on the far-field x axis.

By defining

$$q^2 \equiv 2\pi^2L^2/b^2,$$

$$\omega_0 \equiv 2\pi v_\xi/b,$$

$$K \equiv s/\sin\theta_0 = \sin\theta/\sin\theta_0,$$

we now express Eq. (14) in a more transparent form:

$$|\gamma(s, 0, \tau)|^2 = \exp(-|v|^2\tau^2/4a^2) \frac{|\sum_n |g_n|^2 \exp[-q^2(K-n)^2]\cos(\omega_0\tau(K-n)]|^2 + |\sum_n |g_n|^2 \exp[-q^2(K-n)^2]\sin[\omega_0\tau(K-n)]|^2}{|\sum_n |g_n|^2 \exp[-q^2(K-n)^2]|^2}. \quad (17)$$

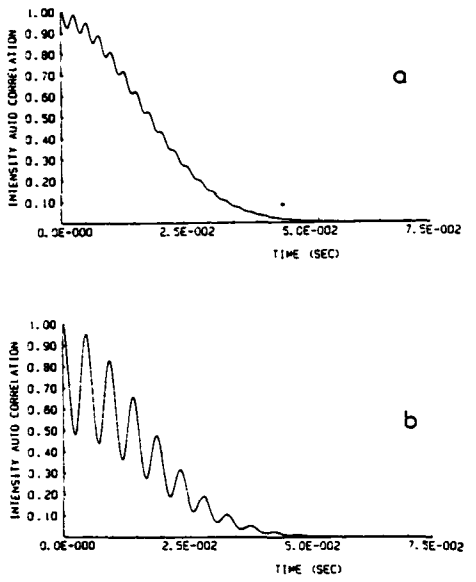

Fig. 5. Theoretical plots of the temporal-intensity autocorrelation at the center of the diffraction field ($s = 0, \sigma = 0$). The diffuser velocity is $v_\xi = 1.3$ mm/sec, and $v_\eta = 30$ mm/sec. The amplitude correlation length $L = 2\ \mu$m, and a, $b = 5.1\ \mu$m; b, $b = 9.2\ \mu$m.

We now restrict our attention to the case $-\lambda/b \le s \le \lambda/b$. That is, we consider an autocorrelation at any point along the far-field x axis that lies within the ± 1 grating diffraction orders. The results obtained are, in fact, quite general, and this merely serves as an illustration of the spatiotemporal behavior in a particular spatial domain. Recollecting that for our case $g_0 \gg |g_{\pm 1}| \gg |g_{\pm 2}|, \ldots$ etc., it is clear by inspection of Eq. (17) that only the terms $n = 0, \pm 1$ contribute significantly whenever $-1 \le K \le 1$ and $L/b \ge 0.05$ (i.e., $q^2 \ge 0.05$). With the above restrictions in mind, a little algebra shows that

$$\begin{aligned}|\gamma(s, 0, \tau)|^2 \cong \exp(-v^2\tau^2/4a^2)/N(K, q)\\ \times [|g_0|^4\exp(-2q^2K^2) + |g_{\pm 1}|^4\exp[-2q^2(K+1)^2]\\ + \exp[-2q^2(K-1)^2]|\\ + 2|g_0|^2|g_{\pm 1}|^2(\exp[-q^2(K^2+(K+1)^2]|\\ + 2\exp[-q^2(K^2+(K-1)^2]|)\cos(\omega_0\tau)],\end{aligned} \tag{18}$$

where

$$\begin{aligned}N(K, q) = (|g_0|^2\exp(-q^2K^2)\\ + |g_{\pm 1}|^2\exp[-q^2(K+1)^2] + \exp[-q^2(K-1)^2]|)^2\end{aligned}$$

is the normalization as a function of K and q.

Careful manipulation of Eq. (17) shows that the inclusion of higher-order terms again introduces cosinusoidal modulation whose frequencies are integral multiples of ω_0. Because of exponential damping and the Fourier coefficients g_n, however, all such terms are small corrections and may be safely dropped in this case.

Equation (18) therefore incorporates all the relevant dynamic features of the spatiotemporal autocorrelation measurements in our experiment and has some interesting features. We first note that, for $-1 \le K \le 1$, Eq. (18) is symmetric in K (i.e., in θ), as might be expected, and has the general form

$$\begin{aligned}&|\gamma(s, 0, \tau)|^2\\ &\cong \frac{\exp(-[v^2\tau^2/4a^2)][A(q, K) + B(q, K)\cos(\omega_0\tau)]}{A(q, K) + B(q, K)},\end{aligned} \tag{19}$$

where

$$A(q, K) = A(q, -K),$$

$$B(q, K) = B(q, -K),$$

and the explicit definitions of each are self-evident from Eq. (18).

Thus the autocorrelation at any point along $-\lambda/b \le \sin\theta \le \lambda/b$ consists of a Gaussian envelope of temporal width $t_0 = 2a/|v|$ modulated by a cosine of period $t_M = b/v_\xi$, where v_ξ is the diffuser's component of velocity parallel to the far-field x axis. Whenever $t_M < t_0$ and $B(q, K) > 0$, this modulation clearly presents itself in routine autocorrelation measurements, as shown in Figs. 5–7. The remarkable feature of Eq. (18) and hence of Eq. (19) is that the period of this modulation

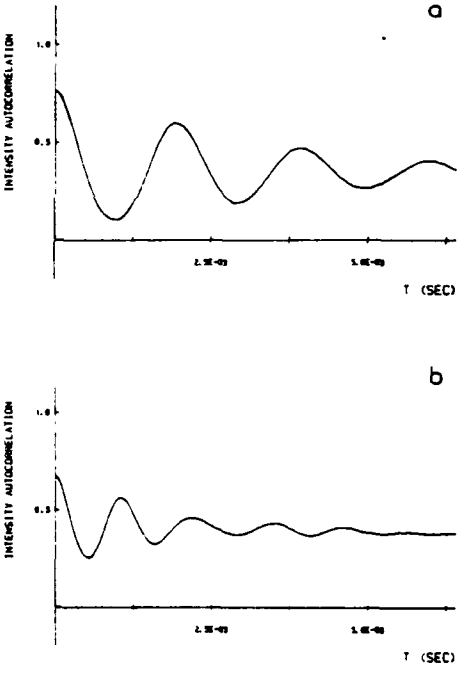

Fig. 6. Experimental measurements of the intensity autocorrelation function at the center of the diffraction field ($s = 0, \sigma = 0$). The diffuser velocity is $v_\xi = 0.5$ mm/sec, $v_\eta = 0$ (pure translation along ξ). The diffuser has an amplitude correlation length of $L \cong 0.9\ \mu$m, and a, $b = 9.2\ \mu$m; b, $b = 5.1\ \mu$m. Note that the period of oscillation varies as σ is, to a high degree of accuracy, and the modulation strength increases as L/b is reduced.

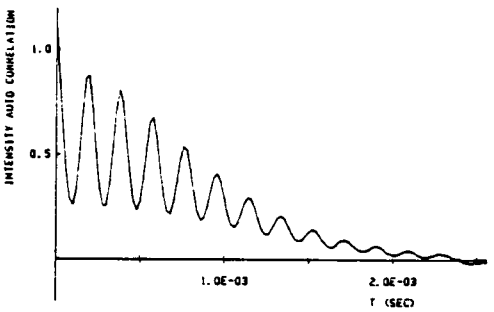

Fig. 7. Experimental measurement of the temporal-intensity autocorrelation function at the center of the diffraction field ($s = 0$, $\sigma = 0$) with parameters $L \cong 0.9$ μm, $b = 9.2$ μm, $a = 0.33$ mm, $v \cong 50$ mm sec^{-1}, $v_x \cong 560$ mm sec^{-1}. Note the modulation period $\tau_m \cong 1.8 \times 10^{-3}$ sec, and the Gaussian envelope has a $1/e$ time of $\tau_0 = 1.2 \times 10^{-3}$ sec, as predicted by theory.

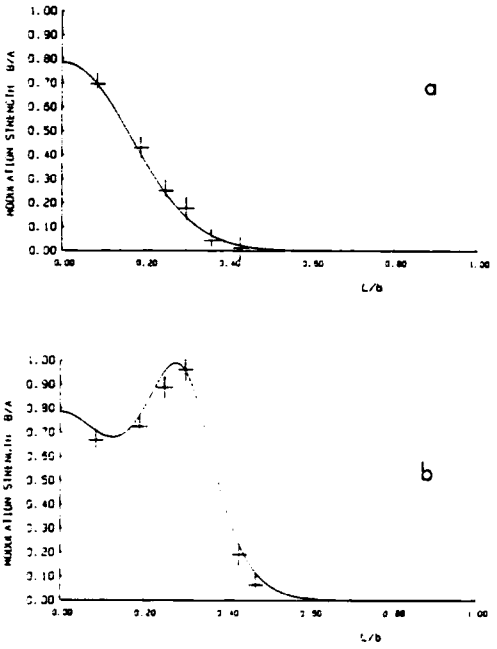

Fig. 8. Modulation strength as a function of intensity overlap L/b at fixed scan angle: a, $K = 0$; b, $K = 1$. The solid curve is a theoretical plot; the +'s refer to experimental measurements.

is entirely independent of the detector location. The detector location K and the overlap parameter σ along with the Fourier coefficients g_n determine the strength of the modulation that we define here as

$$S(q, K) = B(q, K)\, A(q, K), \tag{20}$$

where $A(q, K)$ is a measure of the relative amplitude strength of the [illegible] modulation [illegible]

For fixed diffuser velocity v, Eq. (18) enables us to measure the spatial period a of the grating by a simple measurement of the modulation frequency $\omega_0 = 2\pi v_x/b$. This frequency clearly manifests itself as a series of equally spaced fringes within the Gaussian envelope, as shown in Figs. 5–7. For fixed b and K, Eq. (18) allows one to measure the scattering source term L by an equally simple measurement, that of measuring the relative strength of these fringes.

Figure 8 shows theoretical and experimental plots of the modulation strength $S(q, K)$ against L/b for fixed scan angles $K = 0$ and $K = 1$. In both cases the modulation strength tends to zero for $L/b > 0.5$ and increases dramatically for $L/b < 0.5$, although at very different rates. Figure 9 shows theoretical and experimental plots of the modulation strength versus scan angle K for fixed $L/b = 0.18, 0.25, 0.30$. It is clear from the curves, and the excellent experimental agreement, that the modulation strength is a sensitive measure of the degree of intensity overlap L/b and therefore allows one to estimate L for a given b to a reasonable degree of accuracy.

Figures 6 and 7 show experimental measurements of the period of these modulations. The period is indeed seen to be proportional to the component of velocity parallel to the far-field x axis, whereas the Gaussian envelope has a width pro-

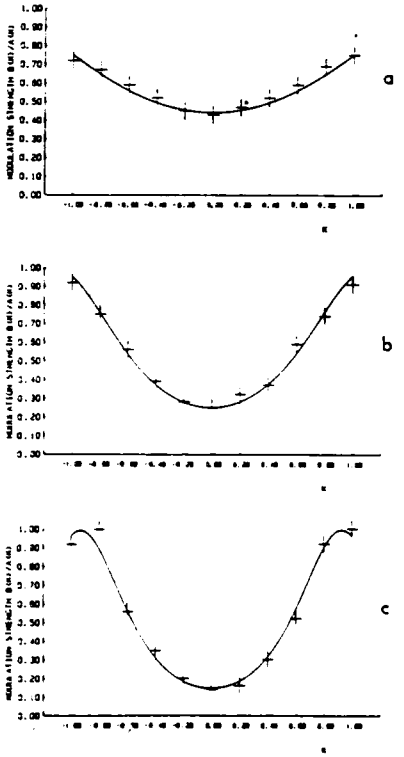

Fig. 9. Modulation strength as a function of scan angle $K = s/\sin\theta_0$ (where $\sin\theta_0 = \lambda/b$) for fixed overlap parameter L/b = a, 0.18; b, 0.25; c, 0.30. The solid curve refers to theory; the +'s refer to experimental measurements.

portional to the total diffuser velocity $(v_\xi^2 + v_\eta^2)^{1/2}$. For our experimental parameters a and b, it was necessary to have $v_\xi < v_\eta$ whenever the full Gaussian envelope was to be observed with fewer than 10 full periods of modulation. We are limited here by the 128 channels of correlation data in our resolution. Figure 6 shows autocorrelation data for a pure translational diffuser velocity $|v| = v_\xi$, $v_\eta = 0$ and confirms our analysis that the modulation frequency varies as v_ξ/b to a high degree of accuracy.

6. PHYSICAL ORIGINS OF THE MODULATION AND COHERENCE PEAKS

Figures 8(a) and (b) show how the modulation of the Gaussian envelope $\exp(-|v|^2\tau^2/4a^2)$ increases dramatically for $L/b < 0.5$ and essentially disappears for $L/b > 0.5$. This may be understood by considering a diffuser correlation cell of linear dimension L traversing the phase grating of spatial period b and noting that the phase grating is uniform in the $\hat{\eta}$ direction and periodic in the $\hat{\xi}$ direction. Whenever $L/b \ll 1$ the instantaneous random phase associated with a particular diffuser element has added to it a periodic component that is due to the grating. This gives rise in the far field to a strong cosinusoidal modulation of period b/v_ξ. As L increases, the diffuser element still has a periodic component added to it; however, the strength of the component is now smaller since it is the value of the phase of the grating averaged over a distance L; thus the modulation disappears as $L/b \to \infty$.

The Gaussian envelope of width $t_0 = 2a/|v|$ is a well-known[18] property of dynamic speckle-intensity correlation measurements. It may be understood in a somewhat elementary way as the time taken for a speckle in the far field to evolve into an essentially new speckle with no memory of its previous configuration. The speckle field evolves because of the motion of the diffuser with respect to the laser beam. After a translation of a laser beam width $(2a)$, the diffraction field is formed by an entirely different set of scatters; hence the decorrelation time of each speckle in the far field is approximately $2a/|v|$.

It is instructive to view the spatial cross-correlation peak in the antisymmetric scan and its associated width in terms of speckle phenomena. Our experiment measures the normalized correlation of speckle intensity fluctuations, and this has a value of one for an autocorrelation. Figure 4 shows that the normalized cross correlation is also equal to 1 when one is correlating the ± 1 diffraction orders and $L/b \geq 1$. As shown in Fig. 2, whenever $L/b \geq 1$, the diffraction field consists of identical and well-separated speckle patterns whose intensities at the ± 1 diffraction orders are identical because of the choice of grating. Correlating the ± 1 diffraction orders then yields the same result as an autocorrelation of either of these since the detectors are fixed on essentially the same speckle of identical intensity. As L/b is reduced, the neighboring speckle patterns overlap the ± 1 diffraction orders. The correlation peak therefore decreases as the far field becomes more diffuse, i.e., the signal-to-noise ratio is reduced.

The spatial width of this peak has a measured value of $\Delta x = 2R\lambda/\pi a$ (see Fig. 3), which is approximately a speckle diameter. Whenever the net alignment error of the detectors exceeds a speckle diameter, the detectors are fixed on two different speckles; hence the correlation peak must vanish.

CONCLUSIONS

We have verified experimentally that the presence of a sinusoidal phase grating of period b hidden behind a diffuser of correlation length L can be revealed by measurements of the spatial-intensity cross correlation of the scattered field, confirming the theories presented in Refs. 1–6. By extension of this theory to the space–time domain, we have confirmed our own analysis that the hidden periodicity of the grating is more easily measured by a temporal autocorrelation of the dynamic speckle field. The presence of the grating in this case manifests itself as a cosinusoidal modulation within a Gaussian envelope. The period of this modulation is inversely proportional to the spatial period b of the grating. It has been verified that this effect is easily measured for highly diffuse fields ($L/b \ll 1$) by using a single detector with minimal demands on the spatial orientation of the detector, in contrast to the spatial cross-correlation method.

ACKNOWLEDGMENTS

This research was supported by grants from the U.S. Army Research Office (DAAG-29-80-K-0048) and the U.S. Air Force Office of Scientific Research (AFOSR-81-0003).

* Present address, Blackett Laboratory, Imperial College, London SW7 2BZ, England. J. C. Dainty is also with the Institute of Optics, The University of Rochester, Rochester, New York 14627.

REFERENCES

1. H. P. Baltes, H. A. Ferwerda, A. S. Glass, and B. Steinle, "Retrieval of structural information from the far-zone intensity and coherence of scattered radiation," Opt. Acta 28, 11–28 (1981).
2. H. P. Baltes and H. A. Ferwerda, "Inverse problems and coherence," IEEE Trans. AP-29, 405–406 (1981).
3. H. P. Baltes, A. S. Glass, and K. M. Jauch, "Multiplexing of coherence by beam-splitters," Opt. Acta 28, 873–876 (1981).
4. H. P. Baltes and K. M. Jauch, "Multiplex version of the van Cittert–Zernike theorem," J. Opt. Soc. Am. 71, 1434–1439 (1981).
5. A. S. Glass and H. P. Baltes, "The significance of far-zone coherence for sources or scatterers with hidden periodicity," Opt. Acta 29, 269–285 (1982).
6. A. S. Glass, H. P. Baltes, and K. M. Jauch, "The detection of hidden diffractors by coherence measurements," Proc. Soc. Photo-Opt. Instrum. Eng. 369, 681–686 (1982).
7. K. M. Jauch and H. P. Baltes, "Coherence of radiation scattered by gratings covered by a diffuser. Experimental evidence," Opt. Acta 28, 1013–1015 (1981).
8. A. S. Glass, "The significance of image reversal in the detection of hidden diffractors by interferometry," Opt. Acta 29, 575–583 (1982).
9. K. M. Jauch and H. P. Baltes, "Reversing-wave-front interferometry of radiation from a diffusely illuminated phase grating," Opt. Lett. 7, 127–129 (1982).
10. K. M. Jauch, H. P. Baltes, and A. S. Glass, "Measurements of coherence of radiation from diffusely illuminated beamsplitters," Proc. Soc. Photo-Opt. Instrum. Eng. 369, 687–690 (1982).
11. J. C. Dainty and D. Newman, "Detection of gratings hidden by diffusers using photon-correlation techniques," Opt. Lett. 8, 608–610 (1983).
12. J. W. Goodman, "The role of coherence concepts in the study of speckle," Proc. Soc. Photo-Opt. Instrum. Eng. 194, 86–94 (1979).
13. J. C. Leader, "Similarities and distinctions between coherence theory relations and laser scattering phenomena," Opt. Eng. 19, 500–501 (1980).

14. H. M. Pederson, "Intensity correlation metrology: a comparative study," Opt. Acta **29**, 105–118 (1982).
15. J. W. Goodman, in *Laser Speckle and Related Phenomena*, J. C. Dainty, ed. (Springer-Verlag, Heidelberg, 1975), p. 63.
16. P. F. Gray, "A method of forming optical diffusers of simple known statistical properties," Opt. Acta **25**, 765–775 (1978).
17. B. M. Levine and J. C. Dainty, "Non-Gaussian image plane speckle: measurements for diffusers of known statistics," Opt. Commun. **45**, 252–257 (1983).
18. T. Asakura and N. Takai, "Dynamic laser speckles and their application to velocity measurements of a diffuse object," Appl. Phys. **25**, 179–194 (1981).

Variable threshold discrimination in a photon-imaging detector

Thomas Gonsiorowski

The photon statistics of a particular photon-imaging detector are studied, and the conditional probability of photon counts in the output given a certain number of counts in an associated reference channel is derived. This result is applied in a variable level discrimination technique which significantly reduces detection errors approaching the ideal limit. These results can be applied to other photon-limited detectors with nonideal pulse height distributions.

I. Introduction

The photon-imaging detector which we are currently constructing is a modified version of the device first described by Papaliolios and Mertz.[1] We have named this device the Space–Time Analysis Camera (STAC). The STAC is designed to detect the spatiotemporal coordinates of a photoevent, i.e., the interaction of a photon with the photocathode of an image-intensifying tube. Before embarking on the statistical analysis of the STAC, we describe its operation. After presenting some general results in Sec. II we will consider a standard approach to photoevent discrimination using a fixed discrimination level. Finally, in Sec. IV we consider a variable discrimination technique suggested by Papaliolios[2] which improves the detection statistics.

The STAC consists of five major components: (1) the image-intensifier tube; (2) the multiplexing optics; (3) the image plane masks; (4) the photomultiplier tubes (PMTs); and (5) the discrimination electronics. The image tube serves to amplify the optical signal from a photoevent producing a pulse of light containing many photons yet retaining the spatial location of the original photoevent. The multiplexing optics form multiple images of the intensifier output face; in all, seventeen images are produced, each containing a fraction of the photons emitted by the intensifier. It is important to remember that each image is a small spot of light centered on the original photoevent location. In the following analysis we ignore channel to channel variations of the imaging properties and assume that all seventeen images are statistically identical, i.e., each image contains the same average number of photons. We do not ignore the aberrations of the optical system but simply assume that the image spot can be represented by a Gaussian point-spread function.

To encode the image spot location, a high-contrast binary transmittance grating is placed over each image. The period and orientation of each grating or mask are chosen to encode a particular bit of the digital photoevent coordinate. Eight masks are used to encode the x coordinate and eight are used for the y coordinate. The finest mask has a period about equal to the FWHM of the optical point-spread function and the period then doubles in each successive mask up to the coarsest mask which is half transparent and half opaque. The four coarsest masks are shown in Fig. 1. The seventeenth channel has no mask and serves both as a timing reference and event trigger, and in the variable threshold discrimination scheme this seventeenth channel also serves as a reference for the adjustable discrimination level. To complete the encoding, all light transmitted by the mask is collected by a photon counting PMT with a fast preamplifier/counter registering the number of detected photocounts. The final encoding step is to decide based on this number of counts whether the photoevent fell over an opaque region of the image plane mask (and hence the digital bit is assigned a 0) or over a transparent region (digital bit is a 1).

It is in this final step that some discrimination must take place. The number of counts registered in each channel will be a random variable with a statistical distribution determined by the characteristics of the various STAC elements. The form of this distribution will determine how effectively we can discriminate between a blocked event and a transmitted event.

II. Modeling the STAC

In an ideal system, the image tube would produce a fixed number of photons in the output pulse for each photoevent, and the optical system, masks, and PMTs

The author is with University of Rochester, Institute of Optics, Rochester, New York 14627, but at the present time is at Harvard University, Center for Earth & Planetary Physics, Cambridge, Massachusetts 02138.

Received 19 December 1983.
0003-6935/84/071060-06$02.00/0.

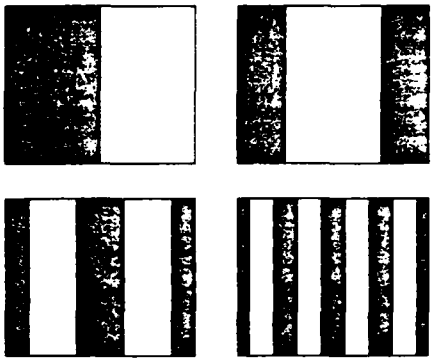

Fig. 1. Four coarsest masks of the STAC would encode the four most significant bits of the digital x coordinate. Note that Gray code is used as opposed to binary to minimize multibit errors.

would also give a fixed output depending only on the event location. In such a deterministic system it would be an easy matter to decide on the digital coordinate, and errors would be eliminated. Unfortunately, nature is not so obliging; at best the image tube produces not a fixed number of photons but instead a random number N with some probability $p(N)$. Also, each successive stage of the system behaves in a probabilistic way; if N photons enter a stage, rather than a fixed fraction emerging, the number output N' again has some distribution $p(N'|N)$, which does, however, depend on the input number. Ultimately, the number of photocounts registered in each channel n will also be a random variate with a distribution $p(n)$; as a result, any decision method which we use to select the various bits in the digital coordinate will err for some events, assigning a 1 instead of a 0 and vice versa. Thus, in the real system we must ask, what is the probability of making an error in the event coordinate?

In modeling the system we consider two possible distributions for the number of photons emitted by the image tube: (1) $p(N)$ is Poisson,

$$p(N) = \frac{\langle N \rangle^N}{N!} \exp[-\langle N \rangle], \tag{1}$$

and (2) $p(N)$ is Bose-Einstein,

$$p(N) = \frac{\langle N \rangle^N}{[1 + \langle N \rangle]^{N+1}}. \tag{2}$$

In both cases, $\langle N \rangle$ is the mean number of photons produced by the image tube for each photoevent. The Poisson distribution represents the optimum realizable distribution, i.e., the realistic ideal case, while the Bose-Einstein distribution approximates the actual image tube we are using. The Bose-Einstein distribution can be considered as the convolution of the ideal Poisson statistics with a broader noise distribution which increases the fluctuation of the photon numbers. Each successive stage of the STAC performs a binomial selection on the input to that stage

$$p(N'|N) = \binom{N}{N'} T^{N'}(1 - T)^{N-N'}, \tag{3}$$

where T is just the intensity transmittance of the stage. Another reason for selecting distributions (1) and (2) is that both are invariant under binomial selection, i.e., the form of the distribution does not change although the mean is modified. The transmittance of the multiplexing optics is T_0, the masks have a transmittance T_m, which is position dependent, and the PMT preamplifier/counter combination has some effective efficiency (transmittance) η. To obtain numerical results, it will be necessary to choose values for these parameters; we will use approximate values for our particular system:

$$\begin{aligned} \langle N \rangle &\approx 5.0 \times 10^4, \\ T_0 &\approx 1.1 \times 10^{-2}, \\ \eta &\approx 0.15. \end{aligned} \tag{4}$$

Also, a derived quantity which will appear frequently is the mean number of counts generated in the reference channel, i.e., without any mask,

$$\langle n \rangle = \eta T_0 \langle N \rangle \approx 8.3. \tag{5}$$

Although the exact values of these parameters does not affect the following analysis, some results do depend on their relative magnitudes.

As mentioned above, we model the optical point-spread function by a Gaussian function. The mask grating integrates periodic portions of this point-spread function resulting in a total transmittance T_m given by

$$T_m = \sum_{k=-\infty}^{\infty} \left[\frac{1}{\pi} \int_{2kw}^{(2k+1)w} \exp[-(x - x_0)^2/2\sigma^2] dx\right], \tag{6}$$

where x_0 is the centroid of the image spot, $2\sqrt{2\sigma}$ is the FWHM of the point-spread function, w is the width of a bar or space in the mask, and k is an integer. In reality, the limits on the sum should be finite since the mask has a finite extent; in practice, however, the point-spread function will become negligible before the mask edge is reached. Of course, this does not apply to events very near the edge of the field, but we will ignore such cases. To simplify the above formula, we define two dimensionless parameters

$$\alpha = \frac{w}{\sqrt{2\sigma}} \text{ and } s = \frac{x_0}{w}. \tag{7}$$

Because of the mask periodicity, the normalized event position s has a fundamental range $-\frac{1}{2} \le s \le \frac{1}{2}$; while the mask–spot ratio α has approximate values of 1, 2, 4, . . . 128 in our system. Introducing the error function and using s and α we can write

$$T_m(s,\alpha) = \frac{1}{2} \sum_{k=-\infty}^{\infty} \{\operatorname{erf}[\alpha(2k - s + \tfrac{1}{2})] - \operatorname{erf}[\alpha(2k - s)]\}. \tag{8}$$

Figure 2 shows the variation of T_m with s for various values of α. For low mask–spot ratios ($\alpha = 1$), the point-spread function covers several mask periods producing a poorly modulated transmittance function. But as α increases, the transmittance approaches a step

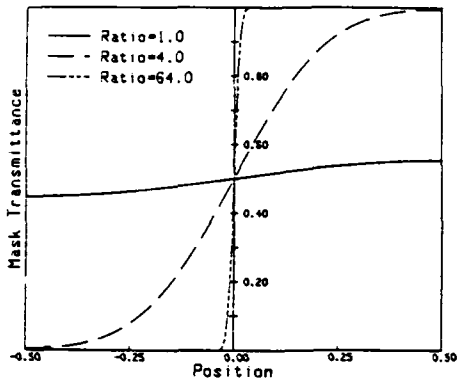

Fig. 2. $T_m(s,\alpha)$ plotted over the fundamental range of s for $\alpha = 1$, 4, and 64.

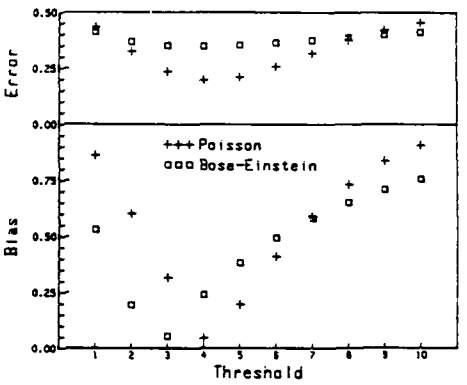

Fig. 3. Typical variation of bias B and error E with threshold n_t for the mask-spot ratio $\alpha = 2$.

function. The poor modulation of T_m for smaller α results in larger detection errors, thus ultimately limiting the detector resolution.

III. Fixed Threshold Discrimination

Consider the output of a particular masked channel of the STAC which consists of a series of counts $n_1, n_2, \ldots n_k$. For each count we must decide the event location—was it over a space or a bar? The simplest decision method is to choose some threshold value n_t, and whenever $n_k \geq n_t$ we assign the event to a space ($0 \leq s \leq \frac{1}{2}$), otherwise the event is assigned to a bar ($-\frac{1}{2} \leq s < 0$). Since the number of counts n_k is random for any position s, there will be a probability of incorrectly assigning the event location. Given the probability distribution of counts $p(n)$, the probability of assignment error is

$$E(s) = \begin{cases} p(n \geq n_t), & \text{for } -\frac{1}{2} \leq s < 0; \\ p(n < n_t), & \text{for } 0 \leq s \leq \frac{1}{2}. \end{cases} \quad (9)$$

Note that, for each value of s and each mask, the distribution $p(n)$ will be different since it depends on the mask transmittance T_m. Having no *a priori* information about the event location, we will assume that all positions are equally likely allowing us to spatially average the error

$$\begin{aligned} E_0 &= \langle p(n \geq n_t) \rangle_s, \text{ for } s < 0; \\ E_1 &= \langle p(n < n_t) \rangle_s, \text{ for } s \geq 0; \\ E &= \frac{1}{2}(E_0 + E_1). \end{aligned} \quad (10)$$

In choosing n_t we must minimize E. However, there is another constraint: if the difference between E_0 and E_1 is large, we introduce a bias into the measurement in that a disproportionate number of events are assigned to either bars or spaces. This would cause a spatially uniform input signal to produce a striped output pattern. So we must also minimize the bias, which can be characterized by

$$B = |E_1 - E_0| \quad (11)$$

As we will see, choosing n_t to minimize B will also tend to give a minimum E.

From the arguments of Sec. II, we know that $p(n)$ will be of the same form as $p(N)$, the distribution of photon number emitted by the image tube, but having a mean given by

$$\langle n \rangle = T_m \langle r \rangle \quad (12)$$

Once we have tabulated T_m vs s and α, it is easy to numerically evaluate B and E vs n_t for the cases of Poisson and Bose-Einstein statistics. Note that B and E will be different for each mask-spot ratio α. The plots in Fig. 3 show typical results of this analysis. For both distributions we see that an optimum threshold which minimizes the bias or the error exists. Although room does not permit, inspection indicates that for most values of α the same threshold minimizes both. The minimum error and bias obtained for each mask is plotted in Fig. 6.

IV. Variable Threshold Discrimination

In an attempt to reduce the probability of detection errors, we consider making a second simultaneous measurement for each event—besides counting the number of photons in each masked channel, we also measure the number of counts in an unmasked reference channel which has a position independent transmittance, $T_m = 1$. We hope that the reference channel measurement will give us added information about the number of photons produced by the image tube for a particular event, thereby decreasing the probability of detection errors. Now we ask, what is the conditional distribution of counts in one of the masked channels $p(n|r)$ given that we have measured r counts in the reference channel?

We begin by noting that, if in a particular event the image tube produces N photons (not a random number), the probability of producing r counts in the reference channel is just a binomial distribution

$$p(r|N) = \begin{cases} \binom{N}{r} (\eta T_0)^r (1-\eta T_0)^{N-r}, & \text{for } r \le N; \\ 0, & \text{for } r > N. \end{cases} \quad (13)$$

Since we also know both $p(N)$ and $p(r)$, we can apply Bayes's theorem to find $p(N|r)$, which is the distribution of photon output by the image tube given that r counts are measured in the reference channel. From Bayes's theorem,[3]

$$p(N|r) = \frac{p(r|N)p(N)}{p(r)}. \quad (14)$$

Equation (13), the formula for $p(r|N)$, also applies to the output of any masked channel with r replaced by n and T_0 replaced by T_0T_m. Given both $p(n|N)$ and $p(N|r)$, we can find $p(n|r)$ from

$$p(n|r) = \sum_{N=0}^{\infty} p(n|N)p(N|r). \quad (15)$$

Once we have found $p(n|r)$ we are again in a position to consider choosing n_t to minimize B and E. However, n_t is now a function of r, having a different value for each r; but since we know the unconditional distribution of counts in the reference channel $p(r)$, we can average over r to obtain a single bias and error figure for each mask–spot ratio.

Consider first the Poisson case, where $p(N)$ and $p(r)$ are each Poisson distributions with respective means $\langle N \rangle$ and $\langle r \rangle$. Applying Eq. (14) we obtain

$$p(N|r) = \begin{cases} \dfrac{[(1-\eta T_0)\langle N \rangle]^{N-r}}{(N-r)!} \exp[-(1-\eta T_0)\langle N \rangle], & \text{for } r \le N, \\ 0, & \text{for } r > N. \end{cases} \quad (16)$$

Defining

$$u = (1-\eta T_0)\langle N \rangle = \langle N \rangle - \langle r \rangle, \quad (17)$$

this becomes

$$p(N|r) = \begin{cases} \dfrac{u^{N-r}}{(N-r)!} \exp(-u), & \text{for } N \ge r, \\ 0, & \text{for } N < r. \end{cases} \quad (18)$$

The binomial distribution $p(n|N)$ can be written as

$$p(n|N) = \begin{cases} \binom{N}{n} \beta^n (1-\beta)^{N-n}, & \text{for } n \le N, \\ 0, & \text{for } n > N. \end{cases} \quad (19)$$

where

$$\beta = \eta T_0 T_m. \quad (20)$$

Combining Eqs. (18) and (19) gives

$$p(n|r) = \sum_{N=N_0}^{\infty} \binom{N}{n} \beta^n (1-\beta)^{N-n} \frac{u^{N-r}}{(N-r)!} \exp(-u) \quad (21)$$

with

$$N_0 = \max(n, r). \quad (22)$$

After some manipulation the sum can be transformed to the confluent hypergeometric function[4] giving

$$p(n|r) = \begin{cases} \binom{r}{n} (1-\beta)^{r-n} \beta^n \exp(-\mu) M[r+1; r-n+1; \mu(1-\beta)], & n \le r; \\ \dfrac{\mu^{n-r}}{(n-r)!} \beta^n \exp(-\mu) M[n+1; n-r+1; \mu(1-\beta)], & n \ge r. \end{cases} \quad (23)$$

To facilitate numerical computation we apply Kummer's transformation[5]

$$M(a; b; z) = \exp(z) M(b-a; b; -z), \quad (24)$$

which reduces the confluent hypergeometrics in Eq. (23) to terminating series or polynomials:

$$p(n|r) = \begin{cases} \binom{r}{n} \beta^n (1-\beta)^{r-n} \exp(-\mu\beta) M[-n; r-n+1; \mu(\beta-1)], & n \le r; \\ \dfrac{(\mu\beta)^{n-r}}{(n-r)!} \exp(-\mu\beta) \beta^r M[-r; n-r+1; \mu(\beta-1)], & n \ge r. \end{cases} \quad (25)$$

Although this result is exact, it offers little insight to the advantage of the reference channel measurement. For our particular system, however, we can approximate the formula by noting that

$$u \gg 1, \beta \ll 1, \text{ and } u(1-\beta) \approx u \gg 1. \quad (26)$$

For the confluent hypergeometric function we use an asymptotic approximation[6]

$$M(a; b; z) = \frac{\Gamma(b)}{\Gamma(a)} \exp(z) z^{a-b} [1 + O(|z|^{-1})], \quad (27)$$

noting that $|z|^{-1} = 2 \times 10^{-5}$. Surprisingly, within this approximation we find

$$p(n|r) \approx \frac{\langle n \rangle^n}{n!} \exp(-\langle n \rangle), \quad (28)$$

where $\langle n \rangle$ is given in Eq. (12), this result being valid for all values of n and r. Numerical computations using both the exact and approximate expressions show the approximation to be accurate within 10^{-4}. The approximate formula shows quite clearly that, for Poisson statistics, the measurement in the reference channel gives us no new information, and thus the variable threshold technique would be fruitless. This result seems quite reasonable and suggests that the exact expression (25) should reduce to a Poisson for all values of u and β, but we have not proved this except in the limit [Eq. (26)].

For the Bose-Einstein distribution of photons emitted by the image tube, the probability of having N photons produced by the intensifier given r counts in the reference channel is

$$p(N|r) = \begin{cases} \binom{N}{r} \dfrac{(1+\langle r\rangle)^{r+1}}{(1+\langle N\rangle)^{N+1}} \mu^{N-r}, & \text{for } N \geq r, \\ 0, & \text{for } N < r. \end{cases} \quad (29)$$

where μ is given in Eq. (17). Now the probability of receiving n counts in a masked channel when the image tube produces N photons is still given by Eq. (19), thus

$$p(n|r) = \sum_{N=N_0}^{\infty} \binom{N}{n}\binom{N}{r} \beta^n(1-\beta)^{N-n} \frac{(1+\langle r\rangle)^{r+1}}{(1+\langle N\rangle)^{N+1}} \mu^{N-r}, \quad (30)$$

where again N_0 is given by Eq. (22). This sum can be transformed into the hypergeometric function[7] resulting in a conditional probability distribution

$$\begin{aligned} p(n|r) &= \binom{r}{n} \beta^n(1-\beta)^{r-n} \left[\frac{(1+\langle r\rangle)}{(1+\langle N\rangle)}\right]^{r+1} \\ &\quad \times F\left[r+1, r+1; r-n+1; \frac{\mu(1-\beta)}{1+\langle N\rangle}\right], \quad n \leq r \\ &= \binom{n}{r} \beta^r(\mu\beta)^{n-r} \frac{(1+\langle r\rangle)^{r+1}}{(1+\langle N\rangle)^{n+1}} \\ &\quad \times F\left[n+1, n+1; n-r+1; \frac{\mu(1-\beta)}{1+\langle N\rangle}\right], \quad n \geq r. \end{aligned} \quad (31)$$

As before we can transform the hypergeometric function to a terminating series with the transformation[8]

$$F(a,b;c;z) = (1-z)^{c-a-b} F(c-a, c-b; c; z), \quad (32)$$

which leads to

$$\begin{aligned} p(n|r) &= \binom{r}{n} \beta^n(1-\beta)^{r-n} \frac{(1+\langle r\rangle)^{r+1}(1+\langle N\rangle)^n}{(1+\langle r\rangle+\mu\beta)^{r+n+1}} \\ &\quad \times F\left[-n, -n; r-n+1; \frac{\mu(1-\beta)}{1+\langle N\rangle}\right], \quad n \leq r \\ &= \binom{n}{r} \beta^r(\mu\beta)^{n-r} \frac{(1+\langle r\rangle)^{r+1}(1+\langle N\rangle)^r}{(1+\langle r\rangle+\mu\beta)^{r+n+1}} \\ &\quad \times F\left[-r, -r; n-r+1; \frac{\mu(1-\beta)}{1+\langle N\rangle}\right], \quad n \geq r. \end{aligned} \quad (33)$$

Using the relations in Eq. (26) we discover that

$$\frac{\mu(1-\beta)}{1+\langle N\rangle} \approx 1 \quad (34)$$

suggesting use of the relation[9]

$$F(a,b;c;1) = \frac{\Gamma(c)\Gamma(c-a-b)}{\Gamma(c-a)\Gamma(c-b)}, \quad (35)$$

which is valid for $\mathcal{R}(c-a-b) > 0$ and $c \neq 0, -1, -2, \ldots$. From Eq. (33), we see that $c-a-b = r+n+1$ is always positive, while for all n and r; $c \geq 1$. With this approximation, the conditional probability reduces to

$$p(n|r) \approx \binom{r+n}{n} \frac{(1+\langle r\rangle)^{r+1}\langle n\rangle^n}{(1+\langle r\rangle+\langle n\rangle)^{r+n+1}}, \quad (36)$$

where $\langle n\rangle$ is given in Eq. (12), this formula holding for all values of n and r. Although this result is only an approximation, it has all the properties of a true probability density and

$$\sum_{r=0}^{\infty} p(n|r)p(r) = \frac{\langle n\rangle^n}{(1+\langle n\rangle)^{n+1}}, \quad (37)$$

when $p(r)$ is a Bose-Einstein with mean $\langle r\rangle$. Thus,

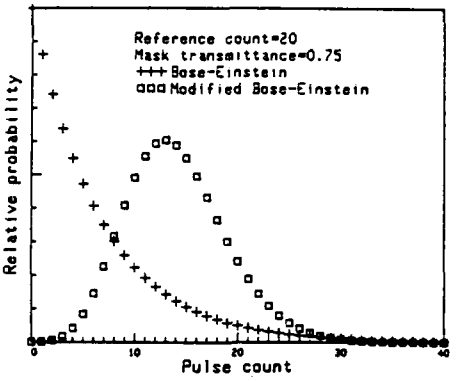

Fig. 4. Comparison of the unconditional Bose-Einstein distribution and the conditional or modified Bose-Einstein distribution for r = 20 and T_m = 0.75.

$p(n|r)$ as given in Eq. (36) is a proper conditional probability. Comparison of the exact and approximate formulas again shows excellent agreement. Henceforth, we shall call the distribution [Eq. (36)] the modified Bose-Einstein or MBE.

The significance of the MBE is vividly demonstrated in Fig. 4, which compares the MBE obtained by including the reference channel measurement to the unconditional Bose-Einstein distribution. Clearly the MBE is much narrower, a result which can be formally shown by calculating the ratio of the variance to the mean for each distribution. Letting $\langle n_r\rangle$ represent the mean of the MBE, we find

$$\begin{aligned} \text{MBE:} \quad & \frac{\sigma^2}{\langle n_r\rangle} = 1 + \langle n\rangle - \left(\frac{\langle r\rangle}{1+\langle r\rangle}\right)\langle n\rangle, \\ \text{Bose-Einstein:} \quad & \frac{\sigma^2}{\langle n\rangle} = 1 + \langle n\rangle, \\ \text{Poisson:} \quad & \frac{\sigma^2}{\langle n\rangle} = 1. \end{aligned} \quad (38)$$

clearly showing that the width of the MBE is bounded by the Bose-Einstein from above and by the Poisson from below. Thus, including the reference channel measurement does add information, and we can consider $\langle r\rangle/(1+\langle r\rangle)$ as a quantitative measure of the improvement.

To see how much of an improvement the MBE gives, we consider the error and bias analysis as in Sec. II. In this case, however, there is a different optimum threshold for each value r and each mask–spot ratio α as shown in Fig. 5. As one would guess, the threshold rises with increasing r since larger values of r imply larger image tube output pulses which also give higher counts in the masked channels. That $n_t \approx r/2$ is indicative of the spatial averaging used to compute n_t, since the averaged transmittance of the mask is just $\frac{1}{2}$. Figure 6 compares the bias and error figures for the three cases: (1) Poisson statistics with fixed (or variable) threshold; (2) Bose-Einstein statistics with fixed threshold; and (3) MBE statistics (i.e., Bose-Einstein

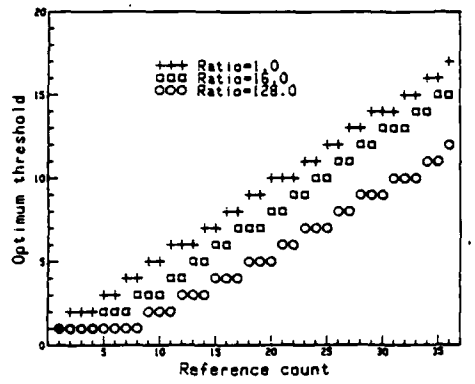

Fig. 5. Optimum threshold vs reference channel count r for several mask–spot ratios.

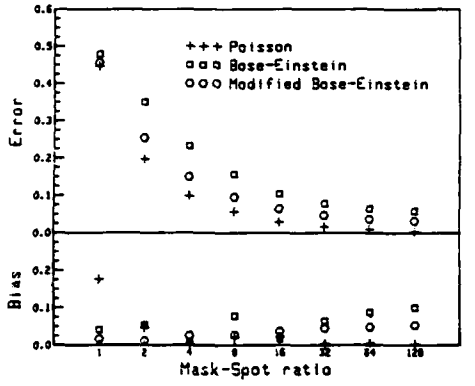

Fig. 6. Comparison of the three discrimination schemes presented in the text.

with variable threshold). In case (3) we averaged the results over r with $p(r)$ being Bose-Einstein. For all three cases, the error is very large for the mask–spot ratio $\alpha = 1$ due to the poor mask transmittance modulation but quickly improves as α increases. Variable level discrimination improves the error (compared with the Bose-Einstein case) for all mask–spot ratios, most notably for intermediate values $\alpha = 2, 4$, and 8. It also decreases the bias for most mask–spot ratios and surprisingly results in very small biases for $\alpha = 1$ and 2—surpassing even the Poisson case. Clearly, variable threshold discrimination significantly improves both the bias and the error offering performance which approaches the Poisson (ideal) case. This improvement results because variable level discrimination removes the large fluctuations in photon numbers partially recovering the ideal pulse height distribution of the system.

V. Conclusion

We have presented a statistical analysis of a photon-imaging detector which uses a mask structure in the image plane to encode the digital coordinate of a photoevent. The distribution of photocounts at the output was derived both unconditionally and conditioned upon counting r photons in a reference channel. The conditional case allows the use of a variable discrimination level, which depends on the value of r. That this conditional distribution is at least approximately unchanged for the case of Poisson statistics indicates the optimum nature of this distribution. However, for the broader Bose-Einstein distribution, the conditional probability affords considerable improvement. Although the particular formulas obtained herein may not apply to other detectors, we feel that the general concept of a variable threshold could prove useful in other photon-counting devices where improvement of the pulse height statistics is desired.

References

1. C. Papaliolios and L. Mertz, Proc. Soc. Photo-Opt. Instrum. Eng. 331, 360 (1982).
2. C. Papaliolios, personal communication.
3. A. Papoulis, *Probability, Random Variables, and Stochastic Processes* (McGraw-Hill, New York, 1965), pp. 38 and 39.
4. M. Abramowitz and I. A. Stegun, Eds., *Handbook of Mathematical Functions* (Dover, New York, 1965), p. 504.
5. Ref. 4, p. 505, Eq. (13.1.27).
6. Ref. 4, p. 504, Eq. (13.1.4).
7. Ref. 4, p. 556.
8. Ref. 4, p. 559, Eq. (15.3.3).
9. Ref. 4, p. 556, Eq. (15.1.20).

I wish to thank J. C. Dainty and B. M. Levine for their helpful comments and suggestions. This work was supported by the Air Force Office of Scientific Research under grant AFOSR-81-0003 and by a fellowship from the Eastman Kodak Co.

Volume 52, number 2 OPTICS COMMUNICATIONS 15 November 1984

TESTING FOR UNIQUENESS OF PHASE RECOVERY IN TWO DIMENSIONS

M. NIETO-VESPERINAS [1] and J.C. DAINTY [2]
The Institute of Optics, The University of Rochester, Rochester, NY 14627, USA

Received 9 July 1984

The uniqueness of phase retrieval for two dimensional sampled functions of finite extent is equivalent to the irreducibility of their z-transform. We put forward a method of characterizing the uniqueness (or non-uniqueness) in the absence of noise based on a theorem that gives a necessary and sufficient condition for irreducibility of univariate polynomials over finite fields.

It is well-known that the question of uniqueness of phase recovery for sampled functions is equivalent to that of the irreducibility of the polynomial which represents the z-transform of the object samples [1,2] $\{a_{ij}\}$ $(i = 0, 1, ..., m, j = 0, 1, ..., n)$:

$$F(z_1, z_2) = \sum_{i,j=0}^{m,n} a_{ij} z_1^i z_2^j. \tag{1}$$

It has been shown that the set of reducible polynomials in more than one variable is a set of measure zero [3] and also that irreducibility is stable in the sense that it is not sensitive to arbitrary but small noise on the coefficients [4].

The only means available so far of testing for uniqueness has been to use many random starts in any one of the iterative methods of phase retrieval [5,6]. Only for a special class of objects, those that satisfy Eisenstein's [7] irreducibility criterion, has phase uniqueness been established [8]. Since this criterion puts forward a *sufficient* but *not necessary* condition for the irreducibility of (1), there may be many other polynomials that do not satisfy it that are, however, irreducible. In this letter we propose a method of testing for irreducibility in the case in which the coefficients a_{ij} are not perturbed by noise. This ideal noise-free situation will be useful in those cases in which phase-reconstruction algorithms are to be inspected for digital objects; since in this case the test of irreducibility can provide a priori information on the extent of the expected ambiguity in the reconstruction. Also the study of noise-free cases has an interpretative interest of the problem.

Since we shall be interested in distributions (1) corresponding to digital pictures, we shall assume the coefficients a_{ij} to be *non-negative integers* in the noise-free situation (or even when noise is weak enough to give no ambiguity as to the value of the last digit of the coefficients a_{ij}).

Writing (1) as a polynomial in the main variable z_1 with the coefficients being polynomials in z_2:

$$F(z_1, z_2) = p_m(z_2) z_1^m + p_{m-1}(z_2) z_1^{m-1} + \cdots + p_1(z_2) z_1 + p_0(z_2). \tag{2}$$

$F(z_1, z_2)$ is *monic* with respect to z_1 if its *leading coefficient* $p_m(z_2) = 1$. $F(z_1, z_2)$ is *primitive* in z_1 when the $p_i(z_2)$ are relatively prime. If $F(z_1, z_2)$ is not primitive, the *content*, cont$[F]$, is the greatest common divisor (gcd) of the coefficients $p_i(z_2)$. The *principal part* of $F(z_1, z_2)$ with respect to z_1 is then defined as pp$[F] = F/\text{cont}[F]$. Starting with a non-monic polynomial, such as (2) with $p_m(z_2) \neq 1$, it is always possible to construct the following monic polynomial [9]:

[1] On leave from: Instituto de Optica, C.S.I.C., Serrano 121, Madrid 6, Spain.
[2] Permanent address: Blackett Laboratory, Imperial College, London SW7 2BZ, England.

0 030-4018/84 $03.00 © Elsevier Science Publishers B.V. (North-Holland Physics Publishing Division)

$$G(z_1, z_2) = [p_m(z_2)]^{m-1} F(z_1/p_m(z_2), z_2). \quad (3)$$

If the complete factorization of the monic polynomial (3) into irreducible factors $G_k(z_1, z_2)$ is

$$G(z_1, z_2) = \prod_{k=1}^{r} G_k(z_1, z_2), \quad (4)$$

then it may be shown [9] that

$$F(z_1, z_2) = \prod_{k=1}^{r} \{\mathrm{pp}[G_k(p_m(z_2)z_1, z_2)]\}. \quad (5)$$

Thus, we may assume in the following that $F(z_1, z_2)$ is monic in z_1, since otherwise eqs. (3)–(5) reduce to the situation of factoring a monic polynomial.

According to a well known lemma by Gauss [7], factorization of a polynomial with rational coefficients is equivalent to that of a polynomial with integer coefficients (this is seen by multiplying the polynomial with rational coefficients by their least common denominator).

Proposition 1: The factorization of $F(z_1, z_2)$ is such that if it has a factor $F_{km}(z_1, z_2)$ with complex coefficients then it must necessarily have another factor $F_{km^*}(z_1, z_2)$ whose coefficients are the complex conjugates of those of $F_{km}(z_1, z_2)$.

Proof: Let us write F in the x and y variables factorized as:

$$F(x, y) = F_{k_m}(x, y) \prod_{k \neq k_m}^{r} F_k(x, y).$$

The complex conjugate of $F(x, y)$ is:

$$F^*(x, y) = F^*_{k_m}(x, y) \prod_{k \neq k_m}^{r} F^*_k(x, y).$$

Since $F(x, y)$ has real coefficients $F(x, y) = F^*(x, y)$; i.e.:

$$F_{k_m}(x, y) \prod_{k \neq k_m}^{r} F_k(x, y) = F^*_{k_m}(x, y) \prod_{k \neq k_m}^{r} F^*(x, y).$$

The above can be possible only if the product $\Pi^r_{k \neq k_m} F_k(x, y)$ contains the factor $F^*_{k_m}(x, y)$, which also means that the product $\Pi^r_{k \neq k_m} F^*(x, y)$ contains the factor $F_{k_m}(x, y)$.

This proposition is a generalization in two dimensions of a well known theorem of algebra for univariate polynomials according to which a polynomial with real coefficients has roots in complex conjugate pairs.

Proposition 2: There is a unique monic polynomial $F(z_1, z_2)$ with integer coefficients, irreducible over integers, with a given factor $F_{km}(z_1, z_2)$ with irrational or complex coefficients, and every other polynomial with integer coefficients containing the same factor $F_{km}(z_1, z_2)$ is a multiple of $F(z_1, z_2)$.

As will be seen, we shall call $F(z_1, z_2)$ the *minimal polynomial* with integer coefficients containing the factor $F_{km}(z_1, z_2)$.

Proof: By ordering on the set of degrees of polynomials with integer coefficients containing the factor $F_{km}(z_1, z_2)$, there is a monic polynomial $F(z_1, z_2)$ with smallest degree. $F(z_1, z_2)$ is irreducible over integers since otherwise $F(z_1, z_2) = A(z_1, z_2)B(z_1, z_2)$ both A and B with integer coefficients. But then either A or B has the factor $F_{km}(z_1, z_2)$ which is a contradiction with our assumption that $F(z_1, z_2)$ has smallest degree.

Let $G(z_1, z_2)$ be any polynomial with integer coefficients with $F_{km}(z_1, z_2)$ as a factor. By the division algorithm [7]:

$$G(z_1, z_2) = F(z_1, z_2)\, Q(z_1, z_2) + R(z_1, z_2),$$

with R having lower degree than F. From the assumption on G and F it follows that also R has F_{km} as a factor, thus R must be zero since it was assumed that F has the lower degree amongst the polynomials with F_{km} as a factor. Therefore G is a multiple, over integers, of F.

Proposition 2 is a generalization for two dimensional polynomials of another well known theorem of algebra for univariate polynomials [e.g. 7], according to which there is a unique monic polynomial with rational coefficients having a given algebraic root and being irreducible over rationals. The generalization of these propositions can obviously be made to any dimension.

Before quoting the main theorem that characterizes irreducibility, we first establish the following facts:

Fact 1: The factorization of $F(z_1, z_2)$ with ordinary integers a_{ij} into r irreducible factors $F_k(z_1, z_2)$ is such that the coefficients of these factors are ordinary integers. Thus the factorization may be considered over integers.

To see this we observe the following:

First, if we admit decomposition into factors with some complex coefficients, they will appear in complex conjugate coefficient pairs. Flipping factors with such coefficients has to be done in those pairs since if one flips one factor of the pair only, according to Proposition 1, the polynomial built will no longer have integer coefficients and thus cannot be considered representing a valid object under our assumption of absence of noise. Of course, pairs of complex conjugate factors combine giving higher degree polynomials with integer coefficients.

Secondly, if we admit a decomposition with factors having some irrational coefficients, flipping some of such factors and leaving others unflipped will lead to a new polynomial with some factors of irrational coefficients (those unflipped) equal to those of the old polynomial, i.e. before flipping some of them. According to Proposition 2 that new polynomial built after flipping cannot have integer coefficients as well.

E.g., the object $F(z_1, z_2) = z_1^2 + 9z_2^2 + 8z_1z_2$ admits the factorization $(z_1 + (4 + \sqrt{7})z_2)(z_1 + (4 - \sqrt{7})z_2)$. However, none of the possible objects obtained by flipping any of the factors has integer coefficients. Flipping the second factor, for instance, would yield the object $\bar{F}(z_1, z_2) = (z_1 + (4 + \sqrt{7})z_2) \times (z_2 + (4 - \sqrt{7})z_1) = (4 - \sqrt{7})z_1^2 + (4 + \sqrt{7})z_2^2 + 10z_1z_2$.

Fact 2: Let gcd $[F(z_1, z_2), \partial F/\partial z_1] = D(z_1, z_2)$; then F has a repeated factor $v(z_1, z_2)$ if and only if v divides $D(z_1, z_2)$ and F/D is square-free.

For example, if $F(z_1, z_2) = v^{\alpha}(z_1, z_2)w(z_1, z_2)$, α being an integer greater than 1 and v and w not necessarily irreducible, then $\partial F/\partial z_1 = \alpha v^{\alpha-1}w\partial v/\partial z_1 + v^{\alpha}\partial w/\partial z_1$, so that $D(z_1, z_2) = v^{\alpha-1}$ and $F/D = vw$. If $D = 1$, then $F(z_1, z_2)$ has no repeated factors. Otherwise the factorization of F is speeded up by studying that of D and F/D separately. The process may be repeated.

Fact 3: A polynomial in one or more variables which has a certain factorization over integers into r irreducible factors has an equivalent factorization modulo q^n (n being a positive integer and q a prime number and such that with respect to some variable the degree of the polynomial is the same as over the integers) with at least as many factors. In addition, the arithmetic operations are conserved when passing from the field of integers to the finite field of integers modulo q^n [10].

For instance, the univariate polynomial $21z^4 + 52z^3 + 24z^2 + 9z + 2 = (z + 2)(1 + 3z)(1 + z + 7z^2)$ over integers, whereas modulo 2 is factored as $z^4 + z = z(1 + z)(1 + z + z^2)$ and we note that $21z^4 + 52z^3 + 24z^2 + 9z + 2 \equiv z^4 + z \pmod 2$, $z + 2 \equiv z \pmod 2$; $1 + 3z \equiv 1 + z \pmod 2$; $1 + z + 7z^2 \equiv 1 + z + z^2 \pmod 2$ (the sign $\equiv$ denotes *congruence*). On the other hand, the polynomial $z^3 + 217z^2 + 116z + 1$ is irreducible over integers, whereas modulo 5 becomes

$$z^3 + 217z^2 + 116z + 1 \equiv z^3 + 2z^2 + z + 1 \pmod 5,$$

$$z^3 + 2z^2 + z + 1 \equiv (z^2 + 3z - 1)(z + 4) \pmod 5.$$

As a consequence, in order for a polynomial to be irreducible over integers, it is sufficient that it be irreducible modulo some q^n which conserves its degree. Obviously, the higher n or q, the more likely it is that the polynomial has the same factors modulo q^n as over integers. The condition that the polynomial has the same degree over integers and modulo q^n is very important. For instance, $5z^3 + 30z^2 + 47z + 6 = (z + 3)(5z^2 + 15z + 2)$ over integers, whereas modulo 5 becomes $2z + 1$ which is irreducible.

We shall now quote the theorem with which the irreducibility of $F(z_1, z_2)$ can be established.

Theorem [11]: Let $F(z) = z^m + p_{m-1}z^{m-1} + \ldots + p_1z + p_0$ be a univariate polynomial in z, with coefficients being in the finite field of integers modulo q (q is a prime) and such that F(z) is square-free (or has repeated factors all with the same multiplicity); then F(z) is irreducible over q if and only if the matrix

$$\|A_{ij} - \delta_{ij}\|, \quad (i = 0, 1, \ldots m - 1, j = 0, 1, \ldots m - 1) \tag{6}$$

has rank s equal to $m - 1$. The elements A_{ij} are defined by the congruences:

$$z^{iq} \equiv \sum_{j=0}^{m-1} A_{ij}z^j \pmod{F(z)} \quad (i = 0, 1, \ldots m - 1) \tag{7}$$

and δ_{ij} is the Kronecker delta. Moreover, if F(z) is factorizable into r different irreducible factors with the same multiplicity, then the rank of the matrix (6) is $s = m - r$.

The first row of the matrix A is always $(1, 0, 0, \ldots 0)$ representing z^0 (modulo $F(z)$) which is 1. The second row corresponds to z^q (modulo $F(z)$). In general z^i

(mod $F(z)$) is determined as follows. If

$$z^i \equiv b_{i,0} + b_{i,1}z + \ldots + b_{i,m-1}z^{m-1} \pmod{F(z)}, \quad (8)$$

then

$$z^{i+1} \equiv b_{i,0}z + b_{i,1}z^2 + \ldots + b_{i,m-1}z^m$$
$$\equiv b_{i,0}z + \ldots + b_{i,m-2}z^{m-1}$$
$$+ b_{i,m-1}(-p_{m-1}z^{m-1} - \ldots - p_1 z - p_0)$$
$$\equiv b_{i+1,0} + b_{i+1,1}z + \ldots + b_{i+1,m-1}z^{m-1}, \quad (9)$$

where

$$b_{i+1,j} = b_{i,j-1} - b_{i,m-1}p_j. \quad (10)$$

The recurrence relation (10) may easily be implemented in a computer; $b_{i,-1}$ is considered to be zero so that $b_{i+1,0} = -b_{i,m-1}p_0$. (Note that analogy of the polynomial $Q(A_{ij})$ obtained from a minor of order $m-1$ of the matrix $\|A_{ij} - \delta_{ij}\|$ being different from zero with the polynomial $Q \neq 0$ quoted in ref. [4].)

In general, no matter how large the degree of the polynomial is, it is possible to find in practice a small integer q such that the rank of $\|A_{ij} - \delta_{ij}\|$ is $m-1$ if the polynomial is irreducible over integers. However, one should be aware that some pathological cases exist [12]; for instance, there are polynomials irreducible over integers but reducible modulo every prime.

To test the irreducibility of a two dimensional polynomial like (1), we proceed as follows:

1) Reduce $F(z_1, z_2)$ to a primitive polynomial.

2) Check whether $F(z_1, z_2)$ has repeated factors according to Fact 2. If $D(z_1, z_2) \neq 1$, the polynomial is of course reducible.

3) If $D(z_1, z_2) = 1$, then fix a value of $z_2 = z_0$ so that the degree of $F(z_1, z_0)$ is the same as the degree of $F(z_1, z_2)$ and $F(z_1, z_2)$ has no repeated factors. According to Fact 1, z_0 may be an integer.

4) Transform $F(z_1, z_0)$ into a polynomial $\tilde{F}(z_1, z_0)$ with coefficients modulo q as stated in Fact 3.

5) Build the matrix $\|A_{ij} - \delta_{ij}\|$ for $\tilde{F}(z_1, z_0)$ according to the above Theorem. It might be possible that several values of z_0 and several modulo q have to be tried (in increasing order) until one obtains a rank of $m-1$ (for irreducible $F(z_1, z_2)$).

Example

$$F(z_1, z_2) = z_1^3 + (813z_2^5 + 1314z_2^4$$
$$+ 579z_2^3 + 75z_2^2 + 60z_2 + 815)z_1^2$$
$$+ (23z_2^5 + 17z_2^4 + 213z_2^3 + 119z_2 + 75)z_1$$
$$+ (83z_2^4 + 13z_2^3 + 42z_2^2 + 27z_2 + 23).$$

For $z_2 = 1$ this becomes

$$F(z_1, 1) = z_1^3 + 3656z_1^2 + 447z_1 + 188.$$

By reducing $F(z_1, 1)$ modulo 5 we have

$$\tilde{F}(z_1, 1) = z_1^3 + z_1^2 + 2z_1 + 3 \pmod 5.$$

Eqs. (7) are, working in arithmetic modulo 5:

$z_1^0 \equiv 1 = (1\ 0\ 0)$

$z_1 \equiv z_1 = (0\ 1\ 0)$

$z_1^2 \equiv z_1^2 = (0\ 0\ 1)$

$z_1^3 \equiv -3 - 2z_1 - z_1^2 \equiv 2 + 3z_1 + 4z_1^2$
$= 2(1\ 0\ 0) + 3(0\ 1\ 0) + 4(0\ 0\ 1)$
$\equiv (2\ 3\ 4)$

$z_1^4 \equiv -3z_1 - 2z_1^2 - z_1^3 \equiv 2z_1 + 3z_1^2 + 4z_1^3$
$= 2(0\ 1\ 0) + 3(0\ 0\ 1) + 4(2\ 3\ 4)$
$\equiv (3\ 4\ 4)$

$z_1^5 \equiv -3z_1^2 - 2z_1^3 - z_1^4 \equiv 2z_1^2 + 3z_1^3 + 4z_1^4$
$= 2(0\ 0\ 1) + 3(2\ 3\ 4) + 4(3\ 4\ 4)$
$\equiv (3\ 0\ 0)$

$z_1^6 \equiv 2(2\ 3\ 4) + 3(3\ 4\ 4) + 4(3\ 0\ 0) \equiv (0\ 3\ 0)$

$z_1^7 \equiv 2(3\ 4\ 4) + 3(3\ 0\ 0) + 4(0\ 3\ 0) \equiv (0\ 0\ 3)$

$z_1^8 \equiv 2(3\ 0\ 0) + 3(0\ 3\ 0) + 4(0\ 0\ 3) \equiv (1\ 4\ 2)$

$z_1^9 \equiv 2(0\ 3\ 0) + 3(0\ 0\ 3) + 4(1\ 4\ 2) \equiv (4\ 2\ 2)$

$z_1^{10} \equiv 2(0\ 0\ 3) + 3(1\ 4\ 2) + 4(4\ 2\ 2) \equiv (4\ 0\ 0)$

(all powers of z_1 are modulo $(z_1^3 + z_1^2 + 2z_1 + 3)$).

For example, z_1^4 is obtained as follows: one takes the remainder of dividing z_1^4 by $z_1^3 + z_1^2 + 2z_1 + 3$, which is $-3z_1 - 2z_1^2 - z_1^3$; this is congruent with $2z_1 + 3z_1^2 + 4z_1^3$ (mod 5). Then z_1, z_1^2 and z_1^3 are substituted by their former representations (0 1 0), (0 0 1) and (2 3 4) respectively, yielding (3 4 4).

The A and $A-I$ matrices are therefore

$$A = \begin{pmatrix} 1 & 0 & 0 \\ 3 & 0 & 0 \\ 4 & 0 & 0 \end{pmatrix}; \quad A - I = \begin{pmatrix} 0 & 0 & 0 \\ 3 & 4 & 0 \\ 4 & 0 & 4 \end{pmatrix}.$$

The minor $\begin{vmatrix} 4 & 0 \\ 0 & 4 \end{vmatrix} = 1 \pmod 5$. Hence the rank of the matrix $A - I$ is 2 and $\tilde{F}(z_1, 1)$ is irreducible and therefore $F(z_1, z_2)$ is also irreducible.

The above procedure can obviously be used to test whether a given object intensity will give rise to a unique solution in the phase problem by applying it to the autocorrelation polynomial $Q(z_1, z_2) = F(z_1, z_2)\, F(z_1^{-1}, z_2^{-1}) z_1^m z_2^n$; in this case of course one expects a minimum of two factors. In fact, as will be seen in a forthcoming paper, this scheme may provide a means of finding the actual factors, when noise is absent, in $Q(z_1, z_2)$.

A small amount of noise would not change the assessment of irreducibility found from the rank of $A - I$. However, the presence of noise will change the field of reducibility of $F(z_1, z_2)$; i.e. if the noiseless polynomial was reducible into factors with all integer coefficients, the polynomial affected by noise may become reducible into factors with irrational coefficients – these representing approximations to the true integer coefficients –, complex coefficients, or even not reducible at all. Thus the test put forward in this note would become insufficient in this case. Even with a large amount of noise it would be difficult to have the exact perturbation which yields the correct combination of coefficients in $F(z_1, z_2)$ for the rank of $A - I$ to be smaller than $m - 1$ if the noiseless object is reducible; the more complicated the object (i.e. the more information the a_{ij} contain), the more difficult would be to reduce the rank.

We are grateful to B.J. Brames, M.A. Fiddy and J.L.C. Sanz for valuable discussions.

This work was supported by grant AFOSR-81-0003 from the U.S. Air Force Office of Scientific Research.

References

[1] Yu.M. Bruck and L.G. Sodin, Optics Comm. 30 (1979) 304.
[2] M.H. Hayes, IEEE Trans. Acoust. Speech Signal Process. ASSP-30 (1982) 140.
[3] M.H. Hayes and J. McClellan, Proc. IEEE 70 (1982) 197.
[4] J.L.C. Sanz, T.S. Huang and F. Cukierman, J. Opt. Soc. Am. 73 (1983) 1442.
[5] J.R. Fienup, Optics Lett. 3 (1978) 27; Appl. Optics 21 (1982) 2758.
[6] A.V. Oppenheim, M.H. Hayes and J.S. Lim, Opt. Eng. 21 (1982) 122.
[7] B.L. Van der Waerden, Algebra (Ungar, N.Y. 1970) Vol. 1;
L. Childs, A concrete introduction to higher algebra (Springer Verlag, N.Y. 1979).
[8] M.A. Fiddy, B.J. Brames and J.C. Dainty, Optics Lett. 8 (1983) 96.
[9] N.K. Bose, Applied multidimensional systems theory (Van Nostrand, N.Y. 1982). Ch. 1.
[10] D.E. Knuth, The art of computer programming. (Addison Wesley, Mass. 1981) Vol. 2, Ch. 4.
[11] M.C.R. Butler, Quart. J. Math. Oxford (2) 5 (1954) 102.
[12] H.P.F. Swinnerton-Dyer, quoted by E.R. Berlekamp in Math. Comp. 24 (1970) 713.

December 1984 / Vol. 9, No. 12 / OPTICS LETTERS 555

Regenerative amplifiers with one phase-conjugate mirror

M. Nieto-Vesperinas*

The Institute of Optics, University of Rochester, Rochester, New York 14627

Received June 11, 1984; accepted September 13, 1984

We study the operating characteristics of a cavity with a gain medium inside and one phase-conjugate mirror as a regenerative amplifier. We show that, for this cavity to work efficiently, the phase-conjugate mirror must have a reflectivity in a certain range determined by the reflectivity of the ordinary mirror. The difference between the phase shift of the incident wave and twice that introduced in the phase-conjugation process should be nonzero.

Optical resonators with one end phase-conjugate mirror (PCM) are a subject of active research[1-4] (see Ref. 5 for a review) because of the property of the PCM to correct, or partially compensate for, phase distortions inside the cavity.

Recently, a Fabry–Perot cavity with one PCM of unity reflectivity was shown to produce cancellation of the wave that is specularly reflected from the ordinary mirror, yielding an emerging output wave with the same amplitude as that of the incident wave and with conjugate phase.[6,7] This phenomenon constitutes in fact a particular case of the correction of scattering distortions of a wave front by the presence of a PCM.[8]

In this Letter we report some properties not yet studied of cavities with a PCM and filled with a gain medium. We show that interesting interference phenomena take place when the system operates below threshold as a regenerative amplifier,[9,10] so the behavior of the system may be quite different from that of ordinary amplifiers.

We assume an incident linearly polarized electromagnetic wave u_0 and reflections in the mirrors P and PCM such that complete reversal of the state of polarization of the wave at the PCM takes place (see Ref. 8, Sec. 7), so that one can work with scalar quantities. The output wave emerging from the cavity will be denoted by u (see Fig. 1). Let r be the reflection coefficient of the ordinary mirror P from the left-hand side; then the reflection coefficient of P from the right-hand side is $-r$, and its transmission coefficient on either side is $t^2 = 1 - r^2$. The PCM is assumed to have a reflectivity $\mu = |\mu|e^{i\Phi}$, so if u_p is the wave reflected at P inside the cavity and propagating back to PCM, the wave at P after a round trip through reflection at the PCM will be $\mu e^{\gamma L}u_p^*$, in contrast with an ordinary cavity in which a phase factor $2kL$ would be accumulated in every round trip. k is the wave number, and L is the length of the cavity.

The gain coefficient γ of the medium inside the cavity is given by the imaginary part of the complex propagation constant $\hat{k}$,[10] so

$$\hat{k} = k - i\gamma/2. \tag{1}$$

The single-pass gain[10] of the traveling wave across the cavity is

$$G_0 = e^{\gamma L}. \tag{2}$$

The complex amplitude of the output wave u may be obtained either by using the boundary conditions for the fields at P and PCM or by adding the geometrical series that results by considering the multiple reflections in the plates. The second method, for instance, gives

$$\begin{aligned} A &= ru_0 + \mu t^2 e^{\gamma L}u_0^* - t^2 r|\mu|^2 e^{2\gamma L}u_0 \\ &\quad + t^2|\mu|^2\mu r^2 e^{3\gamma L}u_0^* - t^2 r^3|\mu|^4 e^{4\gamma L}u_0 \\ &\quad + t^2|\mu|^4\mu r^4 e^{5\gamma L}u_0^* + \ldots \\ &= ru_0 - t^2 r|\mu|^2 e^{2\gamma L}(1 + |\mu|^2 r^2 e^{2\gamma L} + \ldots)u_0 \\ &\quad + e^{\gamma L}t^2\mu(1 + |\mu|^2 r^2 e^{2\gamma L} + \ldots)u_0^* \\ &= \frac{r(1 - |\mu|^2 e^{2\gamma L})u_0 + \mu(1 - r^2)e^{\gamma L}u_0^*}{1 - r^2|\mu|^2 e^{2\gamma L}}. \end{aligned} \tag{3}$$

The condition for the convergence of the series, which also corresponds to the stability of the feedback system, is

$$r^2|\mu|^2 e^{2\gamma L} < 1. \tag{4}$$

Figure 2 shows the plots of $|\mu|^2$ versus the critical values $(\gamma L)_c$ at which

$$r^2|\mu|^2 e^{2(\gamma L)_c} = 1 \tag{5}$$

for several reflectivities r^2.

The overall gain of the system is given by the intensity of the output wave $I = |u|^2$:

$$\begin{aligned} I &= \left[\frac{r(1 - |\mu|^2 e^{2\gamma L}) + |\mu|(1 - r^2)e^{\gamma L}\cos\phi}{1 - r^2|\mu|^2 e^{2\gamma L}}\right]^2 \\ &\quad + \left[\frac{|\mu|(1 - r^2)e^{\gamma L}}{1 - r^2|\mu|^2 e^{2\gamma L}}\sin\phi\right]^2, \end{aligned} \tag{6}$$

where $\phi = \Phi - 2\phi_0$, ϕ_0 being the phase of the incident wave u_0, and where the amplitude of the wave is assumed normalized to unity, i.e., $u_0 = e^{i\phi_0}$.

We compare the expression given by Eq. (6) with the overall gain of a cavity with two ordinary mirrors of reflectivities r_1 and r_2 in the resonant situation, namely, when $2kL = 2n\pi$ (n is an integer):

0146-9592/84/120555-03$2.00/0

$$I_{12}^{\text{ord}} = \left|\frac{r_1(1 - r_2^2 e^{2\gamma L}) - r_2(1 - r_1^2)e^{\gamma L}}{1 - r_1^2 r_2^2 e^{2\gamma L}}\right|^2 \quad (7)$$

or in the particular case when $r_1 = r_2 = r$ in which Eq. (7) become

$$I_{11}^{\text{ord}} = \left|\frac{r(1 - e^{\gamma L})}{1 - r^2 e^{\gamma L}}\right|^2. \quad (8)$$

From Eqs. (6)–(8) we observe the following:

(1) For $\phi = m\pi$ (m is an odd integer), I becomes identical with I_{12}^{ord} and has a zero at

$$G_0 = e^{\gamma L} = r/|\mu|, \quad (9)$$

which occurs for γL positive (i.e., single-pass gain G_0 greater than unity) when $r > |\mu|$. (Observe that this is in agreement with the law of conservation of energy of the electromagnetic wave.) *This fact permits the determination of the phase ϕ_0 of the incident wave in this device for G_0, r, and $|\mu|$ given satisfying Eq. (9) (which can be attained, e.g., by varying the length L of the cavity) if the phase shift at the PCM Φ is known and matched to satisfy $\Phi - 2\phi_0 = m\pi$.* [When $\gamma = 0$, Eq. (9) implies that $r = |\mu|$.]

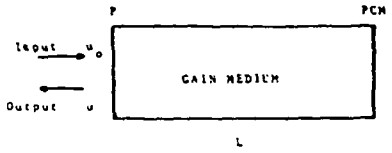

Fig. 1. Diagram of the regenerative amplifier.

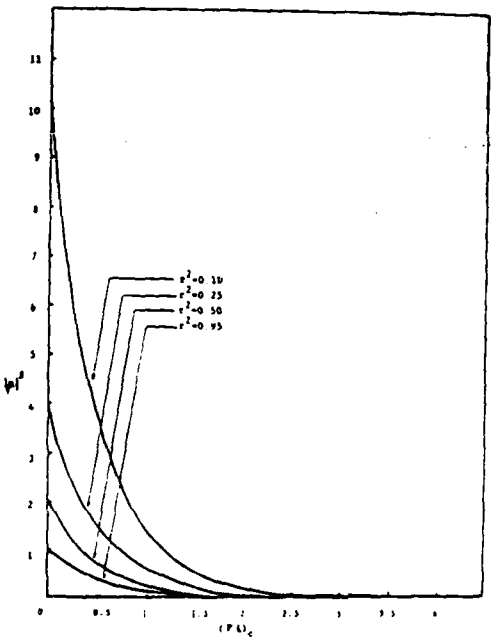

Fig. 2. Values of $|\mu|^2$ versus the critical $(\gamma L)_0$ for several reflectivities r^2.

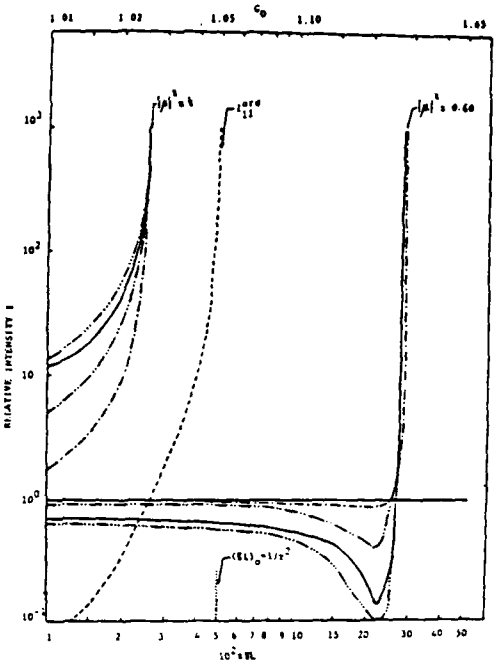

Fig. 3. Overall gains versus γL and G_0 for $r^2 = 0.95$: – – –, I_{11}^{ord}. The horizontal solid line represents I for $\phi = 0$ and any $|\mu|^2$, $|\mu|^2 = 0.20$ and any ϕ, and $|\mu|^2 > 1.05$ (e.g., $|\mu|^2 = 1.2$ and higher). — · —, I for $\phi = \pi/4$; — · · — · ·, I for $\phi = \pi/2$; — · · · — · · ·, I for $\phi = \pi$ ($= I_{12}^{\text{ord}}$); —— other than horizontal, I for $\phi = 3\pi/4$.

(2) The overall gain is enhanced below threshold by working near its resonance point $(\gamma L)_c$ given by Eq. (5), while maintaining condition (4). Since $(\gamma L)_c$ is positive for a cavity with gains, one should have, according to Eq. (5), $|\mu|^2 < 1/r^2$. This leads to the result that no overall amplification is obtained by increasing the PCM reflectivity beyond the value $1/r^2$.

(3) For $\phi = 2n\pi$ (n is an integer), I does not present any resonant value. At $(\gamma L)_c$, I has the finite value $(1 + r^2)/2r$. *Therefore, when $\Phi = 2\phi_0$, the cavity will not work as a regenerative amplifier. This will be so in particular when $\phi_0 = 0$ and there is perfect phase conjugation at the PCM, i.e., when $\Phi = 0$.*

Figure 3 illustrates these points. The overall gain I has been compared with the ordinary case I_{11}^{ord} given by Eq. (8) ($r^2 = 0.95$), and I_{12}^{ord} given by Eq. (7) appears plotted as the limit of I when $\phi = \pi$. The curves of I versus γL and G_0 are shown for different values of ϕ and $|\mu|^2$ while r^2 is maintained at 0.95.

For $\phi = 0$, I remains around unity, and no regenerative amplification takes place independently of $|\mu|^2$.

For low $|\mu|^2$ ($|\mu|^2 \simeq 0.20$), I also takes values around unity even when γL is large and independent of ϕ.

For $|\mu|^2 = 1.2$ ($1.2 > 1/r^2 = 1/0.95$) and higher, I also remains around unity, and no improvement of the overall gain is obtained by increasing $|\mu|^2$ above the value $1/0.95 = 1.05$.

For intermediate values of $|\mu|^2$ (e.g., $|\mu|^2 = 0.60$) one obtains first, constant I for low γL, then, as γL increases, a minimum followed by a sharp increase of I. These minima are deeper as ϕ increases from 0 to π, until the situation corresponding to I_{12}^{ord} is reached when $\phi = \pi$ with a zero minimum around $\gamma L \simeq 0.23$ ($G_0 \simeq 1.26$).

Finally, when $1/r^2 > |\mu|^2 \geq r^2$ (e.g., when $|\mu|^2 = 1$), the cavity works efficiently as a regenerative amplifier with overall gain higher than I_{11}^{ord} but lower than I_{12}^{ord} since the amplification increases with ϕ.

In conclusion, we have shown that, under the assumptions that there are no saturation effects and that μ remains constant independently of the intensity of the wave incident upon the PCM, a cavity with a gain medium inside and a PCM presents interesting interference phenomena. It permits (with or without gains) the determination of the phase of the incident field if the phase shift of the PCM can be known and adjusted so that the emerging field is zero. It also requires certain conditions in order to work as a regenerative amplifier: The phase shift at the PCM should be twice that of the incident wave, and, in particular, if the phase of the input is zero there should not be perfect phase conjugation, i.e., Φ must be different from zero. Also, the reflectivity $|\mu|^2$ of the PCM must be in the range $r^2 \leq |\mu|^2 < 1/r^2$. For large r^2, $|\mu|^2 = 1$ is a good value.

The author wishes to thank E. Wolf for introducing him to the subject of phase conjugation and for many suggestions that motivated this work. He also thanks him and R. W. Boyd for many interesting comments that shaped this work. M. Raymer also made interesting remarks. Some comments of a referee are also acknowledged. This research was partly supported by the U.S. Air Force Office of Scientific Research through grant AFOSR-81-0003 and by the National Science Foundation.

* On leave from Instituto de Optica, C.S.I.C., Serrano 121, Madrid 6, Spain.

References

1. J. Au Yeung, D. Fekete, D. M. Pepper, and A. Yariv, IEEE J. Quantum Electron. **QE-15**, 1180 (1979).
2. J. M. Bel'dyugin, M. G. Galushkin, and E. M. Zemskov, Sov. J. Quantum Electron. **9**, 20 (1979).
3. P. A. Belanger, A. Hardy, and A. E. Siegman, Appl. Opt. **19**, 602 (1980); **19**, 479 (1980).
4. J. F. Lam and W. P. Brown, Opt. Lett. **5**, 61 (1980).
5. A. E. Siegman, P. A. Belanger, and A. Hardy, in *Optical Phase Conjugation*, R. A. Fisher, ed. (Academic, New York, 1983), Chap. 13.
6. A. T. Friberg and P. D. Drummond, J. Opt. Soc. Am. **73**, 1216 (1983); J. Appl. Phys. **54**, 5618 (1983).
7. M. Nazarathy, Opt. Commun. **45**, 117 (1983).
8. G. S. Agarwal, A. T. Friberg, and E. Wolf, J. Opt. Soc. Am. **73**, 529 (1983).
9. H. Boersch and G. Herziger, IEEE J. Quantum Electron. **QE-2**, 549 (1966).
10. A. E. Siegman, *An Introduction to Masers and Lasers* (McGraw-Hill, New York, 1971), Sec. 5.5.

Reprinted from Journal of the Optical Society of America A, Vol. 2, p. 22, January 1985

K distributions from doubly scattered light

D. Newman

Applied Optics Group, Blackett Laboratory, Imperial College, London SW7 2BZ, England

Received May 21, 1984; accepted September 13, 1984

It has been experimentally demonstrated that the effect of doubly scattering coherent light within the limitations of a particular model gives rise to probability densities that are *K* distributed. The probability distribution of photon counts $P(n)$ therefore has an exact analytic form and has been favorably compared with the experimental values, as have the normalized moments of intensity.

INTRODUCTION

A recent theoretical paper by O'Donnell[1] has examined the probability distribution of intensity and the correlation structure of coherent light that has been scattered on two distinct occasions. The model is essentially one in which dynamic Gaussian speckles arising from a primary scattering mechanism are themselves scattered by a translating diffuser (see Fig. 1). The secondary scatterer (diffuser) is located in the far field of the primary scatterer, and it is assumed that the microstructure of this diffuser is much finer than the incident coherence domains (speckles) that illuminate it. All measurements are made in the far field of the secondary diffuser.

Using these assumptions together with a nonrestrictive approximation, it was shown[1] that this process exhibits a probability density of intensity that is *K* distributed.[2] The moments of this distribution are well known[3] and agree favorably with the experimental results presented in this paper. Further, it is demonstrated here that the Mandel transform of the intensity distribution may also be expressed in an exact analytic form to yield the probability distribution of photon counts. These curves are shown to fit the data extremely well and confirm the analysis that this process is indeed *K* distributed and hence capable of exhibiting highly non-Gaussian fluctuations under circumstances that are explained below.

THEORY

Only the most basic elements of the theory are presented here, a more detailed account being given in Ref. 1. The experimental arrangement is shown in Fig. 1. A laser source illuminates a rotating ground-glass diffuser, producing dynamic Gaussian speckle in the far field, where the second translating diffuser is located. A hard circular aperture is placed on axis immediately behind the second diffuser to limit the number of speckles that illuminate it. If the correlation scale (i.e., the speckle size) is much larger than this aperture, we may assume that, at any instant of time, the complex speckle amplitude denoted by a_0 is approximately constant over the scattering aperture. The complex amplitude seen by the detector may then be expressed as

$$A(x,y) = a_0 \iint_D t(\xi,\eta)\exp\left[\frac{-ik}{z}(x\xi + y\eta)\right]d\xi d\eta, \quad (1)$$

where $t(\xi, n)$ is the transmission function of the second diffuser and D is the domain of integration [an unimportant phase term and scaling constant were ignored in Eq. (1)]. Hence $A(x, y) = a_0 A_0(x, y)$, where a_0, A_0 are independent and are themselves Rayleigh distributed according to

$$p(|a_0|) = \frac{2|a_0|}{\sigma_1^2}\exp(-|a_0|^2/\sigma_1^2),$$
$$p(|A_0|) = \frac{2|A_0|}{\sigma_2^2}\exp(-|A_0|^2/\sigma_2^2), \quad (2)$$

with $\sigma_1^2 = \langle|a_0|^2\rangle$ and $\sigma_2^2 = \langle|A_0|^2\rangle$.

The probability density of $A = a_0A_0$ is then

$$p(|A|) = \iint_0^\infty d|A_0|d|a_0|p(|a_0|)p(|A_0|)\hat{\delta}(|A| - |A_0||a_0|), \quad (3)$$

where $\hat{\delta}$ is the Dirac delta function.

By carrying out the integral over A_0 first and by making the substitution $e^t = a_0^2\sigma_2/(|A|\sigma_1)$ for the second integral, we find that

$$p(|A|) = \frac{4|A|}{\sigma_1^2\sigma_2^2}\int_0^\infty dt \exp\left[\frac{-2|A|}{\sigma_1^2\sigma_2^2}\cosh(t)\right]. \quad (4)$$

This is an integral representation of the zero-order Bessel function of the second kind; thus

$$p(|A|) = \frac{4|A|}{\beta}K_0\left(\frac{2|A|}{\sqrt{\beta}}\right), \quad (5)$$

where $\beta = \langle|A|^2\rangle = \sigma_1^2\sigma_2^2$.

If many speckles are illuminating the second diffuser, an intuitive approximation is made, in that the complex amplitude of each speckle is spatially constant over equal-sized domains within the scattering aperture. We may then express the complex amplitude seen by the detector as

$$A(x,y) = \sum_{i=1}^{N} a_i \iint_{D_i} t(\xi,\eta)\exp\left[\frac{-ik}{z}(x\xi + y\eta)\right]d\xi d\eta, \quad (6)$$

where a_i is the spatially constant complex amplitude of the ith domain D_i, and N is the number of domains present within the scattering aperture of the diffuser. The central-limit theorem ensures that each integral within the sum represents

0740-3232/85/010022-05$02.00

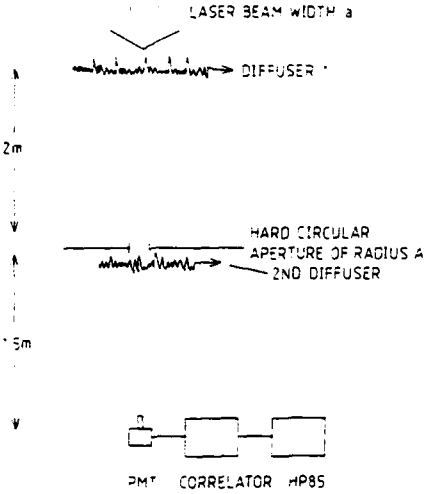

Fig. 1. Experimental setup.

a complex amplitude, which has circular Gaussian statistics. By the theorem of Jakeman and Pusey,[4] a random walk of the N steps in Eq. (6) is distributed as

$$p(|A|) = \frac{4|A|}{\Gamma(N)}\frac{1}{\sqrt{\beta}}\left(\frac{|A|}{\sqrt{\beta}}\right)^{N} K_{N-1}\left(\frac{2|A|}{\sqrt{\beta}}\right), \tag{7}$$

which may be rewritten in terms of the normalized intensity distribution as

$$P(I) = \frac{2}{\Gamma(N)}\frac{1}{\beta}\left(\frac{I}{\beta}\right)^{(N-1)/2} K_{N-1}\left(2\sqrt{\frac{I}{\beta}}\right), \tag{8}$$

where $\langle I\rangle = N\beta = \langle |A|^2\rangle$ is the average intensity, K_{N-1} is the modified Bessel function, and $\Gamma(N)$ is the gamma function. Thus a random walk of N steps, in which each step length is given by a K distribution, leads to another K distribution of the order $N-1$. The normalized moments of intensity are therefore

$$\frac{\langle I^m\rangle}{\langle I\rangle^m} = \frac{m!\,\Gamma(m+N)}{N^m\Gamma(N)}, \tag{9}$$

where we note that, when $N = 1$,

$$\frac{\langle I^m\rangle}{\langle I\rangle^m} = (m!)^2,$$

which represents strong intensity fluctuations, whereas for large N it is easy to show that

$$\lim_{N\to\infty}\frac{\langle I^m\rangle}{\langle I\rangle^m} = m!,$$

which represents a Rayleigh or circular Gaussian distribution. The present experiment explicitly measures the probability distribution of photon events $P(n)$ from which the normalized intensity moments are found by computation of the normalized factorial moments of $P(n)$. A theoretical calculation of $P(n)$ may be achieved by taking the Mandel transform of the intensity distribution [Eq. (8)].

The Mandel transform is defined by

$$P(n) = \int_0^\infty dI\, P(I)\frac{(\epsilon t I)^n}{n!}\exp(-\epsilon t I), \tag{10}$$

where ϵ is the detector efficiency and t denotes the experimental sampling time. It is a necessary condition that the sampling time t be much less than the average intensity-fluctuation time τ_c for Eq. (10) to be considered valid. Direct substitution of Eq. (8) into Eq. (10) yields a Bessel transform whose solution[5] is

$$P(n) = \langle n\rangle^{-N/2}\frac{\Gamma(N+n)}{\Gamma(N)}\exp\left(\frac{1}{2\langle n\rangle}\right) W_{k,y}(1/\langle n\rangle), \tag{11}$$

where $\langle n\rangle = N\epsilon t\beta$ is the average number of photons per sample time and $W_{k,y}(x)$ is the Whittiker function with $k = -(n + N/2)$ and $y = \frac{1}{2}(N-1)$.

Again, substitution of the appropriate form[6] of the Whittiker function in Eq. (11) yields the result

$$P(n) = \frac{1}{\Gamma(N)}\left(\frac{\langle n\rangle}{N}\right)^n\int_0^\infty dx\,\frac{x^{N+n-1}\exp(-x)}{\left(1+\frac{\langle n\rangle x}{N}\right)^{n+1}}. \tag{12}$$

The integral in Eq. (12) was calculated numerically for each value of n, as it is an exponential integral and cannot be reduced analytically. Although our heuristic derivation of Eq. (12) was based on a model with implicitly integer values of N (approximately equal to the number of speckles illuminating the second diffuser), it is not restricted to integer values, provided that $N \geq 1$. Numerous examples of distributions involving noninteger values of N were analyzed and agreed well with the predictions of Eq. (12).

EXPERIMENT

An 8-W argon-ion laser, $\lambda = 490$ nm, was used as the primary source of coherent light, which passed through a microscope objective of 16-mm focal length before transmission through the first diffuser. The distance between the microscope objective and the diffuser was varied in order to control the diameter of the primary source and therefore to control the speckle size in the far field of the first diffuser. A second diffuser was placed on axis at a distance of approximately 1.65 m from the first diffuser, and a hard circular aperture preceded it. The detector was located along the optical axis at a distance of approximately 1.5 m from the second diffuser. The detector consisted of a 50-μm-core optical fiber coupled to a photomultiplier tube (PMT) and to a pulse amplifier/discriminator. Digital output from the discriminator was sent to a photon correlator and an on-line computer for processing the moments of intensity and the photon-count histogram.

The sample time for all measurements was 5×10^{-5} sec, and a typical 30-sec run yielded a total of approximately 6×10^5 samples. The $1/e$ correlation time of the doubly scattered intensity fluctuations had a measured value of $\tau_c \simeq 5\times10^{-4}$ sec; hence the total number of independent samples was approximately $M = 6\times10^4$ for a 30-sec run. Corrections for dead time and dark counts were made in calculating the normalized moments, although both effects were small. A lower limit of the rms variance for the moment calculations was made using the following simple argument: If x represents the value of the mth intensity moment, as estimated from M

Table 1. Experimental Measurements of the Normalized Moments of Intensity

	$\frac{\langle I^2\rangle}{\langle I\rangle^2}$	$\frac{\langle I^3\rangle}{\langle I\rangle^3}$	$\frac{\langle I^4\rangle}{\langle I\rangle^4}$	$\frac{\langle I^5\rangle}{\langle I\rangle^5}$	Number of Independent Samples
$N = 1$					
Predicted value	4	36	576	14400	
Experimental values	4.03 ± 0.12	35.13 ± 3.6	470 ± 200	7425 ± 18000	6×10^4
	4.06 ± 0.12	36.55 ± 3.6	520 ± 200	9075 ± 18000	6×10^4
	4.003 ± 0.12	34.42 ± 3.6	440 ± 200	6850 ± 18000	6×10^4
$N = 2$					
Predicted value	3	18	180	2700	
Experimental values	3.06 ± 0.09	18.50 ± 1.7	163 ± 50	1610 ± 1800	3×10^4
	2.94 ± 0.09	16.44 ± 1.7	134 ± 50	1240 ± 1800	
$N = 3$					
Predicted value	2.66	13.3	106.6	1244	
Experimental values	2.67 ± 0.05	13.4 ± 0.7	100 ± 17	922 ± 480	6×10^4
	2.66 ± 0.09	12.9 ± 1.2	88 ± 31	665 ± 800	3×10^4
$N = 4$					
Predicted value	2.5	11.25	78.75	787.75	
Experimental values	2.53 ± 0.07	11.52 ± 0.09	73.6 ± 18	521 ± 530	3×10^4

statistically independent samples I_j, i.e.,

$$x = \frac{1}{M}\sum_{j=1}^{M} I_j{}^m,$$

then the variance of x is

$$\sigma_x{}^2 = \sum_{j=1}^{M} \frac{\langle I_j{}^{2m}\rangle - \langle I_j{}^m\rangle^2}{M^2} = \frac{\langle I^{2m}\rangle - \langle I^m\rangle^2}{M}. \quad (13)$$

The normalized rms variance is obtained by dividing Eq. (13) by $\langle I^m\rangle^2$ and taking the square root. This yields a lower bound for the error, as no account of the error in the denominator or the photon noise was folded in. It is clear from Eq. (9), however, that the rms variance increases dramatically with increasing m.

A comparison of the experimental measurements of the normalized moments of intensity with those predicted by theory is shown in Table 1. The values are seen to agree with theory well within the experimental error. Experimental determinations of the parameter N may be achieved by a straightforward calculation of the speckle size incident upon the scattering aperture; however, it is more consistent to define N by comparing the experimental value of the second moment of intensity with that predicted by Eq. (9). This convention is used in establishing the experimental values of N in this paper.

The value of N approximately corresponds to the number of speckles illuminating the second diffuser. This is easily controlled in the experiment by adjusting the beam diameter incident upon the first diffuser and/or by varying the diameter of the hard aperture. For the experiments, the combinations shown in Table 2 were used.

A comparison of the theoretical distribution of photon counts $P(n)$ with the experimental results is shown in Fig. 2 for $N = 1, 2, 3, 4$ and various values of $\langle n\rangle$. The model fits the data extremely well. For fixed $\langle n\rangle$, the curves show how the distribution of $P(n)$ gradually broadens toward a negative exponential distribution as N is increased.

DISCUSSION

The experimental values of the normalized moment of intensity, shown in Table 1, indicate good general agreement with the predictions of Eq. (9). However, it is clear that almost all values fall slightly below the predicted value. This is probably due to a truncation error, since only 64 channels were used in the histogram and the effect of cutting off the tail of this distribution would certainly result in a lower value of the calculated moment. The run times were also a bit short in terms of gathering a good statistical base for the fourth and the fifth moments [see Eq. (13)].

The distribution of photon counts $P(n)$ fits the theoretical curves [Eq. (12)] to at least the 5% level for $N = 1, 2$, as shown in Fig. 2. For $N = 3, 4$, the theoretical curves again show excellent agreement with the data; however, the first few points tend to be slightly more spread out than those predicted in theory.

It is instructive to compare this model with other systems that exhibit K-distributed probability densities. These

Table 2. Typical Parameters Used for Selecting Various Values of N

N	Beam Diameter a (mm)[a]	Aperture Diameter $2A$ (mm)
1	0.24	1.0
2	0.32	2.0
3	0.32	2.5
4	0.48	2.5

[a] The beam diameter refers to the primary beam diameter at the $1/e^2$ intensity.

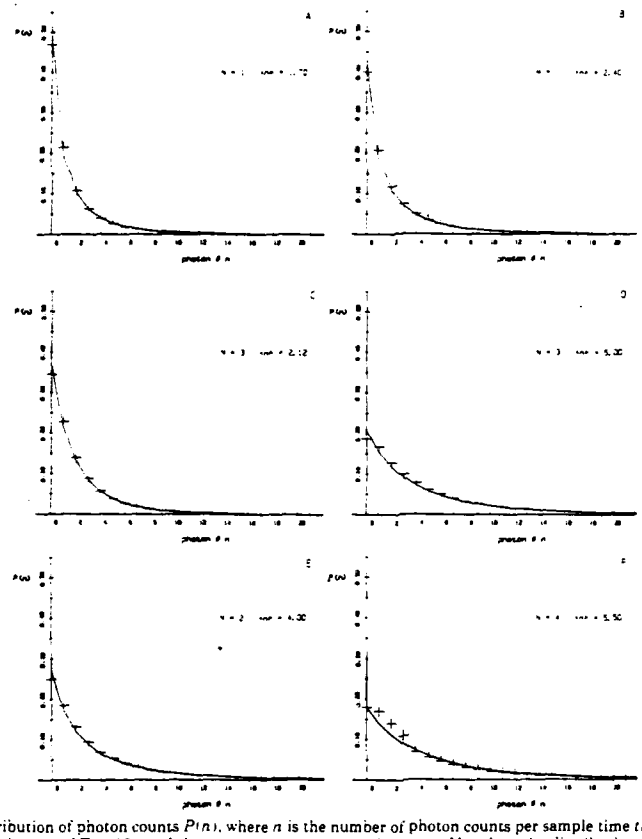

Fig. 2. Probability distribution of photon counts $P(n)$, where n is the number of photon counts per sample time t_0 ($t_0 = 5 \times 10^{-5}$ sec). The solid line is the theoretical curve of Eq. (12), and the crosses are experimental points. Note how the distribution depends on the number of speckles within the scattering aperture N and the average number of photons per sample time $\langle n \rangle$. This is seen most clearly by comparing C and D.

systems include the *single* scattering of laser light from (a) a turbulent layer of nematic liquid crystal,[7] (b) a turbulent layer of air,[8] (c) the scattering of starlight from the upper atmosphere,[9] and (d) the scattering of microwave radiation from a small patch of turbulent seas.[10] According to the limit theorem of Jakeman and Pusey,[4] if a scattering medium is made up of a finite number N of independent scattering centers, each of which contains a *correlated* group of lesser scatterers (which obey negative binomial statistics), then the amplitude scattered by each independent region is K distributed. In the present context, however, the K distributions arise for a different reason, in that they are explicitly generated by the multiplicative effects of double scattering, each process being independently Rayleigh distributed.

Finally, for $N = 1$ the problem reduces to that of scattering a single Gaussian correlated source from an optically rough diffuser. In other words, this may be interpreted as a Gaussian–Gaussian scattering process, which has been investigated in a different context by Bertolotti[11] and others. It is straightforward to show that, in this case, the temporal autocorrelation of intensities takes the form

$$C^{(2)}(\tau) = [1 + |\gamma_1(\tau)|^2][1 + |\gamma_2(\tau)|^2], \tag{14}$$

where $|\gamma_1(\tau)|$, $|\gamma_2(\tau)|$ are the amplitude correlations of the independent processes 1 and 2. In our experiments

$$|\gamma_1(\tau)|^2 = \exp\left(\frac{-V_1^2\tau^2}{4a^2}\right),$$

$$|\gamma_2(\tau)|^2 = J_1^2\left(\frac{2\pi A V_2 \tau}{\lambda z}\right) \Big/ \left(\frac{2\pi A V_2 \tau}{\lambda z}\right)^2,$$

where V_1, V_2 are the diffuser velocities, a is the laser-beam diameter, A is the scattering aperture radius, and $J_1(x)$ is the Bessel function of the first kind. The correlation functions were measured with the the photon correlator, and the shape and the time scales were in agreement with Eq. (14). However, the results are not reproduced here.

ACKNOWLEDGMENTS

The author thanks J. C. Dainty for his support of this research and for many helpful discussions. I also thank L. Mandel and

S. Friberg for their generosity in providing the major equipment that made this experiment possible. Thanks finally to B. M. Levine for the use of his program MOMENTS, which greatly simplified the data acquisition.

This research was sponsored by the U.S. Air Force Office of Scientific Research under grant AFOSR-81-0003.

The author is also with the Department of Physics and Astronomy, University of Rochester, Rochester, New York 14726.

REFERENCES

1. K. A. O'Donnell, J. Opt. Soc. Am. 72, 1459 (1982).
2. E. Jakeman and P. N. Pusey, "A model for non-Rayleigh sea echo," IEEE Trans. Ant. Prop. AP-24, 806 (1976).
3. B. E. A. Saleh, "Photoelectron statistics," in Vol. 6 of Springer Series in Optical Sciences (Springer-Verlag, Berlin, 1978), p. 70.
4. E. Jakeman and P. N. Pusey, "Significance of K distributions in scattering experiments," Phys. Rev. Lett. 40, 546 (1978).
5. A. Erdely, W. Magnus, F. Oberhettinger, and F. G. Tricomi, *Tables of Integral Transforms* (McGraw-Hill, New York, 1954), Vol. 2, p. 132.
6. E. T. Whittiker and G. N. Watson, *A Course in Modern Analysis* (Cambridge U. Press, Cambridge, 1954), p. 340.
7. E. Jakeman and P. N. Pusey, J. Phys. A 8, 392 (1975).
8. G. Parry, P. N. Pusey, E. Jakeman, and J. G. McWhirter, Opt. Commun. 22, 195 (1977).
9. E. Jakeman, E. R. Pike, and P. N. Pusey, Nature (London) 263, 215 (1976).
10. E. Jakeman and P. N. Pusey, *Radar 77* (Institute of Electronics Engineers, London, 1977), p. 105.
11. M. Bertolotti, B. Crosignani, and P. DiPorto, J. Phys. A 3, L37 (1970).

Fields generated by a Fabry–Perot interferometer with a phase-conjugate mirror

M. Nieto-Vesperinas*

Institute of Optics, University of Rochester, Rochester, New York 14627

Received June 29, 1984; accepted October 29, 1984

We study theoretically a Fabry–Perot interferometer with one phase-conjugate mirror. Comparisons with results previously obtained by Kastler [Appl. Opt. 1, 17 (1962)] for an ordinary Fabry–Perot interferometer are made. Specifically, we discuss the field intensity of the light both outside and inside the interferometer. We also study the intensity of the exterior field that is due to atoms radiating incoherently inside the interferometer. The operating characteristics below the threshold of the interferometer when it is filled with a gain medium are also analyzed and are found to be different from those of the ordinary interferometer. Finally, conditions are obtained under which the cavity can act as a regenerative amplifier.

1. INTRODUCTION

In an interesting paper[1] Kastler studied the fields generated inside an ordinary Fabry–Perot interferometer and also those generated outside the interferometer by atoms radiating incoherently inside the cavity.

In recent years, phase-conjugate optics has experienced rapid development,[2–4] and phase-conjugate reflectivities of the order of unity and higher have been achieved.[5–7] There has also been progress in the understanding of scattering of phase-conjugate fields (see, e.g., Ref. 8 and the references cited therein).

Optical resonators with one phase-conjugate mirror (PCM) have also been actively investigated,[9–13] and the amplitudes of the field emerging from a cavity without gains when a plane wave is incident upon the system have been calculated.[14–16]

In this paper, we investigate theoretically an interferometer that consists of a lossless dielectric mirror and a PCM. We calculate the field that emerges from the cavity for several reflectivities of the ordinary mirror, and the results are compared with those of Refs. 14–16. We also compute the field intensity inside the cavity and compare it with the intensity inside an ordinary Fabry–Perot interferometer that was investigated in Ref. 1. The case of atoms radiating incoherently inside the cavity is also considered and is contrasted with the more usual case treated in Ref. 1. In both cases, we find that there is higher amplification of the fields in an interferometer with a PCM compared with the ordinary interferometer.

We also compute the intensity of the field emerging from the cavity when it is filled with a gain medium and the ordinary mirror is illuminated at normal incidence. We will see that there are interesting interference phenomena for the output wave when the system operates below threshold as a regenerative amplifier[17,13]: it may give rise to emerging fields that are quite different from those produced by ordinary amplifiers.

All the calculations assume monochromatic linearly polarized input waves and also reflectivity of the PCM that is independent of the intensity and propagation direction of the wave incident upon it; hence this reflectivity remains constant during multiple reflections inside the interferometer.

2. FIELDS GENERATED BY AN INTERFEROMETER WITH A PHASE-CONJUGATE MIRROR

Let us consider a system consisting of a lossless nonmagnetic dielectric partially transmitting plane mirror P, whose amplitude, reflection, and transmission coefficients are r and t, respectively, and a plane PCM, which is parallel to P (see Fig. 1). We shall assume for the moment that the space between both planes is a vacuum. As is well known (see, e.g., Ref. 14 and references cited therein), if t and τ are the transmission coefficients of P from left to right and from right to left, respectively, then $t = \tau$: also, if r and ρ are the reflection coefficients of P from left to right and from right to left, respectively, then $r = -\rho$. As in Ref. 1, we assume that r, ρ, t, and τ are real quantities satisfying the relations

$$r^2 + t^2 = 1, \tag{1a}$$

$$rt + t\rho = 0. \tag{1b}$$

Let an electromagnetic plane wave, which is linearly polarized either in the plane of incidence or perpendicular to it, be incident at angle θ on the mirror P. We take its amplitude to be normalized to unity. We assume that the reflected wave at the PCM suffers complete reversal of the state of polarization (see Ref. 8, Sec. 7, and Refs. 14–16), so that we can employ a scalar description. The incident wave will be

$$E_i = \exp(i\mathbf{k}_i \cdot \mathbf{r}), \tag{2}$$

where $\mathbf{k}_i$ is its wave vector.

The transmitted wave E_t at P will be in the same direction $\mathbf{k}_i$[18]:

$$E_t = t \exp(i\mathbf{k}_i \cdot \mathbf{r}). \tag{3}$$

0740-3232/85/030427-10$02.00

The reflected wave E_r at P will be (Fig. 1)

$$E_r = r \exp(i\mathbf{k}_r \cdot \mathbf{r}), \tag{4}$$

$\mathbf{k}_r$ being the wave vector of this wave.

When the field E_i reaches the PCM, a reflected wave, which is the conjugate of the incident field E_i, is generated that has the wave vector $-\mathbf{k}_i$[19]: $\mu t^* \exp(-i\mathbf{k}_i \cdot \mathbf{r})$. μ is a parameter, assumed constant (see Ref. 12), which represents the amplitude reflection coefficient of the PCM. This field is partly reflected and partly transmitted at P, and this process continues. As a result of the multiple reflections between P and PCM there are four series that represent the fields E_1, E_2, E_3, and E_4 inside the cavity formed by P and PCM (see Fig. 1) as well as a total reflected field E_R and a phase-conjugate field E_C outside the interferometer. The amplitudes of all these fields are

$$A_1 = t + t|\mu|^2 r^2 + t|\mu|^4 r^4 + \ldots = \frac{t}{1-|\mu|^2 r^2}, \tag{5}$$

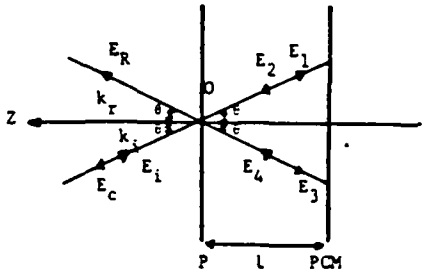

Fig. 1. Reflection of an incident plane wave E_i from an interferometer consisting of a dielectric plate P and a PCM.

$$A_2 = \mu t + \mu t|\mu|^2 r^2 + \mu t|\mu|^4 r^4 \ldots = \frac{\mu t}{1-|\mu|^2 r^2}, \tag{6}$$

$$A_3 = \mu t r + \mu t r|\mu|^2 r^2 + \mu t r|\mu|^4 r^4 + \ldots = \frac{\mu t r}{1-|\mu|^2 r^2}, \tag{7}$$

$$A_4 = |\mu|^2 r t + |\mu|^2 r t|\mu|^2 r^2 + |\mu|^2 r t|\mu|^4 r^4 + \ldots = \frac{|\mu|^2 r t}{1-|\mu|^2 r^2}. \tag{8}$$

Here, the geometric series have been summed under the assumption that

$$|\mu|^2 r^2 < 1. \tag{9}$$

Hence the intensities of these four fields inside the interferometer are given by the expressions

$$I_1 = \frac{1-r^2}{(1-|\mu|^2 r^2)^2}, \tag{10}$$

$$I_2 = \frac{|\mu|^2(1-r^2)}{(1-|\mu|^2 r^2)^2}, \tag{11}$$

$$I_3 = \frac{|\mu|^2 r^2(1-r^2)}{(1-|\mu|^2 r^2)^2}, \tag{12}$$

$$I_4 = \frac{|\mu|^4 r^2(1-r^2)}{(1-|\mu|^2 r^2)^2}, \tag{13}$$

where condition (1a) has been taken into account. It is to be noted that Eqs. (5)–(8) could have also been obtained by using the electromagnetic boundary conditions at P and at the PCM.

Figures 2–5 show the plots of the intensities given by Eqs. (10)–(13) versus $|\mu|^2$ for different values of r^2. For low reflectivities r^2, the field intensities can become large when $|\mu|^2$ is large enough, because energy is then provided by the

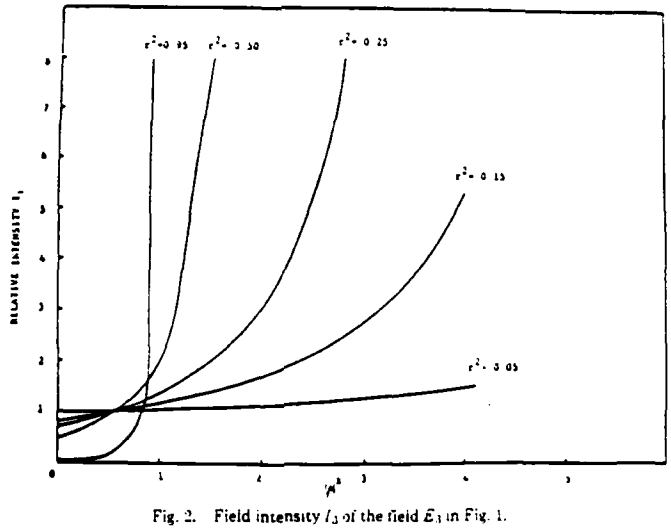

Fig. 2. Field intensity I_3 of the field E_3 in Fig. 1.

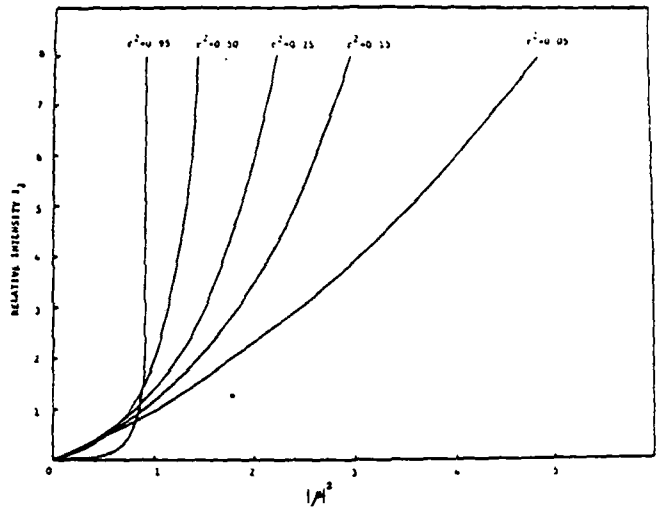

Fig. 3. Field intensity I_2 of the field E_3 in Fig. 1.

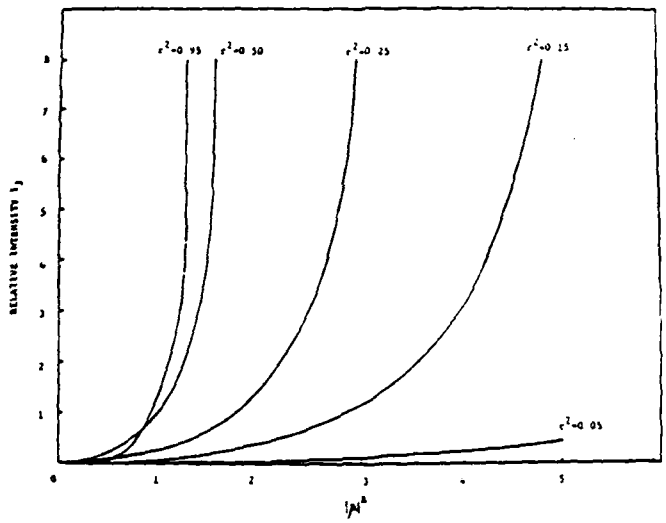

Fig. 4. Field intensity I_1 of the field E_1 in Fig. 1.

pump fields at the PCM. For large reflectivity, $r = 0.95$; these field intensities become very large as $|\mu|^2$ approaches unity; in fact, they may be 20 times larger than the intensity of the incident wave. For values of $|\mu|^2$ such that $|\mu|^2 r^2 \geq 1$, then theory does not provide a stable solution [the constraint described in expression (9) is then not satisfied].

The fields E_R and E_C were calculated in Refs. 12 and 13 by adding the series

$$A_R = r + |\mu|^2 r t^2 (1 + |\mu|^2 r^2 + \ldots) = \frac{r(1 - |\mu|^2)}{1 - |\mu|^2 r^2} \quad (14)$$

and

$$A_C = \mu t^2 (1 + |\mu|^2 r^2 + \ldots) = \frac{\mu(1 - r^2)}{1 - |\mu|^2 r^2}, \quad (15)$$

subject to the constraint in expression (9). The corresponding intensities then are

$$I_R = \frac{r^2(1-|\mu|^2)^2}{(1-|\mu|^2r^2)^2} \tag{16}$$

and

$$I_C = \frac{|\mu|^2(1-r^2)^2}{(1-|\mu|^2r^2)^2}. \tag{17}$$

The intensities I_R and I_C are plotted as functions of $|\mu|^2$ in Figs. 6 and 7. These plots generalize those of Ref. 16 for r^2 other than 0.95 or 0.50. The intensity I_R is exactly zero at $|\mu|^2 = 1$ for every value of r^2, in agreement with a general theorem (Ref. 8); it increases quite rapidly for values of r^2 and $|\mu|^2$ greater than 1, provided that condition (9) is maintained. For low reflectivities, high pumping energy, giving large values of $|\mu|^2$, can yield large I_R. For $|\mu|^2 = 1$, I_C is equal to 1 independently of r^2 and also takes large values near the resonance region $r^2|\mu|^2 = 1$. Of course, the theory does not provide stable values of I_R and I_C when $r^2|\mu|^2 > 1$.

We also note that since all waves reach any point outside the interferometer with the same phase, *there is no dependence of E_R and E_C on the separation between the plates.*

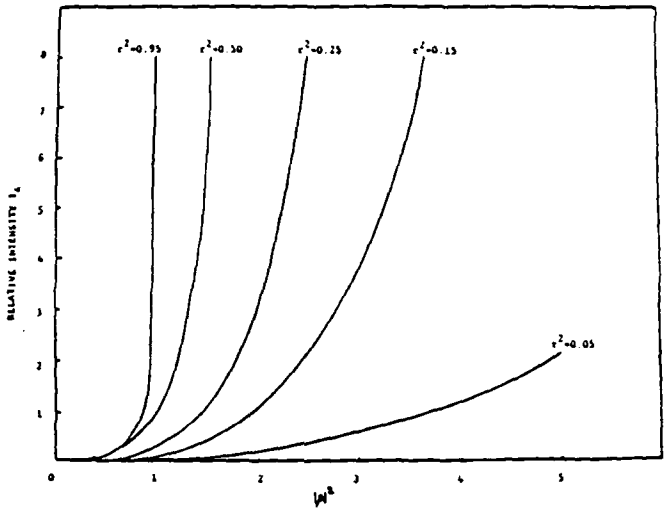

Fig. 5. Field intensity I_4 of the field E_4 in Fig. 1.

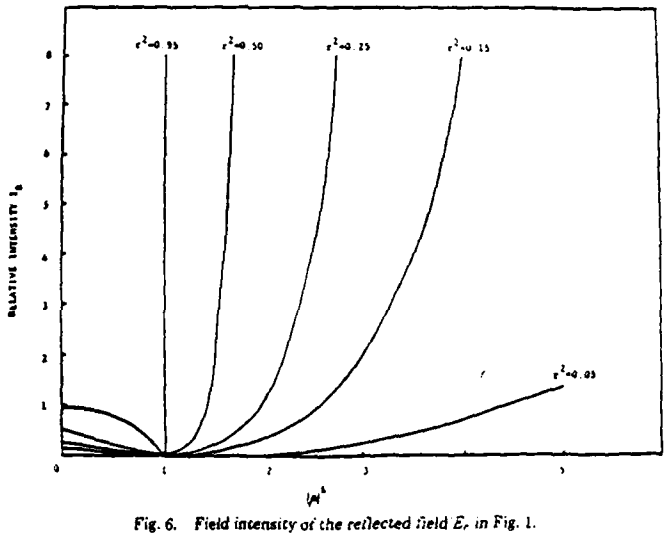

Fig. 6. Field intensity of the reflected field E_r in Fig. 1.

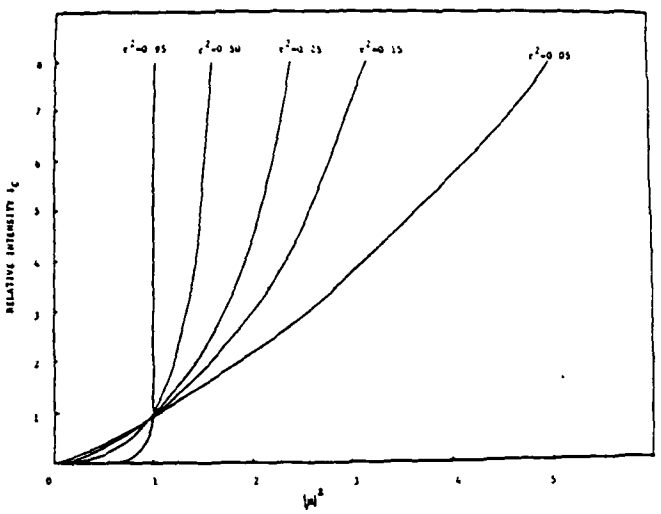

Fig. 7. Intensity of the phase-conjugate field E_c in Fig. 1.

3. TOTAL FIELD INTENSITY INSIDE THE INTERFEROMETER

Consider now under the same conditions as before, a point P of coordinates (x, z) between the two plates P and the PCM as shown in Fig. 8. The waves meeting at P are E_3, E_2, E_1, and E_4, whose respective amplitudes A_3, A_2, A_1, and A_4 are given by Eqs. (5)–(8). These waves have the following complex amplitudes:

$$E_3 = A_3 \exp[ik(x \sin\theta - z\cos\theta)], \tag{18}$$

$$E_2 = A_2 \exp[ik(-x \sin\theta + z\cos\theta)], \tag{19}$$

$$E_1 = A_1 \exp[ik(-x \sin\theta - z\cos\theta)], \tag{20}$$

$$E_4 = A_4 \exp[ik(x \sin\theta + z\cos\theta)]. \tag{21}$$

The total intensity at P is therefore

$$I = |E_3 + E_2 + E_1 + E_4|^2, \tag{22}$$

which, on taking Eqs. (18)–(21) into account, yields

$$\begin{aligned} I = {} & |A_3 + A_4 \exp(2ikz\cos\theta)|^2 \\ & + |A_2 + A_1 \exp(-2ikz\cos\theta)|^2 \\ & + 2\,\mathrm{Re}[A_3 + A_4 \exp(2ikz\cos\theta)] \\ & \times [A_2^* + A_1^* \exp(2ikz\cos\theta)]\exp(2ik(x\sin\theta - z\cos\theta)], \end{aligned} \tag{23}$$

where Re indicates that the real part is taken.

By substituting from Eqs. (5)–(8) into Eq. (23) and writing μ as

$$\mu = |\mu| e^{i\phi}, \tag{24}$$

one finds after a lengthy but straightforward calculation that

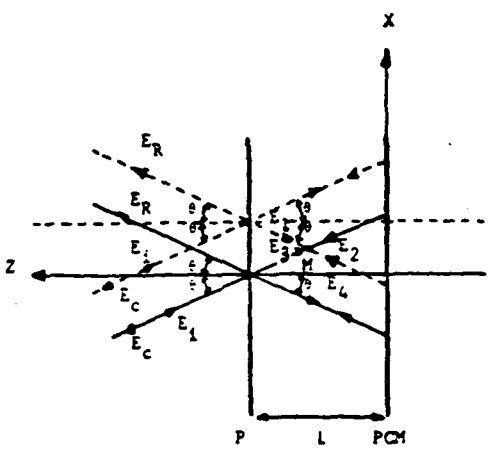

Fig. 8. Total field at a point P inside the interferometer.

$$\begin{aligned} I = {} & \frac{1-r^2}{(1-r^2|\mu|^2)^2}(1+r^2|\mu|^4 \\ & + |\mu|^2(1+r^2) + 4r|\mu|^2\cos(2kz\cos\theta) \\ & + 2|\mu|[\cos[2k(x\sin\theta - z\cos\theta) - \phi] \\ & + r(1+|\mu|^2)\cos(2kx\sin\theta - \phi) \\ & + |\mu|^2 r^2\cos[2k(x\sin\theta + z\cos\theta) - \phi]]), \end{aligned} \tag{25}$$

which represents a rather complicated system of fringes.

The case $|\mu|^2 = 1$ is interesting and provides some insight. Expression (25) then reduces to

$$I = \frac{4}{1-r^2}|\cos[k(x\sin\theta - z\cos\theta) - \phi] + r^2\cos[k(x\sin\theta + z\cos\theta) - \phi]|^2. \quad (26)$$

It is interesting to compare Eq. (26) with the corresponding expression I_{or} for the intensity resulting from an ordinary Fabry–Perot interferometer given by Kastler in Sec. II of Ref. 1 for large r^2:

$$I_{or} = \frac{4r}{1-r^2}\cos^2(kz\cos\theta). \quad (27)$$

When r^2 is large (near unity), Eq. (26) may be approximated by the expression

$$I = \frac{16}{1-r^2}\cos^2(kx\sin\theta - \phi)\cos^2(kz\cos\theta). \quad (28)$$

This expression represents a system of fringes along OZ of width $\Delta z = \lambda/2\cos\theta$, just as in the ordinary case described by Eq. (27); however, these fringes are modulated by another system along the OX direction of width $\Delta x = \lambda/2\sin\theta$.

Existence of fringes along the x direction may appear somewhat surprising at first. Their separation is well defined by Eq. (28); however, their origin is determined by the *absolute phase* of the incident wave. When $r^2 = 0.95$, the maximum intensity of the fringes given by Eq. (28) is

$$I = \frac{16}{1-r^2} = 320, \quad (29)$$

which is more than four times larger than the maximum value of the intensity in the ordinary Fabry–Perot interferometer given by Eq. (27) under the same conditions:

$$I_{or} = 78. \quad (30)$$

Also, the overall amplification factor of the interferometer, which is given by the mean intensity, is in this case

$$\langle I\rangle = 320\langle\cos^2(kx\sin\theta - \phi)\cos^2(kz\cos\theta)\rangle = 80. \quad (31)$$

On the other hand, in the ordinary interferometer, one has (see Sec. II of Ref. 1).

$$\langle I_{or}\rangle = 78\langle\cos^2(kz\cos\theta)\rangle = 39. \quad (32)$$

4. EMISSION FROM ATOMS RADIATING INCOHERENTLY INSIDE THE INTERFEROMETER

Suppose that there are atoms inside the interferometer emitting light (for instance, by irradiating them laterally to excite their optical resonance, as suggested in Ref. 1). The waves emitted by these atoms will be assumed to be mutually incoherent.

We shall consider the radiation emitted by an atom located at a point M toward the outside through the plate P, at angle θ. Let E_A denote this field (see Fig. 9). E_A has an amplitude that is given by the sum of four sequences of rays:

Sequence 1: $t(1 + |\mu|^2r^2 + |\mu|^4r^4 + \ldots)$

$$= \frac{t}{1-|\mu|^2r^2}, \quad (33)$$

Sequence 4: $\mu t'(1 + |\mu|^2r^2 + |\mu|^4r^4 + \ldots)$

$$= \frac{\mu t'}{1-|\mu|^2r^2}, \quad (34)$$

Sequence 3: $\mu rt(1 + |\mu|^2r^2 + |\mu|^4r^4 + \ldots)$

$$= \frac{\mu rt}{1-|\mu|^2r^2}, \quad (35)$$

Sequence 2: $|\mu|^2rt'(1 + |\mu|^2r^2 + |\mu|^4r^4 + \ldots)$

$$= \frac{|\mu|^2rt'}{1-|\mu|^2r^2}. \quad (36)$$

The series has been summed under the assumption expressed by relation (9). Since on reflection at the PCM the fields emerge with the phase reversed with respect to the incident one, all four of the sequences of waves emerge in the direction A with the same phase factor $\exp[ik(x\sin\theta + z\cos\theta)]$; thus, unlike in the ordinary interferometer, they will not produce interference fringes. The field E_A is therefore given by

$$E_A = \frac{(1-r^2)^{1/2}}{1-|\mu|^2r^2}(1 + \mu + \mu r + |\mu|^2r) \times \exp[ik(x\sin\theta + z\cos\theta)], \quad (37)$$

and its intensity is given by

$$I_A = \frac{1-r^2}{(1-|\mu|^2r^2)}[1 + (1+r)^2|\mu|^2 + r^2|\mu|^4 + 2r|\mu|^2 + 2(1+r)(1+r|\mu|^2)|\mu|\cos\phi], \quad (38)$$

where Eq. (24) has been used; the total intensity emitted by N atoms radiating incoherently inside the cavity will be just NI_A.

When $|\mu|^2 = 1$, $\phi = 0$, and $r^2 = 0.95$, I_A is equal to 312, which indicates a considerable amplification of the intensity compared with the intensity emitted by the atom at M in the direction A in the absence of the mirrors, when it would have the value unity. In fact, I_A is considerably greater than the intensity generated by atoms radiating incoherently inside an ordinary Fabry–Perot interferometer under the same conditions; it would then have the value of 32 (cf. Ref. 1, Sec. III).

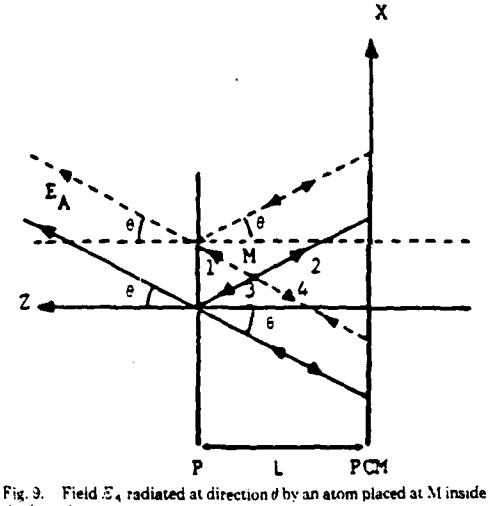

Fig. 9. Field E_A radiated at direction θ by an atom placed at M inside the interferometer.

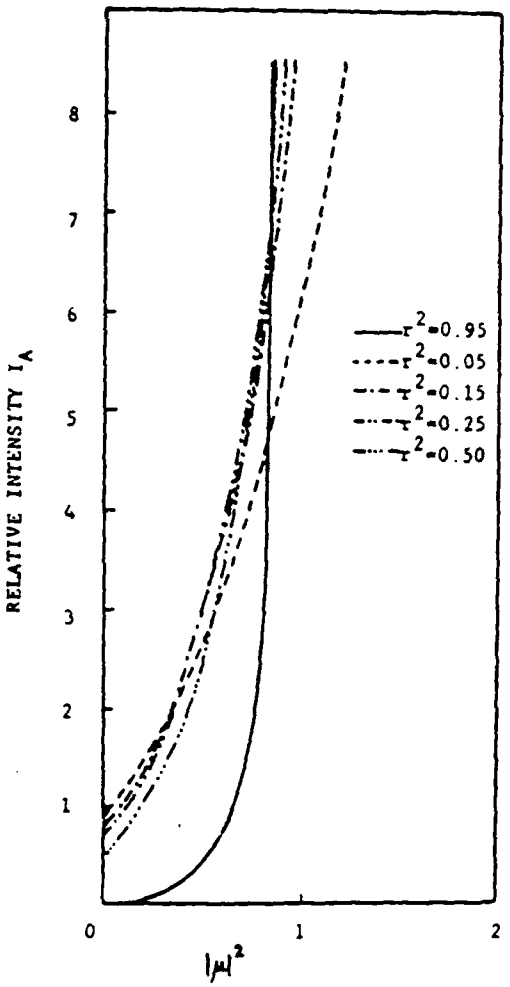

Fig. 10. Intensities I_A of E_A for $\phi = 0$ and different values of the reflectivity r^2 of P.

I_A is plotted versus $|\mu|^2$ (see Fig. 10) for $\phi = 0$ and for different values of r^2. For high r^2, e.g., $r^2 = 0.95$, the intensity is low for low values of $|\mu|^2$; but it increases rapidly once values of $|\mu|^2$ around 0.9 are reached. A dramatic change in the value of I_A occurs when we pass from low values of $|\mu|^2$ to high values: Whereas in the first case higher reflectivity r^2 at P implies a lower value of I_A, in the second case higher values of r^2 may produce very large values of I_A.

5. EXISTENCE OF GAINS INSIDE THE INTERFEROMETER

We will now consider the situation depicted in Fig. 11, in which a wave U_0 is incident normally upon the cavity of length L. Let U be the output wave emerging from this cavity when it is filled with a gain medium. If U_p is the wave reflected at P inside the cavity and sent back toward the PCM, the wave at P, after a round trip involving reflection at the PCM, will be $|\mu| e^{i\phi} e^{\gamma L} U_p$, in contrast with an ordinary cavity where a phase factor $2kL$ is accumulated during each round trip [cf. Eq. (24)].

The gain coefficient γ of the medium inside the cavity is given by the imaginary part of the complex-propagation constant (assuming no absorption losses), i.e., by the imaginary part of

$$\tilde{k} = k - i\frac{\gamma}{2}. \tag{39}$$

Hence the single-pass gain[18] of the wave across the cavity is

$$G_0 = e^{\gamma L}. \tag{40}$$

The amplitude of the output wave U may be again calculated in a way similar to that described in the preceding sec-

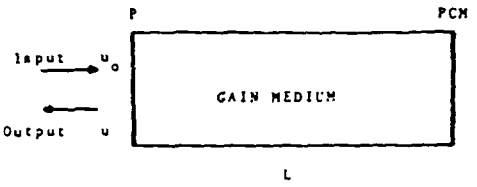

Fig. 11. Diagram of the regenerative amplifier.

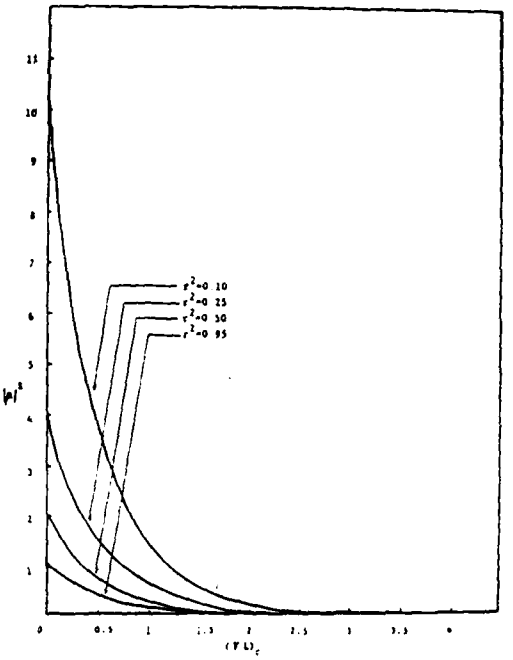

Fig. 12. Values of $|\mu|^2$ versus the critical $(\gamma L)_0$ for several reflectivities r^2.

tions. Making use of the geometrical-series method, we obtain, with the amplitude of U_0 normalized to unity,

$$\left.\begin{aligned} A &= r + \mu t^2 e^{\gamma L} - t^2 r |\mu|^2 e^{2\gamma L} + t^2 |\mu|^2 \mu r^2 e^{3\gamma L} \\ &\quad - t^2 r^3 |\mu|^4 e^{4\gamma L} + t^2 |\mu|^4 \mu r^4 e^{5\gamma L} + \dots \\ &= r - t^2 r |\mu|^2 e^{2\gamma L}(1 + |\mu|^2 r^2 e^{2\gamma L} + \dots) \\ &\quad + t^2 \mu e^{\gamma L}(1 + |\mu|^2 r^2 e^{2\gamma L} + \dots) \\ &= \frac{r(1 - |\mu|^2 e^{2\gamma L}) + \mu(1 - r^2) e^{\gamma L}}{1 - r^2 |\mu|^2 e^{2\gamma L}}. \end{aligned}\right\} \quad (41)$$

The condition for convergence of the series, which also corresponds to the stable solution of the feedback system, is

$$r^2 |\mu|^2 e^{2\gamma L} < 1. \quad (42)$$

Figure 12 shows plots of $|\mu|^2$ versus the critical values $(\gamma L)_c$ at which

$$r^2 |\mu|^2 e^{2(\gamma L)_c} = 1 \quad (43)$$

for several reflectivities r^2.

The intensity $I = |U|^2$ gives the overall gain of the system

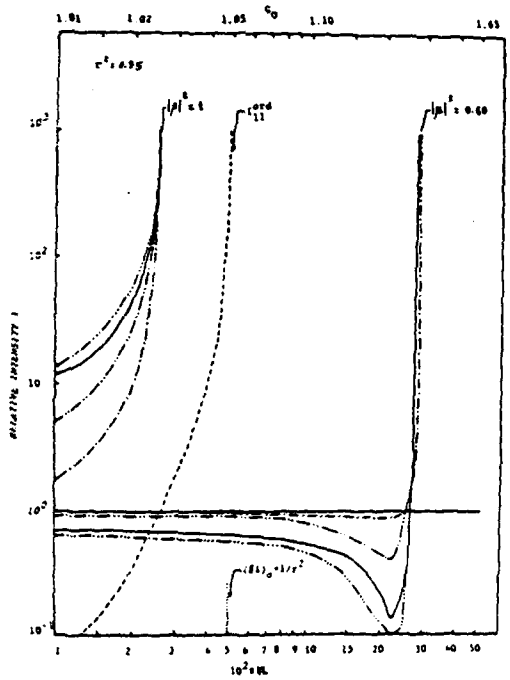

Fig. 13. Overall gains versus γL and G_0 for $r^2 = 0.95$. Dashed line (- - - -): I_{11}^{ord}. Horizontal solid line (——): I for $\phi = 0$ and any $|\mu|^2$, $|\mu|^2 = 0.20$ and any ϕ, and $|\mu| > 1.05$ (e.g., $|\mu|^2 = 1.2$ and higher). Dashed–dotted lines: (——) I for $\phi = \pi/4$, (——) I for $\phi = \pi/2$, (——) I for $\phi = \pi$ ($= I_{12}^{ord}$), and nonhorizontal solid line, I for $\phi = 3\pi/4$.

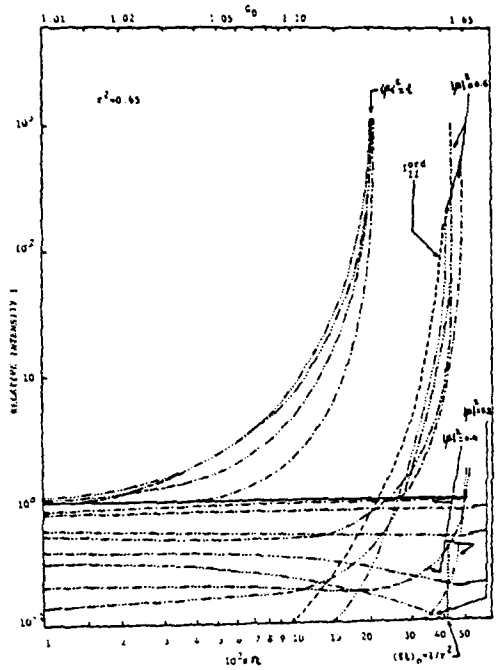

Fig. 14. Overall gains versus γL and G_0 for $r^2 = 0.65$. Dashed line, I_{11}^{ord}. Horizontal solid line, I for $\phi = 0$ and any $|\mu|^2$. Dashed–dotted lines: (——) $\phi = \pi/4$, (——) $\phi = \pi/2$, (——) $\phi = 3\pi/4$, and (——) $\phi = \pi$ ($= I_{12}^{ord}$).

$$I = \left\{\frac{r(1 - |\mu|^2 e^{2\gamma L}) + |\mu|(1 - r^2) e^{\gamma L} \cos\phi}{1 - r^2 |\mu|^2 e^{2\gamma L}}\right\}^2 + \left\{\frac{|\mu|(1 - r^2) e^{\gamma L} \sin\phi}{1 - r^2 |\mu|^2 e^{2\gamma L}}\right\}^2. \quad (44)$$

This expression should be compared with the overall gain corresponding to a cavity with two ordinary mirrors of reflectivities r_1 and r_2, respectively, in the resonant situation, i.e., when $2kL = 2n\pi$ (n is an integer):

$$I_{12}^{ord} = \left\{\frac{r_1(1 - r_2^2 e^{2\gamma L}) - r_2(1 - r_1^2) e^{\gamma L}}{1 - r_1^2 r_2^2 e^{2\gamma L}}\right\}^2. \quad (45)$$

In the special case when $r_1 = r_2 = r$, Eq. (45) becomes

$$I_{11}^{ord} = \left\{\frac{r(1 - e^{\gamma L})}{1 - r^2 e^{\gamma L}}\right\}^2. \quad (46)$$

The results following immediately from Eq. (44) are

(1) When $\phi = m\pi$ (m is an odd integer), I becomes identical to I_{12}^{ord} and has a zero at

$$G_0 = e^{\gamma L} = \frac{r}{|\mu|}, \quad (47)$$

which occurs for positive γL (i.e., G_0 is greater than unity) when $r > |\mu|$; this is in agreement with the law of conservation of energy of the electromagnetic wave. It should be noted that

if the amplitude U_0 of the incident wave is considered to have a phase factor ϕ_0 (i.e., U_0 is not unity), then the first term of Eq. (41) should appear to be multiplied by U_0, whereas the second term of that equation would appear to be multiplied by U_0^*. Assuming that $U_0 = \exp(i\phi_0)$, the phase in Eq. (44) will now be $\phi - 2\phi_0$ instead of ϕ. In this case, the condition $\phi - 2\phi_0 = m\pi$ with which I has a zero when Eq. (47) is satisfied [observe that when $\gamma = 0$, Eq. (47) implies that $r = |\mu|$] *can allow the determination of the phase* ϕ_0 of the incident amplitude U_0 if G_0, r and $|\mu|$ are given to satisfy Eq. (47) (this can be adjusted in an experiment by varying L and $|\mu|$), and one determines the value of γL at which I becomes zero. ϕ_0 is then given by $\phi_0 = 1/2(\phi - m\pi)$.

(2) The overall gain is enhanced below threshold by working near its resonance point $(\gamma L)_c$ while satisfying condition (42). Since $(\gamma L)_c$ is positive, for a cavity with gains according to Eq. (43), one must have $|\mu|^2 < 1/r^2$. This leads to the result that no overall amplification is obtained by increasing the PCM reflectivity $|\mu|^2$ beyond the value $1/r^2$.

(3) For $\phi = 2n\pi$ (n is an integer), I does not have any resonant value. At $(\gamma L)_c$, it has instead the finite value $(1 + r^2)/2r$. The interferometer with gains therefore will not work as a regenerative amplifier when there is perfect phase conjugation at the PCM, i.e., when $\phi = 0$ [if $U_0 = \exp(i\phi_0)$, this will happen when $\phi = 2\phi_0$].

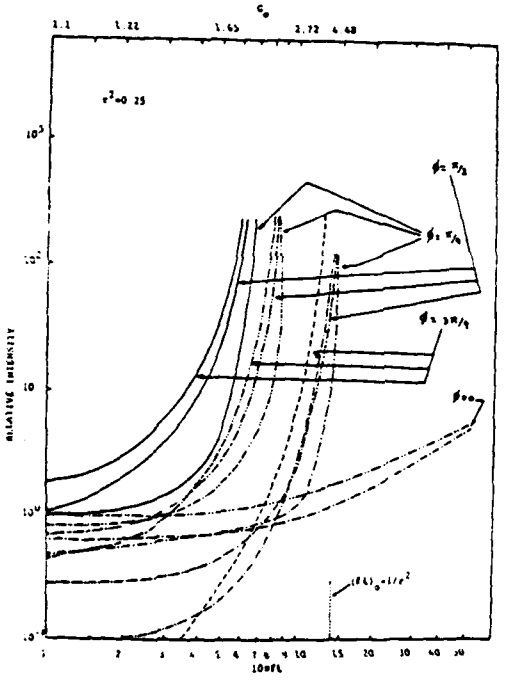

Fig. 15. Overall gains versus γL and G_0 for $r^2 = 0.25$. Dashed line: $I_{(1)}^{3rd}$. Dashed-dotted lines: (——) $|\mu|^2 = 0.20$, (——) $|\mu|^2 = 0.60$, and (——) $|\mu|^2 = 1$. For $\phi = 0$, the curve corresponding to $|\mu|^2 = 1$ is not distinguished from that of $|\mu|^2 = 0.60$.

Figures 13–15 illustrate these points: The continuous horizontal line in Figs. 13 and 14 represents the overall gain I for $r^2 = 0.95$ and $r^2 = 0.65$, respectively, and for $\phi = 0$, independently of $|\mu|^2$. For low values of $|\mu|^2$ ($|\mu|^2 \cong 0.20$), I is also close to unity for $r^2 = 0.95$, independently of ϕ. For $|\mu|^2 = 0.20$ and $r^2 = 0.65$ and 0.25, the low values of I are seen in Figs. 14 and 15. When $|\mu|^2 > 1/r^2$, independently of ϕ, the values of I in any of Figs. 13–15 are similar to those with $\phi = 0$. Hence there is no amplification when the reflectivity of the PCM exceeds the value $1/r^2$.

For $r^2 = 0.95$ and intermediate values of $|\mu|^2$, constant values of I are obtained. These are followed by minima (which are zero at $\phi = \pi$) and by abrupt increases. For these values of $|\mu|^2$ and for $r^2 = 0.65$ and 0.25, these minima either are less pronounced or do not appear at all.

Finally, when $1/r^2 > |\mu|^2 \geq r^2$ (e.g., $|\mu| = 1$ for $r^2 = 0.95$ or $r^2 = 0.65$ and $r^2 = 0.25$), regenerative amplification takes place.

6. CONCLUSIONS

We have investigated theoretically the fields generated by an interferometer of the Fabry–Perot type but with one of the plates replaced by a PCM.

We made a comparison of this system with the ordinary interferometer that was studied fully by Kastler, and we concluded that the system with a PCM can generate more intense fields than the ordinary cavity with the ordinary mirrors having the same reflectivities.

When the interferometer is filled with a gain medium, we obtained stringent conditions that allow the cavity to work as a regenerative amplifier: No perfect conjugation at the PCM must take place [i.e., ϕ should be different from zero, or, if $U_0 = \exp(i\phi_0)$, ϕ should be different from $2\phi_0$], and the reflectivity $|\mu|^2$ must be in the range $r^2 = |\mu|^2 < 1/r^2$.

For large values of r^2, $|\mu|^2 = 1$ is a very good value. As ϕ increases from 0 to π, the amplification increases until the ordinary-cavity situation is reached at $\phi = \pi$.

A Fabry–Perot interferometer with a PCM permits the determination of the phase of the incident wave. When $U = \exp(i\phi_0)$, $\gamma = 0$, and $\mu = r$ ($\phi = 0$), then Eq. (44) yields ($\phi \to \phi - 2\phi_0$).

$$I = \frac{2r^2}{(1 + r^2)^2}[1 \cos(2\phi_0)]; \tag{48}$$

hence the output intensity depends in a simple way on the phase ϕ_0 of the incoming wave. The measurement of I thus may provide information of ϕ_0.

It is clear that a Fabry–Perot cavity with a PCM has some remarkable properties that also deserve to be investigated experimentally.

ACKNOWLEDGMENTS

I am indebted to E. Wolf for introducing me to the subject of phase conjugation and for many suggestions and discussions that originated and shaped this research. I wish also to thank R. W. Boyd and M. Raymer for helpful comments. This research was partially supported by the U.S. Air Force Office of Scientific Research and by the National Science Foundation. Kind hospitality from J. C. Dainty made this work possible.

* On leave from Instituto de Optica, CSIC, Serrano 121, 28006, Madrid, Spain.

REFERENCES

1. A. Kastler, "Atomes a l'intérieur d'un interferomètre Perot–Fabry," Appl. Opt. 1, 17–24 (1962).
2. A. Yariv, "Phase-conjugate optics and real-time holography," IEEE J. Quantum Electron. QE-14, 650–660 (1978).
3. D. M. Pepper, "Non-linear optical phase conjugation," Opt. Eng. 21, 156–183 (1982).
4. R. A. Fisher, ed., *Optical Phase Conjugation* (Academic, New York, 1983).
5. A. Yariv and D. M. Pepper, "Amplified reflection, phase conjugation, and oscillation in degenerate four-wave mixing," Opt. Lett. 1, 16–18 (1977).
6. D. M. Bloom, P. F. Liao, and N. P. Economov, "Observation of amplified reflection by degenerate four-wave mixing in atomic sodium vapor," Opt. Lett. 2, 58–60 (1978).
7. J. Feinberg and R. W. Hellwarth, "Phase conjugate mirror with continuous-wave gain," Opt. Lett. 5, 519–521 (1980).
8. G. S. Agarwal, A. T. Friberg, and E. Wolf, "Scattering theory of distortion correction by phase conjugation," J. Opt. Soc. Am. 73, 529–538 (1983).
9. J. Au Yeung, D. Fekete, D. M. Pepper, and A. Yariv, "A theoretical and experimental investigation of the modes of optical resonators with phase-conjugate mirrors," IEEE J. Quantum Electron. QE-15, 1180 (1979).
10. I. M. Bel'dyugin, M. G. Galushkin, and E. M. Zemskov, "Properties of resonators with wavefront-reversing mirrors," Sov. J. Quantum Electron. 9, 20 (1979).
11. P. A. Belanger, A. Hardy, and A. E. Siegman, "Resonant modes of optical cavities with phase-conjugate mirrors," Appl. Opt. 19, 602 (1980); 19, 479 (1980).
12. J. F. Lam and W. P. Brown, "Optical resonators with phase-conjugate mirrors," Opt. Lett. 5, 61–63 (1980).
13. A. E. Siegman, P. A. Belanger, and A. Hardy, "Optical resonators using phase conjugate mirrors," in *Optical Phase Conjugation*, R. A. Fisher, ed. (Academic, New York, 1983), Chap. 13.
14. A. T. Friberg and P. D. Drummond, "Reflection of a linearly polarized plane wave from a lossless stratified mirror in the presence of a phase-conjugate mirror," J. Opt. Soc. Am. 73 1216–1219 (1983).
15. M. Nazarathy, "A Fabry–Perot étalon with one phase-conjugate mirror," Opt. Commun. 45, 117–121 (1983).
16. P. D. Drummond and A. T. Friberg, "Specular reflection concellation in an interferometer with a phase-conjugate mirror," J. Appl. Phys. 54, 56183–5625 (1983).
17. H. Boersch and G. Herziger, "Theoretical and experimental investigation of regenerative laser amplifiers and their applications," IEEE J. Quantum Electron. QE-2, 549–552 (1966).
18. A. E. Siegman, *An Introduction to Masers and Lasers* (McGraw-Hill, New York, 1971), Sec. 5.5.
19. E. Wolf, "Phase conjugacy and symmetries in spatially band limited wave fields containing no evanescent components," J. Opt. Soc. Am. 70, 1311–1319 (1980).

THE ASTROPHYSICAL JOURNAL, 293:530–536, 1985 June 15

SPATIALLY RESOLVED INFRARED OBSERVATIONS OF THE RED RECTANGLE

J. C. DAINTY,[1,2] J. L. PIPHER,[1] AND M. G. LACASSE[1,3]
Department of Physics and Astronomy, University of Rochester

AND

S. T. RIDGWAY
Kitt Peak National Observatory
Received 1984 October 1, accepted 1984 December 19

ABSTRACT

Infrared one-dimensional (E-W and N-S) speckle interferometric observations centered on HD 44179 (the "Red Rectangle") reveal spatially resolved extended emission at *K*, *L*, and *M*, of i.e diameter 1".05 N-S and 0".4 E-W, as well as a central source of 1 *e* diameter 0".2. Polarimetry at *K* with a beam size encompassing both sources was also obtained; the low resultant polarization suggests that scattering off grains associated with the bipolar flow is not a plausible source of the infrared emission. The spatially resolved extended emission is elongated in the direction of the bipolar flow and is interpreted as thermal dust emission.

Subject headings: infrared: sources — interferometry — nebulae: individual — polarization

I. INTRODUCTION

Since the discovery (Cohen *et al.* 1975) of the bipolar nebula associated with HD 44179 (the "Red Rectangle") and the infrared source AFGL 915, an increasing number of bipolar nebulae with bright central infrared point sources have been identified. It is now clear that all these objects do not represent the same phenomenon. A large number of bipolar nebulae are apparently associated with evolved mass-losing stars and may even be "protoplanetary nebulae" as proposed by Zuckerman *et al.* (1976) and supported by Calvet and Cohen (1978). However, young objects are also associated with bipolar phenomena on various scales, e.g., L1551 IRS 5 (Beichman and Harris 1981) and S106 (Pipher *et al.* 1976). Icke (1981) has demonstrated that bipolar shapes arise from a biconical outflow above a disk geometry: for example, Bally and Scoville (1982) observe a constraining disk for the bipolar flow in S106.

The Red Rectangle is a peculiar object in a number of ways, and is to date unique. Some of its properties are outlined below.

1. The optical nebulosity differs at various wavelengths, but the bipolar nature is best outlined with a red filter, and is predominantly a N-S bicone (Cohen *et al.* 1975): spikes tangent to the edge of the bicone are observed, implying that material in the nebula is distributed in an optically thin shell rather than throughout the biconical volume (Webster 1979).

2. The visible object at the center, HD 44179, contains a well-established binary. The most recent published determination is a separation of 0".20 ± 0".02 at a position angle of 146° ± 3° in 1981.87 by Meaburn *et al.* (1983). The near-equality of the two components makes it difficult to determine the orbital elements, but Meaburn *et al.* propose a plausible progression of the position angle with time.

3. The visible star(s) have been tentatively identified as spectral class ~B9–A0 III by Cohen *et al.* (1975), although a normal B-star atmosphere cannot be fitted to the spectrum, because of the large observed Balmer jump and infrared excess. Greenstein and Oke (1977) provide two alternative models of HD 44179, one a B star with an extended neutral shell, and one an unusual Population II F giant. The UV spectra of HD 44179 show features in emission and absorption unlike those of other early-type stars with circumstellar shells (Sitko, Savage, and Meade 1981; Sitko 1983). At wavelengths ≤ 1600 Å, there is a precipitous decline in flux: the distribution of flux at wavelengths < 1400 Å suggests that the star has a spectral type of ~A0.

4. An optical spectrum of the nebulosity includes a peculiar broad red emission feature which Schmidt, Cohen, and Margon (1980) and Warren-Smith, Scarrott, and Murdin (1981) have resolved into narrow emission lines from a very low excitation plasma, in addition to diffuse features which remain unidentified but may be carbon-rich molecular emission. This feature is shown by Schmidt, Cohen, and Margon (1980) and Perkins *et al.* (1981) to be nebular emission rather than scattered starlight.

5. Infrared spectroscopy of the point source reveals a signature quite different from those of other protoplanetary nebula or pre-main-sequence candidates. High-resolution near-IR observations by Thronson (1982) of the Red Rectangle show a featureless spectrum from 1.5 to 2.3 μm, although there is possible marginal detection of three $\Delta v = 2$ overtone CO bands. This is in contrast to spectra of candidate protoplanetary nebulae GL 2688 and GL 618, which are dominated by molecular hydrogen emission, and HM Sge, which exhibits weak lines in the Brackett series. The infrared photometry to 27 μm of the infrared point source in the Red Rectangle shows a broad infrared excess, not identifiable with a single, cool blackbody temperature (as is the case, for example, with GL 2688; Ney *et al.* 1975). If the infrared radiation is thermal emission, it is optically thin: this is supported by the presence of unidentified emission features at 3.28, 6.2, 7.7, 8.6, and 11.3 μm, normally associated with optically thin thermal dust emission in planetary nebulae, H II regions, and reflection nebulae.

[1] Visiting Astronomers at Kitt Peak National Observatory, operated by the Association of Universities for Research in Astronomy, Inc., under contract with the National Science Foundation.

[2] Now at Blackett Laboratory, Imperial College, London, England SW7 2BZ.

[3] Harvard College Observatory, Cambridge, MA 02138.

6. The low polarization of the blue scattered light within the bipolar nebula can be understood from the polarimetric maps of Perkins *et al.* (1981) and Lacasse (1984). Substantial polarizations ($\sim 20\%$) are observed along the spikes and just outside the bicone, while values of 5%–10% are common in the nebula itself.

7. Geldzahler and Cohen (1983) give a 3 σ upper limit of 0.09 mJy at 1.5 and 4.9 GHz to radio emission from their VLA observations of the Red Rectangle, and similarly only an upper limit to the ^{12}CO $J = 1$–0 line emission was obtained (L. Blitz, as quoted by Schmidt, Cohen, and Margon 1980).

Previous investigators have proposed the following model for bipolar nebulae. The central star is located in an equatorial disk (or torus) which may obscure the star in the visible if the disk is sufficiently dense. If viewed edge-on or at a slight inclination, the star may be visible and the bicones may exhibit differing intensities. The central object is often a strong infrared source. A thin cloud of dust and gas located on either side of the disk is responsible for the bipolar reflection nebulae.

In this paper, we present infrared speckle interferometry on AFGL 915, the central source associated with HD 44179, as well as infrared polarimetry of the point source and the surrounding nebula. These observations serve to refine models of this enigmatic object.

II. OBSERVATIONS

The Red Rectangle was observed in 1981 December and 1982 May using the Kitt Peak Infrared Speckle Interferometer on the 3.8 m Mayall telescope. One-dimensional measurements were made at K (2.2 μm), L (3.5 μm), and M (4.9 μm) with E-W scans and at K and L with N-S scans.

The technique of one-dimensional infrared speckle interferometry is well established (Sibille, Chelli, and Léna 1979), although several observational problems remain, some of which are discussed below. A scanning secondary mirror is used to sweep the image across a selectable narrow slit at a rate of 50″–100″ s^{-1}. The detector was the Kitt Peak "TTT" InSb photometer, cooled to liquid helium temperatures. Each scan consisted of 128 data points whose angular sampling interval was selected to give roughly 25% oversampling compared with the Nyquist rate. Table 1 summarizes the scan parameters at K, L, and M.

In a typical observation sequence, 1000 scans of the object would be made (~ 150 s), followed by a similar number of scans on the sky and a reference object (BS 2305 at K and L, α CMa at M). This was repeated up to 5 times. On-line data reduction enabled the quality of observations to be estimated, although all the data presented here are the result of off-line data reduction. The operation of the Kitt Peak Speckle Interferometer, scanning secondary and on-line data analysis, is controlled by a computer program written by D. Conners.

Data reduction consisted of computing an estimate of the "power spectrum" (i.e., the average squared modulus of the discrete Fourier transform) of object, sky, and reference scans, subtracting the sky power spectrum from those of the object and reference, and finally dividing the corrected object power spectrum by the corrected reference power spectrum to yield an estimate of the power spectrum of the object intensity. This resultant one-dimensional power spectrum is a section through the origin of the two-dimensional power spectrum at an angle dependent on the scan direction. Figure 1 summarizes the data obtained on the Red Rectangle, and gives some idea of the random errors inherent in this observational technique.

Average object power spectra corresponding to the five sets of observations are shown in Figure 2. Denoting the estimate of the power spectrum of the sky-corrected object scans by $\hat{P}_1(f)$ and that of the sky-corrected reference scans by $\hat{P}_2(f)$ then Figure 2 shows averages of the form av $[\hat{P}_1(f)]$, av $[\hat{P}_2(f)]$; the average of the curves shown in Figure 1, i.e., av $[\hat{P}_1(f)\,\hat{P}_2(f)]$, is a biased estimate of the object power spectrum when there is substantial variability in the data.

It is impossible to determine a unique object profile from a knowledge of the object power spectrum. We have fitted a symmetric model of the object,

$$O(r) = F \exp\left[-\left(\frac{r}{W_1}\right)^2\right] + (1 - F) \exp\left[-\left(\frac{r}{W_2}\right)^2\right],$$

consisting of two Gaussian profiles, to the observed object power spectra; the best-fit power spectra are shown in Figure 3*a*. There $W_1 = 0''.52$, $W_2 = 0''.1$, and $F = 0.58$ for N-S scans, while $W_1 = 0''.2$, $W_2 = 0''.1$, and $F = 0.58$ for E-W scans, where the W_i are 1/*e* radii. The object profiles along the N-S and E-W axes are shown in Figure 3*b*: it must be stressed that while these object profiles are consistent with the observed power spectra data, they are only one possible object distribution.

In summary, the speckle measurements reveal the following:

1. The Red Rectangle is clearly resolved N-S and E-W. The

TABLE 1

SCAN PARAMETERS

Parameter	K 1981 Dec	K 1982 May	L	M
Mean wavelength λ (μm)	2.2	2.2	3.45	4.8
Diffraction-limited angular frequency of 3.8 m aperture, f_{diff} (arcsec^{-1})	8.4	8.4	5.3	3.8
Sampling interval Δx (arcsec)	0.076[a]	0.047	0.073	0.105
Sampling interval Δt (s)	0.001	0.001	0.001	0.001
Max observable frequency in power spectrum, $f_{max} = 1/2\Delta x$ (arcsec^{-1})	6.6[a]	10.7	6.8	4.7
Sampling interval in power spectrum, $\Delta f = 1/128\Delta x$ (arcsec^{-1})	0.102[a]	0.167	0.106	0.074
Slit width (arcsec):				
N-S	0.09	0.09	0.13	...
E-W	0.09	0.09	0.13	0.21

[a] The scan parameters were not optimized in the 1981 December observations, owing to a calibration error discovered afterward.

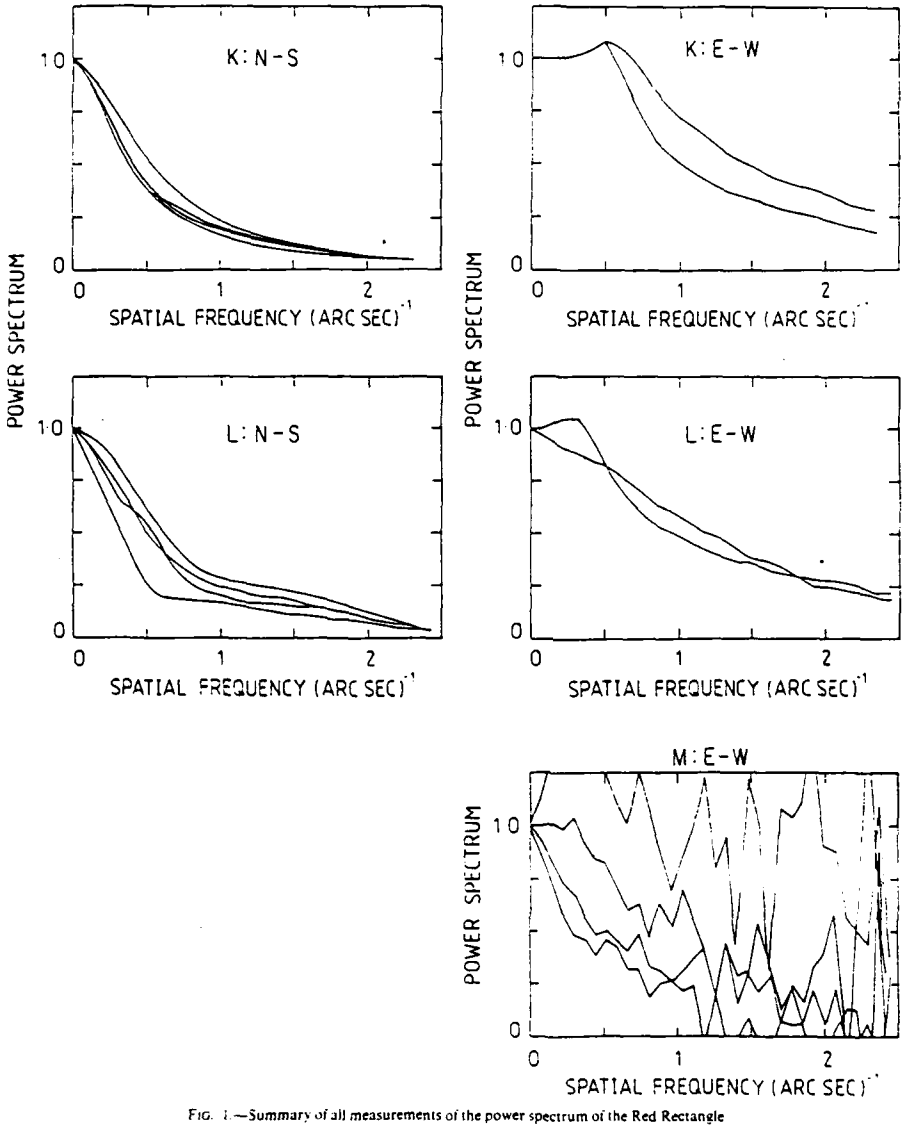

FIG. 1.—Summary of all measurements of the power spectrum of the Red Rectangle

shape of the power spectrum indicates that the object intensity is more concentrated toward the center than a single Gaussian would predict. Fitting a double Gaussian model for the object to the observations indicates the presence of a (possibly) centro-symmetric concentration of intensity of diameter 0"2 and an asymmetric distribution of intensity of diameter 0"4 E-W and 1"05 N-S (i.e., the elongation is along the N-S axis).

2. No systematic variation of the power spectra with wavelength, in the range 2.2–4.8 μm, was detectable, although our probable errors in diameter estimates are ~20%.

Polarimetric observations at K of the Red Rectangle were obtained in 1980 October on the 2.1 m telescope using the Blue Toad Rapid-Pol polarimeter. Observations on HD 44179, as well as 8"0 north, south, east, and west of the star(s) were obtained with a 10" beam and a beam separation of 80" N-S. In addition, multiaperture polarimetric observations at K were

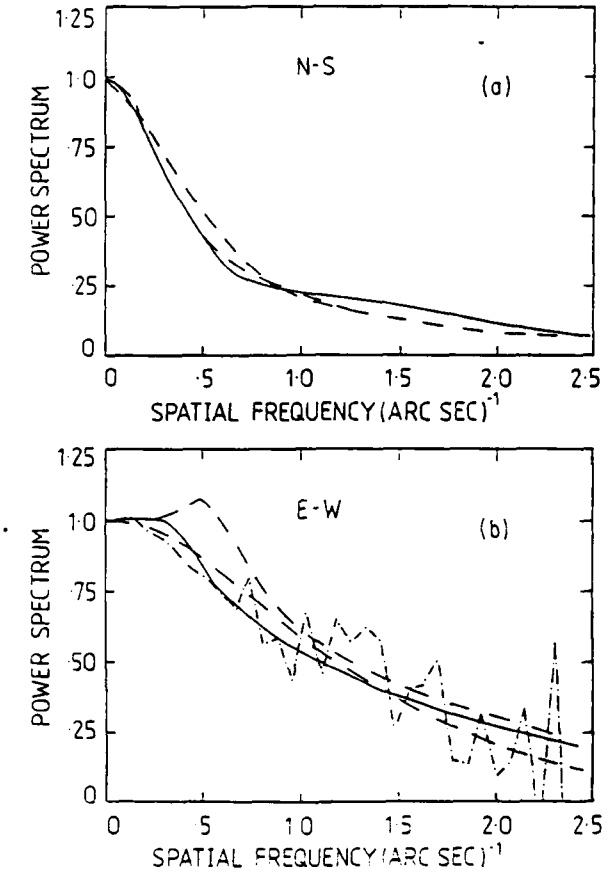

FIG. 2.—Average power spectra for each observation night of the Red Rectangle. *Dashed lines*: *K* wavelength; *solid line*: *L* wavelength; *dot-dash line*: *M* wavelength.

obtained in 1982 September with the same instrument. Instrumental polarization was determined by observing several unpolarized stars, and corrections for the instrumental polarization have been applied to the data. The efficiency of the system and the zero position angle correction were measured by obtaining observations of VI Cygni No. 12 and Walker 67. Photometric data are also extracted from the polarimetry, and the results are presented graphically in Figure 4. The central source is 0.3% polarized at *K*, with a position angle of 45° ± 2°. A previous polarization measurement by Jones and Dyck (1978) at *K* gave a polarization of 0.5% ± 0.2%, and their position angle (measured at *J*) was $\theta = 45° \pm 7°$. While nebulosity 8" from the central source is slightly more polarized, we do not find the Red Rectangle to be similar to typically highly polarized bipolar nebulae (e.g., AFGL 2688, NGC 2261, and S106.

III. DISCUSSION

Previous IR photometry and spectrophotometry, as well as the polarimetry reported here, of the central region around HD 44179 were obtained with observing apertures larger than the largest dimension resolved here (1"05). Russell, Soifer, and Willner (1978, hereafter: RSW), illustrate combined spectra from 2 to 14 μm, attribute the observed radiation to thermal dust emission, and point out that the emission is broader than that from a single-temperature blackbody, as had been previously noted by Cohen *et al.* (1975). For example, at $\lambda \sim 3$ μm, the gray body color temperature is ~900–1000 K, while at $\lambda \sim 10$ μm, it is ~500 K. Since HD 44179 is apparently bipolar nearly in the plane of the sky, they conclude that the dust emission detected from 2 to 14 μm must be optically thin. This conclusion is substantiated by the observed presence of the

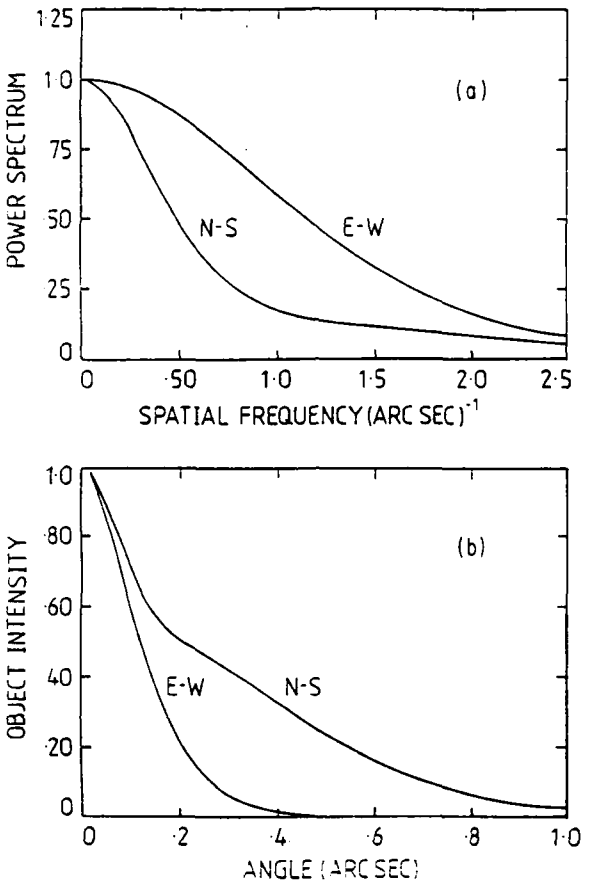

FIG. 3.—Best-fit models to the experimental data of Fig. 2

unidentified emission features generally associated with optically thin dust emission nebulae.

RSW attributed most of the near-IR emission to a reddened central star, and by assuming a brightness temperature no higher than the 500 K color temperature derived for the nebulosity in their beam, deduced from the observed flux density a diameter in excess of 0".1.

Our speckle measurements of the power spectrum can be (nonuniquely) modeled by a two Gaussian components, one with 1 *e* diameter 0".2 and another of total size 0".4 E-W by 1".05 N-S. We find no systematic variations of the power spectra with wavelength. In fact, we cannot easily model the *intensity associated with each component because we have no a priori* knowledge of the geometry. What seems clear, however, is the separation into a central component and an elongated component. We presume that the "central" object (1 *e* diameter = 0".2) is identifiable with an extensive shell around the star(s) HD 44179 and that the extended emission (0".4 E-W by 1".05 N-S) represents an axisymmetric distribution of dust surrounding the central object. Both the lack of detectable free-free radio emission and the color temperature rule out a free-free component. Although RSW considered only thermal emission, there is a distinct possibility that the observed infrared radiation associated with the bipolar flow could be due to dust scattering in the lobes north and south of the torus. For example, many protoplanetary nebulae exhibit large infrared polarizations in the bicone (e.g., NGC 2261, P_K = 16%; Jones and Dyck 1978), as do young objects like S106 (P_K = 20%; Lacasse *et al.* 1981). The nebula OH 0739−14 (Allen *et al.* 1980) has been spatially resolved into a late M star and an IR reflection nebula (Forrest *et al.*, *in preparation*), and exhibits polarization P_K = 29%, (Kobayashi 1978). We now consider the evidence for scattering versus thermal emission in the Red Rectangle.

We have obtained polarimetry at *K* with a 10" beam centered on the central object, as well as positions ~5" from the

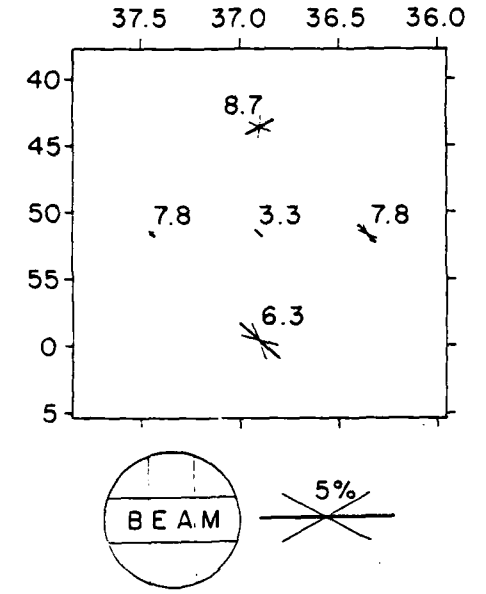

FIG. 4.—Polarimetry of the Red Rectangle at 2.2 μm. The heavy solid lines are in the direction of the polarization vector, and the lengths are proportional to the polarization. The light lines indicate the uncertainty in polarization angle. The number above each vector represents the *K*-magnitude at that beam position.

center, east, west, north, and south. The polarimetry of the central object (which includes the two components spatially resolved here) yields $P = 0.3\%$ and $\theta = 45°$. This result is in agreement with the earlier measurements by Jones and Dyck (1978) at *K* as well as their position angle at *J*. In addition, we obtained multiaperture polarimetry at *K*, centered on HD 44179, with apertures of 6"–20", and the polarization and position angles were identical within the errors. Although the intensity level 8" away from HD 44179 is extremely low, we find the polarization level to be only ~1%–2% north and south of HD 44179. If the IR scattering is similar to the scattering in the blue, conditions favorable for higher polarization occur only along the bicone in the bipolar nebula. Thus, although we cannot discount the possibility of scattering in the bipolar regions 8" from HD 44179, we cannot on the basis of these observations prove it, either. However, since both components spatially resolved by speckle interferometry, namely, the elongated source of size 0"4 E-W by 1"05 N-S observed at *K*, *L*, and *M*, as well as the 0"2 diameter central object, were included in the beam used for the polarimetric observations centered on HD 44179, we show below that dust scattering plays only a minor role in that observed emission. Our *K* band polarimetry can be considered in conjunction with the observation at *J* by Jones and Dyck 1978), and the visual polarimetry obtained by G. V. Coyne, as reported in Cohen *et al.* (1975). Coyne accounted for his observations with a three-component model consisting of a small circumstellar electron-scattering component (approximately neutral) with $P = 0.97\%$ and $\theta = 43°$, an interstellar component, and a small dust-scattering component at $\theta = 8°$ along the long axis of the nebula. If Coyne's model is correct, the near-IR polarization is due predominantly to electron scattering from an asymmetric distribution of circumstellar material. The puzzle about this interpretation is the peculiar angle of this asymmetry as compared with the N-S bipolar nebula and the inferred E-W torus. Another interpretation is based on the polarimetry of Perkins *et al.* (1981), which shows relatively higher polarizations along the bicone, where enhanced densities in the dust distribution are inferred. Since one axis of the bicone is approximately perpendicular to $\theta = 43°$, an enhancement in dust density along that axis close to the source might result in polarization perpendicular to that axis as the dominant polarization. In any event the small magnitude of the polarization at *K* precludes substantial right-angle scattering in a particular direction. For example, if the emission from the observed 0"4 E-W by 1"05 N-S component were due to right-angle scattering off dust in small lobes 0"52 north and south of the torus, the polarization at *K* would be substantial and at a position angle of approximately 90° (see, e.g., Elsässer and Staude 1978). Thus we suggest that both the emission associated with the symmetric shell around HD 44179, and that associated with the bipolar extended material are due to thermal dust emission. That conclusion is strengthened by the color temperatures observed by RSW.

A dust grain situated 0"5 from the central star(s) will attain a cooler temperature than a grain in the circumstellar shell at 0"1 from the star. The grain temperature will vary with distance d as $d^{-0.4}$ if the IR grain emissivity is proportional to λ^{-1}, and as $d^{-0.33}$ if the grain emissivity is proportional to λ^{-2}. Thus the grain temperature at $d = 0"5$ will be 0.53 (0.59) times the grain temperature at $d = 0"1$, corresponding to λ^{-1} (λ^{-2}) emissivity. The range of color temperatures observed, namely, 500–1000 K by RSW, fits this hypothesis well as long as the thermal dust emission associated with the bipolar flow region is optically thin.

Are dust temperatures of this magnitude realistic? Following Cohen *et al.* (1975), we assume that the binary star components are identical, of type A0 III, with bolometric luminosities of $\sim 360\ L_\odot$ each. The observed bolometric flux (integrating the IR spectrum and extrapolating to unmeasured longer IR wavelengths as in Cohen *et al.*) is $\sim 3 \times 10^{-7}$ ergs cm^{-2} s^{-1}, so that the distance corresponding to the bolometric luminosity is $D \sim 280$ pc. The IR optical emission ratio is ~12, which suggests $A_V \sim 2.7$ mag, and this is probably due to the small dust torus normally associated with bipolar nebulae. At a distance of 280 pc, the observed spatial scales of 0"1 and 0"5 from the star(s) correspond to 4×10^{14} and 2×10^{15} cm, respectively. If the grain emissivity ratio $\epsilon_{IR}\,\epsilon_{opt}$ is 0.1 (0.01), grain temperatures of 1580 K (890 K) are expected at a distance 0"1 from the star(s) and 700 K (400 K) at a distance 0"5 from the star(s). Hence dust temperatures within the 500–1000 K range are entirely reasonable.

IV. CONCLUSION

Speckle interferometric observations centered on HD 44179 at *K*, *L*, and *M* reveal spatially resolved information on this source. The data are compatible with a model consisting of a central source of 1 *e* diameter 0"2 and extended emission 1"05 N-S by 0"4 E-W. Polarimetry at *K* including both sources in the beam is inconsistent with scattering as the main source of the observed emission in the infrared. We show that thermal

emission by dust is a plausible source of the observed emission. Polarimetric IR speckle observations would allow quantitative estimates of the role played by scattering in the extended emission region. If the extended emission is associated with the bipolar lobes, as seems reasonable, then scattering is expected to contribute partially to the emission. With the present data it is impossible to build a quantitative model of the source, because of the unknown geometry and the lack of a complete set of spatially resolved spectroscopic observations. An elliptical geometry (e.g., Lefèvre, Daniel, and Bergeat 1983) might eventually prove useful. Subsequent IR speckle observations of resolved structure close to the central star of a bipolar nebula at other angles and wavelengths are planned.

J. C. Dainty acknowledges the support of the National Science Foundation (AST 7926461) and the Air Force Office of Scientific Research (AFOSR-81-0003).

REFERENCES

Allen, D. A., Barton, J. R., Gillingham, P. R., and Phillips, B. A. 1980, *M.N.R.A.S.*, **190**, 531.
Bally, J., and Scoville, N. Z. 1982, *Ap. J.*, **255**, 497.
Beichman, C., and Harris, S. 1981, *Ap. J.*, **245**, 589.
Calvet, N., and Cohen, M. 1978, *M.N.R.A.S.*, **182**, 687.
Cohen, M., *et al.* 1975, *Ap. J.*, **196**, 179.
Elsässer, H., and Staude, H. J. 1978, *Astr. Ap.*, **70**, L3.
Geldzahler, B. J., and Cohen, N. L. 1983, *Pub. A.S.P.*, **95**, 489.
Greenstein, J. C., and Oke, J. B. 1977, *Pub. A.S.P.*, **89**, 131.
Icke, V. 1981, *Ap. J.*, **247**, 152.
Jones, T. J., and Dyck, H. M. 1978, *Ap. J.*, **220**, 159.
Kobayashi, Y. 1978, *Pub. Astr. Soc. Japan*, **30**, 377.
Lacasse, M. G. 1984, private communication.
Lacasse, M. G., Boyle, D., Levrault, R., Pipher, J. L., and Sharpless, S. 1981, *Astr. Ap.*, **104**, 57.
Lefèvre, J., Daniel, J.-Y., and Bergeat, J. 1983, *Astr. Ap.*, **121**, 51.
Meaburn, J., Walsh, J. R., Hebden, J. C., Morgan, B. C., and Vine, H. 1983, *M.N.R.A.S.*, **205**, 53P.
Ney, E. P., Merrill, K. M., Becklin, E. E., Neugebauer, G., and Wynn-Williams, C. G. 1975, *Ap. J. (Letters)*, **198**, L129.
Perkins, H. G., Scarrott, S. M., Murdin, P., and Bingham, R. G. 1981, *M.N.R.A.S.*, **196**, 635.
Pipher, J. L., Sharpless, S., Savedoff, M. P., Kerridge, S. J., Krassner, J., Schurmann, S., Soifer, B. T., and Merrill, K. M. 1976, *Astr. Ap.*, **51**, 255.
Russell, R. W., Soifer, B. T., and Willner, S. P. 1978, *Ap. J.*, **220**, 568 (RSW).
Schmidt, G. D., Cohen, M., and Margon, B. 1980, *Ap. J. (Letters)*, **239**, L133.
Sibille, F., Cheili, A., and Lena, P. 1979, *Astr. Ap.*, **79**, 315.
Sitko, M. L. 1983, *Ap. J.*, **265**, 848.
Sitko, M. L., Savage, B. D., and Meade, M. R. 1981, *Ap. J.*, **246**, 161.
Thronson, H. 1982, *A.J.*, **87**, 1207.
Warren-Smith, R. F., Scarrott, S. M., and Murdin, P. 1981, *Nature*, **292**, 317.
Webster, A. 1979, *M.N.R.A.S.*, **189**, 33P.
Zuckerman, B., Gilra, D. P., Turner, B. E., Morris, M., and Palmer, P. 1976, *Ap. J. (Letters)*, **205**, L15.

J. C. Dainty: Blackett Laboratory, Imperial College, London SW7 2BZ, England

Marc G. Lacasse: Center for Astrophysics, 60 Garden Street, Cambridge, MA 02138

Judith L. Pipher: University of Rochester, Department of Physics and Astronomy, Rochester, NY 14627

Stephen T. Ridgway: Kitt Peak National Observatory, P.O. Box 26732, Tucson, AZ 85726

REF. 17

ev. Optique 6

ical engineering,
980) p. 31.
d techniques in
n, 1983) p. 109.
975) 87.
ki. Opt. Laser

Am. 73 (1983)

) 972.
52) 193.
70) 255.
ptics 11 (1972)

).
i. Optics 16

13 (Sapparo,

74) 1287.

A NOTE ON EISENSTEIN'S IRREDUCIBILITY CRITERION FOR TWO-DIMENSIONAL SAMPLED OBJECTS

M. NIETO-VESPERINAS [1]

The Institute of Optics, The University of Rochester, Rochester, NY 14627, USA

and

J.C. DAINTY

Blackett Laboratory, Imperial College, London SW7 2BZ, UK

Received 2 May 1985

A proof of uniqueness of phase retrieval for a certain class of objects is given, based on Eisenstein's irreducibility criterion. Some consequences are discussed.

The uniqueness of phase recovery for two dimensional positive sampled functions can be assessed from the irreducibility of the so-called object polynomial whose coefficients are sampled values of the object [1–3], $\{a_{mn}\}$, $m = 0, 1, 2, \ldots, M$, $n = 0, 1, 2, \ldots, N$:

$$F(z_1, z_2) = \sum_{m=0}^{M} \sum_{n=0}^{N} a_{mn} z_1^m z_2^n, \tag{1}$$

where the $\{a_{mn}\}$ are real positive numbers.

It was recently proposed by Fiddy, Brames and Dainty [4] that Eisenstein's irreducibility criterion [5] of one dimensional polynomials can be applied to two dimensional ones by writing (1) as a polynomial in one of the variables z_1 with coefficients being polynomials in the other variable z_2, namely:

$$F(z_1, z_2) = \sum_{m=0}^{M} f_m(z_2) z_1^m, \tag{2}$$

where the coefficients are

$$f_m(z_2) = \sum_{n=0}^{N} a_{mn} z_2^n. \tag{3}$$

[1] On leave from Instituto de Optica, Serrano 121, 28006 Madrid, Spain.

0 030-4018/85 $03.30 © Elsevier Science Publishers B.V. (North-Holland Physics Publishing Division)

This generalisation is not evident and no proof was given in ref. [4]. In this note we give a proof of this proposition.

For the sake of clarity, we shall first quote the Eisenstein irreducibility criterion in its usual form [5].

Eisenstein's Criterion: Given a univariate polynomial $F(z)$ with integer coefficients, if there exists a prime p in Z (Z being the ring of integers), such that (i) p does not divide the leading coefficient of $F(z)$, (ii) p divides all other coefficients of $F(z)$ and (iii) p^2 does not divide the coefficient of the term in z^0, then $F(z)$ is irreducible over the integers (and, by Gauss' theorem [5], over the ring Q of rationals).

To see the generalisation proposed in ref. [4] with the above formulation of the criterion, we next quote it in the form given by van der Waerden (ref. [6], p. 95).

Eisenstein's Criterion (van der Waerden): Let G be an integral domain [6] with identity element in which unique factorisation holds. Let

$$F(z) = \sum_{m=0}^{M} f_m z^m \tag{4}$$

be a polynomial with coefficients f_m in G. If there exists a prime element p in G such that (i) p does

not divide f_M, (ii) p divides all other elements f_m, $m \neq M$ and (iii) p^2 does not divide f_0, *then* $F(z)$ is irreducible in the set of polynomials with coefficients over G, *except for constant factors.*

Let us observe that since Z (and G) are integral domains, the first form of the criterion is a particular case of the second formulation. Moreover, from this more general form of the criterion we infer the following corollary of interest in our problem which constitutes the formulation of the criterion given in ref. [5]:

Corollary: Consider the polynomial $F(z_1, z_2)$ as a polynomial in the main variable z_1 with coefficients $f_m(z_2)$ as in eqs. (2) and (3), the a_{mn} belonging to the field C of complex numbers. If there exists a prime factor $p(z_2)$ such that: (i) $p(z_2)$ does not divide to $f_M(z_2)$, (ii) $p(z_2)$ divides any other $f_m(z_2)$, $m \neq M$, (iii) $p^2(z_2)$ does not divide $f_0(z_2)$, then $F(z_1, z_2)$ is irreducible over the set $C[z_2]$ of one dimensional polynomials with coefficients in C, i.e. is irreducible in the set $C[z_1, z_2]$ of two dimensional polynomials with coefficients in C, apart from factors being polynomials in z_2.

Proof: The set of polynomials

$$f_m(z_2) = \sum_{n=0}^{N} a_{mn} z_2^n$$

with a_{mn} in the field C is an integral domain with the identity element 1, with unique factorization (see e.g. ref. [5], p. 126); therefore this set satisfies the requirements for the three conditions of the criterion.

As quoted in ref. [4], the only prime in $C[z_2]$ is of the form $z_2 + b$, with b in C; this leads to the configuration of fig. 1 of ref. [4] for an Eisenstein object. However, if one is interested only in real functions $f(x, y)$ then the coefficients $f_m(z_2)$ will be in the integral domain $R[z_2]$ of one dimensional polynomials with real coefficients. Then a prime factor in $R[z_2]$, satisfying the three conditions of the criterion, will be a polynomial with real coefficients, irreducible in $R[z_2]$. Also, the irreducibility of $F(z_1, z_2)$ in the set $R[z_1, z_2]$ of two dimensional polynomials with real coefficients is guaranteed *apart from factors that are polynomials in* z_2. This, so far not quoted for Eisenstein's objects, is important since it accounts for the possibility of repeatability of a support in the z_2-direction by discrete steps, and its subsequent addition. For instance, if $G(z_1, z_2)$ is a polynomial which represents the z-transform of an Eisenstein object, then

$$F(z_1, z_2) = (az_2^2 + bz_2 + c)G(z_1, z_2)$$

also represents an Eisenstein object and corresponds to the sum of $G(z_1, z_2)$ taken with weight c, shifted along z_2 one step with weight b and shifted two steps with weight a.

The example given by Bruck and Sodin [1] in which a reference point is placed to one side of a one-dimensional array $F(z_1, z_2) = g(z_2) + z_2^n z_1^m$ corresponds to an Eisenstein object *provided* $g(z_2)$ has *at least* either a simple real root (different from zero if $n \neq 0$) or a simple pair of complex conjugate roots. Also a two-dimensional array with a reference point:

$$F(z_1, z_2) = G(z_1, z_2) + z_2^{N'} z_1^{M'},$$

$$G(z_1, z_2) = \sum_{m=0}^{M} \sum_{n=0}^{N} a_{mn} z_2^n z_1^m,$$

where $M < M'$, will be an Eisenstein object providing $G(z_1, z_2)$ may be decomposed as $G(z_1, z_2) = A(z_2) \times B(z_1, z_2)$, with $A(z_2)$ a simple factor polynomial with at least either one simple real root (different from zero if $N' \neq 0$) or a simple pair of complex conjugate roots. These are just a few instances of distributions satisfying the conditions of the criterion. Of course, any other case among the many that can satisfy the three conditions quoted above will correspond to a unique solution, apart, of course, from the polynomial factor in z_2.

This work was supported by grants from the US Air Force of Scientific Research (AFOSR-81-0003) and the UK Science and Engineering Research Council (SG/C 18190).

References

[1] Yu.M. Bruck and L.G. Sodin, Optics Comm. 30 (1979) 304.
[2] H.H. Hayes, IEEE Trans. Acoust. Speech Signal Process. ASSP-30 (1982) 140.
[3] M. Nieto-Vesperinas and J.C. Dainty, Optics Comm. 52 (1984) 94.
[4] M.A. Fiddy, B.J. Brames and J.C. Dainty, Optics Lett. 8 (1983) 96.
[5] L. Childs, A concrete introduction to higher algebra (Springer-Verlag, New York, 1979) p. 116.
[6] B.L. van der Waerden, Algebra, Vol. 1 (Unger, New York, 1970).

REF. 18

0740-3232/85/010000-00$02.00

Phase conjugation and symmetries with wave fields in free space containing evanescent components

Manuel Nieto-Vesperinas* and Emil Wolf

Department of Physics and Astronomy, University of Rochester, Rochester, New York 14627

Received December 4, 1984; accepted May 10, 1985

Several theorems are known concerning symmetry relations between monochromatic wave fields that propagate either into the same half-space ($z > 0$) or into complementary half-spaces ($z > 0$ and $z < 0$) and that are complex conjugates of each other in some cross-sectional plane z = constant. The theorems derived up to now apply only to wave fields that do not contain inhomogeneous (evanescent) components. In the present paper two of the main theorems are generalized to a wider class of fields. It is found that homogeneous and inhomogeneous components of a wave field have quite different symmetry properties under phase conjugation. The results are illustrated by a discussion of the behavior of plane waves, both homogeneous and evanescent ones, which undergo phase conjugation followed by transmission or by reflection.

Paper unavailable at present time.

PHASE RECOVERY FOR TWO-DIMENSIONAL DIGITAL OBJECTS BY POLYNOMIAL FACTORISATION*

M Nieto-Vesperinas**

The Institute of Optics
The University of Rochester
Rochester
NY 14627 , USA

J C Dainty
Blackett Laboratory
Imperial College
London SW7 2BZ, UK

ABSTRACT

Phase retrieval for sampled, real, positive objects in two-dimensions is studied from the point of view of factorisation of the z-transform. This decomposition is considered over the field of integers for noise-free autocorrelations of digital objects and the formulation provides a means of calculating all possible objects with a given autocorrelation. A brief discussion on the influence of noise is carried out using some simple examples which show the existence of an approximate factorisation over reals.

* A preliminary account of this work was presented at the 1984 Annual Meeting of the Optical Society of America, San diego, CA.
** On leave from Instituto de Optica, CSIC, Serrano 121, 28006 Madrid, Spain.

INTRODUCTION

It is known[1,2] that the phase retrieval problem for sampled data is equivalent to that of obtaining the so-called object polynomial which represents the z-transform of the object samples $\{a_{mn}\}$, $m = 0,1,2...M$, $n = 0,1,2...N$:

$$F(z_1,z_2) = \sum_{m=0}^{M} \sum_{n=0}^{N} a_{mn}\, z_1^m\, z_2^n \qquad (1)$$

by finding the factorisation of the so-called autocorrelation polynomial :

$$Q(z_1,z_2) = \sum_{m=0}^{2M} \sum_{n=0}^{2N} b_{mn}\, z_1^m\, z_2^n \qquad (2)$$

(whose coefficients b_{mn} represent the data) in the form :

$$Q(z_1,z_2) = z_1^M\, z_2^N \Big[\sum_{m=0}^{M} \sum_{n=0}^{N} a_{mn}\, z_1^m\, z_2^n \Big] \Big[\sum_{m'=0}^{M} \sum_{n'=0}^{N} a_{m'n'}\, z_1^{m'}\, z_2^{n'} \Big]$$

$$= z_1^M\, z_2^N\, F(z_1,z_2)\, F(1/z_1,1/z_2) \; . \qquad (3)$$

However, apart from procedures based on modifications of the Gerchberg-Saxton algorithm[3], whose convergence are not yet well understood, no other attempts of performing such factorisation have been made, although recently some computational results for small

arrays based on our analysis below have been reported[4].

In a recent paper[5] we proposed a test of uniqueness of the factorisation in the absence of noise for digital objects, based on an analysis of factorisation of polynomials over the ring of integers Z, which for real digital objects and noise-free autocorrelations was shown[5] to be the necessary domain of factorisation. Thus, the coefficients a_{mn} and b_{mn} of Eqs. (1) and (2) are assumed to be non-negative integers. In Ref. 5 it was pointed out also that the scheme used for assessing uniqueness of the reconstruction could be extended to find the factors of $Q(z_1, z_2)$ and hence the solution(s) to the phase problem. The purpose of this paper is to show how this is done.

This noise-free factorisation is useful where other phase reconstruction algorithms are tested for digital objects. In this case the factorisation procedure proposed in this paper can give all possible objects with integer sampling values.

2. FACTORING OVER INTEGERS IN ONE DIMENSION

The procedure of factorizing a one dimensional polynomial F(z) in Z consists of factoring modulo p^{2^k}, (p prime) by successive lifts of factorisation starting modulo p. This method yields factorisation modulo an integer as large as one needs. (What follows is based on the facts quoted in Ref. 5 .)

The following lemmas state how to lift the factorisations (see e.g. Refs. 6, Ch.II.13 and 7):

Lemma 1 (Hensel): Let p be a prime and F(z) a monic polynomial in Z[z]. Let $g_1(z)$ and $h_1(z)$ be two monic relatively prime** polynomials in $Z_p[z]$ such that $F(z) \equiv g_1(z)\, h_1(z) \pmod p$. Then for any integer $k > 1$ there exist polynomials $g_k(z)$ and $h_k(z)$ in $Z_q[z]$ such that $F(z) \equiv g_k(z)\, h_k(z) \pmod q$, where $q = p^k$, $g_k \equiv g_1 \pmod p$ and $h_k \equiv h_1 \pmod p$.

Lemma 2 (Zassenhaus extension[8]): Let p, F(z), $g_1(z)$ and $h_1(z)$ be given as in Lemma 1: for any integer $k > 0$ there are polynomials $g_k(z)$ and $h_k(z)$ in $Z_q[z]$ such that $F(z) \equiv g_k(z)\, h_k(z) \pmod q$, where $q = p^{2^{k-1}}$ and $g_k \equiv g_1 \pmod p$ and $h_k \equiv h_1 \pmod p$.

Based on these lemmas the procedure for factorizing over Z (or equivalently, modulo $p^{2^{k-1}}$ large enough so that the coefficients of F(z) and its factors are the same as those over Z) is as follows:

** Footnote If q is a natural number and g and h polynomials in Z[z], g and h are relatively prime modulo q if there exist polynomials r and s in Z[z] such that $rg + sh \equiv 1 \pmod q$.

1) Factorize the monic $F(z)$ in Z_p, the ring of integers modulo p (p prime), by means of Berlekamp's method[7] into two relatively prime factors g_1 and h_1.

2) Write the difference $F(z) - h_1 g_1$ where $F(z)$ and the product of h_1 and g_1 is taken over integers. Then reduce that difference modulo p^2 obtaining a polynomial $k_1(z)$ in p by extracting p as a multiple.

3) Find two polynomials $H_1(z)$ and $G_1(z)$ such that $k_1(z) \equiv g_1(z)\, H_1(z) + h_1(z)\, G_1(z) \pmod{p}$, the degrees (deg) of H_1 and G_1 being such that: deg G_1 < deg g_1 and deg H_1 < deg h_1.

4) Build the new factors (mod p^2): $g_2 = g_1 + p^1 G_1$ and $h_2 = h_1 + p^1 H_1$.

5) Iterate the procedure as many times as necessary until the factorisation mod p^2 coincides with the factorisation over Z.

The details, with examples for the procedure to factorise a polynomial $F(z)$ modulo p^2 can be found in Section 13.B of Ref. 6.

3. FACTORIZATION OVER INTEGERS OF 2-DIMENSIONAL Z-TRANSFORMS

Based on the above ideas, the factorisation of the autocorrelation polynomial $Q(z_1,z_2)$ into irreducible factors (whose number is expected to be even) with integer coefficients, or, if it is of interest, the factorisation of the object polynomial $F(z_1,z_2)$, can be carried out by means of algorithms that generalise univariate polynomial factorisation to several variables. A suitable algorithm is that put forward by Wang[9], which is an improved version of another method previously established by Wang and Rothschild[10]. The algorithm is as follows:

Let

$$P(z_1, z_2) = P_M(z_2)\, z_1^M + P_{M-1}(z_2)\, z_1^{M-1} + \ldots\ldots + P_0(z_2) \qquad (4)$$

be the polynomial in z_1 whose coefficients $P_m(z_2)$ are:

$$P_m(z_2) = \sum_{n=1}^{N} c_{mn}\, z_2^n \quad . \qquad (5)$$

(1) Extract the content[5] of $P(z_1,z_2)$ by obtaining the greatest common divisor (gcd) of the coefficients $P_m(z_2)$. This will be a factor in z_2 of $P(z_1,z_2)$.

(2) Obtain $\gcd[P(z_1,z_2), \partial P/\partial z_1] = D(z_1,z_2)$, which accounts for multiple factors as in Fact 2 of Ref. 5. The algorithm can be carried out by factoring D and P/D separately if $D \neq 1$.

(3) Factorize the leading coefficient $P_M(z_2)$ into irreducible factors according to the procedure described in Section 2:

$$P_M(z_2) = F_1(z_2)...F_r(z_2) \quad .$$

(4) Find an integer z_0 such that: (i) $P_m(z_0) \neq 0$. (ii) For each factor F_i of P_M, $\widetilde{F}_i = F_i(z_0)$ has at least one prime divisor P_i which does not divide any F_j, $j < 1$, or the content of $P(z_1,z_0)$.
(iii) $P(z_1,z_0)$ has no repeated factors.

(5) Factorize over integers $pp[P(z_1,z_0)] = P_1(z_1)...P_r(z_1)$, where pp[ ] denotes the principal part[5].

(6) Denote by $P_{ii}^{(1)}(z_1,z_2)$ the polynomial obtained by substituting the leading coefficient of $P_i(z_1)$ by $F_i(z_2)$ such that, of course, this leading coefficient is equal to $F_i(z_0)$. Then construct the function $R_1(z_1,z_2)$:

$$R_1(z_1,z_2) = P_{11}^{(1)}...P_{rr}^{(1)} - P(z_1,z_2)$$

Note that $R_1(z_1,z_0) = 0$.

Evaluate

$$C_1(z_1) = \frac{\partial R_1}{\partial z_2}\Bigg|_{z_2 = z_0}$$

7) Find polynomials $a_i^{(1)}(z_1)$, $(i = 1,...r)$, such that

$$a_1^{(1)}P_2\ldots P_r + a_2^{(1)}P_1.P_3..P_r + a_3^{(1)}P_1P_2P_4\ldots P_r +$$
$$\ldots + a_r^{(1)}P_1\ldots P_{r-1} = C_1(z_1) ,$$

such that $\deg(a_i) < \deg(P_i)$, $(i = 1,\ldots r)$.

(8) Obtain new approximations to the factors:

$$P_{ii}^{(2)} = P_{ii}^{(1)} - a_i^{(1)}(z_2 - z_0) .$$

(9) Obtain a new $R_2(z_1,z_2)$:

$$R_2(z_1,z_2) = P_{11}^{(2)}\ldots P_{rr}^{(2)} - P(z_1,z_2)$$

and evaluate:

$$C_2(z_1) = \frac{1}{2}\frac{\partial^2 R_2}{\partial z_2}\Bigg|_{z_2 = z_0} .$$

In general, after obtaining $P_{11}^{(m)}\ldots P_{rr}^{(m)}$ in the mth iteration one will evaluate:

$$R_m(z_1,z_2) = P_{11}^{(m)}\ldots P_{rr}^{(m)} - P(z_1,z_2)$$
$$R_m(z_1,z_0) = 0$$

and:

$$C_m(z_1) = \frac{1}{m!}\frac{\partial^m R_m}{\partial z_2^m}\Bigg|_{z_2 = z_0} .$$

Then one will obtain polynomials $a_1^{(m)}(z_1)$ such that:

$$a_1^{(m)}P_2....P_r + a_2^{(m)}P_1P_3...P_r + a_3^{(1)}P_1P_2P_4...P_r + ... + a_r^{(m)}P_1....P_{r-1} = C_m(z_1) \ ,$$

so that

$$P_{ii}^{(m+1)} = P_{ii}^{(m)} - a_i^{(m)}(z_2 - z_0)^m \ .$$

The following example illustrates the above, but of course the procedure would be implemented on a computer for larger arrays.

Example 1

Let us find all possible objects, with integer sampling values, compatible with the autocorrelation of Table 1. The greatest common divisor of $Q(z_1,z_2)$ and $\partial Q(z_1,z_2)/\partial z_1$ is found to be (see e.g. Ref. 7 for the calculation procedure):

$$P(z_1,z_2) = \gcd[Q, \frac{\partial Q}{\partial z_1}]$$

$$= (9z_2^3 + 9z_2^2 + 5z_2 + 1)z_1^4 + (3z_2^3 + 4z_2^2 + 2z_2 + 1)z_1^3 + (3z_2^4 + 11z_2^3 + 25z_2^2 + 11z_2 + 3)z_1^2 + (z_2^4 + 2z_2^3 + 4z_2^2 + 3z_2)z_1 + (z_2^4 + 5z_2^3 + 9z_2^2 + 9z_2)$$

which is a double factor of $Q(z_1,z_2)$. In fact, a straightforward calculation gives:

$$Q(z_1,z_2) = P(z_1,z_2)^2 \ .$$

$P(z_1,z_2)$ is found to have no multiple factors.

Let us apply Wang's algorithm to find the factors of $P(z_1,z_2)$. An analysis based on the methods of Ref. 5 shows that $P(z_1,z_2)$ has two factors.

The leading coefficient $9z_2^3 + 9z_2^2 + 5z_2 + 1$ is factored according to Section 2 as:

$$F_1(z_2) = 3z_2 + 1$$
$$F_2(z_2) = 3z_2^2 + 2z_2 + 1 .$$

An integer satisfying the conditions of point (4) of Wang's algorithm is $z_0 = 1$. Then

$$P(z_1,1) = 24z_1^4 + 10z_1^3 + 53z_1^2 + 10z_1 + 24 ,$$

which, using the procedure of Section 2, factors into:

$$P_1(z_1) = 4z_1^2 + z_1 + 6 \quad \text{and} \quad P_2(z_1) = 6z_1^2 + z_1 + 4 .$$

Then:

$$P_{11}^{(1)}(z_1,z_2) = (3z_2 + 1)z_1^2 + z_1 + 6$$
$$P_{22}^{(1)}(z_1,z_2) = (3z_2^2 + 2z_2 + 1)z_1^2 + z_1 + 4 .$$

$R_1(z_1,z_2)$ is given by

$$R_1(z_1,z_2) = [(3z_2 + 1)z_1^2 + z_1 + 6][(3z_2^2 + 2z_2 + 1)z_1^2 + z_1 + 4] - P(z_1,z_2)$$

$$= (-3z_2^3 - z_2^2 + 3z_2 + 1)z_1^3 + (-3z_2^4 - 11z_2^3 - 7z_2^2 + 13z_2 + 8)z_1^2 + (-z_2^4 - 2z_2^3 - 4z_2^2 - 3z_2 + 10)z_1 + (-z_2^4 - 5z_2^3 - 9z_2^2 - 9z_2 + 24)$$

and

$$C_1(z_1) = \left.\frac{\partial R_1}{\partial z_2}\right|_{z_2 = 1} = -8z_1^3 - 46z_1^2 - 21z_1 - 46 .$$

Let us now find polynomials $a_2^{(1)} = az_1 + b$ and $a_1^{(1)}(z_1) = cz_1 + d$ satisfying:

$$a_2^{(1)}(4z_1^2 + z_1 + 6) + a_1^{(1)}(z_1)(6z_1^2 + z_1 + 4) = -8z_1^3 - 46z_1^3 - 21z_1 - 46 ,$$

which gives the linear system:

$$\begin{aligned} 4a + \quad 6c \quad &= -8 \\ a + 4b + c + 6d &= -46 \\ 6a + b + 4c + d &= -21 \\ 6b + 4d &= -46 \end{aligned}$$

from which $a = -2$, $b = -5$, $c = 0$ and $d = -4$.

Thus: $a_2^{(1)}(z_1) = -2z_1 - 5$, $\quad a_1^{(1)}(z_1) = -4$

Then:

$$P_{11}^{(2)}(z_1, z_2) = P_{11}^{(1)}(z_1, z_2) + 4(z_2 - 1) = (3z_2 + 1)z_1^2 + z_1 + 4z_2 + 2$$

$$P_{22}^{(2)}(z_1, z_2) = P_{22}^{(1)}(z_1,z_2) + (2z_1 + 5)(z_2 - 1)$$
$$= (3z_2^2 + 2z_2 + 1)z_1^2 + (2z_2 - 1)z_1 + (5z_2 - 1) .$$

The procedure is repeated with $P_{11}^{(2)}(z_1,z_2)$ and $P_{22}^{(2)}(z_1,z_2)$ until the following factorisation is obtained:

$$Q(z_1,z_2) = [P_{11}^{(3)}(z_1,z_2)]^2 [P_{22}^{(3)}(z_1,z_2)]^2$$

with

$$P_{11}^{(3)}(z_1,z_2) = (3z_2+1)z_1^2 + z_1 + (z_2^2+2z_2+3)$$

$$P_{22}^{(3)}(z_1,z_2) = (3z_2^2+2z_2+1)z_1^2 + z_2^2z_1 + (z_2^2+3z_2) .$$

The two possible objects $F_1(z_1,z_2) = P_{11}^{(3)}(z_1,z_2)\ P_{22}^{(3)}(z_1,z_2)$ and $F_2(z_1,z_2) = [P_{11}^{(3)}(z_1,z_2)]^2$ are shown in Tables 2a and 2b respectively.

4. INFLUENCE OF NOISE

All of the above analysis is applicable to digital, noise-free objects and thus will fail in the presence of noise. In fact, although the noise-free autocorrelation polynomial $Q(z_1,z_2)$ is factorisable into an even number of polynomials with integer coefficients, the noisy autocorrelation will probably become reducible into factors with irrational coefficients (the first decimals of these representing approximations to the ideal noise-free integer coefficients), or even reducible over complex fields, in which case no possible real and positive object distribution can be found.

The following example illustrates the above comments. This example does not attempt to be an exhaustive analysis of the influence of noise on the problem, since this paper is mainly concerned with the noise-free situation. However, the example illustrates to some extent how noise can affect the factorisation.

Example 2

The polynomial $Q(z_1,z_2)$ of Table 3a is found by the method of Section 3 to correspond to the object of Table 3b. This solution can be seen to be unique by using the test of Ref. 5.

The autocorrelation polynomial of Table 4a, whose coefficients are perturbed values of Table 3a, no longer factorises into polynomial z-transforms with integer coefficients, but into the product $F(z_1,z_2)\ F(z_1^{-1},z_2^{-1})\ z_1^4\ z_2^4$, with $F(z_1,z_2)$ having irrational coefficients. Table 4b shows the object with coefficients obtained by

approximating these irrationals by decimals. The coefficients of this object are simply perturbations of those of Table 3b.

However, the situation can be much worse. Table 5a represents another perturbation of the autocorrelation of Table 3a, and Table 5b shows the corresponding complex object. In this case no real approximation to the true ideal noise-free object of Table 3a can be found, and, neglecting the phase, the modulus of this complex object represents a poor approximation to the original object.

Even for a noisy autocorrelation $Q(z_1,z_2)$, one expects a minimum of two factors, (one flipped with respect to the other). However for $F(z_1,z_2)$ perturbed by noise one would expect to lie in a region of irreducibility even if the noise-free F is reducible over Z. This is likely to be so since according to Ref.11 the set of reducible polynomials in two variables has measure zero.

Acknowledgements

We are grateful to B J Brames, M A Fiddy and J Sanz for discussions, to a referee for suggestions for shortening the original manuscript and to B J King for typing the paper. This work was supported by grants from the US Air Force Office of Scientific Research (AFOSR-81-0003) and the UK Science Research Council (SG/C 18190).

References

1. Yu M Bruck and L G Sodin, Opt. Commun., 30, 304-308 (1979).

2. M H Hayes, IEEE Trans. Acoust. Speech. Signal. Process., ASSP-30, 140-154 (1982).

3. J R Fienup, Opt. Lett., 3, 27-29 (1978).

4. H M Berenyi, H V Deighton and M A Fiddy, submitted to Opt. Acta

5. M Nieto-Vesperinas and J C Dainty, Opt. Commun., 52, 94-98 (1984).

6. L Childs, 'A Concrete Introduction to Higher Algebra' (Springer-Verlag, New York, 1979).

7. D E Knuth, 'The Art of Computer Programming' (Addison-Wesley, Mass. 1981) Vol. 2, Ch. 4.

8. H Zassenhaus, J. Number Theory, 1, 291-311 (1969).

9 . P S Wang, Math. Comp., 32, 1215-1231 (1978).

10. P S Wang and L P Rothschild, Math. Comp., 29, 935-950 (1975).

11. M H Hayes and J H McClellan, Proc. IEEE, 70, 197-198 (1982).

TABLE 1

Autocorrelation Function

1	2	7	6	9				
10	14	56	40	90	36	54		
43	46	226	156	399	144	261	54	81
108	100	546	326	922	368	702	126	162
171	138	792	464	1321	464	792	138	171
162	126	702	368	922	326	546	100	108
81	54	261	144	399	156	226	46	43
		54	36	90	40	56	14	10
				9	6	7	2	1

TABLE 2a

Object (F_1) obtained from the autocorrelation of Table 2

1	1	3		
5	2	11	3	9
9	4	25	4	9
9	3	11	2	5
		3	1	1

TABLE 2b

Object (F_2) obtained from autocorrelation of Table 2

1				
4		6		
10	2	14		9
12	4	22	6	6
9	6	7	2	1

TABLE 3a

Noise-free autocorrelation

25				
115	50	115		
126	115	352	115	126
		115	50	115
				25

TABLE 3b

Corresponding object

5			
14	5	9	
		5	

TABLE 4a

Noisy autocorrelation

28	1	1		
119	57	123	4	3
124	119	352	119	124
3	4	123	57	119
		1	1	28

TABLE 4b

Corresponding object approximated by decimals

5.35	0.12	0.2
13.86	5.17	8.84
	0.11	5.16

TABLE 5a

Noisy autocorrelation

20				
100	40	100		
130	120	340	120	130
		100	40	100
				20

TABLE 5b

Corresponding object

$\sqrt{10} + i\sqrt{10}$				
$\sqrt{90} + i\sqrt{40}$		$\sqrt{40}$	$\sqrt{90} + i\sqrt{40}$	
			$\sqrt{10} + i\sqrt{10}$	

Modulus:

$\sqrt{20}$				
$\sqrt{130}$	$\sqrt{40}$	$\sqrt{130}$		
		$\sqrt{20}$		

Phase:

$\pi/4$			
0.588	0	0.588	
			$\pi/4$

A STUDY ON THE PERFORMANCE OF NON-LINEAR LEAST-SQUARE OPTIMIZATION METHODS IN THE PROBLEM OF PHASE RETRIEVAL

M. Nieto-Vesperinas*

Department of Physics and Astronomy
and
The Institute of Optics
University of Rochester
Rochester, NY 14627, USA

ABSTRACT

The efficiency of an important class of Newton methods (the Levenberg-Marquardt algorithm) for solving overdetermined sets of non-linear equations is tested in finding the solution to the 2-D phase problem. It is seen that the non-linearity and number of local minima of the cost function increases dramatically with the size of the object array, making these methods of little practical use for sizes greater than 6 x 6.

AD-A168 755 HIGH ANNULAR RESOLUTION STELLAR INTERFEROMETRY(U) 3/3
ROCHESTER UNIV NY INST OF OPTICS J C DAINTY 31 JUL 85
AFOSR-TR-86-0312 AFOSR-81-0003

UNCLASSIFIED F/G 3/1 NL

END
DATE FILMED
2 86

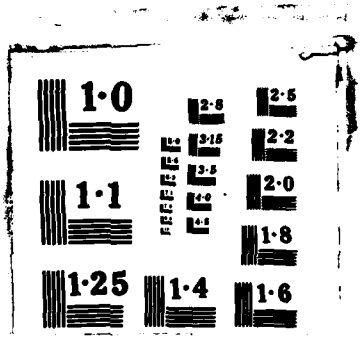
1·0
1·1
1·25
1·4
1·6
1·8
2·0
2·2
2·5

1. Introduction

There is much current effort in obtaining algorithms to retrieve the phase from knowledge of the modulus of the Fourier transform of a 2-D real and positive sampled object function[1-3]. Although this problem has no unique solution in 1-D, it is now understood that in the majority of 2-D cases the solution is likely to be unique[4-7].

Let $a(x,y)$ be the 2-D object sampled function to be found:

$$a(x,y) = \sum_{m=1}^{M} \sum_{n=1}^{M} a_{mn}\, \delta(x - m\Delta)\, \delta(y - n\Delta) \qquad (1)$$

(Δ being the sampling interval; for the sake of simplicity the number of samples and the interval between samples are considered equal in the x and y directions).

The phase problem in object space then consists of finding $a(x,y)$ from knowledge of its autocorrelation function $Q(x,y)$ by solving the non-linear integral equation:

$$Q(x,y) = \iint_D d\xi\, d\eta\, a(\xi,\eta)\, a(\xi + x, \eta + y) \qquad (2)$$

D being the object support.

Taking into account the discrete character (1) of $a(x,y)$, this amounts to solving the overdetermined system of non-linear equations:

$$Q_{ij} = \sum_{m=1}^{M} \sum_{n=1}^{M} a_{mn}\, a_{m+i,\,n+j} \qquad (3)$$

$$(i = 1, \ldots, 2M-1 \quad j = 1, \ldots, 2M-1)$$

Q_{ij} being the samples of $Q(x,y)$.

In spite of the progress made in computer simulations with the algorithms used so far, no reconstruction procedure seems yet to have been systematically successful except for small arrays or when the starting guess introduced in the iteration process is close to the true solution. Otherwise the iterations tend to stagnate and get stuck in the so-called local minimum of the cost function. Also, the convergence criteria of these algorithms are generally not well understood.

On the other hand, there is now available a wide and complete study of optimization methods for solving systems of non-linear equations based on gradient search. Among these, an important and well established class includes Newton and conjugate gradient methods[8,9]. Their convergence has been extensively analyzed and is known to be quadratic. It is therefore of interest to study the performance of these methods in the problem of phase retrieval, namely in obtaining the solution to Eq. (3). If $F(\underline{x})$ is the cost function associated with this system of non-linear equations and it is given by the norm of the residuals of (3)[9], gradient methods operate by searching the line $\underline{P}$ at which $F(\underline{x}^{(k+1)})$ in the $(k+1)$th iteration satisfies:

$$F(\underline{x}^{(k+1)}) = F(\underline{x}^{(k)} + P) < F(\underline{x}^{(k)}) \qquad (4)$$

Hence, these procedures lead directly to a minimum of the cost function $F(\underline{x})$.

An important class of line search methods is the steepest descent. Fienup[2] has shown the equivalence of this method and his error-reduction algorithm. However, steepest descent methods seem to be inefficient and unreliable in practice to find minima[8,9]; they are very sensitive to scaling and round-off errors and hence, although their convergence can be theoretically

proven to be linear, it is in practice either very slow or non-existent as the successive iterations become unstable and end far from a minimum.

Newton and conjugate gradient methods provide, on the other hand, very robust and stable codes of implementation. Their main disadvantage, however, is that the computing time may become long as they require to produce and invert an $M^2 \times M^2$ matrix for an $M \times M$ object. These operations can be made stable, though, and their time be substantially reduced with the aid of an array processor. Also their quadratic convergence requires only a few iterations, and no inclusion of noisy autocorrelation data is required at each iteration as in refs. 1 and 2.

In this work we have tested a least-square (L-S) optimization; more specifically, the Levenberg-Marquardt (L-M) modification[10,11] of Gauss-Newton method[8,9]. This is an appropriate procedure for an overdetermined set of non-linear equations such as (3): For an object array with M^2 unknown elements, there are $M^2 + (M - 1)^2$ equations. This fact may also account for the uniqueness of the solution in 2-D. Earlier attempts for 1-D phase problems by using the Newton-Raphson method (which is established for a set with the same number of equations and unknowns) have been done in Refs. 12 and 13. In the 1-D case, however, because the number of equations and unknowns is the same and the equations are non-linear, the solution is not unique.

As we shall show in this work, although the stability and convergence of existing L-S codes is very good, the structure of the problem increases dramatically in complication as the size of the array increases. The cost function becomes highly non-linear with a huge number of local minima, both far and near the global zero minimum that constitutes the solution to the

problem. Thus, although these gradient methods are well established and provide good convergence, they always yield local minima and fail to reach the solution to the problem (except for $M < 6$). At the same time they give, however, an account of its complexity.

2. Description of the numerical method

Given the system of non-linear equations:

$$\left.\begin{aligned} f_1(x_1, \dots, x_M) &= g_1 \\ \cdots\cdots\cdots & \\ f_N(x_1, \dots, x_M) &= g_N \end{aligned}\right\} \qquad (5)$$

with N data $g_1, \dots, g_N$ and M unknowns $x_1, \dots, x_M$ ($N > M$), the non-linear L-S method for solving (5) consists of seeking the global minimum of the cost function:

$$F(x_1, \dots, x_M) = \frac{1}{2} \sum_{j=1}^{N} r_j^2 \qquad (6)$$

where the residuals r_j are:

$$r_j = f_j(x_1, \dots, x_M) - g_j \qquad (7)$$

We shall use the vector notation:

$$\begin{aligned} \underline{x} &= (x_1, \dots, x_M) \\ \underline{R}(\underline{x}) &= (r_1(\underline{x}), \dots, r_N(\underline{x})) \end{aligned} \qquad (8)$$

So (6) may be written as:

$$F(\underline{x}) = \frac{1}{2} \underline{R}^T(\underline{x}) \underline{R}(\underline{x}) \qquad (9)$$

the superscript T denoting 'transposed'.

The iterative procedure that yields a minimum of $F(\underline{x})$ is[8,9]

$$\underline{x}^{(k+1)} = \underline{x}^{(k)} + \underline{\delta}^{(k)} \qquad (10)$$

where the increment vector $\underline{\delta}^{(k)}$ is obtained by solving the linear system

$$[\underline{\underline{\nabla^2} F}(\underline{x}^{(k)})]\, \underline{\delta}^{(k)} = -\underline{\nabla} F(\underline{x}^{(k)}) \qquad (11)$$

$\nabla^2 F(\underline{x}^{(k)})$ is the Hessian matrix of $\underline{F}$ evaluated in the kth-iteration $\underline{x}^{(k)}$; its elements are:

$$\left[\nabla^2 F(\underline{x}^{(k)})\right]_{ij} = \left.\frac{\partial^2 F}{\partial x_i \partial x_j}\right|_{\underline{x}=\underline{x}^{(k)}} \qquad (12)$$

It is straightforward to see from Eq. (6) that:

$$\underline{\underline{\nabla}}^2 F(\underline{x}^{(k)}) = \underline{\underline{J}}^T(\underline{x}^{(k)})\,\underline{\underline{J}}(\underline{x}^{(k)}) + \left(\begin{array}{l}\text{terms with second order}\\ \text{derivatives of } r_j\end{array}\right) \qquad (13)$$

where $\underline{\underline{J}}^T(\underline{x}^{(k)})$ is the transposed of the Jacobian $\underline{\underline{J}}(\underline{x}^{(k)})$ of Eq. (5), whose elements are:

$$\left[J(\underline{x}^{(k)})\right]_{ij} = \left.\frac{\partial r_i}{\partial x_j}\right|_{\underline{x}=\underline{x}^{(k)}} \qquad (14)$$

On the other hand, $\nabla F(\underline{x}^{(k)})$ is obtained from Eq. (6) to be:

$$\underline{\nabla} F(\underline{x}^{(k)}) = \underline{\underline{J}}^T(\underline{x}^{(k)})\,\underline{R}(\underline{x}^{(k)}) \qquad (15)$$

By inserting Eqs. (11) - (15) into Eq. (10) and approximating the Hessian by the first term of Eq. (13) one obtains the algorithmic scheme:

$$\underline{x}^{(k+1)} = \underline{x}^{(k)} - \left[\underline{\underline{J}}^T(\underline{x}^{(k)})\,\underline{\underline{J}}(\underline{x}^{(k)})\right]^{-1} \underline{\underline{J}}^T(\underline{x}^{(k)})\,\underline{R}(\underline{x}^{(k)}) \qquad (16)$$

The iterative procedure corresponding to Eq. (16) is the Gauss-Newton method. In order that the fixed point $\underline{x}^*$ of the sequence (16) when $k \to \infty$ be a minimum of $F(\underline{x})$ the Hessian (13) should be positive definite. Sometimes the neglect of the terms of (13) from the second onwards prevents this property of the Hessian and is convenient to add a multiple of the identity matrix. The result is the L-M algorithm:

$$\underline{x}^{(k+1)} = \underline{x}^{(k)} - \left[\underline{\underline{J}}^T(\underline{x}^{(k)})\,\underline{\underline{J}}(\underline{x}^{(k)}) + \mu_k \underline{\underline{I}}\right]^{-1} \underline{\underline{J}}^T(\underline{x}^{(k)})\,\underline{R}(\underline{x}^{(k)}) \qquad (17)$$

There are several codes for finding the optimum μ_k. An efficient one for adequate line search is due to Moré[14].

For the system (3) the vector $\underline{x}$ has the M^2 components a_{mn}. Then $\underline{\underline{J}}^T(\underline{x}^{(k)})\underline{\underline{J}}(\underline{x}^{(k)}) + \mu_k\underline{\underline{I}}$ is an $M^2 \times M^2$ matrix.

A very efficient implementation code of (17) that controls numerical instabilities due to round-off errors that appear in (17) for M large (we have observed them for $M > 5$), is the one contained in MINPACK[15]. The subroutine LMSTR contained there seems appropriate since it uses minimum storage. It is the one we have used to implement (17).

Since the autocorrelation array:

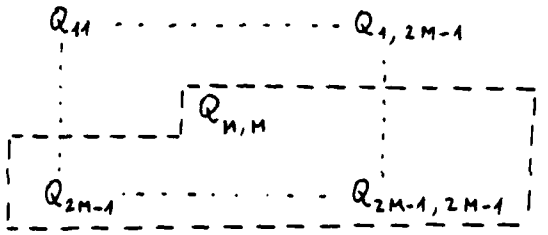

(18)

is even around the central sampling point $Q_{M,M}$, the necessary number of data Q_{ij} is $M^2 + (M-1)^2$, namely $Q_{M,M},\ldots,Q_{M,2M-1},Q_{M+1,1},\ldots,Q_{M+1,2M-1},\ldots,Q_{2M-1,1},\ldots,Q_{2M-1,2M-1}$.

For the sake of clarity, the technique used for establishing the set of non-linear equations and to find the Jacobian will be illustrated with a 2 x 2 array. Numerical results for larger arrays will be shown in the next section.

For example, the 2 x 2 array

$$\begin{matrix} a_{11} & a_{12} \\ a_{21} & a_{22} \end{matrix} \qquad (19)$$

has the autocorrelation

$$\begin{matrix} Q_{11} & Q_{12} & Q_{13} \\ Q_{21} & Q_{22} & Q_{23} \\ Q_{31} & Q_{32} & Q_{33} \end{matrix} \qquad (20)$$

Since $Q_{11} = Q_{13}$, $Q_{12} = Q_{32}$, $Q_{13} = Q_{31}$ and $Q_{21} = Q_{23}$, we have to consider as data the five elements Q_{22}, Q_{23}, Q_{31}, Q_{32} and Q_{33}. The set (3) of equations would be in this case

$$\begin{aligned} Q_{22} &= a_{11}^2 + a_{12}^2 + a_{21}^2 + a_{22}^2 \\ Q_{23} &= a_{11}a_{12} + a_{21}a_{22} \\ Q_{31} &= a_{12}a_{21} \\ Q_{32} &= a_{11}a_{21} + a_{12}a_{22} \\ Q_{33} &= a_{11}a_{22} \end{aligned} \qquad (21)$$

which has 2^2 unknowns and 5 equations.

In general, the set (3) may be formed by the following matrix procedure:

$$\begin{bmatrix} a_{11} \cdots a_{1M} \overbrace{0 \cdots 0}^{M-1 \text{ times}} a_{21} \cdots a_{2M} \overbrace{0 \cdots 0}^{M-1 \text{ times}} a_{M,1} \cdots a_{M,M} \\ 0\, a_{11} \cdots a_{1,M-1}\, a_{1,M} \overbrace{0 \cdots 0}^{M-1 \text{ times}} a_{21} \cdots a_{2,M-1}\, a_{2,M} \overbrace{0 \cdots 0}^{M-1 \text{ times}} a_{M,1} \cdots a_{M-1,M-1} \\ 0\,0\, a_{11} \cdots \cdots \cdots \cdots \cdots \cdots a_{M-2,M-2} \\ \cdots \cdots \cdots \cdots \cdots \cdots \cdots \\ \cdots \cdots \cdots \cdots \cdots \cdots \cdots \\ 0\,0\,0 \cdots \cdots \cdots \cdots 0\,0\,0 \cdots a_{11} \end{bmatrix} \begin{bmatrix} a_{11} \\ \vdots \\ a_{1M} \\ \overbrace{0}^{M-1} \\ a_{21} \\ \vdots \\ a_{2M} \\ \overbrace{0}^{M-1} \\ a_{M1} \\ \vdots \\ a_{MM} \end{bmatrix} = \begin{bmatrix} Q_{MM} \\ Q_{M,M+1} \\ \vdots \\ Q_{M,2M-1} \\ Q_{M+1,1} \\ \vdots \\ Q_{2M-1,2M-1} \end{bmatrix} \qquad (22)$$

For example, for the 2 x 2 array (19), Eqs. (21) are expressed according to (22) as:

$$\begin{bmatrix} a_{11} & a_{12} & 0 & a_{21} & a_{22} \\ 0 & a_{11} & a_{12} & 0 & a_{21} \\ 0 & 0 & a_{11} & a_{12} & 0 \\ 0 & 0 & 0 & a_{11} & a_{12} \\ 0 & 0 & 0 & 0 & a_{11} \end{bmatrix} \begin{bmatrix} a_{11} \\ a_{12} \\ 0 \\ a_{21} \\ a_{22} \end{bmatrix} = \begin{bmatrix} Q_{22} \\ Q_{23} \\ Q_{31} \\ Q_{32} \\ Q_{33} \end{bmatrix} \qquad (23)$$

From Eq. (22) the Jacobian (14) is now easy to evaluate. For example:

$$J_{11} = \frac{\partial r_1}{\partial a_{11}} = [1\,0\,0\,0\cdots 0] \begin{bmatrix} a_{11} \\ \vdots \\ a_{1M} \\ 0 \\ \vdots \\ 0 \\ a_{21} \\ \vdots \\ a_{2M} \\ 0 \\ \vdots \\ 0 \\ a_{M,1} \\ \vdots \\ a_{M,M} \end{bmatrix} \begin{matrix} \\ \\ \\ \}M-1 \\ \\ \\ \\ \\ \}M-1 \\ \\ \\ \\ \end{matrix} \begin{bmatrix} 1 \\ 0 \\ \vdots \\ 0 \\ \vdots \\ 0 \\ \vdots \\ 0 \end{bmatrix}$$

$$+ [a_{11}\,a_{12}\cdots a_{1M}\,\overbrace{0\cdots 0}^{M-1}\,a_{21}\,a_{22}\cdots a_{2M}\,\overbrace{0\cdots 0}^{M-1}\cdots a_{M,1}\cdots a_{MM}] \qquad (24)$$

and so on.

For example, in the expression (23)

$$J_{11} = \frac{\partial r_1}{\partial a_{11}} = [1\,0\,0\,0\,0] \begin{bmatrix} a_{11} \\ a_{12} \\ 0 \\ a_{21} \\ a_{22} \end{bmatrix} + [a_{11}\,a_{12}\,0\,a_{21}\,a_{22}] \begin{bmatrix} 1 \\ 0 \\ 0 \\ 0 \\ 0 \end{bmatrix} \qquad (25)$$

and so on. In this way one obtains easily for the Jacobian of (23):

$$\underline{\underline{J}} = \begin{bmatrix} 2a_{11} & 2a_{12} & 2a_{21} & 2a_{22} \\ a_{12} & a_{11} & a_{22} & a_{21} \\ 0 & a_{21} & a_{12} & 0 \\ a_{21} & a_{22} & a_{11} & a_{12} \\ a_{22} & 0 & 0 & a_{11} \end{bmatrix} \qquad (26)$$

The recursive procedure given by Eqs. (22) and (24) and illustrated for a 2 x 2 array in Eqs. (23) and (25), can be straightforwardly programmed in a computer. For an M x M object array, the product $\underline{\underline{J}}^T\underline{\underline{J}}$ contained in Eq. (17) is an $M^2 \times M^2$ matrix. This product and the subsequent inversion procedure can cause instability of the algorithm due to round-off errors for

M larger than a certain value (we have experienced this for $M > 5$ in a VAX-11/750). However, Moré's et al. subroutine LMSTR and other subroutines of MINPACK in ref. 15 control this and complete convergence is obtained. In the following section we describe our results with this subroutine to which we provide the system of non-linear equations and the Jacobian as described in Eqs. (22) and (24).

3. Numerical results

The performance of the L-M algorithm by using the LMSTR subroutine of ref. 15 is discussed here.

Tables 1 show two objects 5 x 5. Table 1a shows an object array with random elements, whereas Table 1b shows an object with a certain ordered structure. The reconstruction of these two objects by solving the system of non-linear equations (22)—41 equations and 25 unknowns—from the auto-correlation data without noise, is accurate 100% and perfect convergence is obtained in about 15 iterations. The time per iteration in a VAX 11/750 was about 2 sec. Apart from the correct solutions, trial and error with different random starts also provided, in each case, about another ten local minimum solutions completely different from these correct reconstructions. No positivity constraints were used, since no advantage was found in imposing them. In fact, the inclusion of positivity conditions introduces a non-linear constraint such that the convergence process becomes difficult to understand and in fact, it was observed to increase the number of local solutions.

For these small arrays the stability of the reconstruction versus the noise introduced in the autocorrelation data was found to be robust. Table 2 shows the autocorrelation of the object of Table 1a. Table 3a shows the reconstruction of the object of Table 1a by adding to the autocorrelation data of Table 2 a noise uniformly distributed with values between -5 and +5. Table 3b shows the reconstruction of the same object when the noise is uniformly distributed with values between -50 and +50. For a noise with values between -500 and +500 the reconstruction becomes poorer. Results for other 5 x 5 arrays are similar.

The number of local minimum solutions increases dramatically with the size of the array. Since L-S operates following the scheme of Eq. (4), the minimum of F which is closer to the starting guess is going to be encountered. This is illustrated with the 11 x 11 array of Table 4. For this size it took about six minutes per iteration and perfect convergence (in the sense that the successive iterations were exactly equal) was obtained in about seven iterations; from noiseless data, however, many trials with different starting guesses always gave local minima of F. If G is the value of the square root of F, and for the starting guess it was of the order of 10^6, all local minima were found at $G \simeq 10^5$ and, of course, these reconstructions were very far from the correct one. The autocorrelation arrays of these local minima were all similar to the correct one near the center but very different towards the borders. A Monte Carlo procedure allowed us to obtain a start as close to the correct solution as $G \simeq 29$, however the L-M algorithm got stuck in this start showing that it was already a local solution. In fact, in order to get an idea of how many local minima were existent also in regions of lower G and even near the correct solution for which $G = 0$, a starting guess equal to the correct solution perturbed by noise uniformly distributed between 0 and 1 was introduced in the L-M algorithm. After four or five iterations the algorithm got stuck without having substantially approached the correct solution. This suggests the existence of a "swarm" of local minima very close to the absolute minimum of F. In practice, if this region of F is reached, it will be very difficult to distinguish between these local solutions and also from the ideal noiseless correct reconstruction; of course the existence of noise in the autocorrelation data will always lead to these local minima if such low regions of G are found.

4. Conclusions

We have tested the performance of an important class of Newton methods--specifically the Levenberg-Marquardt modification of the Gauss-Newton algorighm for non-linear least square optimization--in the problem of phase retrieval for 2-D array objects.

Since this method leads directly to a minimum of the cost function and also is numerically stable and quadratically convergent, it provides, on the other hand, a good test of the complexity in the number of the local minima solutions. For small arrays the algorithm always worked, since a small number of local solutions was found. However, the algorithm showed a dramatic increase of the number of these local minima with the size of the array, showing the existence of swarms of local minima, both far and close to the correct global minimum solution.

Therefore, although much consideration has been paid to the ambiguity of the phase reconstruction problem, i.e. to the number of global minima of the cost function, and it has been shown that in 2-D there is likely to exist just one global minimum which constitutes the correct solution, the real practical problem that one has to overcome to establish an efficient algorithm to reconstruct an object from its autocorrelation data (or what is equivalent, to reconstruct the phase from the modulus of its spectrum) is that of developing a strategy to avoid the huge number of local minima of the cost function. This number seems to increase as one approximates the global minimum, and the practical uniqueness problem in 2-D is going to be the distinction between these and the correct solution. This distinction is going to be hard to make in the presence of noise in the data. A decomposition of the problem in small arrays would be obviously desirable, however we have been unable to

find a de-coupling of the unknowns in the set of non-linear equations that would make such decomposition possible.

Finally, it should be mentioned that by the time this work is finished a very interesting paper[16] has appeared presenting a successful reconstruction of a 32x32 object array from the zero location of the analytic continuation of 1-D strips of the object spectrum in the absence of noise. Its efficiency for real noisy data is under current investigation by those authors. It is worthwhile to remark, however, that the performance of the optimization method used in this paper should be investigated for 1-D strips of the object which would involve only M unknowns at each time. The number of local minima of the corresponding cost function will be much lower than in the case treated here. However a procedure similar to that of Ref.16 that eliminates the possible ambiguities by crossing strips in object space has yet to be found.

ACKNOWLEDGMENTS

The author would like to thank Dr. J. J. Moré for his help concerning the MINPACK subroutine. J. E. Dennis and J. L. Sanz also made helpful comments concerning the L-M algorithm, and useful discussions were held with B. J. Brames. Comments and hospitality from J. C. Dainty and E. Wolf made this work possible.

Research supported by the U.S. Air Force Office of Scientific Research, grant AFOSR-81-0003 and by the National Science Foundation.

* Also at the Institute of Optics, University of Rochester. Currently on leave from Instituto de Optica, CSIC, Serrano 121, Madrid 28006, Spain.

TABLES

1	3	7	18	9
7	1	35	12	2
20	10	1	9	6
18	31	7	15	20
6	40	1	20	25

Table 1a: An object with random values. The reconstruction from noiseless data is exactly coincident with this object.

50	50	50	50	50
50	0	0	0	50
50	0	50	0	50
50	0	0	0	50
50	0	50	0	50

Table 1b: An object with an orderer structure. The reconstruction from noiseless data coincides with this object.

25	95	236	633	718	496	771	468	54
195	240	1094	1798	1017	1990	1439	755	174
646	802	1079	2228	1746	1675	1717	1022	252
894	1722	1434	2835	3881	2411	2205	1633	331
653	2381	2129	3051	7126	3051	2129	2381	653
331	1633	2205	2411	3881	2835	1434	1722	894
252	1022	1717	1675	1746	2228	1079	802	646
174	755	1439	1990	1017	1798	1094	240	195
54	468	771	496	718	633	236	95	25

Table 2: Autocorrelation of the object of Table 1a.

1.009	3.010	7.003	18.003	9.019
7.022	1.004	35.005	12.004	1.996
19.997	9.999	1.002	8.993	6.003
18.019	31.010	6.999	15.000	20.005
5.996	39.984	0.945	19.978	24.998

Table 3a: Reconstruction of the object of Table 1a from the auto-correlation data plus a noise with values in the interval (-5, +5).

1.085	3.101	7.032	18.033	9.198
7.227	1.042	35.048	12.038	1.964
19.968	9.996	1.021	8.925	6.031
18.197	31.102	6.987	15.012	20.052
5.966	39.832	0.955	19.776	24.983

Table 3b: Reconstruction of the object of Table 1a from the auto-correlation data plus a noise with values in the interval (-50, +50).

0	1	4	25	7	6	1	2	49	33	56
4	2	29	36	74	2	14	0	3	68	12
35	44	51	12	17	27	2	30	78	14	1
14	80	26	4	98	19	42	38	2	0	13
6	14	13	23	45	23	12	30	3	89	67
0	26	12	14	80	12	33	16	23	2	23
49	2	11	33	16	1	14	12	57	78	32
15	1	10	2	1	0	16	1	67	93	23
0	3	5	45	36	80	34	79	12	98	0
23	19	32	0	44	34	2	49	16	64	2
5	23	43	51	6	17	31	95	33	0	56

Table 4: An 11 x 11 object array.

REFERENCES

1. J. R. Fienup, Opt. Lett. 3, 27 (1978).

2. J. R. Fienup, Appl. Opt. 21, 2758 (1982).

3. P. L. Van Hove, M. H. Hayes, J. S. Lim and A. V. Oppenheim, IEEE Trans. Acoust. Speech Signal Proc. ASSP-31, 1286 (1983).

4. Y. M. Bruck and L. G. Sodin, Opt. Commun. 30, 304 (1979).

5. M. H. Hayes and J. H. McClellan, Proc. IEEE 70, 197 (1982).

6. M. Nieto-Vesperinas and J. C. Dainty, Opt. Commun. 52, 94 (1984).

7. M. Nieto-Vesperinas and J. C. Dainty, J. Opt. Soc. Amer. (submitted).

8. R. Fletcher, 'Practical Methods of Optimization', Vol. 1 (J. Wiley, New York, NY, 1980).

9. J. E. Dennis Jr. and R. B. Schnabel, 'Numerical Methods for Unconstrained Optimization and Non-linear Equations' (Prentice Hall, New York, NY, 1983).

10. K. Levenberg, Quart. Appl. Math. 2, 164 (1944).

11. D. Marquardt, SIAM J. Appl. Math. 11, 431 (1963).

12. R. Barakat and G. Newsam, J. Opt. Soc. Amer. 70, 1255 (1980).

13. B. R. Frieden and D. G. Currie, J. Opt. Soc. Amer. 66, 1111 (1976).

14. J. J. Moré, in Numerical Analysis (G. A. Watson Ed.), Lecture Notes in Math. 630, 105-116 (Springer-Verlag, Berlin, 1977).

15. J. J. Moré, B. S. Garbow and K. E. Hillstrom, "User Guide for MINPACK-1", Argonne National Labs Report ANL-80-74 (1980).

16. H.V.Deighton, M.S.Scivier and M.A.Fiddy, Opt. Lett. 10,250 (1985).

S T E L L A R I N T E R F E R O M E T R Y

A Bibliography

Chris Dainty
The Institute of Optics
The University of Rochester
Rochester, NY 14627

Address from 1st January 1984:
Blackett Laboratory
Imperial College
London SW7 2BZ

July 1983

Aime, C.
Some Solar Granulation Observations using Speckle Interferometry Techniques
In Future Solar Optical Observations , Florance, 1978.

Aime, C.
Solar Seeing and the Statistical Properties of the Photospheric Granulation. I - Noise in Michelson and Speckle Interferometry.
Astron. and Astrophys. 47, 5-7 (1976)

Aime, C.
Interferometric Techniques Applied to High Resolution Observation of the Solar Granulation
IAU Colloquium #50, paper 30, Maryland 1978

Aime, C.
The Influence of Scanning Rate in Sequential Analysis of Fringes Produced by a Michelson Interferometer
Opt. Commun. 26, 139-142 (1978)

Aime, C. et al
Temporal Autocorrelation Functions of Solar Speckle Patterns
Opt. Commun., 39, 287-292 (1981)

Aime, C. et al
Measurements of Stellar Speckle Interferometry Lens-atmosphere Modulation Transfer Function
Optica Acta, 26, 575-581 (1979)

Aime, C. et al
One-Dimensional Telescope Aperture for Brightness and Velocity Speckle Interferometry Measurements
Opt. Engng., 22, 224-226 (1983)

Aime, C., et al.
Changes in the Atmosphere-Lens Modulation Transfer Function Used For Calibration in Solar Speckle Interferometry
J. Opt. Soc. Am. 68, 1063-1066 (1978)

Aime, C., C. Roddier, F. Roddier
Holographic Recording and Reconstruction of Astronomical Images in Imaging in Astronomy
Conference Preprints, Boston (June, 1975)

Aime, C., F. Roddier
Imaging Through Turbulence With Telescope Arrays
Opt. Commun. 19, 57-60 (1976)

Aime, C., F. Roddier
One Dimensional Stellar and Solar Speckle Interferometry
Opt. Commun. 21, 435-438 (1977)

Aime,C. and G. Ricort
Speckle Interferometric Techniques Applied To The Observation
Of Solar Photosphere
SPIE Seminar Proc., 243, 58-64 (1980)

Aitken, G. J. M., D. L. Desaulniers
Restoration of Atmospherically Degraded Images Using Complex
Spectral Ratios
Opt. Commun. 28, 26-29 (1979)

Aitken, G.J.M.
Split-band Interferomters
Opt. Commun., 40, 5-9 (1981)

Aitken, G.J.M., J.P. Corteggiani and J. Gay
Partially Redundant Apertures for Infrared Stellar Imaging
J. Opt. Soc. Am., 71, 759-763 (1981)

Allen, D.A., J.R. Barton and P.T. Wallace

Mon. Not. R. Astr. Soc., 196, 797-800 (1981)

Anderson, J. A.
Application of Michelson's Interferometer Method to the Measurement
of Close Double Stars
Astrophys. J. 51, 263-275 (1920)

Arnold, S. J., A. Boksenberg, W. L. W. Sargent
Measurement of the Diameter of Pluto by Speckle Interferometry
Astrophys. J., 234, L159-L163 (1979)

Arnot, N.R.
A Technique for Obtaining Diffraction Limited Pictures from a Single
Large-aperture Small-exposure Image
Opt. Commun. 45, 380-384 (1983)

Asakura, T., H. Fujii, K. Murata
Measurement of Spatial Coherence Using Speckle Patterns
Optica Acta 19, 273-290 (1972)

Bagnuolo, W.G.
Bates' Algorithm and Application to Capella
Mon. Not. R. Astro. Soc.

Baier, G., N. Hetterich and G. Weigelt
Digital Speckle Interferometry of Juno, Amphitrite and
Pluto's Moon Charon
ESO Messenger, 30, 23-26 (1983)

Baier,G.,J.Ebersberger,A.Lohmann,G.Weigelt
Applications of Digital and Optical-Digital Stellar Speckle Interferometry
SPIE Seminar Proc., 264, 58-63 (1980)

Baldwin, J. E., P. J. Warner
Phaseless Aperture Synthesis
Mon. Not. R. Astr. Soc. 182, 411-422 (1978)

Balega, Yv. Yv., N. A. Tikhonov
Speckle Interferometry of Some Bright Stars with the 6-Meter Telescope
Sov. Astron. Lett. 3, 272-273 (1977)

Barakat, R. and P. Nisenson
The Effectiveness of Astronomical Speckle Transfer Function Reweighting Algorithms
Opt. Commun., 45, 311-316 (1983)

Barnett, M. E., G. Parry
Photon Noise Limitations on the Recovery of Stellar Images by Speckle Interferometry
Opt. Commun. 21, 60-62 (1977)

Bates, R. H. T and P.T. Gough
New Outlook on Processing Radiation Received From Objects Viewed Through Randomly Fluctuating Media
IEEE Trans. Comp. c-24, 449-456 (1975)

Bates, R. H. T.
A Stochastic Image Restoration Procedure
Opt. Commun. 19, 240-244 (1976)

Bates, R. H. T.
Recovery of Fringe Visibility from Recorded Speckle Images Quantised to Two Levels
Mon. Not. R. Astr. Soc. 181, 365-374 (1977)

Bates, R. H. T.
Contributions to the Theory of Intensity Interferometry
Mon. Not. R. Astr. Soc. 142, 413-428 (1969)

Bates, R. H. T., M. J. Mcdonnell, P. Gough
Imaging through Randomly Fluctuating Media
Proc. IEEE 65, 138-143 (1977)

Bates, R. H. T., M. O. Milner, G. I. Lund, A. D. Seager
Towards High Resolution Imaging by Speckle Interferometry
Opt. Commun. 26, 22-26 (1978)

Bates, R. H. T., M. O. Milner
Towards Imaging of Star Clusters by Speckle Interferometry
Image Formation from Coherence Functions in Astronomy,
edited by C. van Schooneveld (D. Reidel, 1979) 187-193

Bates, R. H. T., P. Gough, P. J. Napier
Speckle Interferometry Gives Holographs of Multiple Star
Systems
Astron. and Astrophys. 22, 319-320 (1973)

Bates, R. H. T., P. J. Napier
Identification and Removal of Phase Errors in Interferometry
Mon. Not. R. Astr. Soc. 158, 405-424 (1972)

Bates, R.H.T.
Astronomical Speckle Imaging
Physics Reports, 90, 203-297 (1982)

Bates, R.H.T.
Uniqueness of Solutions to Two-Dimensional Fourier Phase Problems
for Localised and Positive Images
Comp. Graph. Image Proc., (1983)

Bates, R.H.T. and F.M. Cady
Towards True Imaging by Wideband Speckle Interferometry
Opt. Commun., 32, 365-369 (1980)

Bates, R.H.T. and W.R. Fright
Reconstructing Images from their Fourier Intensities
In Advances in Computer Vision and Image Processing, Vol.1,
(Ed. T.S. Huang) 1983

Bates, R.H.T. and W.R. Fright
A Composite Two-dimensional Phase Restoration Procedure
J. Opt. Soc. Am., 73, 358-365 (1983)

Bates, R.H.T., K.L. Garden and W.R. Fright
Fourier Phase Problems are Uniquely Solvable in more than One
Dimension : Parts 1 - 3
Optik, 61, 247-262 ; 62, 131-142 ; 62, 219-230 (1982)

Beckers, J.M.
Differential Speckle Interferometry
Opt. Acta, 361-362 (1982)

Beckers, J.M.
Differential Speckle Interferometry
Current Techniques in Double and Multiple Star Research,
IAU Collquium #62, Flagstaff, Az. May 1981.

Beckers, J.M.
Differential Speckle Interferometry : A New Tool for Double Star Research
IAU Coolquium #62, Flagstaff, 1981

Beddoes, D. R., J. C. Dainty, B. L. Morgan, R. J. Scaddan
Speckle Interferometry on the 2.5 mm Isaac Newton Telescope
J. Opt. Soc. Am. 66, 1247-1251 (1976)

Bender, P. L.
Effects of Ground Motions on Amplitude Interferometry
IAU Colloquium #50, paper 5, Maryland 1978

Bialetzki, J., A.W. Lohmann and G.P. Weigelt
Astro-speckle Interferometry with Multiple Mirror Telescopes
Optik, 53, 323-331 (1979)

Bialetzki,J. and G.P. Weigelt
Speckle Interferometry Measurements of Astronomical Objects With Simulated Multiple Mirror Telescopes
Optik, 55, 199-206 (1980)

Blazit, A., et al.
The Angular Diameters of Capella A and B From Two Telescope Interferometry
Astrophys. J. 217, L55-L57 (1977)

Blazit, A., D. Bonneau, L. Koechlin
Premier Resultats D'observation l'interferometre a deux telescopes
C. R. Acad. Sci. Paris 285B, 149-152 (1977)

Blazit, A., D. Bonneau, L. Koechlin, A. Labeyrie
The Digital Speckle Interferometer. Preliminary Results on S9 Stars and 3C273
Astrophys. J. 214, L79-L84 (1977)

Blazit, A., L. Koechlin, J. L. Oneto
Online Digital Correlation of Photon Counting TV Images for Stellar Interferometry
Image Processing Techniques in Astronomy (D. Reidel, Holland 1975)

Bohm,H.,A.W.Lohmann,G.P. Weigelt
Optical Processing of Optical Data
SPIE Seminar Proc., 232, 191-196 (1980)

Bonneau, D. and R. Foy
Interferometrie au 3.6 m CFH . I. Resolution du systeme Pluto-Charon
Astron. & Astrophys., 92, L1-L4 (1980)

Bonneau, D., A. Labeyrie
Speckle Interferometry: Color Dependent Limb Darkening Evidence on Alpha Orionis and Omicron Ceti
Astrophys. J. 181, L1-L4 (1973)

Bonneau,D. and R. Foy
Speckle Interferometric Observations of Binary Systems With The Haute-Provence 1.93m Telescope
Astron. Astrophys. 86, 295-298 (1980)

Bonneau,D.,A. Blazit,R. Foy,A.Labeyrie
Speckle Interferometric Measurements of Binary Stars
Astron.Astrophys. Suppl. Ser. 42, 185-188 (1980)

Bonneau,D.,M. Faucherre,L. Koechlin, F. Vakii
Observational Speckle Interferometry
SPIE Seminar Proc., 243, 80-82 (1980)

Brames, B.J. and J.C.Dainty
A Method of Determining Object Intensity Distributions in Stellar Speckle Interferometry
J. Opt. Soc. Am., 71, 1542-1545 (1981)

Breckinridge, J. B.
Coherence Interferometer and Astronomical Applications
Appl. Opt. 11, 2996-2998 (1972)

Breckinridge, J. B.
Obtaining Information Through the Atmosphere at the Diffraction Limit of a Large Aperture
J. Opt. Soc. Am. 65, 755-759 (1975)

Breckinridge, J. B.
A Two-Dimensional White Light Amplitude Interferometer
IAU Colloquium #50, paper 31, Maryland 1978

Breckinridge, J. B.
Interference in Astronomical Speckle Patterns
J. Opt. Soc. Am. 66, 1240-1242 (1976)

Breckinridge, J. B.
Measurement of the Amplitude of Phase Excursions in the Earth's Atmosphere
J. Opt. Soc. Am. 66, 143-144 (1976)

Breckinridge, J. B., H. A. McAlister, W. G. Robinson
Kitt Peak Speckle Camera
Appl. Opt. 18, 1034-1041 (1979)

Breckinridge, J.B.
Two-dimensional white light coherence interferometer
Appl. Opt., 13, 2760-2762 (1974)

Bridges, E. T., et al.
Coherent Optical Adaptive Techniques
Appl. Opt. 13, 291-300 (1974)

Brown, T. M.
Reconstruction of Turbulence-Degraded Images Using Nonredundant
Aperture Arrays
J. Opt. Soc. Am. 68, 883-889 (1978)

Bruck, Yu. M. and L.G. Sodin
On the Ambiguity of the Image Reconstruction Problem
Opt. Commun., 30, 304-308 (1979)

Bruck, Yu.M. and L.G. Sodin
Speckle Interferometry Image Reconstruction from the Fourier
Transform Phase
J. Opt. Soc. Am. (1983)

Bruck, Yu.M. and L.G. Sodin
A Method for Processing Speckle Images Requiring No Reference
Point Source
Astron. and Astrophys. 87, 188-191 (1980)

Burke, J. J., J. B. Breckinridge
Passive Imaging Through the Turbulent Atmosphere: Fundamental Limits
on the Spatial Frequency Resolution of a Rotational Shearing Interferometer
J. Opt. Soc. Am. 68, 67-77 (1978)

Cady, F.M. and R.H.T. Bates
Speckle Processing Gives Diffraction-limited True Images from
Severely Aberrated Instruments
Opt. Letters, 5, 438-440 (1980)

Cagnet, M.
Measures Interferometriques des Diametres Apparents Stellaires
Opt. Commun. 8, 430-434 (1973)

Chelli, A. et al
Modulation Transfer Function for Infra-red Stellar Speckle
Interferometry ; evidence for a log-normal statistic
Optica Acta, 26, 583-595 (1979)

Chelli, A., C. Perrier and Y.G. Biraud
One-Dimensional High Resolution Image Reconstruction on
Eta Carinae at 4.6 Microns with Speckle Data
Astron. Astrophys. (1983)

Chelli, A., P. Lena and F. Sibille
Angular Dimensions of Accreting Young Stars
Nature, 278, 143-146 (1979)

Christou, J. and S. P. Worden
The Diameter of ChiCygni given by Speckle Interferometry
Astron. J., 85, 302-304 (1980)

Christou,J.
Imaging ofStar Clusters From Speckle Interferometry
Opt. Commun., 37, 331 -334 (1981)

Cocke, W.J.
Computer Simulation Comparisons of Speckle Image Reconstruction
Techniques
SPIE Seminar Proc.,

Cole, T.W.
A Fast Real-time Processor for Speckle Interferometry
Proc. A.S.A., 4, 19-21 (1980)

Cole, T.W.
A Fast Real-time Processor for Speckle Interferometry
Proc. A.S.U., 4, 19-21 (1980)

Coulman, C. E.
Quantitative Treatment of "Seeing" in Syst. Design of Solar Astr. Telescopes
In Optical Instruments and Techniques, edited by Hone-Dickinson,
Oriel Press (UK), 1978

Coulman, C. E.
A Quantitative Treatment of Solar Seeing, II
Solar Phys. 34, 491-506 (1974)

Currie, D. G.
Amplitude Interferometry and High Resolution Image Information
Proc. of Optical Propagation Through Turbulence, Boulder, 1974

Currie, D. G.
On Astrometric Applications of the Very Long Baseline Amplitude
Interferometer
IAU Colloquium #50, paper 22, Maryland 1978

Currie, D. G.
On the Amplitude Interferometer Program at the University of Maryland
IAU Colloquium #50, paper 7, Maryland 1978

Currie, D. G.
The Development, Fabrication and Astronomical Application of a Wide-Band Long Baseline Optical Amplitude Interferometer
Tech. Rep. 77-075 University of Maryland (1977)

Currie, D. G.
Amplitude Interferometry on the Large Space Telescope
Tech. Rep. 77-056 University of Maryland (1977)

Currie, D. G., et al.
Stellar Disk Diameter Measurements by Amplitude Interferometry
Tech. Rep. 76-125 University of Maryland (1976)

Currie, D. G., S. L. Knapp, K. M. Wiewer
Four Stellar Diameter Measurements by a New Technique, Amplitude Interferometry
Astrophys. J. 187, 131-134 (1974)

Dainty, J. C.
Telescope Requirements for Speckle Interferometry in Optical Telescopes of the Future
ESO Conference, Geneva 1977

Dainty, J. C.
The Statistics of Speckle Patterns
Progress In Optics, Vol. 14, edited by E. Wolf (North-Holland, 1976)

Dainty, J. C.
Stellar Speckle Interferometry in Laser Speckle and Related Phenomena
Edited by J. C. Dainty (Springer-Verlag, 1975)

Dainty, J. C.
The Transfer Function, Signal-to-noise Ratio and Limiting Magnitude in Stellar Speckle Interferometry
Mon. Not. R. Astr. Soc. 169, 631-641 (1974)

Dainty, J. C.
Diffraction-limited Imaging of Stellar Objects Using Telescopes of Low Optical Quality
Opt. Commun. 7, 129-134 (1973)

Dainty, J. C.
Computer Simulations of Speckle Interferometry of Binary Stars in the Photon-counting Mode
Mon. Not. R. Astr. Soc. 183, 223-236 (1978)

Dainty, J. C., A. H. Greenaway
The Signal-to-Noise Ratio in Speckle Interferometry
IAU Colloquium #50, paper 23, Maryland 1978

Dainty, J. C., A. H. Greenaway
Estimation of Spatial Power Spectra in Speckle Interferometry
J. Opt. Soc. Am. 69, 786-790 (1979)

Dainty, J.C.
Stellar Speckle Interferometry
In Laser Speckle and Related Phenomena, Edited by J.C. Dainty
Springer-Verlag, 2nd. Edition, 1983

Dainty, J.C.
Speckle Interferometry in Astronomy
In Symposium on Recent Advances in Astronomy, Ensenada, Mexico,
1981 pp5=11. Eds: H.L. Johnson and C. Allen.

Dainty, J.C. and R.J. Scaddan
Measurements of the Atmospheric Transfer Function at Mauna Kea, Hawaii
Mon. Not. R. Astr. Soc. 170, 519-532 (1975)

Dainty, J.C., D.R. Hennings and K.A. O'Donnell
Space-time Correlation of Stellar Speckle Patterns
J. Opt. Soc. Am., 71, 490-492 (1981)

Davies, C.L. et al
The Use of a CCD in the Reduction of Speckle Interferometry Data
"Photoelectronic Imaging Devices", London, Sept.1978 (Academic
Press)

Davis, J.
An 11 Metre Michelson Stellar Interferometer
NZ J. Science, 22, 431-455 (1983)

Davis, J.
A Prototype II Meter Modern Michelson Stellar Interferometer
IAU Colloquium #50, paper 14, Maryland 1978

Davis, J.
The Application of High Angular Resolution Stellar Interferometry to
the Study of Single Objects in the Visible Region of the Spectrum
IAU Colloquium #50, paper 1, Maryland 1978

Davis, J.
High Angular Resolution Stellar Interferometry
Proc. Astr. Soc. Australia 3, 26-32 (1976)

Deitz, P.H.
Image Information by Means of Speckle-Pattern Processing
J. Opt. Soc. Am. 65, 279-285 (1975)

Deitz, P.H., P. F. Carlson
Spatial Irradiance Interferometry with Sources of Arbitrary Symmetry
J. Opt. Soc. Am. 64, 11-17 (1975)

Deron, R. and J.C. Fontanella
Uncertainty on Phase Reconstruction using the Knox-Thompson Algorithm
OSA Topical Meeting on Image Proc in Astron, Minn., June 1983

Dyck, H.M. and R.R. Howell
Speckle Interferometry of Molecular Cloud Sources at 4.8 Microns
Astron. J., 87,400-405 (1982)

Dyck, H.M., S. Beckwith and B. Zuckerman
Speckle Interferometry of IRC+10216 in the Fundamental Vibration-Rotation Lines of CO
Astrophys. J. (in press)

Dyck, H.M., T. Simon and B. Zuckerman
Discovery of an Infrared Companion to T-Tauri
Astron. J. (in press)

Dyson, F. J.
Photon Noise and Atmospheric Noise in Active Optical Systems
J. Opt. Soc. Am. 65, 551- 558 (1975)

Ebersberger, J. and G.P. Weigelt
Speckle Interferometry and Speckle Holography with the 1.5 and 3.6m ESO telescopes
The Messenger, #18, 24-27 (1979)

Englander, A.
Probabalistic Diffraction Limited Imaging through Turbulence
Opt. Engng., 22, 143-148 (1983)

Estes, L. E., R. Boucher
Temporal- and Spatial-Intensity-Interferometer Imaging Through a Random Medium
J. Opt. Soc. Am. 65, 760-764 (1975)

Fante, R. L.
Some Results on the Imaging of Incoherent Sources Through Turbulence
J. Opt. Soc. Am. 66, 574-580 (1976)

Fante, R. L.
On the Imaging of Incoherent Objects in a Turbulent Medium
Afcrl-Tr-75-0546 (1975)

Fante, R.L.
Comments on a Method for Processing Stellar Speckle Data
J. Opt. Soc. Am., 69, 1394-1396 (1979)

Fienup, J. R.
Space Object Imaging Through the Turbulent Atmosphere
Opt. Engng., 18, 529-534 (1979)

Fienup, J. R.
Reconstruction of an Object from the Modulus of its Fourier Transform
Opt. Lett. 3, 27-29 (1978)

Fienup, J. R.
Iterative Method Applied to Image Reconstruction and to Computer-Generated Holograms
SPIE Seminar Proc. 207-02 and Opt. Engrg. (1980)

Fienup, J.R.
Fourier Modulus Image Construction
RADC-TR-81-63 (May, 1981) (Rome Air Development Center, Griffiss AFB, NY 13441)

Fienup, J.R.
Phase Retrieval Algorithms : a Comparison
Appl. Opt.,21, 2758-2769 (1982)

Fienup,J.R.,G.B. Feldkamp
Astronomical Imaging By Processing Stellar Speckle Interferometry Data
SPIE Seminar Proc., 243, 95-102 (1980)

Finsen, W. S.
Twenty Years of Double-Star Interferometry and its Lessons
Astrophys. and Space Sci. 11, 13-19 (1971)

Finsen, W. S.
Interferometer Observation of Binary Stars
Astron. J. 69, 319-324 (1964)

Fizeau
Report on the Prix Bordin (in French)
Compt. Rend., 66, 932-934 (1868)

Foy, R et al
Angular Diameter of IRC+10216, Mira, R Cas and GL2591 in the Near Infrared
Astron. Astrophys., 79, L3-L8 (1979)

Fried, D. L.
Angular Dependence of Atmospheric Turbulence Effect in Speckle Interferometry
IAU Colloquium #50, paper 26, Maryland 1978

Fried, D. L.
The Nature of Atmospheric Turbulence Effects of Imaging and Pseudo-Imaging Systems, and Its Quantification
IAU Colloquium #50, paper 4, Maryland 1978

Fried, D.L.
Angular Dependence of the Atmospheric Turbulence Effect in Speckle Interferometry
Optica Acta, 26, 597-613 (1979)

Fried, D.L.
Analysis of Techniques for Imaging through the Atmosphere
RADC-TR-78-285 (1979)

Fright, W.R. and R.H.T. Bates
Fourier Phase Problems are Uniquely Solvable in more than One Dimension III
Optik, 62, 219-230 (1982)

Frost, R. L., C. K. Rushforth, B. S. Baxter
Fast FFT-Based Algorithm for Phase Estimation in Speckle Imaging
Appl. Opt. 18, 2056-2061 (1979)

Garden, K.L. and R.H.T. Bates
Fourier Phase Problems are Uniquely Solvable in more than One Dimension II
Optik, 62, 131-142 (1982)

Gezari, D. Y., A. Labeyrie, R. V. Stachnik
Speckle Interferometry: Diffraction Limited Measurements of Nine Stars with the 200-inch Telescope
Astrophys. J. 173, L1-L5 (1972)

Golay, M.J.E.
Point Arrays having Compact, Nonredundant Autocorrelations
J. Opt. Soc. Am., 61, 272-273 (1971)

Goodman, J. W.
Analogy Between Holography and Interferometric Image Formation
J. Opt. Soc. Am. 60, 506-509 (1970)

Goodman, J. W., J. F. Belsher
Fundamental Limitations in Linear Invariant Restoration of Atmospherically Degraded Images
SPIE Seminar Proc. 75, 141-154 (1976)

Gough, P. T., R. H. T. Bates
Speckle Holography
Optica Acta 21, 243-254 (1974)

Greenaway, A. H.
The Phase Problem in Astronomy
Presented at Bordeaux Conference, 1979

Greenaway, A. H.
The Potential of a Telescope Array for Long-Baseline Michelson Interferometry with Two or More Large Telescopes
Kitt Peak Report, 1978

Greenaway, A. H.
The Interferometric Observing Efficiency of Arrays of Large Aperture Telescopes
Opt. Commun. 29, 279-283 (1979)

Greenaway, A. H., C. Roddier
A 180-degree Rotation Shearing Interferometer with Increased Optical Efficiency
Opt. Commun., 32, 48-50 (1980)

Greenaway, A. H., J. C. Dainty
The Formal Equivalence Between Autocorrelation and Power Spectral Analysis of Photon-Limited Data
Opt. Commun., 35, 307-310 (1980)

Greenaway, A. H., J. C. Dainty
On Long-Baseline Amplitude Interferometers in Astronomical Applications
Optica Acta 25, 181-189 (1978)

Greenaway, A.H.
Diffraction Limited Pictures from a Single Turbulence-Degraded Image in Astronomy
Opt. Commun., 42, 157-161 (1982)

Greenaway, A.H.
The Signal-to-noise Ratio in Long Baseline Stellar Interferometry
Optica Acta, 26, 1147-1171 (1979)

Greenaway, A.H.
Interferometry with Arrays of Large Aperture Telescopes
"Optical and Infrared Telescopes for the 1990s",
KPNO, 1980.

Greenaway, A.H.
Isoplanatism in Speckle Interferometry and Adaptive Optics
"Solar Instrumentation - What's Next ? ", Sunspot, NM, 1980

Hanbury Brown, R.
Intensity Interferometry versus Michelson Interferometry
Optical Telescopes of the Future, CERN, Geneva 1977

Hanbury Brown, R.
The Intensity Interferometer
Taylor and Francis (London) 1974

Hanbury Brown, R.
A Review of the Achievements and Potential of Intensity Interferometry
IAU Colloquium #50, paper 11, Maryland 1978

Hanbury Brown, R., J. Davis, L. R. Allen
The Stellar Interferometer at Narrabri Observatory
Mon. Not. R. Astr. Soc. 137, 375-392 and 393-417 (1967)

Hanbury Brown, R., J. Davis, R. J. W. Lake, R. J. Thompson
The Effects of Limb Darkening on Measurements of Angular Size
with an Intensity Interferometer
Mon. Not. R. Astr. Soc. 167, 475-484 (1974)

Hanbury Brown, R., J. Davis, L. R. Allen
The Angular Diameters of 32 Stars
Mon. Not. R. Astr. Soc. 167, 121-136 (1974)

Hanbury Brown, R., R. Q. Twiss
Interferometry of the Intensity Fluctuations in Light
Proc. Roy. Soc. A242, 300-324 (1957), A243, 291-319 (1957)
and A248, 199-221 (1958)

Hardy, J. W., E. P. Wallner
Active Control for Michelson Stellar Interferometers
IAU Colloquium #50, paper 10, Maryland 1978

Harvey, J. W., J. B. Breckinridge
Solar Speckle Interferometry
Astrophys. J. 182, L137-L139 (1973)

Harvey, J. W., M Schwartschild
Photoelectric Speckle Interferometry of the Solar Granulation
Astrophys. J. 196, 221-226 (1975)

Hege, E.K. et al
Speckle Interferometry Observations of the Triple QSO
PG 1115+08
Astrophys. J., 248, L1-L3 (1981)

Hege, E.K., E.N. Hubbard and P.A. Strittmatter
An Intensified Event-detecting Television System for
Astronomical Speckle Interferometry
SPIE Seminar Proc., 264, 29-33 (1980)

Heide, K von der
Image Restoration by the Method of Least Squares
Astron. Astrophys., 70, 777-784 (1978)

Howell, R.
Near Infrared Interferometry of the Galilean Satellites
IAU Colloquium #50, paper 17, Maryland 1978

Howell, R.R., D.W. McCarthy and F.J. Low
One-Dimensional Infrared Speckle Interferometry
Astrophys. J., 251, L21-L25 (1981)

Hubard, G., et al.
Speckle Interferometry I: The Steward Observatory Speckle Camera
Astron. J.84, 1437- (1979)

Hubard, G., et al.
Digital Speckle Interferometry to Measure the Angular Diameters of
Faint Objects
IAU Colloquium #50, paper 28, Maryland 1978

Hufnagel, R. E., N. R. Stanley
Modulation Transfer Function Associated with Image Transmission
Through Turbulent Media
J. Opt. Soc. Am. 54, 52-61 (1964)

Hughes, D.W.
Speckle Interferometry of Pluto
(a news report)
Nature, 284, 123 (1980)

Huiser, A.M.J.
A Procedure to Correct the Images of Astronomical Objects for the
Distortions due to Atmospheric Turbulence
Opt. Commun., 42, 226-230 (1982)

Hunt, B. R.
Matrix Formulation of the Reconstruction of Phase Values from
Phase Differences
J. Opt. Soc. Am. 69, 393-399 (1979)

Hunt, B.R., W.R. Fright and R.H.T. Bates
Analysis of the Shift and Add Method for Imaging through
Turbulent Media
J. Opt. Soc. Am., 73, 456-465 (1983)

Itoh, K.
Analysis of the Phase Unwrapping Algorithm
Appl. Opt., 21, 2470 - (1982)

Itoh, K. and Y. Ohtsuka
Photon Noise Limitations in Wavefront Folding Interferometry
J. Opt. Soc. Am., 73, 479-485 (1983)

Itoh, K. and Y. Ohtsuka
Interferometric Image Reconstruction through the Turbulent Atmosphere
Appl. Opt., 20, 4239-4244 (1981)

Itoh,K., Y. Ohtsuka
Spatial Coherence Measurements Through Turbulent Atmosphere Using a Computer Aided Interferometer
Optics Commun., 36, 250-254 (1980)

Johnson, M. A., A. L. Betz, C. H. Townes
Ten Micron Heterodyne Stellar Interferometer
Phys. Rev. Lett. 33, 1617-1620 (1974)

Karo, D. P., A. M. Schneiderman
Speckle Interferometry at Finite Bandwidths and Exposure Times
J. Opt. Soc. Am. 68, 480-485 (1978)

Karo, D. P., A. M. Schneiderman
Transfer Functions, Correlation Scales and Phase Retrieval in Speckle Interferometry
J. Opt. Soc. Am. 67, 1583-1587 (1977)

Karo, D. P., A. M. Schneiderman
Speckle Interferometry with Severley Aberrated Telescopes
J. Opt. Soc. Am. 67, 1277-1278 (1977)

Karo, D. P., A. M. Schneiderman
Speckle Interferometry Lens-Atmosphere MTF Measurements
J. Opt. Soc. Am. 66, 1252-1256 (1976)

Karo, D. P., A. M. Schneiderman
Image Reconstruction in Speckle Interferometry
Imaging in Astronomy, Conference Preprints, Boston, June 1975

Karo, D.P. and A.M. Schneiderman
Laboratory Simulation of Stellar Speckle Interferometry
Appl. Opt., 18, 828-833 (1979)

Kenknight, C. E.
A Statistical Method for the Post-Detection Compensation for Atmospheric Distortions of Images of Faint Scenes
SPIE Seminar Proc. 75, 163-167 (1976)

Kenknight, C. E.
Autocorrelation Methods to Obtain Diffraction Limited Resolution with Large Telescopes
Astrophys. J. 176, L43-L45 (1972)

Klemperer, W. K.
Non-Redundant Phased-Array Radar
IEEE (UK) Conference Publication #105, 74-80 (1973)

Knox, K. T.
Image Retrieval from Astronomical Speckle Patterns
J. Opt. Soc. Am. 66, 1236-1239 (1976)

Knox, K. T., B. J. Thompson
New Methods of Processing Speckle Pattern Star Images
Astrophys. J. 182, L133-L136 (1973)

Knox, K. T., B. J. Thompson
Recovery of Images from Atmospherically Degraded Short-Exposure Images
Astrophys. J. 193, L45-L48 (1974)

Koechlin, L.
Proposals for Phase Recovery in High Resolution Techniques
Optical Telescopes of the Future, CERN, Geneva 1977

Koechlin, L.
Observational Speckle Interferometry
IAU Colloquium #50, paper 24, Maryland 1978

Koechlin, L.
Amplitude Interferometry at CERGA
IAU Colloquium #50, paper 9, Maryland 1978

Koechlin, L., D. Bonneau and F. Vakili
Detection d'un effet de phase a l'interferometre du CERGA, application du movement de Capella
Astron. Astrophys., 80, L13-14 (1979)

Korff, D.
Analysis of a Method for Obtaining Near-Diffraction-Limited Information in the Presence of Atmospheric Turbulence
J. Opt. Soc. Am. 63, 971-980 (1973)

Korff, D., G. Dryden, M. G. Miller
Information Retrieval from Atmospheric Induced Speckle Patterns
Opt. Commun. 5, 187-192 (1972)

Korff, D., G. Dryden, R. P. Leavitt
Isoplanicity: The Translation Invariance of the Atmospheric Green's Function
J. Opt.Soc. Am. 65, 1321-1330 (1975)

Kulagin, E.S.
A Variant of Michelson's Stellar Interferometer
Opt. Spectrosc., 23, 459-460 (1967)

Kulagin, E.S.
Measurements of Capella with the Pulkovo stellar interferometer
Sov. Astron., 14, 145-147 (1970)

Kulagin, E.S.
A Superposed-ray Interferometer
Sov. Astron., 13, 1023-1028 (1970)

Labeyrie, A.
Speckle Interferometer for 0.02 arc sec Stellar Resolution
Auxillary Instrumentation for Large Telescopes, ESO/CERN, May 1972

Labeyrie, A.
Attainment of Diffraction-Limited Resolution in Large Telescopes by Fourier Analysing Speckle Patterns in Large Telescopes
Astron. and Astrophys. 6, 85-87 (1970)

Labeyrie, A.
Coherent Arrays
Optical Telescopes of the Future, ESO/CERN, Geneva 1977

Labeyrie, A.
High-Resolution Techniques in Optical Astronomy
Progress in ptics, edited by E. Wolf (North-Holland, 1976)

Labeyrie, A.
Interference Fringes Obtained on Vega with Two Optical Telescopes
Astrophys. J. 196, L71-L75 (1975)

Labeyrie, A.
Observations Interferometriques au Mont Palomar
Nouv. Rev. Optique 5, 141-151 (1974)

Labeyrie, A.
Speckle Interferometry
The Messenger No. 15, 9-11 (1979)

Labeyrie, A.
Stellar Interferometry Methods
Ann. Rev. Astron. Astrophys. 16, 77-102 (1978)

Labeyrie, A.
Post-Detection Interferometer Image Processing
Optical Telescopes of the Future, ESO/CERN, Geneva 1977

Labeyrie, A., et al.
strong TiO-Related Variations in the Diameters of Mira and R Leonis
Astrophys. J. 218, L75-L78 (1977)

Labeyrie, A., D. Bonneau, R. V. Stachnik, D. Y. Gezari
Speckle Interferometry III: High Resolution Measurements on Twelve
Close Binary Systems
Astrophys. J. 194, L147-L151 (1974)

Lamy, P., and S. Koutchmy
Infrared Imaging and Speckle Observations with a TV Camera
ESO Messenger (1981)

Lena, P.
Observational Techniques in Infrared Astronomy
In Infrared Astronomy , edited by G. Setti and G.G. Fazio,
D. Reidel, Holland (1978)

Liewer, K. M.
The Prototype Vary Long Baseline Amplitude Interferometer
IAU Colloquium #50, paper 8, Maryland 1978

Linfoot, E. H., R. C. Witcomb
Random Wave-front Perturbations and Telescope Star Images
Mon. Not. R. Astr. Soc. 158, 199-231 (1972)

Lippincott, S.L., D. Braun and D.W. McCarthy
Astrometric and Infrared Speckle Analysis of the Visually
Unresolved Binary BD+41 328
Publ. Astr. Soc. Pac., 95, 271-274 (1983)

Liu, Y. C., A. Lohmann
High Resolution Image Formation Through the Turbulent Atmosphere
Opt. Commun. 8, 372-377 (1973)

Lohmann, A. W., G. P. Weigelt
Astronomical Speckle Interferometry: Measurements of Isoplanicity and of Temporal Correlation
Optik 53, 167-180 (1979)

Lohmann, A. W., G. P. Weigelt
Image Reconstruction from Astronomical Speckle Interferograms
Optical Telescopes of the Future, ESO/CERN, Geneva 1977

Lohmann, A.W. and G.P. Weigelt
Image Restoration of ST Photographs
ESA/ESO Workshop on Astronomical Uses of the ST, Geneva, 1979

Low, F. J.
The Astronomical Potential of Spatial Interferometry in the Infrared
IAU Colloquium #50, paper 2, Maryland 1978

Low, F. J.
Incoherent Infrared Spatial Interferometry
IAU Colloquium #50, paper 15, Maryland 1978

Lynds, C. R., S. P. Worden, J. W. Harvey
Digital Image Reconstruction Applied to Alpha Orionis
Astrophys. J. 207, 174-180 (1976)

Mariotti, J. M. et al
Infrared Speckle Imaging : Improvement of the Method - Results on Miras and Protostars
Astron. Astrophys. (1983)

Martin, F., J. Borgnino, F. Roddier
Localisation de Couches Turbulentes Atmospheriques par Traitment Optiques de Clinches d'ombres Volantes Stellaires
Nouv. Rev. Optiques 6, 15-23 (1975)

McAlister, H. A.
Spectroscopic Binaries as a Source for Astronomic and Speckle Interferometric Studies
Publ. Astr. Soc. Pac. 88, 317-322 (1976)

McAlister, H. A.
Speckle Interferometry of Eta Orionis
Publ. Astr. Soc. Pac. 88, 957-959 (1976)

McAlister, H. A.
Speckle Interferometry of the Hyades Spectroscopic Binary 51 Tauri
Astrophys. J. 212, 459-461 (1977)

McAlister, H. A.
Speckle Interferometric Measurements of Binary Stars II
Astrophys. J., 225, 932-938 (1978)

McAlister, H. A.
Masses and Luminosities for the Spectroscopic/Speckle Interferometric Binary 12 Persei
Astrophys. J, 223, 526-529 (1978)

McAlister, H. A.
Binary Stars Unresolved by Speckle Interferometry
Publ. Astr. Soc. Pac.,90, 288-296 (1978)

McAlister, H. A.
High Angular Resolution Binary Star Interferometry
IAU Colloquium #50, paper 3, Maryland 1978

McAlister, H. A.
Speckle Interferometric Measurement of Binary stars I
Astrophys. J. 215, 159-165 (1977)

McAlister, H. A.
Speckle Interferometry as a Method of Detecting Nearby Extrasolar Planets
Icarus 30, 789-792 (1977)

McAlister, H. A.
Binary Star Speckle Interferometry
Sky and Telescope 53, 346-350 (1977)

McAlister, H. A.
Speckle Interferometric Measurements of Binary Stars IV
Astrophys. J. 230, 497-501 (1979)

McAlister, H. A., K. A. DeGioia
Speckle Interferometric Measurements of Binary Stars III
Astrophys. J. 228, 493-496 (1979)

McAlister, H.A.
Accuracy of Binary Star Speckle Interferometry
In Modern Astrometry , IAU Colloquium #48, Edited by Prochazka and Tucker, University Observatory, Vienna (1978)

McAlister, H.A.
Speckle Interferometry of the Spectroscopic Binary 17 ksi Cephei A
Astrophys. J, 236, 522-525 (1980)

McAlister, H.A.
Speckle Interferometry Of The Spectroscopic/Astrometric Binary Chi Draconis
Astron. J., 85, 1265-1269 (1980)

McAlister, H.A.
The Apparent Orbit of Capella
Astron. J., 86, 795-799 (1981)

McAlister, H.A.
Speckle Interferometry of Tau Persei
Astron. J., 86, 1397-1400 (1981)

McAlister, H.A. and E.M. Hendry
Binary Stars Unresolved by Speckle Interferometry. II.
Publ. Astro. Soc. Pac., 93, 221-224 (1981)

McAlister, H.A. and W.J. Hartkopf
Speckle Interferometry of the Spectroscopic Binary 94 Aquarii A
Publ. Astr. Soc. Pac., 94, 832-834 (1982)

McCarthy, D. W.
Interferometric Measurements of Flattened Circumstellar Envelopes
IAU Colloquium #50, paper 18, Maryland 1978

McCarthy, D. W., F. J. Low
Initial Results of Spatial Interferometry at 5 Microns
strophys. J. 202, L37-40 (1975)

McCarthy, D. W., F. J. Low, R. Howell
Angular Diameter Measurements of Alpha Orionis, VY Canis Majoris and IRC+10216 at 8.3, 10.2 and 11.1 Micrometers
Astrophys. J. 214, L85-89 (1977)

McCarthy, D.W.
Near-Infrared Imaging of Unseen Companions to Nearby Stars
Procedings of IAU Colloquium #76, The Nearby Stars and The Stellar Luminosity Function

McCarthy, D.W.
Triple Structure of Infrared Source 3 in the Monoceros R2 Molecular Cloud
Astrophys. J., L93-97 (1982)

McCarthy, D.W. et al
Infrared Speckle Interferometry of the Nucleus of NGC1068
Astrophys. J., 257, L7-L11 (1982)

McCarthy, D.W. et al
Infrared Detection of the Low-mass Companion to zeta Aquarii B
Astrophys. J., 257, L75-78 (1982)

McCarthy, D.W. et al
The Performance of the Multiple Mirror Telescope : VIII. The MMT as an Optical-Infrared Interferometer and Phased Array
Proc. S.P.I.E., 332, 57-65 (1982)

McCarthy, D.W., F.J. Low and R. Howell
Infrared Spatial Interferometry : Present Status and Future Plans
Proc. S.P.I.E., 172, 140-148 (1979)

McCarthy, D.W., F.J. Low and R.R. Howell
Design and Operation of an Infrared Spatial Interferometer
Opt. Engng., 16, 569-574 (1977)

McCarthy, D.W., R. Howell and F.J. Low
Apparent Variation in the Diameter of o-Ceti at 10.2 Microns
Astrophys. J., 223, L113-116 (1978)

McDonnell, M. J., R. H. T. Bates
Digital Image Restoration of an Image of Betelgeuse
Astrophys. J. 208, 443-452 (1976)

Meaburn, J. et al
Speckle Observations of the Nucleus of NGC1068
Nature, 296, 331-334 (1982)

Mertz, L. N.
Speckle Imaging, Photon by Photon
Appl. Opt. 18, 611-614 (1979)

Mertz, L., T.D. Tarbell and A. Title
Low Noise Imaging Photon Counter for Astronomy
Appl. Opt., 21, 628-634 (1982)

Michelson, A. A.
On the Application of Interference Methods to Astronomical Methods
Phil. Mag. (5), 30, 1-20 (1890)

Michelson, A. A.
On the Application of Interference Methods to Astronomical Measurements
Astrophys. J. 51, 257-262 (1920)

Michelson, A. A., F. G. Pease
Measurement of the Diameter of Alpha Orionis with the Interferometer
Astrophys. J. 53, 249-259 (1921)

Michelson, A.A.
Measurement of Jupiter's Satellites by Interference
Nature, 45, 160-161 (1891)

Miller, M. G.
Noise Considerations in Stellar Speckle Interferometry
J. Opt. Soc. Am. 67, 1176-1184 (1977)

Miller, M. G., A. Schneiderman, P. F. Keller
Comparison of Methods for Processing Short-Exposure Data from Large Telescopes
Astrophys. J. 186, L91-L94 (1973)

Miller, M. G., D. Korff
Resolution of Partially Coherent Objects by Use of Speckle Interferometry
J. Opt. Soc. Am. 64, 155-161 (974)

Miller, M. G., P. F. Keller
Astronomical Differential Angle of Arrival Measurements
Imaging in Astronomy, Conference Preprints, Boston, June 1975

Miller, R. H.
Measurement of Stellar Diameters
Science 153, 581-587 (1966)

Miller, R. H.
A 100 Meter Michelson Interferometer
Aura Eng. Tech. Report #40, KPNO (1971)

Morgan, B. L., et al.
Observations of Binary Stars by Speckle Interferometry
Mon. Not. R. Astr. Soc., 183, 701-710 (1979)

Morgan, B.L. et al
Observations of Binary Stars by Speckle Interferometry III
Mon. Not. R. Astr. Soc., 198, 817-824 (1982)

Morgan, B.L., G.K. Beckmann and R.J. Scaddan
Observations of Binary Stars by Speckle Interferometry -II
Mon. Not. R. Astr. Soc., 192, 143-151 (1980)

Murty, M. V. R. K.
Interference Between Wavefronts Rotated or Reversed with Respect to Each Other and its Relation to Spatial Coherence
J. Opt. Soc. Am. 54, 1187-1190 (1964)

Nelson, M. R.
Computer Controlled Photometer for Speckle Interferometry
Image Processing Techniques in Astronomy, (D. Reidel, Holland, 1975)

Nisenson, P., D. C. Ehn, R. V. Stachnik
Astronomical Speckle Imaging
SPIE Seminar Proc. 75, 83-88 (1976)

Nisenson, P., R. Stachnik and C Papaliolios
High Resolution Imaging at Large Telescopes
Proceedings of "Optical and Infrared Telescopes for the 1990s"
KPNO, 1980

Nisenson, P., R. V. Stachnik
Restoration of Turbulence-Degraded Images, a Review
IAU Colloquium #50, paper 34, Maryland 1978

Nisenson, P., R. V. Stachnik
Measurements of Atmospheric *Isoplanatism Using Speckle Interferometry*
J. Opt. Soc. Am. 68, 169-175 (1978)

Nisenson, P., R. V. Stachnik
Real-Time Speckle Imaging
Imaging in Astronomy, Conference Preprints, Boston, June 1975

Nisenson,P., R. Stachnik,C. Papaliosios, P. Horowitz
Data Recording and Processing for Speckle Image Reconstruction
SPIE Seminar Proc., 243, 88-94 (1980)

O'Donnell, K. A., J. C. Dainty
Space-Time Analysis of Photon-Limited Stellar Speckle Interferometry
J. Opt. Soc. Am., 70, 1354-1361 (1980)

O'Donnell, K.A., B.J. Brames and J.C. Dainty
Measurements of the Spatial-Temporal Statistics of Stellar Speckle Patterns at Mauna Kea, Hawaii
Opt. Commun., (in press)

Papaliolios, C. and L. Mertz
A New Two-Dimensional Photon Camera
Proc. S.P.I.E., 331, 360-365 (1982)

Parry, G., J. G. Walker, R. J. Scaddan
On the Statistics of Stellar Speckle Patterns and Pupil Plane Scintillation
Optica Acta, 26, 563-574 (1979)

Pease, F. G.
The New Fifty-Foot Stellar Interferometer
Sci. Am. 143, 290-294 (1930)

Pease, F. G.
Interferometer Methods in Astronomy
Ergebn. Exacten. Naturwiss. 10, 84-96 (1931)

Pease, F.G.
The Fifty-foot Interferometer Telescope
Armour Engineer, , 125-130 (1925)

Perrier, C.
An Infrared Speckle Interferometer
ESO Messenger, (1981)

Platt, J. R.
Increase of Telescope Resolution with Time Selection and an Image Forming Stellar Interferometer
Journal not known

Pohle, R. H.
The Amplitude Interferometry, Speckle Interferometry and Laser Correlography Systems: A Sensor System Comparison
ARPA Order #1443

Pollaine, S., et al.
Measurement of the Size of the Isoplanatic Patch Using a Phase-Correcting Telescope
J. Opt. Soc. Am. 69, 84-89 (1979)

R.H.T. Bates and W.R. Fright
Towards Imaging with a Speckle Interferometric Optical Synthesis Telescope
Mon. Not. R. Astr. Soc., 198, 1017-1031 (1982)

Readhead, A.C.S. et al
Mapping Radio Sources with Uncalibrated Visibility Data
Nature, 285, 137-140 (1980)

Ribak,E. and S.G. Lipson
Complex Spatial Coherence Function: Its Measurement By Means Of Phase Modulated Shearing Interferometer
Appl. Opt., 20, 1102-1106 (1981)

Rimmer, M. P.
Method for Evaluating Lateral Shearing Interferograms
Appl. Opt. 13, 623-629 (1974)

Roddier, C.
Measurements of the Atmospheric Attenuation of the Spectral Components of Astronomical Images
J. Opt. Soc. Am. 66, 478-482 (1976)

Roddier, C. et al
Twin-image Holography with Spectrally Broad Light
J. Optics (Paris), 11, 149-152 (1980)

Roddier, C., F. Roddier
Seeing Effects Removal in a Michelson Stellar Interferometer
J. Opt. Soc. Am. 66, 1347-1350 (1976)

Roddier, C., F. Roddier
Imaging with a Coherence Interferometer
Image Formation from Coherence Functions in Astronomy, edited by C. van Schooneveld (D. Reidel, 1979) 175-185

Roddier, C., F. Roddier
Correlation Measurements on the Complex Amplitude of Stellar Plane Waves Perturbed by Atmospheric Turbulence
J. Opt. Soc. Am. 63, 661-663 (1973)

Roddier, C., F. Roddier
On the Fringe Visibility in a Michelson Interferometer
J. Opt. Soc. Am. 66, 580-584 (1976)

Roddier, C., F. Roddier
Influence of Exposure Time on Spectral Properties of Turbulence-Degraded Astronomical Images
J. Opt. Soc. Am. 65, 664-667 (1975)

Roddier, F.
Speckle Interferometry Throgh Small Multiple Apertures: Michelson Stellar Interferometer and Aperture Synthesis in Optics
Opt. Commun. 10, 103-105 (1974)

Roddier, F.
Observations of the Sun with Interferometry and Speckle-interferometry Techniques
In Future Solar Optical Observations , Florance, 1978

Roddier, F.
Rotation-Shearing Interferometry
IAU Colloquium #50, paper 32, Maryland 1978

Roddier, F.
Signal-to-Noise Ratio in Speckle Interferometry
Imaging in Astronomy, Conference Preprints, Boston, June 1975

Roddier, F.
The Effects of Atmospheric Turbulence in Optical Astronomy
In "Progress in Optics", XIX, edited by E. Wolf, North-Holland ,1981.

Roddier, F.
Atmospheric Limitations to High Angular Resolution Imaging
ESO Conference on High Angular Resolution, 1981

Roddier, F., C. Roddier and J. Demarcq
A Rotation Shearing Interferometer with Phase-compensated Roof-prisms
J. Optics (Paris), 9, 145-149 (1978)

Roddier, F., G. Ricort, C. Roddier
Defocussing Effects in Astronomical Speckle Interferometry
Opt. Commun. 24, 281-284 (1978)

Roddier, F., J.M Gilli and J. Vernin
On the Isoplanatic Patch Size in Stellar Speckle Interferometry
Opt. Commun., in press

Roddier, F., J.M. Gilli and G. Lund
On the Origin of Speckle Boiling and its Effects in Stellar Speckle Interferometry
J. Optics, 13, 263-271 (1982)

Roddier,F., J.M. Gilli and J. Vernin
On the Isoplanatic Patch Size in Steelar Speckle Interferometry
J. Optics, 13, 63-70 (1982)

Rogers, G. L.
The Stellar Interferometry of a Star Cluster with a Prominent Variable
Opt. Commun. 30, 1-4 (1979)

Rogstad, D.H.
A Technique for Measuring Visibility Phase with an Optical Interferometer in the Presence of Atmospheric Seeing
Appl. Opt., 7, 585-588 (1968)

Ruder, J.
Physical Principles of the New Interferometric Methods
Mitt. Astron. Ges. (Germany) #40, 23-36 (1976)

Sato, T. et al
Differential Detection of Coherence Functions and its Applications
J. Opt. Soc. Am., 70, 97-103 (1980)

Sato, T., S. Wadaka, J. Yamamoto, J. Ishii
Imaging System Using Intensity Triple Correlator
Appl. Opt. 17, 2047-2052 (1978)

Scaddan, R. J., B. L. Morgan, J. C. Dainty
Diffraction-Limited Observations of Binary Star Systems
IAU Colloquium #50, paper 27, Maryland 1978

Scaddan, R. J., J. C. Dainty
A Simple Method of Estimating the RMS Phase Variation Due to Atmospheric Turbulence
Opt. Commun. 21, 51-54 (1977)

Scaddan, R. J., J. G. Walker
Statistics of Stellar Speckle Patterns
Appl. Opt. 17, 3779-3784 (1978)

Schmidt, G.D., J.R.P. Angel and R. Harms
Speckle Interferometry with a Linear Digicon Detector
Pub. Astron. Soc. Pac. 89, 410-414 (1977)

Schneiderman, A. M., D. P. Karo
How to Build a Speckle Interferometer
SPIE Seminar Proc. 75, 70-82 (1976)

Schneiderman, A. M., D. P. Karo
Measurements of RO with Speckle Interferometry
J. Opt. Soc. Am. 68, 348-351 (1978)

Schneiderman, A. M., D. P. Karo
Speckle Interferometry Measurements of Atmospheric Non-Isoplanicity Using Double Stars
J. Opt. Soc. Am. 68, 338-347 (1978)

Schneidermann, A. M., D. P. Karo
Imaging in the Presence of Random Wave Aberrations
J. Opt. Soc. Am. 69, 717-724 (1979)

Schneidermann, A. M., P. F. Keller, M. G. Miller
Laboratory-Simulated Speckle Interferometry
J. Opt. Soc. Am. 65, 1287-1292 (1975)

Selby, M. J., R. Wade, C. Sanchez Magro
Speckle Interferometry in the Near Infra-Red
Mon. Not. R. Astr. Soc. 187, 553-566 (1979)

Shao, M. , D.H. Staelin
First Fringe Measurements with a Phase-tracking stellar Interferometer
Appl. Opt., 19, 1519-1522 (1980)

Shao, M., D. H. Staelin
Long-Baseline Optical Interferometry for Astronomy
J. Opt. Soc. Am. 67, 81-86 (1977)

Shapiro, J. H.
The Seeing Limit Can Resolve the Isoplanatic Patch
J. Opt. Soc. Am. 66, 469-477 (1976)

Shapiro, J. H.
Propagation-Medium Limitations on Phase Compensated Atmospheric Imaging
J. Opt. Soc. Am. 66, 460-469 (1976)

Sherman, J. W.
A-Posteriori Restoration of Atmsopherically Degraded Images Using Multiframe Imagery
SPIE Seminar Proc., 74, 249-258 (1976)

Sherman, J.W.
Speckle Imaging Using the Principal Value Decomposition Method
SPIE Seminar Proc., 149,32-90 (1978)

Sherman,J.W.
Speckle Imaging Under Non-Isoplanatic Conditions
SPIE Vol. 243, Applications of Speckle Phenomena (1980)

Sibille, F., A. Chelli and P. Lena
Infrared Speckle Interferometry
Astron. & Astrophys., 79, 315-328 (1979)

Stachnik, R. V., et al.
Speckle Image Reconstructions of Solar Features
Nature 266, 149-151 (1977)

Stachnik, R., P. Nisenson and C. Papaliolios
Solar Speckle Imaging
In "Solar Instrumentation- What's Next ?", Sunspot, NM, 1980

Stephan
Sur l'extreme petitesse du diametre apparent des etoiles fixes
Compt. Rend., 78, 1008-1112 (1874)

Stephan
Letter to Fizeau
Compt. Rend., 76, 1008-1010 (1873)

Sutton, E. C.
Results and Future Uses of Heterodyne Spatial Interferometry at
11 Microns
IAU Colloquium #50, paper 16, Maryland 1978

Sutton, E. C., J. W. V. Storey, A. L. Betz, C. H. Townes
Spatial Heterodyne Interferometry of VY Canis Majoris, Alpha Orionis,
Alpha Scorpii and R Leonis at 11 Microns
Astrophys. J. 217, L97-L100 (1977)

Sutton, E.C., S. Subramanian and C.H. Townes
Interferometric Measurements of Stellar Positions in the Infrared
Astron. Astrophys., (1982)

Tango, W. J.
The Limiting Sensitivity and Visibility Loss in a Small Aperture
Amplitude Interferometer
IAU Colloquium #50, paper 12, Maryland 1978

Tango, W. J.
A Note on Two Aperture Pupil Plane Stellar Speckle Interferometry
Optica Acta 26, 109-111 (1979)

Tango, W. J.
The Monteporzio Two Meter Amplitude Interferometer
IAU Colloquium #50, paper 13, Maryland 1978

Tango, W. J., et al.
A "Narrabi" Binary Star Resolved by Speckle Interferometry
Mon. Not. R. Astr. Soc.

Tokovinin, A.A.
An Interferometer for Determining the MTF of the Atmosphere
Sov. Astron. Lett. 4, 229-230 (1978)

Tokovinin, A.A.
The Influence of Turbulence on the Operation of a Stellar
Interferometer
Sov. Astron. Lett., 6, 386-388 (1980)

Tokovinin, A.A.
The Diameters of Vesta and Ceres Measured by Interferometry
Sov. Astron. Lett., 6, 100-101 (1980)

Tokovinin, A.A.
A Phase-Grating Stellar Interferometer
Sov. Astron. Lett., 5, 229-231 (1979)

Tokovinin, A.A.
Two-Point Speckle Interferometry
Sov. Astron. Lett. 4, 204-206 (1978)

Townes, C. H., E. C. Sutton, J. W. V. Storey
Infrared Heterodyne Interferometry
Optical Telescopes of the Future, ESO/CERN Conference, Geneva 1977

Twiss, R. Q.
Applications of Intensity Interferometry in Physics and Astronomy
Optica Acta 16, 423-451 (1969)

Van de Stadt
Near Heterodyne Interferometer for the Measurement of Stellar Diameters
In Space Optics , Ed. by Thompson and Shannon, (Nat. Acad. Sci.)

Vokac, P. R.
An Online Digital Autocorrelator for Speckle Interferometry
Proc. SPIE 119, 223-231 (1977)

Wade, R., M. J. Selby
Speckle Interferometry in the Near Infrared
IAU Colloquium #50, paper 29, Maryland 1978

Wagner, R. E.
Postprocessing of Imagery from Active Optics: Some Pitfalls
Appl. Opt. 16, 175-179 (1977)

Walker, J. G.
Optimum Exposure Time and Filter Bandwidth in Speckle Interferometry
IAU Colloquium #50, paper 25, Maryland 1978

Walker, J. G.
Signal to Noise Ratio in Speckle Interferometry in the Photon Counting Autocorrelation Mode at Low Light Levels
Opt. Commun. 29, 273-278 (1979)

Walker, J.G.
Statistical Accuracy in Stellar Speckle Interferometry at
Low Light Levels
Optica Acta, 28, 885-905 (1981)

Walker, J.G.
Signal to Noise Ratio in Speckle Interferometry on the Photon
Counting Autocorrelation Mode at Low Light Levels
Opt. Commun., 29, 273-278 (1979)

Walker, J.G.
Computer Simulation of a Method for Object Reconstruction from
Stellar Interferometry Data
Appl. Opt., 21, 3132-3137 (1982)

Walker, J.G.
Object Reconstruction from Turbulence-degraded Images
Optica Acta, 28, 1017-1019 (1981)

Walker, J.G.
The Phase Retrieval Problem : A Solution Based on Zero Location
by Exponential Apodization
Optica Acta, 28, 735-738 (1981)

Waller,W.
Field of View on Actively Controlled Long Baseline
Stellar Interferometry
J. Opt. Soc. Am., 70, 1096-1100 (1980)

Wang, C. P.
High Resolution Imaging Through Turbulent Media
Opt. Commun. 10, 253-257 (1974)

Wang, C. P.
Isoplanicity for Imaging Through Turbulent Media
Opt. Commun. 14, 200-204 (1975)

Weigelt, G.
Speckle Interferometry and Image Reconstruction
IAU Colloquium #50, paper 33, Maryland 1978

Weigelt, G.
Speckle Interferometry, Speckle Holography, Speckle Spectroscopy,
and Reconstruction of High-resolution Images from ST Data
ESO Conference on High-Angular Resolution, ed. by Ulrich,Kjar,1981

Weigelt, G. and B. Wirnitzer
Image Reconstruction by the Speckle Masking Method
Opt. Lett, 8, 389-391 (1983).

Weigelt, G. P.
Speckle Interferometry Measurements of 12 Binary Stars
Astron. Astrophys. 68, L5-L6 (1978)

Weigelt, G. P.
Speckle Interferometry with a 1 Meter Telescope
Astron. Astrophys. 67, L11-L12 (1978)

Weigelt, G. P.
Speckle Holography Measurements of the Stars Zeta Cancri and ADS 3358
Appl. Opt. 17, 2660-2662 (1978)

Weigelt, G. P.
Modified Astronomical Speckle Interferometry, Speckle Masking
Opt. Commun. 21, 55-59 (1977)

Weigelt, G. P.
Large Field Speckle Interferometry
Optik 43, 111-128 (1975)

Weigelt, G.P.
High-Resolution Astrophotography:New Isoplanicity Measurements
And Speckle Holography Applications
Optica Acta, Vol. 26, No. 11, 1351-1357, (1979)

Weigelt, G.P.
Astronomical Speckle Interferometry and Speckle Holography
Proceedings of ICO-11 Conference, Madrid, Spain, 1978

Weigelt, G.P.
Stellar Speckle Interferometry and Speckle Holography At
Low Light Levels
SPIE Seminar Proc., 243, 103-110 (1980)

Weigelt, G.P.
High Resolution Astrophotography : New Isoplanicity Measurements
and Speckle Holography Apllications
Opt. Acta, 26, 1351-1357 (1979)

Welter, G.L. and S.P. Worden
A Method for Processing Stellar Speckle Interferometry Data
J. Opt. Soc. Am., 68, 1271-1275 (1978)

Wickes, W. C.
Interferometric Measurements of Binary Stars
Astron. J. 80, 655-657 (1975)

Wickes, W. C.
Orbits and Masses of Hyades Visual Binaries
Astron. J. 80, 1059-1064 (1975)

Wickes, W. C., R. H. Dicke
An Automatic Interferometer for Double Star Observations
Astron. J. 78, 757-768 (1973)

Wickes, W. C., R. H. Dicke
Achromatic Double Star Interferometry
Astron. J. 79, 1433-1444 (1974)

Wildey, R. L.
Spatial Filtering of Astronomical Photographs: II Theory
Astron. J. 72, 884-886 (1974)

Wildey, R. L.
Spatial Filtering of Astronomical Photographs: III Remarks on the Knox-Thompson Re-Apodization
Astrophys. J. 186, L47-L50 (1973)

Wilkerson, M. S., S. P. Worden
Further Speckle Interferometric Studies of Alpha Orionis
Astron. J. 82, 642-645 (1977)

Woolf, N.J.
High Resolution Imaging from the Ground
Ann. Rev. Astron. Astrophys.,20, 367-398 (1982)

Worden S.P.
High Angular Resolution Astronomical Techniques:Speckle Interferometry and Related Methods
SPIE Seminar Proc., 243, 66-74 (1980)

Worden, S. P.
Astronomical Image Reconstruction in Astronomy
Vistas in Astron. 20, 301-317 (1977)

Worden, S. P.
Digital Analysis of Speckle Photographs: The Angular Diameter of Arcturus
Pub. Astr. Soc. Pac. 88, 69-72 (1976)

Worden, S. P.
Speckle Interferometry
New Scientist 78, 238-240 (1978)

Worden, S. P., C. R. Lynds, J. W. Harvey
Reconstructed Images of Alpha Orionis Using Stellar Speckle Interferometry
J. Opt. Soc. Am. 66, 1243-1246 (1976)

Worden, S. P., M. K. Stein, G. D. Schmidt, J. R. P. Angel
The Angular Diameter of Vesta from Speckle Interferometry
Icarus 32, 450-457 (1977)

Worden, S.P.
Interferometric Determination of Asteroid Diameters
In "Asteriods", edited by T. Gehrels, U of A Press, 1979

Worden, S.P. , M.K. Stein
Angular Diameter of the Asteroids Vesta and Pallas Determined from
Speckle Observations
Astron. J., 84, 140-142 (1979)

Wynne, C. G.
Extending the Bandwidth of Speckle Interferometry
Opt. Commun. 28, 21-25 (1979)

END

DATE
FILMED

7-86